

**Hyperspectral Remote Sensing of Crop Canopy
Chlorophyll and Nitrogen: The Relative Importance of
Growth Stages**

Inaugural-Dissertation

zur

Erlangung des Doktorgrades

der Mathematisch-Naturwissenschaftlichen Fakultät

der Universität zu Köln

vorgelegt von

Kang Yu

aus Jiangsu, China

2014

Berichtersteller:

Prof. Dr. Georg Bareth

Prof. Dr. Karl Schneider

Tag der mündlichen Prüfung:

April 14, 2014

Abstract

Remote sensing plays an important role in monitoring vegetation dynamics, and has been recognized as a reliable tool for monitoring biochemical and biophysical variations of agricultural crops, such as plant biomass, height, chlorophyll (Chl) and nitrogen (N). Nitrogen is one of the most essential elements in agro-ecosystems because of its direct role in determining crop yield and vegetation productivity, as well as its association with global N and carbon cycles. Canopy remote sensing of plant biochemical (e.g., N) and biophysical parameters (e.g., biomass) is often discussed separately. However, crop canopy structural characteristics and plant morphophysiological variations at different growth stages cause a confounding effect on the analysis and interpretation of the canopy spectral data. This study aimed to (1) understand the underlying mechanisms of canopy structural dynamics (mainly plant biomass and green leaf area) that impact the retrieval of canopy Chl and N at different growth stages, and (2) develop new algorithms and narrow band vegetation indices that may improve the estimation of Chl and N using hyperspectral data collected in the field and simulated by radiative transfer models (RTMs).

To achieve the objectives, barley and rice experiments were conducted in Germany and China, respectively, from experimental plots to farmer fields; both empirical and physical models were employed but with an emphasis on the empirical methods. Results suggest that canopy hyperspectral data allow for the estimation of canopy Chl and N. However, with the advance of growth stages, plant growth rate is much faster than the rate at which N is accumulated in the plant mass until the stage of full heading (canopy closure), which results in a decrease of N concentration — the N dilution effect. Thus, growth stages have a significant effect on the correlation between the optical and biological traits of the crop canopy compared to the differences in crop cultivars and types. This effect is confirmed by five years of experimental data of barley and rice crops. Accordingly, empirical models based on different vegetation indices can be calibrated, before and after the canopy closure, which allows for the monitoring of canopy Chl and N status through the entire growing season. This study also suggests that multivariate models such as partial least squares (PLS) and support vector machines (SVM) are relatively resistant to the influence of growth stages and can be used to improve the estimation of canopy Chl and N compared to univariate models based on vegetation indices.

To devise a simple approach for the estimation of canopy Chl and N status that is relatively insensitive to the confounding effect of canopy structural characteristics, new vegetation indices, the Ratio of Reflectance Difference Indices (RRDIs), were developed based on the multiple scatter correction (MSC) theory. This type of indices conceptually eliminates the linear influence caused by the confounding effect of multiple scattering and soil background as well as their

interactions; therefore, RRDI weakens the effect of canopy structural variations on the analysis of canopy spectra when estimating biochemical variations. For example, the RRDI derived from the red edge (RRDI_{re}) wavelengths proved to be a robust indicator of canopy Chl and N in both barley and rice crops with different cultivars and for the simulated data by RTMs. Therefore, the method is useful for improving the estimation of canopy biochemical parameters.

This study improves the understanding of remote estimation of canopy Chl and N status by considering the dynamical co-variations between plant biomass and N across different growth stages and suggests the potential to improve the ability of canopy hyperspectral data to monitor the canopy biogeochemical cycles of agro-ecosystems using remote sensing. Additionally, this study indicates that hyperspectral vegetation indices based on water absorption bands are useful for the detection of crop diseases at the canopy level.

Zusammenfassung

Fernerkundung spielt eine wichtige Rolle für das Monitoring der Vegetationsdynamik und wurde als zuverlässiges Werkzeug für die Beobachtung von biochemischen und biophysikalischen Unterschieden in Agrarpflanzen, wie z.B. Pflanzenbiomasse, Chlorophyll (Chl), und Stickstoff (N), erkannt. Stickstoff ist aufgrund seiner direkten Rolle in der Ertragsbestimmung von Feldfrüchten und in der Vegetationsproduktivität, als auch in seiner Verbindung mit globalen Stickstoff- und Kohlenstoffflüssen, eines der wesentlichen Elemente im Agrarökosystem. Die Fernerkundung des Stickstoffstatus der Pflanzen und anderer biochemischer Merkmale wird häufig getrennt behandelt, weil es aufgrund von strukturellen und biophysikalischen Eigenschaften in Feldfrüchten und morphophysiologischen Variationen von Pflanzen zu unterschiedlichen Entwicklungsstadien am Verständnis der wechselseitigen Effekte mangelt. Diese Studie bezweckt (1) die zugrundeliegenden Mechanismen zu verstehen, wie die strukturelle Dynamik von Pflanzenbiomasse und grüner Blattfläche die Gewinnung von Chlorophyll und Stickstoff im Bestand beeinflusst, und (2) neue Schmalband Vegetationsindizes aus hyperspektralen Daten, die im Feld erhoben und durch Strahlungstransportmodelle (RTM) simuliert worden sind, zu entwickeln.

Um diese Ziele zu erreichen, wurden Experimente an Gerste und Reis jeweils in Deutschland und China von der Versuchs- bis zur Feldskala durchgeführt und hauptsächlich empirische aber auch physikalische Modelle verwendet. Einhergehend mit einem fortschreitenden Entwicklungsstadium, ist das Wachstum von Kulturpflanzen größer als der Anstieg in der Akkumulationsrate von Stickstoff in der Pflanzenbiomasse, bis zu dem Stadium des Bestandsschlusses. Dies führt zu einer schnellen Abnahme der Stickstoffkonzentration und somit zu einer Stickstoffreduzierung. Dadurch haben Entwicklungsstadien einen signifikanten Einfluss auf den Zusammenhang zwischen optischen und biologischen Merkmalen im Feldfruchtbestand, im Gegensatz zu Unterschieden zwischen Kultursorten und Feldfrüchten. Dieser Einfluss wird durch experimentelle Daten aus fünf Jahren im Gersten- und Reisanbau bestätigt. Dementsprechend können empirische Modelle, die auf unterschiedlichen Vegetationsindizes basieren, jeweils vor und nach dem Bestandsschluss kalibriert werden, was das Monitoring von dem Chl- und N-Status für die gesamte Wachstumsperiode zulässt. Diese Studie legt den Schluss nahe, dass multivariate Modelle wie z.B. Partial Least Squares (PLS) und Support Vector Machine (SVM) verhältnismäßig resistent gegenüber Einflüssen von Entwicklungsstadien sind, und dass sie die Schätzung von Chl und N im Bestand gegenüber Modellen, die auf Vegetationsindizes basieren, verbessern können.

Um einen einfachen Ansatz für die Schätzung von dem Chl- und N-Status zu entwickeln, der relativ unempfindlich gegenüber den wechselseitigen Effekten der Struktureigenschaften im

Bestand ist, wurde ein neuer Vegetationsindex, Ratio of Reflectance Difference Index (RRDI), basierend auf der Strategie einer multiplen Streuungskorrektur (MSC) entwickelt. Dieser Index eliminiert konzeptionell den linearen Einfluss, der durch den wechselseitigen Effekt zwischen multipler Streuung und Bodenhintergrund, als auch durch ihre Interaktionen verursacht wird und mindert somit den Einfluss auf die strukturellen Variationen im Bestand bei der Analyse von Spektren zur Schätzung von biochemischen Variationen. So hat sich z. B. der RRDI, der hier auf den Bereich des Red Edge angepasst wurde (RRDI_{re}), als robuster Chl- und N-Indikator im Bestand, sowohl in Gerste als auch in Reis mit unterschiedlichen Kultursorten, sowie für die durch RTM simulierten Daten erwiesen. Daher ist die Methode für die Verbesserung der Abschätzung von biochemischen Merkmalen aus dem Bestand nützlich.

Diese Studie verbessert das Verständnis der Fernerkundung von dem Chl- und N-Status unter Berücksichtigung von dynamischen Kovariationen zwischen Pflanzenbiomasse und Stickstoff für unterschiedliche Entwicklungsstadien und zeigt das Potential der Verbesserung der Leistungsfähigkeit von hyperspektralen Daten zum Monitoring von biogeochemischen Zyklen in Agrarökosystemen durch die Fernerkundung. Darüber hinaus zeigt diese Studie, dass hyperspektrale Vegetationsindizes, die auf Wasserabsorptionsbändern basieren, für die Detektion von Pflanzenkrankheiten auf Bestandesebene nützlich sind.

Acknowledgements

I came to the Rhine, and my thoughts forced me back to four years ago when I first came to Germany and walked along the river. Fragments of the last four years replayed in my mind, made me feel that the distance between me and other side of the river has never been so close. No words can express my gratitude to all of those who helped me over the past four years.

My most heartfelt thanks go to my advisor, Prof. Georg Bareth who enabled me to become a member of his research group, afforded me freedom in my PhD study, encouraged me to become an independent researcher and allowed me to make mistakes. I thank him for his patient guidance and very helpful criticisms through the four years.

I deeply thank Prof. Karl Schneider, who inspired me a lot during the hydrology seminar and stimulated my interest in coding by demonstrating for us a step by step programming and debugging process. I am also very grateful for his consent on being the second examiner.

I express my deep gratitude to Prof. Xinping Chen, who introduced me to the remote sensing field when I was an undergraduate student at the China Agricultural University (CAU). He always encouraged me and trusted me, even when I was not performing well. Many thanks go to Prof. Yuxin Miao for his enthusiastic guidance and support in the Jiansanjiang project. I also thank Prof. Fei Li for caring for my study and life abroad, and for sharing his experience on writing scientific papers as well as giving me plenty of advice and insightful suggestions.

I thank my dear friends, Zhengrui, Jingbo, Shanchao, Shimeng, Xiaoyan, Meiju, Tian Jing for encouraging and helping each other on the road of “du bo”. I am indebted to all my friends who supported me in their own way, to my Chinese and German colleagues who helped me through the field experiments and laboratory work. Special thanks go to Martin for proofreading my thesis and translating the abstract; Simon and Dirk for proofreading the German abstract; Quanying, Victoria, Thomas, Simon and Jonas and the colleagues at the University of Bonn, Georg Leufen, Dr. Mauricio Hunsche and Prof. Georg Noga for their cooperation. I also extend my gratitude to all the individuals who helped me a lot without knowing they have done so. In particular, I greatly appreciate Prof. Dar Roberts for helping me improve my first journal paper.

Last but not least, to my uncle, Prof. Ye, who has always been my example and is always ready and willing to help me, whenever I need and wherever I am. I also wish to thank his friend Prof. Fuller for editing my English writing.

Beer also deserves thanks!

To my family

Table of Contents

Abstract	i
Zusammenfassung	iii
Acknowledgements	v
Table of Contents	ix
CHAPTER I General introduction	I
<i>1.1 Remote sensing for crop monitoring: Basics</i>	<i>1</i>
<i>1.2 Remote sensing for crop monitoring: Methods</i>	<i>6</i>
1.2.1 Empirical/statistical methods	6
1.2.2 Physical models.....	9
1.2.3 Integration of empirical and physical methods	10
<i>1.3 Introduction to the study areas</i>	<i>11</i>
1.3.1 Study area for rice experiments	11
1.3.2 Study area for barley experiments	12
<i>1.4 Scientific questions and research objectives</i>	<i>15</i>
<i>1.5 Thesis outline</i>	<i>18</i>
CHAPTER 2 Remotely detecting canopy nitrogen concentration and uptake of paddy rice in the Northeast China Plain	20
<i>Abstract</i>	<i>21</i>
<i>2.1 Introduction</i>	<i>22</i>
<i>2.2 Materials and methods</i>	<i>24</i>
2.2.1 Experimental sites.....	24
2.2.2 Experimental design.....	25
2.2.3 Hyperspectral reflectance measurement.....	26
2.2.4 Plant sampling and measurements.....	26
2.2.5 Vegetation indices and data analysis.....	27
<i>2.3 Results</i>	<i>28</i>
2.3.1 Variation in LNC, PNC and PNU and biomass	28
2.3.2 Relationships between published VIs and rice N status	30
2.3.3 Identifying new 2-band vegetation indices using the lambda by lambda band-optimized algorithm.....	33
2.3.4 Identifying the OMNBR models using multiple linear regression analysis	39

2.4	<i>Discussion</i>	43
2.5	<i>Conclusions</i>	48
	<i>Acknowledgements</i>	49
	<i>References</i>	49
CHAPTER 3 Estimate leaf chlorophyll content of rice using spectral indices and partial least squares (PLS)		54
	<i>Summary</i>	55
	<i>Zusammenfassung</i>	55
3.1	<i>Introduction</i>	56
3.2	<i>Material and methods</i>	57
3.2.1	Study area, experimental and farmer fields	57
3.2.2	Spectral measurement	57
3.2.3	Leaf chlorophyll measurement	58
3.2.4	Reflectance indices	58
3.2.5	PLS model	59
3.3	<i>Results</i>	59
3.3.1	NRDI optimization	59
3.3.2	Red edge position	60
3.3.3	RRDI optimization	61
3.3.4	Chl estimation for farmer fields	62
3.3.5	Chl estimation for farmer fields using PLS model	62
3.4	<i>Discussion</i>	64
3.5	<i>Conclusions</i>	65
	<i>Acknowledgements</i>	66
	<i>References</i>	66
CHAPTER 4 Investigation of leaf diseases and estimation of chlorophyll concentration in seven barley varieties using fluorescence and hyperspectral indices		69
	<i>Abstract</i>	70
4.1	<i>Introduction</i>	71
4.2	<i>Materials and methods</i>	73
4.2.1	Experimental design	73
4.2.2	Fluorescence measurements	73

4.2.3	Hyperspectral reflectance measurements	74
4.2.4	Leaf sampling and chlorophyll determination.....	75
4.2.5	Data analysis.....	75
4.3	<i>Results</i>	78
4.3.1	Leaf chlorophyll concentration (LCC).....	78
4.3.2	Discriminatory performances of fluorescence and hyperspectral indices	79
4.3.3	Relationships between LCC and fluorescence and hyperspectral indices.....	84
4.3.4	Estimation of LCC	85
4.4	<i>Discussion</i>	89
4.4.1	Early detection of the risk of disease.....	89
4.4.2	Estimation of LCC	90
4.5	<i>Conclusions</i>	92
	<i>Acknowledgments</i>	93
	<i>Conflict of Interest</i>	93
	<i>References</i>	93
CHAPTER 5 Optimizing spectral indices to reduce effects of soil background and canopy structure for the estimation of leaf chlorophyll of barley at different growth stages		99
	<i>Abstract</i>	100
5.1	<i>Introduction</i>	101
5.2	<i>Materials and methods</i>	104
5.2.1	Barley dataset	104
5.2.2	Synthetic dataset	107
5.2.3	Data analysis.....	107
5.3	<i>Results</i>	112
5.3.1	General purpose models	112
5.3.2	Growth stage specific models	129
5.4	<i>Discussion</i>	136
5.4.1	Confounding effects of soil background, canopy structure and multiple scattering.....	136
5.4.2	Band optimization: green and red edge bands	137
5.4.3	Improvement of RRD type indices relative to other types of indices	138
5.4.4	Connections with previous studies.....	138
5.4.5	Effects of crop type, growth stage and the range of variation in Chl	139
5.5	<i>Conclusions</i>	140
	<i>Acknowledgements</i>	141

References.....	141
Appendix A. Temporal changes in canopy reflectance	149
CHAPTER 6 Validation of N dilution effect and developed vegetation index (RRDI) and evaluation of crop responses to diseases.....	151
Summary.....	151
6.1 Materials and methods.....	152
6.1.1 Experimental design and descriptions of disease symptom	152
6.1.2 Canopy spectral measurement and plant sampling.....	153
6.1.3 Selected vegetation indices for sensitivity comparison with the new index RRDI	154
6.2 Results.....	154
6.2.1 Relationships between Chl and N in different parts of a plant	154
6.2.2 Relationships between Chl and N at different growth stages as observed in different cultivars of barley	155
6.2.3 Relationships between Chl and vegetation indices (VIs)	156
6.2.4 Relationships between N, biomass and VIs	158
6.2.5 Responses of BDW, Chl and N to fungicide treatments	161
6.2.6 Yield response to diseases	163
6.2.7 Responses of VIs to diseases	164
CHAPTER 7 General discussion and conclusions	168
7.1 Remote sensing of canopy N.....	168
7.2 Growth stage and N dilution effect	171
7.3 Relating Chl to N	173
7.4 Decoupling of biochemical and biophysical traits	174
7.5 General model and growth-stage-specific model	177
7.6 Canopy sensing of plant diseases.....	178
7.7 Near-ground remote sensing for PA.....	180
7.8 Main findings and conclusions.....	181
7.9 Limitations and outlook.....	181
General references	183
Eigene Beteiligung an den Veröffentlichungen.....	199
Erklärung.....	200

Curriculum vitae..... 201

List of publications..... 202

CHAPTER 1

General introduction

1.1 Remote sensing for crop monitoring: Basics

Precision agriculture (PA) is a farming management concept that aims to optimize inputs, reduce costs and environmental impacts and meet the increasing environmental, economic, food, market and public pressure on arable agriculture (Stafford, 2000). The basis of PA — the spatial and temporal variability in soil and crop factors within a field — has become increasingly difficult to take account of within-field variability without the development of technologies for observing, measuring and responding to the variability (Stafford, 2000; Zhang et al., 2002). Remote Sensing (RS), Geographic Information Systems (GIS) and Global Positioning Systems (GPS) provide the potential to observe, measure and map the within-field spatial variability and define a decision support system (DSS) for responding to the variability and decision making for management of the entire farm (Bareth, 2009). With this goal, PA requires crop monitoring in a timely fashion to be able to quantify within-field variability and identify key phenological phenomena with greater precisions, both spatially and temporally (Hatfield et al., 2008). However, traditional laboratory-based measurements, i.e., plant- and soil-tests, are destructive, time-consuming and costly; therefore, it is difficult to track the dynamics of crop growth through rapid and repeated measurements with high spatial and temporal resolutions (Atzberger, 2013). Thus, RS — the science of obtaining information about objects or phenomena from a distance without coming into physical contact with them (Elachi & van Zyl, 2006) — provides an attractive and non-destructive method of monitoring crop growth dynamics and measuring the within-field spatial variability at a high frequency.

RS instruments/sensors gather information by measuring the electromagnetic radiation that is absorbed, emitted or reflected by an object in various spectral regions (Elachi & van Zyl, 2006). There are two types of RS sensors: passive (e.g., radiometer and imaging radiometer) and active (e.g., laser, lidar and radar). Passive sensors only sense radiation emitted by the object being sensed or reflected by the object from a source (e.g., sunlight) other than the sensor, active sensors transmit a pulse of energy to the object and then measure the radiation that is reflected or backscattered from the object (NASA Earth Observatory). Accordingly, RS methods can be grouped into two types: passive and active remote sensing. RS techniques can also be divided into different classes according to different standards (Elachi & van Zyl, 2006); for example,

multispectral and hyperspectral methods can be differentiated by spectral resolution or by different sensor carriers, such as airborne, satellite and unmanned aerial vehicles (UAV), and near-ground platforms (Elachi & van Zyl, 2006; Weng, 2011). More recently, a new method for measuring of sun-induced chlorophyll fluorescence (Meroni et al., 2009) has received increasing interest in the RS community and can be categorized as a passive remote sensing method. Because this dissertation focuses mainly on passive remote sensing with an emphasis on hyperspectral narrow band data that were collected at the near ground level using spectroradiometers, the RS methods discussed herein fall primarily into this scope.

RS methods have become widely used in PA for monitoring and understanding plant *in situ* growth status and variability and detecting many environmental stresses (Gausman et al., 1969; Mulla, 2013; Pinter et al., 2003). Generally, the applications of remote sensing in agriculture crop monitoring can be categorized into the following three groups: (1) biochemical trait monitoring, e.g., leaf pigments (Gitelson & Merzlyak, 2004), leaf water content (Ustin et al., 1998), plant nitrogen (N) content (Osborne et al., 2002) and other nutrient statuses or deficiencies (Ayala-Silva & Beyl, 2005); (2) biophysical trait monitoring, e.g., plant height (Tilly et al., 2013), leaf angle distribution (Biskup et al., 2007), leaf area index (LAI) (Wiegand & Richardson, 1990; Xavier & Vettorazzi, 2004), plant biomass production (Aase & Siddoway, 1981) and crop yield (Serrano et al., 2000); and (3) crop growth anomalies, e.g., crop diseases (Huang et al., 2007), pests (Mirik et al., 2012) and weed stresses (Goel et al., 2003) as well as crop lodging detection (Ogden et al., 2002).

Hyperspectral remote sensing (HRS, also known as imaging spectroscopy) is a relatively new technology that can provide detailed spectral information that often has more than hundreds of continuously narrow bands (Thenkabail et al., 2012). HRS is being primarily investigated for the detection and identification of terrestrial vegetation (van der Meer & de Jong, 2001), which facilitates the applications of aforementioned RS methods in PA with high spectral resolution. Green vegetation characterizes unique spectral signatures through the visible (VIS) to shortwave infrared (SWIR) spectrum (Figure 1-1) by absorbing in the red and blue wavelengths and atmospheric water absorption bands in SWIR range and, reflecting in the green wavelength and near infrared (NIR) range (Figure 1-1). Generally, changes in leaf/plant chlorophyll concentration often produce spectral shifts near 700 nm of the VIS, which is known as the red edge, and variations in the leaf/canopy structures, plant nitrogen, cellulose, lignin, starch and water contents as well as other properties form the reflectance spectra over different wavelengths (van der Meer & de Jong, 2001). Therefore, HRS provides the potential for capturing information about plant biochemical and biophysical characteristics. The following sections describe the links between spectral features and individual leaf, plant and vegetation characteristics.

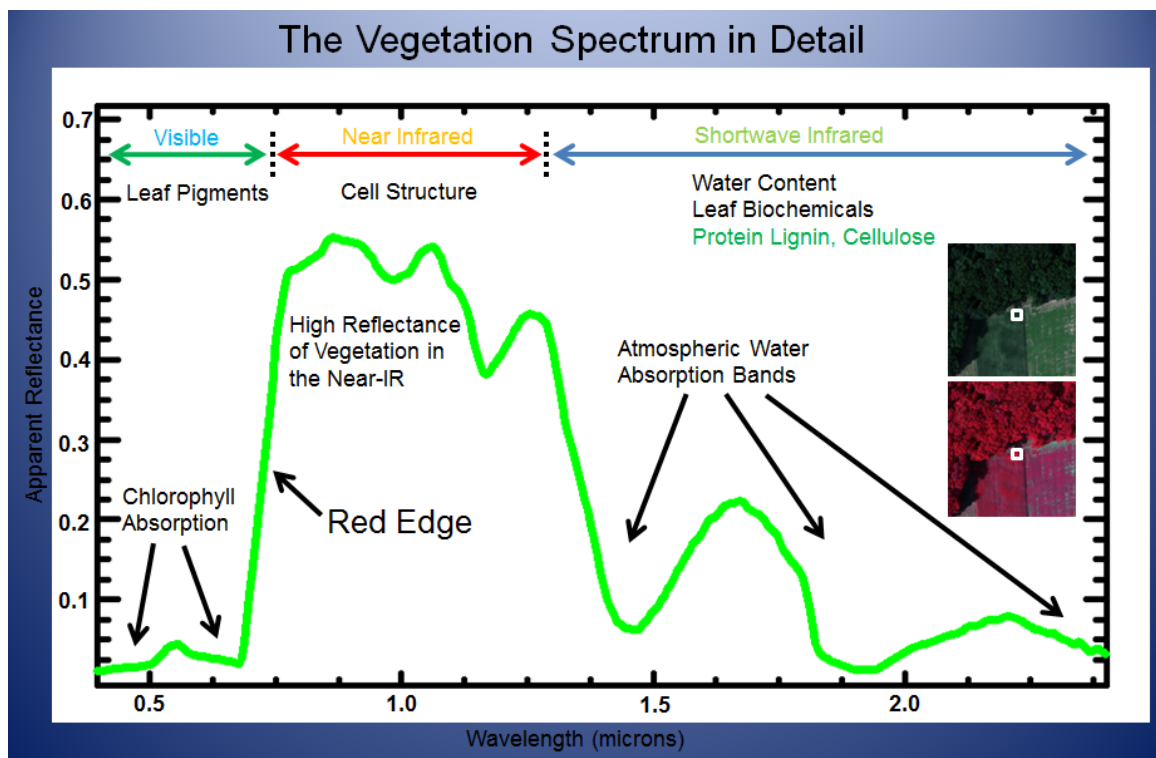


Figure I-1: The reflectance spectrum of green vegetation (Source: Elowitz, 2014).

Plant Pigments: Photosynthetic pigments (mainly chlorophylls and carotenoids) capture light in the process of photosynthesis and convert light energy to carbohydrates (Govindjee & Krogmann, 2004). Chlorophyll is the most important pigment required for photosynthesis and has the maximum absorption of light at approximately 450 and 670 nm, which characterizes the blue and red troughs and the green peak in the reflectance of the visible (VIS, 380-750 nm) spectrum (Lichtenthaler, 1987) (see Figure I-1). In addition to chlorophyll, the amount of anthocyanins, carotenoids and xanthophylls in leaves/plants governs the absorption in the visible spectrum (Davies, 2004). Therefore, variation in these pigments provides unique reflectance signature that allow for the leaf and canopy level sensing of the leaf pigments. For example, a loss of chlorophyll in leaves leads to a red edge shift toward the blue part of the spectrum (van der Meer & de Jong, 2001). Numerous absorption features have been identified for different pigments and foliar chemical components (Curran, 1989). However, the absorption features of different pigments and chemical components are often similar and overlapping (Figure I-2); therefore, a single absorption feature is difficult to be isolated to relate directly to the amount of specific biochemical contents (Kokaly & Clark, 1999). Compared to the majority of light energy (>80%) absorbed by green leaves, only a very small part ($\approx 2\%$) is emitted as leaf fluorescence (Buschmann, 2007), which allows for the characterization of the physiological (photosynthetic) activity of plants. Simultaneous measurement of the red and far-red chlorophyll fluorescence emitted by

leaves as a result of the light absorbed from the ultraviolet (UV) to VIS range permits the estimation of chlorophyll variations (Buschmann, 2007).

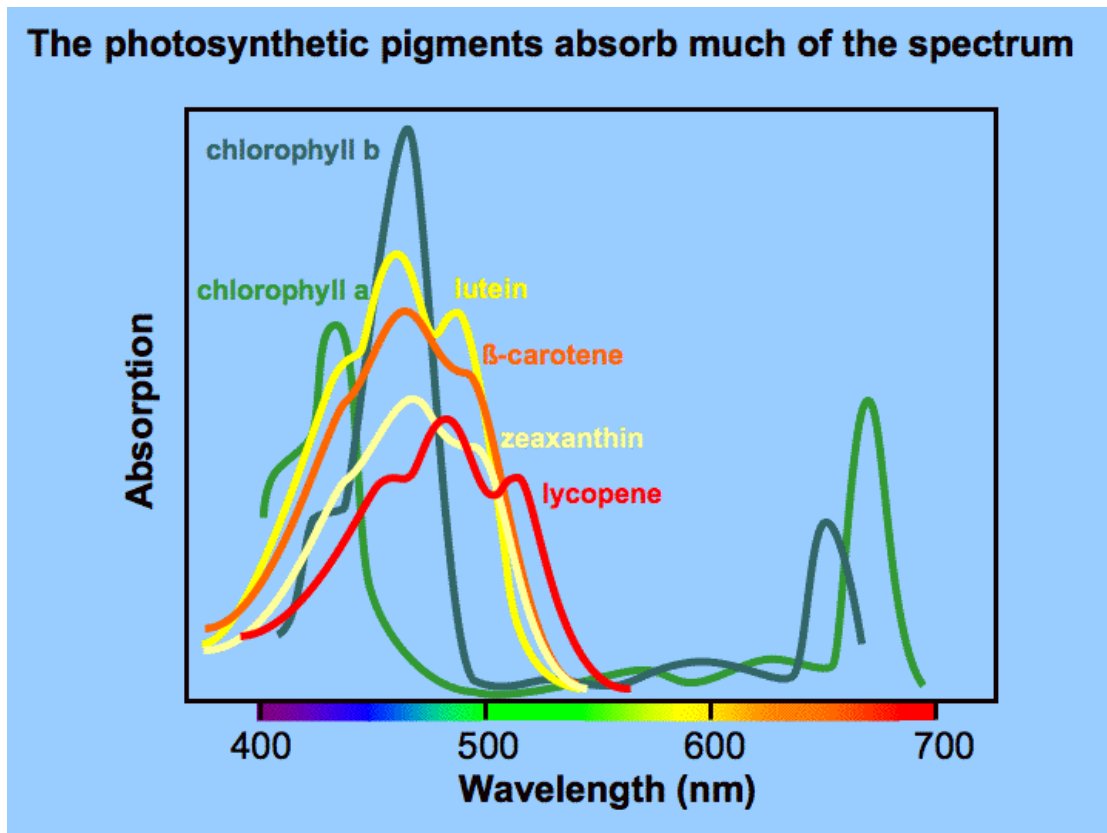


Figure I-2: Absorption spectra of photosynthetic pigments show how these pigments add to the range of wavelengths of light that are useful in photosynthesis (Source: Koning, 1994).

Nitrogen: N is the most important, limiting nutrient element for plant growth and grain production. It is a major component of chlorophyll and part of all amino acids that comprise proteins (Wagner, 2012). The most abundant N-bearing compound in green leaves accounts for 30 to 50 percent of the total N, and it has absorption features at 1500, 1680, 1740, 1940, 2050, 2170, 2290 and 2470 nm (Elvidge, 1990). However, in fresh leaves, the absorption of N compounds is not very strong and is generally masked by water absorption (Kumar et al., 2001). The total leaf N content is known to be related to the rate of CO₂ assimilation and content of chlorophyll (Evans, 1983); thus, N plays a key role in photosynthesis. Normally, plants with an adequate supply of nitrogen have a dark green color as a result of high concentrations of chlorophyll, which is associated with vigorous vegetative growth. Conversely, N deficiency will lead to reduced plant growth and chlorophyll concentrations and is often characterized by the yellowing (chlorosis) of leaves (Beegle, 2013). Therefore, N deficiency often reduces the absorption in the VIS portion and yields high leaf reflectance at green bands near 550 nm (Yoder & Pettigrew-Crosby, 1995).

Water: Absorption by leaf water is dominant in the NIR (750-1000 nm) to SWIR (1000-2500 nm) spectral range (Ustin *et al.*, 2012). Leaf reflectance in the SWIR region, predominantly beyond 1300 nm, increases as an effect of leaf dehydration (Knippling, 1970). Therefore, a reflectance increase in this range allows for the investigation of leaf drought stress. The reflectance sensitivity (changes in leaf reflectance over wavelength relative to its turgid state) to leaf water content has been identified in this range and is greatest in the water absorption bands near 1450, 1920 and 2500 nm (Carter, 1991). In addition to the water absorption bands, leaf dehydration may also lead to high reflectance sensitivity in the VIS bands near the absorption maxima of chlorophyll (480 and 680 nm) (Carter, 1991).

Biomass, LAI and Yield: Plant biomass is an important indicator of the crop population, growth and gross primary production (Gnyp *et al.*, 2014a; Peng & Gitelson, 2011), and LAI is one of the most important structural parameters for studying vegetation status in response to biological and physical processes (Chen & Cihlar, 1996). In agro-ecosystems, biomass and LAI are quantitative measures of the crop yield potential and play important roles in making in-season decisions for crop management (Li *et al.*, 2010a; Serrano *et al.*, 2000). At the canopy level, biomass and LAI have relatively great effects on the NIR reflectance than on the VIS range. High amount of biomass and large LAI often produce higher reflectance in the NIR and SWIR bands (Casanova *et al.*, 1998; Vargas *et al.*, 2002). Therefore, these bands are often used for plant biomass and LAI modeling and yield forecasting (Jégo *et al.*, 2012; Thenkabail *et al.*, 2000).

Diseases, Weeds and Lodging: Plant diseases have significant impacts on physiological functions and may result in severe losses of crop yields (Barkley *et al.*, 2014). For individual leaves, disease stresses appear to affect the VIS reflectance more than the NIR range because chlorophyll is sensitive to physiological disturbances (Knippling, 1970). At the canopy level, however, disease stresses influence morphological traits and lead to smaller leaves/plants and biomass production, and severe stem-based diseases can cause crop lodging (Gröll, 2008). In a developed canopy, disease infection may vary at different leaf layers and is difficult to detect from the top canopy. Weeds and lodging (often caused by wind or rain damages) are common phenomena that reduce crop yield (Seelan *et al.*, 2003). Additionally, weed species often easily out-compete agricultural crops for resources (e.g., sunlight, soil nutrients and water), which affects the crop growth and reduces the yield (Herrmann *et al.*, 2013; Mirik *et al.*, 2013). These field anomalies provide spectrally distinguishable information relative to normal/healthy crop canopies (Hatfield & Pinter, 1993; Lamb & Brown, 2001).

The aforementioned crop characteristics have direct and/or indirect links with the absorption and/or reflectance spectra, which offers many opportunities to monitor these crop

characteristics using HRS that collects spectral data with high spectral resolution (*Thenkabail et al., 2012*). In addition to the requirement for spectral resolution, PA requires high spatial and temporal resolution to detect within-field variability and track key phenological phenomena (*Stafford, 2000*). These three requirements are the pillars that allow RS to play a key role in PA.

1.2 Remote sensing for crop monitoring: Methods

Methods used in agricultural remote sensing for crop monitoring fall into two broad groups: empirical and physical. Empirical methods attempt to explore the statistical relationships between crop growth traits and canopy spectra (*Aparicio et al., 2002*). By contrast, physical methods attempt to determine the underlying mechanisms that generate the empirical relationships to understand the causality principles (*Dorigo et al., 2007*).

1.2.1 Empirical/statistical methods

Among empirical methods, vegetation indices are widely used in a number of investigations that retrieve vegetation characteristics (*Eitel et al., 2008; Gitelson et al., 1996; Oppelt & Mauser, 2004; Perry et al., 2012*). Vegetation indices are derived from combinations of electromagnetic bands that are correlated with specific vegetation features (*Bannari et al., 1995*). The wide use of vegetation indices in applications of agricultural crop monitoring is because of its simplicity. In past decades, a broad range of vegetation/spectral indices have been empirically or semi-empirically developed (*Peñuelas et al., 1995a*). Most of these indices use the chlorophyll absorption bands and NIR range or their related band combinations (*Barton, 2012*), whereas some studies also suggest the usefulness of SWIR bands (*Koppe et al., 2010; Thenkabail et al., 2013*).

Vegetation indices can be classified into three classes (*Daughtry et al., 2000*): (1) intrinsic indices, such as the simple ratio (SR) or ratio vegetation index (RVI), normalized difference vegetation index (NDVI), chlorophyll absorption in reflectance index (CARI) (*Kim et al., 1994*) and its variants such as MCARI (*Daughtry et al., 2000*) and TCARI (*Haboudane et al., 2002*); (2) soil-line related indices, such as the soil-adjusted vegetation index (SAVI) (*Huete, 1988*) and its modifications such as TSAVI (*Baret et al., 1989*) and OSAVI (*Rondeaux et al., 1996*); and (3) atmospherically corrected indices, such as the atmospherically resistant vegetation index (ARVI) (*Kaufman & Tanre, 1992*). Table I-1 lists some of the important vegetation indices and applications for specific biochemical or biophysical parameters

Table I-1: Spectral vegetation indices and their applications for specific vegetation characteristics.

Index	Formula	Application	Reference
<i>Intrinsic indices</i>			
DVI	$R_{NIR} - R_{red}$	Biomass, water	<i>Tucker (1979)</i>
NDVI	$(R_{NIR} - R_{red}) / (R_{NIR} + R_{red})$	LAI, yield	<i>Wiegand & Richardson (1990b)</i>
NDWI	$(R_{857} - R_{1241}) / (R_{857} + R_{1241})$	Water	<i>Gao (1996)</i>
NPCI	$(R_{680} - R_{430}) / (R_{680} + R_{430})$	Chlorophyll	<i>Peñuelas et al. (1994)</i>
SR, RVI	R_{NIR} / R_{red}	LAI, biomass	<i>Casanova et al. (1998); Jordan (1969)</i>
WBI	R_{824} / R_{1225}	Biomass	<i>Koppe et al. (2010)</i>
	R_{900} / R_{970}	Water	<i>Peñuelas et al. (1994; 1997)</i>
Clg	$(R_{NIR} / R_{green}) - 1$	Chlorophyll	<i>Gitelson et al. (2003a)</i>
CAI	$\int R_{600-735} * R(EQ)$	Chlorophyll	<i>Oppelt (2002)</i>
CARI	$R_{700} / R_{670} * \sqrt{[(a * 670 + R_{670} + b)^2] / (a^2 + 1)}$	Chlorophyll	<i>Kim et al. (1994)</i>
MCARI	$[(R_{700} - R_{670}) - 0.2 * (R_{700} - R_{550})] * (R_{700} / R_{670})$	Chlorophyll	<i>Daughtry et al. (2000)</i>
TCARI	$3 * [(R_{700} - R_{670}) - 0.2 * (R_{700} - R_{550}) * (R_{700} / R_{670})]$	Chlorophyll	<i>Haboudane et al. (2002)</i>
PSRI	$(R_{678} - R_{550}) / R_{750}$	Plant senescence	<i>Merzlyak et al. (1999)</i>
<i>Soil-line vegetation indices</i>			
SAVI	$(1 + 0.5) * (R_{NIR} - R_{red}) / (R_{NIR} + R_{red} + 0.5)$	LAI, biomass	<i>Huete (1988)</i>
TSAVI	$a * (R_{NIR} - a * R_{red} - b) / (R_{red} + a * R_{NIR} - a * b)$	LAI	<i>Baret et al. (1989)</i>
OSAVI	$(1 + 0.16) * (R_{800} - R_{670}) / (R_{800} + R_{670} + 0.16)$	LAI, vegetation cover	<i>Rondeaux et al. (1996)</i>
EVI	$2.5 * [(R_{NIR} - R_{red}) / ((R_{NIR}) + (6 * R_{red}) - (7.5 * R_{blue}) + 1)]$	LAI	<i>Huete et al. (2002)</i>
<i>Atmospherically adjusted indices</i>			
ARVI	$(R_{NIR} - R_{rb}) / (R_{NIR} + R_{rb})$, $R_{rb} = R_{red} - p(R_{blue} - R_{red})$, $p = 1$	Vegetation fraction	<i>Kaufman & Tanre (1992)</i>
VARI	$(R_{green} - R_{red}) / (R_{green} + R_{red} - R_{blue})$	Vegetation fraction	<i>Gitelson et al. (2002)</i>
<p>ARVI: atmospherically resistant vegetation index; CAI: chlorophyll absorptions integral, EQ= envelope quotient, see details in <i>Oppelt (2002)</i>; CARI: chlorophyll absorption ratio index, $[a = (R_{700} - R_{550}) / 150$; $b = R_{550} - (a * 550)$]; Clg: chlorophyll index (green model); DVI: difference vegetation index; EVI: enhanced vegetation index; MCARI: modified chlorophyll absorption in reflectance index; NDVI: normalized difference vegetation index; NDWI: normalized difference water index; NPCI: normalized pigment chlorophyll ratio index; OSAVI: optimized soil-adjusted vegetation index; PSRI: plant senescence reflectance index; RVI, ratio vegetation index, also known as SR; SAVI: soil adjusted vegetation index; SR: simple ratio, also known as RVI; TSAVI: transformed soil-adjusted vegetation index, a, b are the soil line coefficients; TCARI: transformed chlorophyll absorption in reflectance index; VARI: visible atmospherically resistant indices; WBI: water band index.</p>			

In terms of canopy biochemistry, almost all of the vegetation indices for pigments are still sensitive to a certain degree to soil background and canopy structural properties (*Daughtry et al., 2000; Haboudane et al., 2002*). The MCARI and OSAVI were combined as the slope of MCARI vs. OSAVI (MCARI/OSAVI) to cancel out the background effect on the canopy spectra (*Daughtry et*

al., 2000). Later, TVARI/OSAVI was proposed to further increase the sensitivity to chlorophyll, particularly for low contents of chlorophyll (*Haboudane et al.*, 2002). Although a number of investigations have demonstrated the improvement of these vegetation indices for chlorophyll, they still have limitations for the lower vegetation cover (e.g., LAI) conditions (*Haboudane et al.*, 2008).

In terms of vegetation biophysical traits, a series of vegetation indices have been developed and modified to enhance their responsiveness to LAI variations. *Haboudane et al.* (2004) developed a modified triangular vegetation index (MTVI2) that was a good indicator of green LAI and less sensitive to chlorophyll content. This index is a modified form of the triangular vegetation index (TVI), which is calculated as the area of the triangle defined by the green peak, chlorophyll absorption minimum, and NIR shoulder (*Broge & Leblanc*, 2001). MTVI2 replaces the NIR shoulder at 750 nm with the reflectance at 800 nm, which is more sensitive to changes in the leaf and canopy structures, and further incorporates a soil adjustment factor for resistance to the soil background (*Haboudane et al.*, 2004; *Huete*, 1988).

Vegetation indices are also widely used to access several abiotic and biotic stresses, including salinity stress (*Hackl et al.*, 2013; *Naumann et al.*, 2009), drought stress (*Gutiérrez-Rodríguez et al.*, 2004; *Zhang et al.*, 2012) and pest damage (*Peñuelas et al.*, 1995b; *Prabhakar et al.*, 2013). The photochemical reflectance index (PRI) (*Gamon et al.*, 1992) has received increased interest in recent studies for a range of plant stresses (*Garbalsky et al.*, 2011; *Inoue & Peñuelas*, 2006; *Zinnert et al.*, 2012). The PRI tracks the action of the xanthophyll cycle that converts xanthophyll pigments from epoxidized to deepoxidized states to avoid damage to the photosynthetic apparatus under excess light conditions; therefore, it is correlated with the efficiency of photosynthesis (*Gamon et al.*, 1992) and stressed plants can be detected by PRI because they often have low photosynthetic radiation use efficiency (RUE) (*Peñuelas et al.*, 1995b).

In addition to vegetation indices, more sophisticated multivariate models, such as the stepwise multiple linear regression (MLR) (*Curran et al.*, 2001; *Kokaly & Clark*, 1999) and more exhaustive MLR methods (*Thenkabail et al.*, 2000; 2002), principal component analysis (PCA) (*Atzberger et al.*, 2010; *Thenkabail et al.*, 2004), partial least squares (PLS) (*Hansen & Schjoerring*, 2003; *Nguyen & Lee*, 2006; *Yu et al.*, 2013a), artificial neural network (ANN) (*Atzberger*, 2004; *Miao et al.*, 2006), and support vector machines (*Verrelst et al.*, 2012), are becoming more widely used in remote sensing applications because of the rapid improvement of computer performance.

These empirical methods have been largely investigated in agricultural remote sensing studies, and applied different vegetation indices alone and in combination. However, the performances of these indices and models are dependent on crop phenological development and

management practices (Hatfield & Prueger, 2010). Some researchers suggest the use of multiple vegetation indices (see Table I-1 for descriptions) for different crop characteristics and growth stages (Hatfield & Prueger, 2010): (a) simple ratios for biomass, (b) NDVI for intercepted photosynthetically active radiation (PAR), (c) SAVI for LAI at early growth stages, (d) EVI for LAI at later stages, (e) Clg for leaf chlorophyll, (f) NPCI for chlorophyll during later stages, and (g) PSRI to quantify plant senescence. There appears to be a trade-off in selecting vegetation indices or multivariate methods because both spectral indices and multivariate models have their advantages and disadvantages (Atzberger et al., 2010). Therefore, multiple and integrated methods are required to best capture crop traits through the whole growing season to obtain the dynamics of crop development. There are additional spectral analysis methods such as techniques for extracting red edge position (Dawson & Curran, 1998; Guyot & Baret, 1988; Miller et al., 1990; Pu et al., 2003) and continuum removal analysis (Huang et al., 2004). All of these empirical methods have demonstrated the usefulness and potential of remote sensing applications in agriculture, although the underlying mechanisms are still not fully understood.

1.2.2 Physical models

Physically based radiative transfer (RT) models have been developed to improve the understanding of the interaction between light and leaves/plants and other canopy structural properties (Jacquemoud et al., 2009). During last three decades, a number of RT models have been developed and widely used; for example, the leaf level RT models PROSPECT (Jacquemoud & Baret, 1990) and LIBERTY (Dawson et al., 1998) and the canopy level model SAIL (Verhoef, 1984).

To monitor crop biochemical and physical properties, physical models can be run in both forward and inverse modes (Jacquemoud et al., 2000). Running RT models in the forward mode allows for the generation of a large database that covers a wide range of combinations of input variables that control the resulting reflectance spectra (Féret et al., 2011). In this mode, the variables of the biochemical or biophysical properties responding to the reflectance bands can be studied, which is useful for identifying and refining spectral indices that are more robust for estimating vegetation biochemical or physical parameters of interest (*continued in section 1.2.3*).

Running RT models in the inverse mode offers the potential of retrieving crop characteristics from hyperspectral reflectance data with a range of 400-2500 nm. A good example is the inversion of the coupled leaf and canopy model PROSAIL (PROSPECT+SAIL) (Jacquemoud & Baret, 1990; Jacquemoud, 1993; Verhoef, 1984). Normally, the inversion of PROSAIL can be conducted in three ways (Jacquemoud et al., 2006): (1) numerical inversion (Botha et al., 2007), (2) look-up table (LUT) (Darvishzadeh et al., 2012) and (3) supervised learning approaches, e.g., ANN

(Atzberger, 2004) and SVM (Camps-Valls et al., 2006). Each method for model inversion has its own advantages and disadvantages (Richter et al., 2009). Some studies have suggested that LUT and supervised learning approaches are more computationally efficient than the numerical inversion (Richter et al., 2011; Weiss et al., 2000).

1.2.3 Integration of empirical and physical methods

To combine empirical and physical methods, simulations of large datasets of leaf and canopy reflectance spectra obtained by forward running the RT models have been used to develop and refine vegetation/spectral indices for retrieving crop biochemical and physical contents at both the leaf (Féret et al., 2011; le Maire et al., 2004) and canopy levels (Broge & Leblanc, 2001; Haboudane et al., 2008). For example, canopy reflectance (CanRefl) can be simulated by the PROSAIL model with 13 input parameters: chlorophyll content (C_{ab}), carotenoids (C_{ar}), leaf equivalent water thickness (C_w), dry matter content (C_m), leaf area index (LAI), average leaf angle (ALA), hot spot parameter (H_{spot}), fraction of diffuse incident radiation (skyl), soil reflectance (R_s), solar zenith angle (θ_s), view zenith angle (θ_v) and relative azimuth angle (φ_{sv}), which are shown in Eq. (I-1):

$$CanRefl = PROSAIL(C_{ab}, C_{ar}, C_w, C_m, N_{stru}, LAI, ALA, H_{spot}, skyl, R_s, \theta_s, \theta_v, \varphi_{sv}) \quad (I-1)$$

Figure I-3 illustrates how the simulated canopy reflectance changes with the LAI variations. The main advantages of the combined mode is its role in developing, modifying and testing various spectral features and vegetation indices for specific vegetation traits of interest and understanding how the distinct biochemical and biophysical characteristics affect the canopy reflectance (Haboudane et al., 2004; Jacquemoud et al., 2009; Salas & Henebry, 2014).

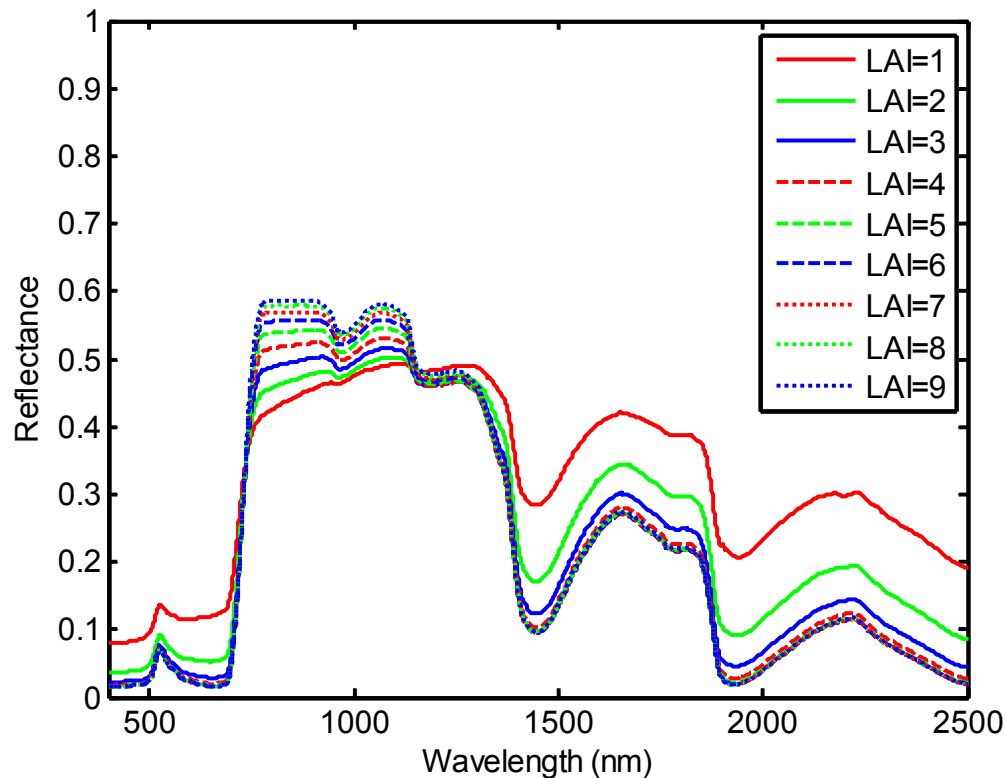


Figure I-3: Effect of LAI variations on canopy reflectance simulated by PROSAIL model ($C_{ab}=30 \mu\text{g cm}^{-2}$, $C_{ar}=0$, $C_w=0.01 \text{ cm}$, $C_m=0.005 \text{ g cm}^{-2}$, $N_{stru}=1.5$, $ALA=\text{spherical}$, $H_{spot}=0.25$, $skyl=0.23$, $\theta_s=30^\circ$, $\theta_v=0^\circ$, $\varphi_{sv}=0^\circ$).

1.3 Introduction to the study areas

1.3.1 Study area for rice experiments

The study area for the rice experiments is located in the Sanjiang Plain, which is the largest marsh area in Northeast China. The Sanjiang Plain is an alluvial plain within the Songhua River Basin that is located in the northeastern part of Heilongjiang Province (Figure I-4). The Sanjiang Plain was originally dominated by marshes and was converted to agricultural production land within the last six decades (Yao *et al.*, 2012). It is rich in natural resources and has become one of the biggest grain production bases in China. The plain results from the alluviation of the Heilong, Songhua and Wusuli Rivers, which earned the plain its name of “Sanjiang” meaning “three rivers” in Chinese. The Sanjiang Plain has a generally flat topography that declines from the southwest to northeast with a slope gradient of approximately 1:5000 – 1:10000 (Cao, Y *et al.*, 2012). The most abundant soils are wet black clays that offer high concentrations of organic matter and nutrients and are favorable for agricultural production (Yao *et al.*, 2012; Zhou & Tong, 2005).

The climate in the Sanjiang Plain is a temperate continental monsoon type with very cold winters and warm summers that has an annual mean temperature of 1.9 °C and a monthly mean temperature in July and January of 22 and -21 °C, respectively (Sun & Song, 2008). The annual mean precipitation is approximately 500-600 mm, which is concentrated in June to August and accounts for more than 60% of the annual precipitation. The characteristic of a hot rainy season is suitable for high quality rice and high-oil soybean growth. Over the last two decades, large scale rice farming has become the dominant land use in the region and is increasingly important in supplying the food market with commercial rice of high quality.



Figure I-4: Rice experiment location in the Sanjiang Plain, Heilongjiang Province, China.

1.3.2 Study area for barley experiments

The study site for the barley experiments is located in the Institute of Crop Science and Resource Conservation – Horticulture Science (Institut für Nutzpflanzenwissenschaften und Ressourcenschutz (INRES) - Gartenbauwissenschaft), University of Bonn, Germany. The institute (latitude 50.72999 °, longitude 7.0754 °, 70 m.a.s.l.) is located in the city of Bonn and the soil is sandy loam with a Nmin value of 20 kg ·N ha⁻¹ (BGR, 1995; Yu et al., 2012). Bonn is located in the southwest region of the federal state of North Rhine-Westphalia (NRW) (Figure I-5) and it has

an area of 141.2 square kilometers that extends from both sides of the Rhine River. The left-bank districts constitute approximately three-quarters of the total area (Figure I-5).

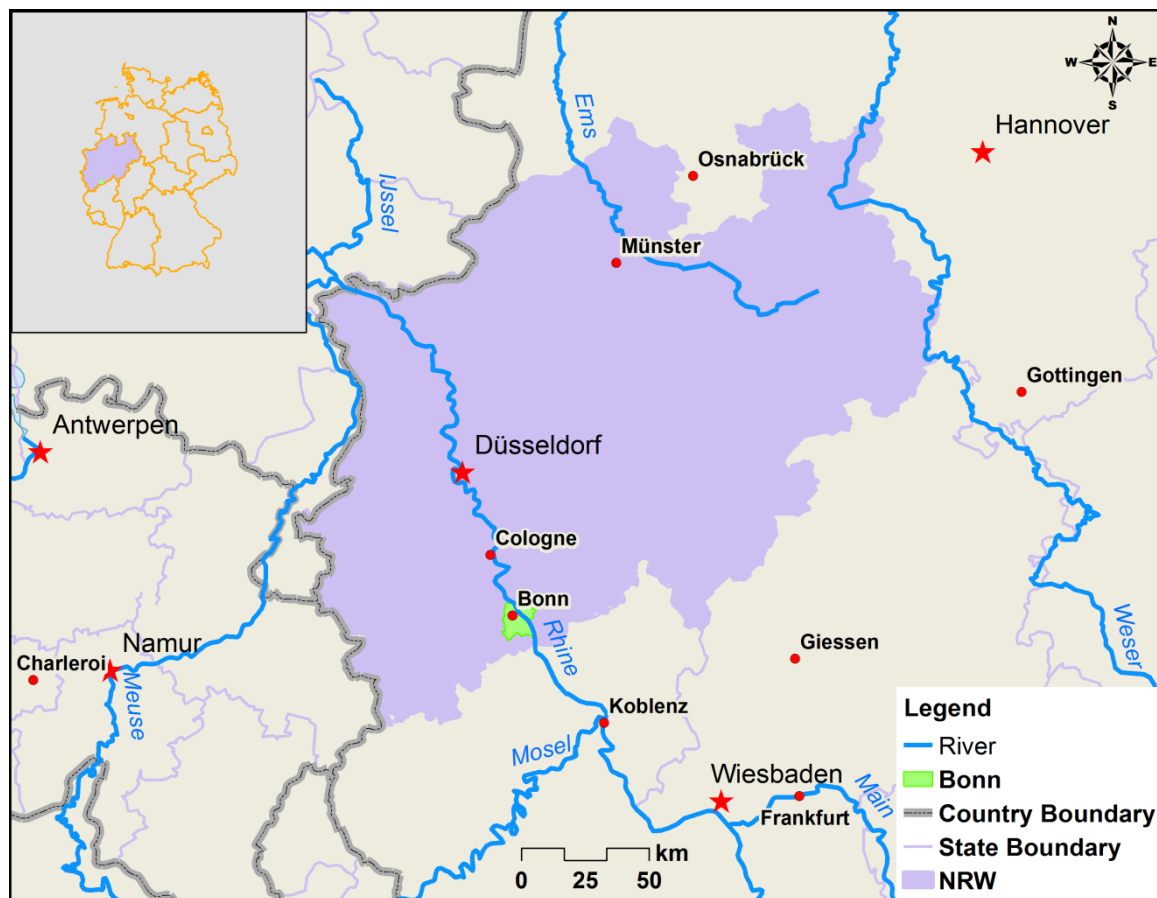


Figure I-5: Barley experiment location in Bonn, North Rhine-Westphalia (NRW), Germany.

Bonn is one of the warmest regions in Germany because of its Atlantic-maritime climate. It has an annual average temperature of 10.3 °C and a monthly average temperature in July and January of 18.7 and 2.0 °C, respectively. The average annual precipitation is 669 mm (source: www.wetteronline.de). Figure I-6 presents an overview (photographs were taken by a Lumix DMC-GF3 (Panasonic Corporation) camera mounted on an unmanned aerial vehicle (UAV), and the panorama for each date was mosaicked from 18 images) of the experimental fields on two different dates in 2012.



Figure I-6: Panoramas of the experimental plots located at the INRES-Horticulture, University of Bonn (courtesy of Dr. Andreas Bolten and taken with a Lumix DMC-GF3 camera mounted on an UAV platform).

1.4 Scientific questions and research objectives

Remote sensing has long been studied in agriculture for crop growth monitoring; however, challenges remain regarding PA because of the rising concern for food security (*Chen et al., 2011; Gebbers & Adamchuk, 2010*). One of the challenges is the “up-scaling” or transfer of quantitative relationships derived from small scales to large scales (*Zarco-Tejada et al., 2001*), from leaf to canopy, field to regional levels. Canopy spectra are not only determined by leaf/plant biochemical and biophysical traits but are also affected by canopy closure, soil/water backgrounds and other factors, as well as their interactions (*van der Meer & de Jong, 2001*). Leaf spectra cannot be directly applied to the canopy level because they have quantitative and qualitative differences (*Hunt et al., 2013; Knipling, 1970*). Therefore, the canopy and leaf spectral properties might be very different even when their constituent leaves have similar spectral properties (*Blackburn, 1998a*). Many factors have been confirmed as affecting the performances of RS methods when up-scaling leaf level relationships to the canopy level (*Zarco-Tejada et al., 2001; 2005*). However, the specific and complete effects that these factors will have either alone or in combination, on the performance are not well understood. The dynamic response of the canopy spectra to crop growth status and the changes in response with crop growth, senescence and phenological features must be qualitatively and quantitatively determined.

Chlorophyll and N are the two biochemical parameters that are of primary interest to both RS and agronomy (*Li et al., 2008; Pinter et al., 2003*); however, the estimation of chlorophyll and N from the canopy level is affected by canopy structures and soil background. Therefore, one of the biggest challenges facing remote sensing is how to decouple spectral contributions of canopy biochemical traits (e.g., chlorophyll and N) from the canopy biophysical traits (e.g., structures, leaf angle and area) (*Jacquemoud et al., 2009*), although a complete decoupling of the contribution of biochemical and structural properties in canopy spectra is difficult and might be impossible in nature. Because hyperspectral canopy sensing of chlorophyll and N are the main goals of this study, this dissertation will attempt to improve the estimation of chlorophyll and nitrogen by weakening the confounding effects of structural properties (mainly biomass variations).

The feasibility of the remote sensing of N is based on a consensus that N is related to chlorophyll (*Perry et al., 2012; Schlemmer et al., 2005*). However, most of the investigations are straightforward and skip the step that links chlorophyll to N when modeling N from spectral measures, which can be explained by the involvement of chlorophyll with the leaf/plant mass and N in a complex organism (Figure I-7), although this retains uncertainties when driving a model to indirectly estimate N from the spectrally modeled chlorophyll. A sufficient amount of N ensures the effective biosynthesis of chlorophyll and thus the photosynthesis efficiency (*Taub & Lerda,*

2000), which can maintain rapid plant growth and carbon assimilation for a high biomass production. However, the rapid increase of plant mass can lead to the dilution of chlorophyll and N per plant mass (Figure I-7). Therefore, the use of spectrally modeled chlorophyll to estimate the N status might be less effective than modeling N directly from the response spectra.

By assuming that the N status can be predicted directly from the leaf and plant optical traits, a large number of studies have demonstrated the strong link between spectral features and leaf and plant N status at both the leaf and canopy levels (*Li et al., 2008; Schlemmer et al., 2013; Smith & Martin, 2001*). These studies show the large potential of remote sensing for crop N management and have promoted the development of crop sensors for field N management. Some researchers have even initiated the application of satellite remote sensing to understand the N cycling of ecosystems (*Ollinger et al., 2008*), which suggests the potential to “watch” the N cycle of earth from the air and space (Figure I-7).

Therefore, we must improve our understanding of the links between canopy optical traits and crop N status and determine the approach that is more applicable for the remote sensing of N status. For this purpose, a synchronous and dynamic comparison must be performed between the correlation of canopy spectra and crop N and the correlation of canopy spectra and chlorophyll. Dynamic monitoring of the relationships is required because the leaf reflectance cannot be related to leaf chlorophyll concentrations when the heterogeneity of the chlorophyll distribution is unknown (*Barton, 2001*). Similarly, a relatively low N concentration might not result in a chlorophyll loss, and the green leaf N content represented only about 30% of shoot N in a wheat crop at the beginning of the grain-filling period (*Gastal & Lemaire, 2002*). Therefore, the remote estimation of N variability cannot be based solely on its relationship with chlorophyll.

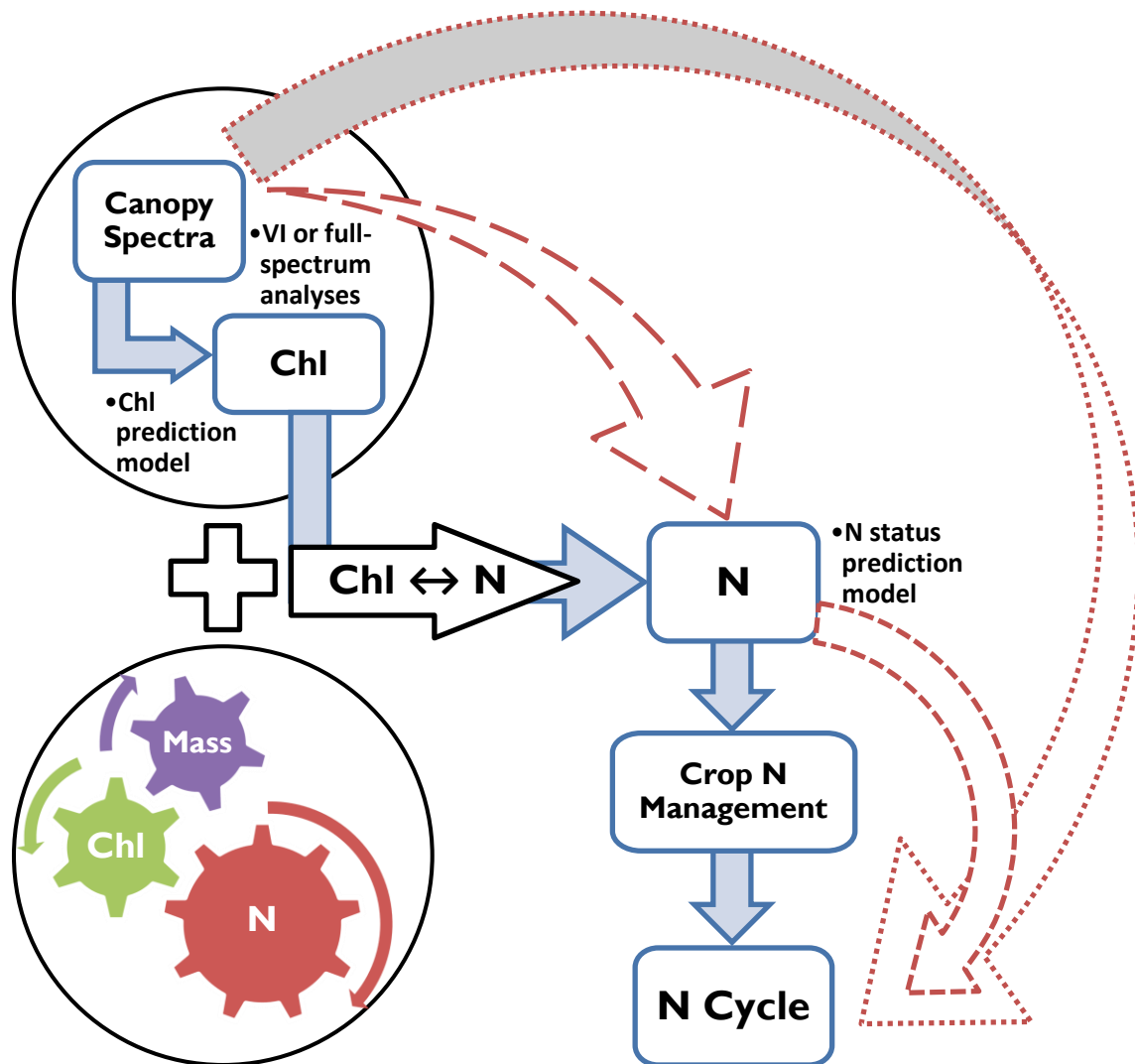


Figure I-7: A schematic diagram shows the indirect remote estimation of nitrogen (N) using spectrally modeled chlorophyll (Chl) and the direct remote estimation of N using canopy spectra.

Precision crop protection is an important subject of PA and becomes increasingly difficult with the enlargement of fields and intensive mechanization (Oerke et al., 2010; Stafford, 2000). Another goal of this study is to detect crop diseases with hyperspectral data. Common sense dictates that diseases will cause chlorophyll functional disturbances; therefore, crop diseases are more likely to affect the canopy spectral signals at chlorophyll absorption bands. However, some studies have found that spectral features in the SWIR range might be more useful for detecting leaf diseases of apple trees (Deldieux et al., 2009). Accordingly, diseases may have specific effects on the spectral traits of water absorption bands compared to the chlorophyll absorption bands. Additionally, the question of whether disease infections will have an earlier effect on crop biomass, chlorophyll and N status than canopy spectra characteristics must be studied. Answers to these questions allow for the selection of disease-sensitive spectral bands and vegetation indices for crop disease early warning.

This thesis is based on five years of canopy-level hyperspectral data collected in field experiments and attempts to extend to answer the above questions by extending our understanding of the remote sensing of agricultural crops through the integration of empirical and physical methods. Briefly, the main objectives of this thesis are to improve the hyperspectral canopy mapping of crop biochemical parameter (mainly chlorophyll and N) and detect crop diseases. More specifically, it aims to:

- Develop and validate hyperspectral remote sensing methods for the estimation of crop chlorophyll and N status;
- Investigate the influence of growth stages and phenological development on the relationships between canopy spectra features and crop biological traits;
- Develop vegetation indices that can help decouple the contributions of crop biochemical and structural properties to canopy spectra and improve the canopy sensing of biochemical parameters; and
- Identify the spectral features and vegetation indices that are sensitive to diseases and develop methods for disease detection.

1.5 Thesis outline

This thesis comprises of seven chapters that begin with a general introduction in Chapter I*, followed by four main chapters (Chapters 2-5) that act as standalone articles that have been published or submitted for publication in peer-reviewed journals. These articles address the specific objectives related to this thesis and are based on rice (Chapters 2 and 3) and barley (Chapters 4 and 5) experiments. Chapter 6 presents some additional data to evaluate and validate the results of the early phase of the whole work. Finally, Chapter 7 provides a general discussion on the results, summarizes the main findings, and defines the limitations of this study as well as the prospects for future study. Chapters 2-7 are briefly summarized in the following sections:

Chapter 2 explores the influence of growth stages on the relationships between the vegetation indices and canopy N status. Because canopy closure (usually at the heading stage) results in a reverse trend of correlations, the narrow 2-band SRs, NDVIs as well the multi-band models were optimized before and after canopy closure. This approach proved to be able to improve the estimation of canopy N status of rice.

Chapter 3 attempts to design a conceptual model/index called the Ratio of Reflectance Difference Index that can reduce the influence of growth stage, canopy structural variations and soil backgrounds to improve the estimation of canopy biochemical parameters (mainly

* Bibliography of Chapter I is included in the General references (page 181).

chlorophyll). This conceptual index showed improved robustness in relating to the chlorophyll content and it was compared with the partial least squares (PLS) model for estimation of the chlorophyll variation in farmer fields, with the results showing that they have comparable performances.

Chapter 4 focuses on the chlorophyll estimation and detection of barley leaf diseases using hyperspectral and fluorescence indices. Canopy hyperspectral data were able to detect disease symptoms that precede significant losses of chlorophyll that result from disease. Multivariate models such as PLS and support vector machines (SVM) were also compared, with the results showing that PLS and SVM improved the estimation of chlorophyll concentration compared to hyperspectral and fluorescence indices.

Chapter 5 combines the empirical and physical methods and includes a large number of the vegetation indices and multivariate models used in previous chapters. Using hyperspectral data collected in the field and simulated by radiative transfer models (RTMs), the potential of the conceptual model/index RRDl was further explored by linking it to the multiple scatter correction theory (MSC). This conceptual model produced a comparable performance to the multivariate models.

Chapter 6 presents additional results from the barley crop experiments to validate the preliminary conclusions made in the previous chapters and verify our hypothesis that hyperspectral vegetation indices based on water absorption bands might be useful for detecting barley diseases. The results corroborated previous results observed in rice crops and demonstrated the usefulness of water absorption bands for disease detection.

Chapter 7 provides a general discussion of the objectives and results of this thesis, and focuses primarily on (1) the importance of growth stages in remote sensing crop chlorophyll and N status, (2) potential of decoupling canopy spectral co-variations that result from leaf/plant biochemical and biophysical characteristics, (3) uses of vegetation indices at different growth stages with different degrees of canopy closure, and (4) uncertainties in disease detection. Finally, the main conclusions and outlook are presented.

CHAPTER 2**Remotely detecting canopy nitrogen concentration and uptake of paddy rice in the Northeast China Plain^{*}**

^{*} *This chapter is based on:*

Yu, K., Li, F., Gnyp, M.L., Miao, Y., Bareth, G., Chen, X. 2013. Remotely detecting canopy nitrogen concentration and uptake of paddy rice in the Northeast China Plain. *ISPRS J. Photogramm. Remote Sens.* **78**: 102-115.

Abstract

The influence of morphophysiological variation at different growth stages on the performance of vegetation indices for estimating plant N status has been confirmed. However, the underlying mechanisms explaining how this variation impacts hyperspectral measures and canopy N status are poorly understood. In this study, four field experiments involving different N rates were conducted to optimize the selection of sensitive bands and evaluate their performance for modeling canopy N status of rice at various growth stages in 2007 and 2008. The results indicate that growth stages negatively affect hyperspectral indices in different ways in modeling leaf N concentration (LNC), plant N concentration (PNC) and plant N uptake (PNU). Published hyperspectral indices showed serious limitations in estimating LNC, PNC and PNU. The newly proposed best 2-band indices significantly improved the accuracy for modeling PNU ($R^2 = 0.75-0.85$) by using the lambda by lambda band-optimized algorithm. However, the newly proposed 2-band indices still have limitations in modeling LNC and PNC because the use of only 2-band indices is not fully adequate to provide the maximum N-related information. The optimum multiple narrow band reflectance (OMNBR) models significantly increase the accuracy for estimating the LNC ($R^2 = 0.67-0.71$) and PNC ($R^2 = 0.57-0.78$) with six bands. Results suggest the combinations of center of red-edge (735 nm) with longer red-edge bands (730-760 nm) are very efficient for estimating PNC after heading, whereas the combinations of blue with green bands are more efficient for modeling PNC across all stages. The center of red-edge (730-735 nm) paired with early NIR bands (775-808 nm) are predominant in estimating PNU before heading, whereas the longer red-edge (750 nm) paired with the center of "NIR shoulder" (840-850 nm) are dominant in estimating PNU after heading and across all stages. The OMNBR models have the advantage of modeling canopy N status for the entire growth period. However, the best 2-band indices are much easier to use. Alternatively, it is also possible to use the best 2-band indices to monitor PNU before heading and PNC after heading. This study systematically explains the influences of N dilution effect on hyperspectral band combinations in relating to the different N variables and further recommends the best band combinations which may provide an insight for developing new hyperspectral vegetation indices.

Keywords: Hyperspectral index; Nitrogen status; Rice; Heading stage; N dilution effect; Stepwise multiple linear regression; Lambda by lambda band-optimized algorithm

2.1 Introduction

Rice production in the Northeast China Plain, a high-latitude northern environment, plays an important role in ensuring food security in step with Chinese population growth. However, an effective method or tool is absent for in-season nitrogen (N) fertilizer management of the paddy rice in the northeast plain of China, and most farmers over apply N fertilizer depending on their own experiences (Miao *et al.*, 2011). The traditional soil-based testing methods widely used for upland crops are not suitable for N recommendations in paddy rice fields due to the flooding and complexity of N cycling in the rice paddy soil during the rice growing period (Dobermann *et al.*, 2003). Even before flooding, the available soil-N test is not accurate enough to lead to confident recommendations for N fertilizer applications (Russell *et al.*, 2006). Particularly in large scale field management in the Northeast China Plain, soil and plant based point measurements are difficult to meet the need of real-time N fertilizer management (Dobermann *et al.*, 2003; Yang *et al.*, 2003). Remotely based canopy reflectance estimation of rice N status may provide an opportunity for greater precision of N management and for reducing N loading into underground water on the large scale farms of the Northeast China Plain.

The development of precision agriculture and remote sensing techniques has enabled us to estimate crop N status in a field or even on a regional scale. In recent decades, a chlorophyll meter has been widely used to estimate crop N status to promote N management of rice (Huang *et al.*, 2008; Peng *et al.*, 1995). However, the chlorophyll meter method is time consuming for a regional measurement and may lose sensitivity at a high chlorophyll level (Ciganda *et al.*, 2009; Steele *et al.*, 2008). As a better alternative, spectral reflectance measurements have been proposed to detect crop N stress and to quantify N amounts (Hansen & Schjoerring, 2003; Read *et al.*, 2002; Reyniers *et al.*, 2006; Yoder & Pettigrew-Crosby, 1995). Read *et al.* (2002) found that leaf chlorophyll and N concentration are more closely associated with canopy-level reflectance (obtained from full canopies) than leaf-level reflectance (obtained from individual leaves), which differed with each other in the spectral band combinations with maximum sensitivity to plant N status. The inconsistencies indicate that the distribution of chlorophyll and N within individual leaves may be heterogeneous (Barton, 2001; Ciganda *et al.*, 2009). Thus, an important uncertainty remains when N or chlorophyll status of individual leaves are used to represent that of a canopy (Ciganda *et al.*, 2009). Since N status of individual leaves may not adequately represent the nutrient condition of whole plants, it is not accurate enough to evaluate canopy N status and guide the N fertilization of crops.

Canopy N status is more important to indicate growth conditions of a crop than leaf N status which mainly involves the information of individual leaves. Plant N concentration (PNC) has

been commonly used as an effective indicator of crop canopy N status, and different threshold values have been established for different crops (Fageria, 2009). Canopy-level reflectance measurements have been used for estimating the PNC as reported in recent studies (Lee et al., 2008; Li et al., 2010; Stroppiana et al., 2009). Stroppiana et al. (2009) proposed an optimal normalized difference index that is highly correlated to the PNC of rice ($R^2 = 0.65$), and they also evaluated the published indices which only explained 33% of the variance by the best performing one. Li et al. (2010) evaluated the performance of 77 published indices and found that only 35% of the variance in PNC of winter wheat was explained by the best performing published vegetation index across site-years and growth stages, whereas 59% of the variation was explained by their newly proposed index. These results reveal that the best performing indices and optimum band combinations in deriving canopy N status vary for different crops and growth stages. Plant N uptake (PNU) indicates N accumulation of plant per unit area and is an important indicator for assessing canopy N status. However, probably due to the difficulty in collecting plant samples of rice, most reports on rice mainly focused on the leaf N uptake and limited studies have been undertaken to estimate rice PNU (Xue et al., 2004).

To date, most of the recent studies for estimating N of rice were conducted to determine leaf N status (Nguyen & Lee, 2006; Xue et al., 2004; Yi et al., 2007; Zhu et al., 2007; 2008), whereas a limited number of studies have been carried out to determine plant N status (Stroppiana et al., 2009). Furthermore, reported results have been inconsistent. For example, an NDVI (1220, 710 nm), which was reported by Zhu et al. (2007), was most highly correlated with rice leaf N concentration (LNC) of individual leaves ($R^2 = 0.79$) across all growth stages. Only 44% of the individual leaf LNC variation was explained across all stages tested by Tian et al. (2011), and this NDVI was very poorly related to PNC ($R^2 = 0.10$), before the heading stage, as reported by Stroppiana et al. (2009). It was noted that LNC was closely related to vegetation indices at each single stage rather than across all growth stages (Xue et al., 2004). Thus, inference can be made that these inconsistencies were due to not only the growth stages but also the limitation of band counts used for these indices, because all of the above mentioned indices are 2-band indices that often constrain the regression analysis (Thenkabail et al., 2000). However, the underlying mechanism to explain the influence of growth stages on remotely estimating canopy N status of rice and the difference between LNC- and PNC-determination has not been systematically addressed and reported in the literature. Therefore, the objective of the present study is to find out how growth stages dynamically influence the performance of hyperspectral indices and the combinations of sensitive narrow bands. We also attempt to identify the best 2-band vegetation indices and construct multi-band models to derive canopy N concentration and uptake at specific growth periods.

CHAPTER 2**2.2 Materials and methods****2.2.1 Experimental sites**

The field experiments were carried out in 2007 and 2008 in the area of Jiansanjiang Branch Bureau (JBB, 46°49'42"-48°13'58" N, 132°31'26"-134°22'26" E, the map shown in Figure 2-1), Heilongjiang Bureau of Agricultural Reclamation (HBAR), Heilongjiang province, northeast China. The climate in the Sanjiang Plain is cool-temperate sub-humid continental monsoon, with very cold winters and warm summers. The annual average temperature, precipitation, and solar amounts are 1-2 °C, 500-600 mm and 2300-2600 hours, respectively. The climatic characteristics are suitable for many field crops (e.g. rice, soybeans, wheat and corn) which have only one harvest per year. As the most widely planted crop in this area, rice is irrigated using groundwater during the entire growing season. The soil characteristics of different experimental sites (Qixing and Keyansuo experiment stations of JBB, Figure 2-1) across two growing seasons/years are summarized in Table 2-1.

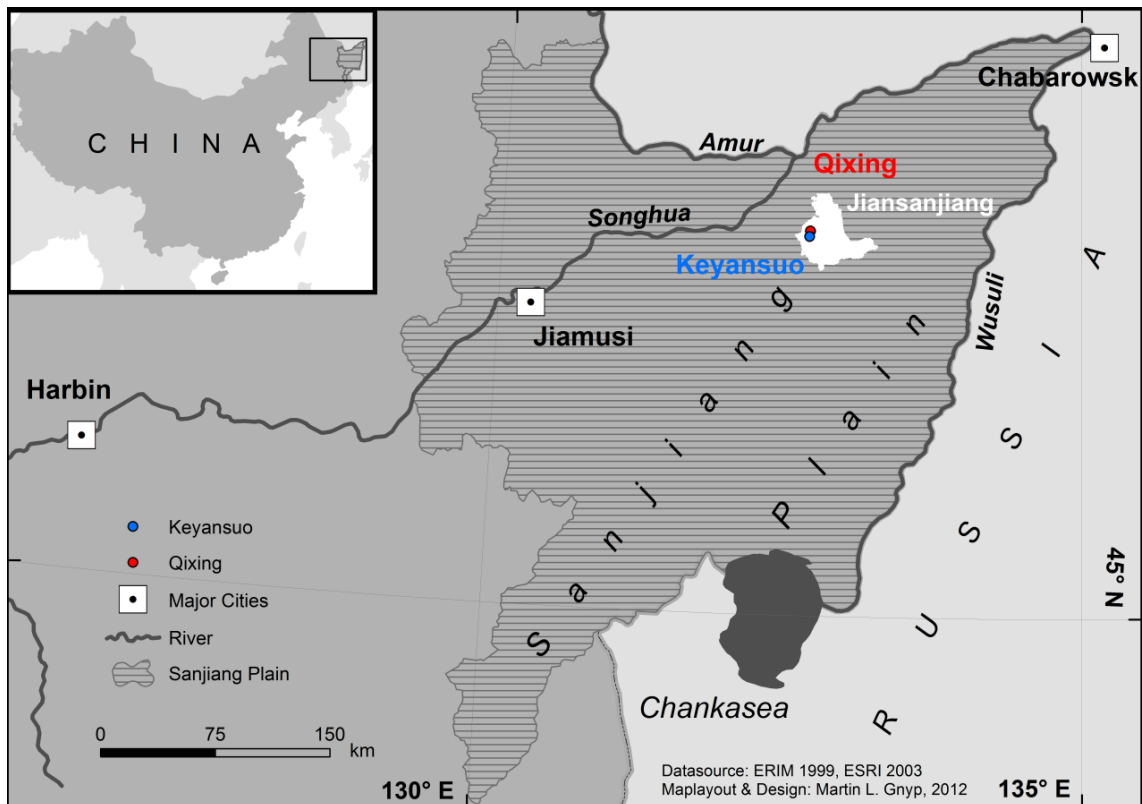


Figure 2-1: Location of the experimental sites Qixing and Keyansuo, Jiansanjiang Branch Bureau, Heilongjiang Bureau of Agricultural Reclamation, Heilongjiang province, China.

Table 2-1: Soil chemical properties (0-30 cm soil layer) of two experimental stations, 2007-2008.

Exp.	Site	Year	Organic matter	Available N	Olsen-P	NH ₄ OAC-K
			g kg ⁻¹	mg kg ⁻¹	mg kg ⁻¹	mg kg ⁻¹
1	Qixing	2007	35.6	97	25	147
2	Keyansuo	2007	31.5	130	32	89
3	Qixing	2008	32.9	175	37	121
4	Keyansuo	2008	35.1	157	30	133

2.2.2 Experimental design

2.2.2.1 Experiments 1 and 2

Experiments 1 and 2 were performed from March to October in 2007 at Qixing and Keyansuo experiment stations respectively with the same experimental design. The rice cultivar Kongyu131, the major cultivar grown in the area of JBB, was used in this study. Three-leaf-old rice seedlings were transplanted in mid May with the transplanting density of 0.12 by 0.30 m with 4-5 plants per hill. Seven N rates (0, 60, 75, 90, 105, 120, and 150 kg N ha⁻¹) of urea were applied, and then the total N rate was distributed in three time splits: 40% was applied before transplanting, 30% in the period of seedling establishment, and 30% at the booting stage. In addition, 60 kg ha⁻¹ P₂O₅ as triple super-phosphate and 75 kg ha⁻¹ K₂O as potassium sulfate were applied mixed with the first-split N application for all the treatment plots. The plots of experiments 1 and 2 were all arranged in a randomized complete block design with four replications. The individual plot size was 5 by 8 m. Field management, such as irrigation, weeding and pesticide applications, followed the local standard practices of JBB rice production.

2.2.2.2 Experiments 3 and 4

Experiments 3 and 4 were conducted at Qixing and Keyansuo experiment stations in 2008 but in different locations than experiments 1 and 2. With the same transplanting strategy, same rice cultivar (Kongyu131) and the analogous experimental design the experiments were carried out from March to October of 2008. Five N rates (0, 35, 70, 105 and 140 kg N ha⁻¹) of urea were applied, and the total N rate was distributed to three time splits: 45% was applied before transplanting, 20% at the period of seedling establishment and 35% at the booting stage. For all the plots, 60 kg ha⁻¹ P₂O₅ of triple super-phosphate and 45 kg ha⁻¹ K₂O of potassium sulfate were applied mixed with the first-split N application. An additional 30 kg K₂O ha⁻¹ was applied at the booting stage. The experiment plots were all arranged in a randomized complete block design with four replications. Each plot size was 10 by 10 m. Other management practices were carried out according to the local standard practices of JBB rice production.

CHAPTER 2**2.2.3 Hyperspectral reflectance measurement**

From a distance of 30 cm above the rice canopy, hyperspectral reflectance was measured between 10:00 and 14:00 local time under clear and cloudless conditions, with the ASD QualitySpec® Pro spectroradiometer (Analytical Spectral Devices Inc., Boulder, CO, USA) for experiments 1 and 2 in 2007 and the ASD FieldSpec® 3 spectroradiometer (Analytical Spectral Devices Inc., Boulder, CO, USA) for experiments 3 and 4 in 2008, respectively. The ASD QualitySpec® Pro spectroradiometer was configured with Visible and NIR spectral range (350 - 1800 nm) and 1.4 nm sampling interval between 350 and 1050 nm, 2 nm sampling interval between 1000 and 1800 nm. The QualitySpec® Pro was operated with 3 nm and 10 nm spectral resolution at 700 nm and 1400 nm respectively. Slightly different, the ASD FieldSpec® 3 spectroradiometer was configured with the spectral range from 350nm to 2500 nm, 1.4 nm sampling interval between 350 and 1050, 2 nm sampling interval between 1000 and 2500 nm, and with 3 nm spectral resolution at 700 nm, 10 nm spectral resolution at 1400 and 2100 nm. Hyperspectral data were subdivided into 1 nm band width by using a self-driven interpolation method of the ASD spectroradiometers and then saved to the connecting PC. The field of view of the both ASD spectroradiometers used in this study is 25 degrees. The diameter for each measurement was approximately 14 cm, which covers an area of canopy for each spectrum of approximately 150 cm² from a measuring distance of 30 cm. Prior to the rice canopy reflectance measurement, calibration measurements included a dark current and reflectance of a white spectralon reference panel. The reflectance measurements were executed consecutively for five random locations per plot and then averaged for the mean of the five repetitions. Table 2-2 shows the acquisition dates of spectral measurements and plant sampling according to the BBCH codes (*Lancashire et al., 1991*).

Table 2-2: Determination dates of both canopy reflectance and rice sampling.

Exp.	Transplanting	Days after transplanting (BBCH code)					
1	May 15 (13)			47 (43)	55 (52)	77 (61)	
2	May 24 (13)	24 (25)	32 (30)	47 (41)	54 (52)		
3	May 21 (13)		37 (32)	47 (41)	63 (54)	74 (61)	88 (75)
4	May 29 (13)		32 (30)	40 (39)	56 (52)	67 (59)	79 (73)
	Principal growth stage	Tillering	Stem elongation	Booting	Heading	Flowering	Filling

2.2.4 Plant sampling and measurements

Immediately after canopy reflectance measurements, above ground biomass of rice was sampled at random locations where plants were scanned with an approximate area of 0.18 m² (5 hills×0.12 m×0.30 m/ hill) per plot. The rice plant samples of experiments 1 and 2 were separated

into leaves and stems. For experiments 3 and 4, samples were left as whole plants because the use of plant N concentration is more precise for the N fertilizer recommendation (Flowers et al., 2003). All of the samples were cleaned, oven-dried for 30 minutes at 105 °C and later at 70°C to a constant weight, then weighted, ground, and their Kjeldahl-N determined. Subsequently, the plant N uptake (kg ha^{-1}) was determined by multiplying plant N concentration and dry biomass weight.

2.2.5 Vegetation indices and data analysis

2.2.5.1 Published hyperspectral vegetation indices

Recently, many vegetation indices (VIs) have been developed to evaluate the N status of crops based on leaf and canopy level reflectance. Reviewing recent reports involving different VIs, and considering the characteristics of different VIs and rice canopy reflectance in the present study, we selected three types of published vegetation indices with the best performance, including the ratio vegetation index, the normalized difference vegetation index and the combined vegetation index, to estimate the canopy N status of rice as listed in Table 2-3. The band selection for each index was deliberately implemented by involving different spectral range for blue, red, green, red edge and NIR.

Table 2-3: Published vegetation indices used in this study.

Index	Equation	Reference
Simple ratio (SR)		
SR1	R_{800}/R_{675}	Jordan (1969)
SR2	R_{810}/R_{560}	Xue et al. (2004)
SR3	R_{750}/R_{710}	Zarco-Tejada et al. (2001)
SR4	R_{750}/R_{700}	Gitelson & Merzlyak (1996)
Normalized difference index		
NDVI	$(R_{800}-R_{680})/(R_{800}+R_{680})$	Blackburn (1998)
GNDVI	$(R_{801}-R_{550})/(R_{801}+R_{550})$	Daughtry et al. (2000)
ND705	$(R_{750}-R_{705})/(R_{750}+R_{705})$	Sims & Gamon (2002)
mSR705	$(R_{750}-R_{445})/(R_{705}-R_{445})$	Sims & Gamon (2002)
MTCI	$(R_{750}-R_{710})/(R_{710}-R_{680})$	Dash & Curran (2004)
NDVI[503,483]	$(R_{503}-R_{483})/(R_{503}+R_{483})$	Stroppiana et al. (2009)
NDVI[565,533]	$(R_{565}-R_{533})/(R_{565}+R_{533})$	Tian et al. (2011)
NDVI[1220,710]	$(R_{1220}-R_{710})/(R_{1220}+R_{710})$	Zhu et al. (2007)
Combined index		
OSAVI	$(1+0.16)(R_{800}-R_{670})/(R_{800}+R_{670}+0.16)$	Rondeaux et al. (1996)
MCARI	$[(R_{700}-R_{670})-0.2*(R_{700}-R_{550})]/(R_{700}/R_{670})$	Daughtry et al. (2000)
MCARI[705,750]	$[(R_{750}-R_{705})-0.2*(R_{750}-R_{550})]/(R_{750}/R_{705})$	Wu et al. (2008)
TCARI	$3*[(R_{700}-R_{670})-0.2*(R_{700}-R_{550})](R_{700}/R_{670})$	Haboudane et al. (2002)
TCARI/OSAVI	TCARI/OSAVI	Haboudane et al. (2002)
TCARI/OSAVI[705,750]	TCARI/OSAVI[705, 750]	Wu et al. (2008)

2.2.5.2 Computing 2-band indices using the lambda by lambda band-optimized algorithm

In order to further check the influences of band combinations and growth stages on the performance of vegetation indices in deriving canopy N status, two classes of indices were calculated involving all possible 2-band combinations from 400 to 1200 nm: simple ratio index ($SR = R_1/R_2$) and normalized difference index ($NDI = (R_1 - R_2)/(R_1 + R_2)$). The computation, “lambda by lambda R² contour” mapping and statistical analyses were done with the MATLAB 7.0 software (The MathWorks, Inc., Natick, MA).

2.2.5.3 Optimum multiple narrow band reflectance (OMNBR) models

It is known that 2-band indices often constrain the regression analysis and that multiple hyperspectral narrow bands can provide additional information (*Thenkabail et al., 2000*). Thus, the OMNBR models (*Thenkabail et al., 2000*) were identified using a multiple stepwise linear regression method called the maximum R² improvement (MAXR) method in SAS (SAS Institute Inc.). The MAXR method tries to find the “best” 1-band model, the “best” 2-band model, and so forth, producing the highest R² in relation to dependent variables (N variables in this study). The MAXR procedure begins by finding the 1-band model that produces the highest R². Then another band, the one that yields the greatest increase in R², is added. Once the 2-band model is obtained, each of the bands in the model is compared to each band not in the model. The MAXR process continues comparing all possible switches until no switch can increase the R² and considers the switch that produces the highest R² as the “best” 2-band model. Another band is then added to the model, and the comparing-and-switching process is repeated to find the “best” 3-band model, and so forth (*SAS Institute Inc., 2008*). The band count to be used for the “best” n-band model was discreetly determined to avoid “over-fitting” and is discussed in the results section.

2.3 Results

2.3.1 Variation in LNC, PNC and PNU and biomass

The LNC in the experimental fields ranged between 1.72% and 3.84% with a CV value of 16.7% during tillering to heading stage while it varied from 0.80 to 3.12% with a CV value of 28.4% during the heading to filling stage (Table 2-4). Similar to LNC, the variation of PNC after heading was greater than that before heading, indicating that canopy N concentration is easy to be remotely derived during heading to filling stage. The LNC and PNC decreased with advance of growth stages due to the dilution effect as mentioned by *Lemaire et al. (2008)*. The dilution effect for PNC was more obvious and yielded higher variation across all stages compared to LNC.

Table 2-4: Descriptive statistics of nitrogen status and biomass in different growing stages rice under different N levels.

Growth stages and years	n	Min	Max	Mean	SD	CV (%)
Leaf N concentration in 2007 (%)						
Tillering to heading (BBCH 13-60)	153	1.72	3.84	2.76	0.46	16.7
Heading to filling (BBCH 51-80)	144	0.80	3.12	2.02	0.57	28.4
All pooled data	297	0.80	3.84	2.38	0.68	28.5
Leaf dry weight in 2007 (t ha ⁻¹)						
Tillering to heading (BBCH 13-60)	153	0.09	1.89	0.79	0.45	56.6
Heading to filling (BBCH 51-80)	144	0.57	2.16	1.21	0.29	24.0
All pooled data	297	0.09	2.16	0.96	0.44	46.3
Plant N concentration in 2008 (%)						
Tillering to heading (BBCH 13-60)	120	1.16	3.35	2.24	0.46	20.4
Heading to filling (BBCH 51-80)	120	0.75	2.18	1.43	0.36	25.3
All pooled data	240	0.75	3.35	1.85	0.62	33.3
Plant dry weight in 2008 (t ha ⁻¹)						
Tillering to heading (BBCH 13-60)	120	0.14	9.92	2.90	2.37	81.7
Heading to filling (BBCH 51-80)	120	2.85	18.3	9.60	3.72	38.7
All pooled data	240	0.14	18.3	6.32	4.97	78.6
Plant N uptake in 2007 and 2008 (kg N ha ⁻¹)						
Tillering to heading (BBCH 13-60)	273	3.1	205.6	45.4	33.9	74.7
Heading to filling (BBCH 51-80)	264	18.6	303.0	96.2	49.7	51.6
All pooled data	537	3.1	303.0	69.2	51.3	74.1
Plant dry weight in 2007 and 2008 (t ha ⁻¹)						
Tillering to heading (BBCH 13-60)	273	0.09	9.92	1.72	1.91	111.3
Heading to filling (BBCH 51-80)	264	0.57	18.30	4.98	4.87	97.8
All pooled data	537	0.09	18.30	3.33	4.25	127.8

SD, standard deviation;
CV, coefficient of variation.

Across growth stages, sites, and years, PNU in the experimental fields ranged from 3.1 to 205.6 kg N ha⁻¹ with a mean of 45.4 kg N ha⁻¹ during tillering to heading stage. During heading to filling, PNU varied from 18.6 to 303.0 kg N ha⁻¹ with a mean value of 96.2 kg N ha⁻¹ and CV of 51.6% (Table 2-4). The plant dry weight ranged from 0.09 to 9.92 t ha⁻¹ with a CV of 111.3% during tillering to heading, and 0.57 to 18.30 t ha⁻¹ with a CV of 97.8% during heading to filling. Both PNU and plant dry weight yielded larger variation before heading compared to that after heading. This is also in agreement with the changing patterns of the tiller count (Figure 2-2). Overall, PNU and plant dry weight yielded very high variation across all growth stages, sites and years with CVs of 74.1% and 127.8 % respectively.

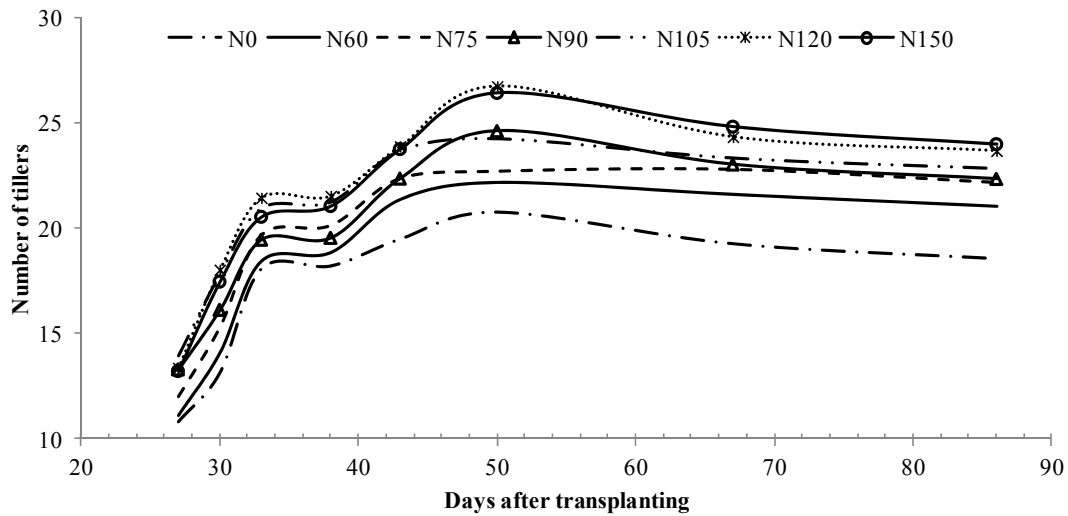


Figure 2-2: Seasonal changes in the number of tillers of rice at seven nitrogen levels for Experiment I in 2007. N0, N60, N75, N90, N105, N120 and N150 represent the seven nitrogen rates of 0, 60, 75, 90, 105, 120 and 150 kg N ha⁻¹ respectively.

2.3.2 Relationships between published VIs and rice N status

In order to understand how growth stages influence hyperspectral vegetation indices in relation to canopy N status, we reviewed many published hyperspectral indices. We plotted the indices versus the three N variables in scatter plots to examine the relationships within all of the data sets. The three best performing and representative vegetation indices that correlated for the three N variables are shown in Figure 2-3. It is shown that LNC and PNC were better related to published indices SRI and MTCI, respectively, after heading. In contrast, PNU was better correlated with the published index MTCI before heading, whereas PNU was poorly correlated after heading (Figure 2-3). In comparison, the published indices yielded lower R^2 across all stages. Table 2-5 shows the correlation analyses for all the published indices relating to the three N variables in the three stage-divisions (before and after heading and across all stages, totally nine cases). The best published indices explained 50% and 75% of the variation in LNC and PNC after the heading stage, respectively, whereas only 35% and 30% of the variation was explained before heading. In contrast, 84% of the variation in PNU before heading and 27% of the variation after heading could be explained by the best published indices. Across all stages, R^2 generally decreased for all published indices relating to LNC, PNC and PNU (Table 2-5). Results also showed that the R^2 for the published indices relating to PNU were generally higher than those were related to LNC and PNC.

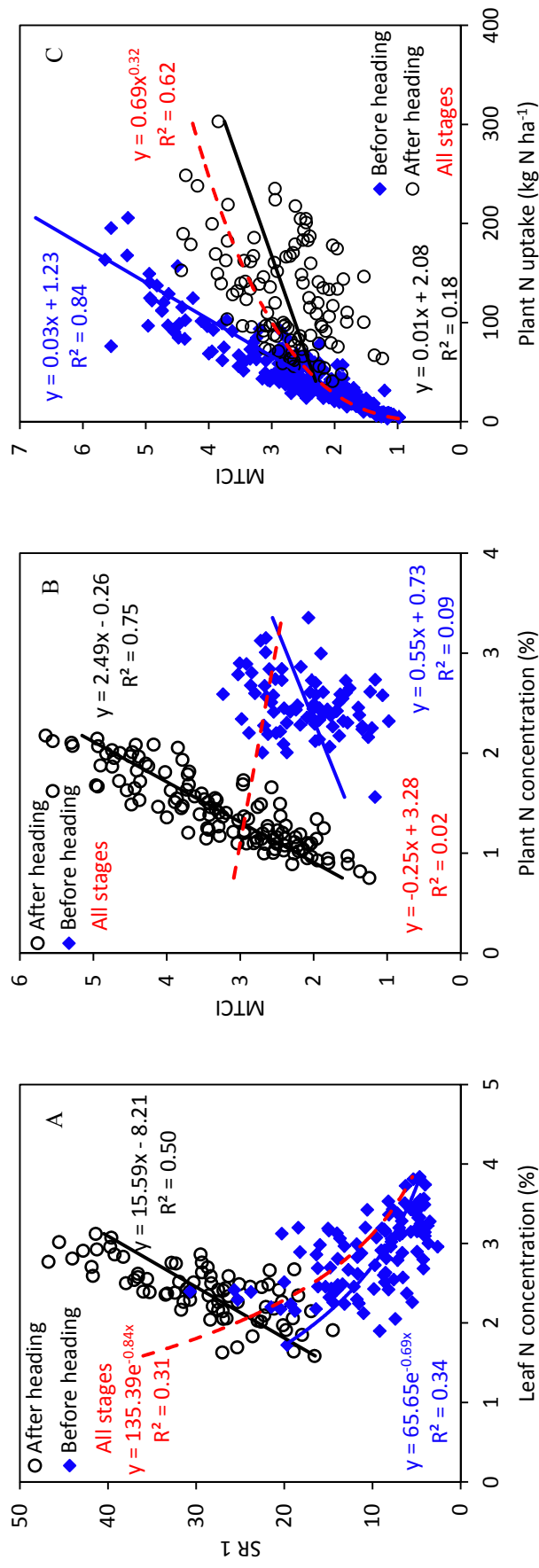


Figure 2-3: Relationships between the best performing published vegetation indices and LNC (A), PNC (B) and PNU (C). Regression lines in blue, black and red colors show the best fit linear or nonlinear relationships for before, after heading and all stages, respectively.

CHAPTER 2**Table 2-5: Squared correlation Coefficients (R^2) for vegetation indices in Table 2-3 in relation to leaf N concentration, plant N concentration and plant N uptake.**

Vegetation index	Leaf N concentration			Plant N concentration			Plant N uptake		
	Tillering to heading	Heading to filling	All stages	Tillering to heading	Heading to filling	All stages	Tillering to heading	Heading to filling	All stages
Simple ratio									
SR1	0.18*	0.50**	0.17*	0.30**	0.62**	0.07*	0.56**	0.01	0.26**
SR2	0.23**	0.21**	0.26**	0.27**	0.68**	0.10*	0.81**	0.16*	0.53**
SR3	0.26**	0.30**	0.25**	0.25**	0.74**	0.03	0.81**	0.05	0.39**
SR4	0.25**	0.38**	0.23**	0.26**	0.73**	0.02	0.78**	0.01	0.32**
Normalized difference index									
NDVI	0.35**	0.43**	0.36**	0.17**	0.48**	0.13*	0.44**	0.02	0.28**
GNDVI	0.29**	0.20**	0.32**	0.22**	0.62**	0.18*	0.66**	0.16*	0.50**
ND705	0.30**	0.36**	0.30**	0.21**	0.68**	0.05**	0.66**	0.01	0.35**
mSR705	0.24**	0.25**	0.20**	0.24**	0.75**	ns	0.83**	0.03	0.29**
MTCI	0.21**	0.20**	0.20**	0.24**	0.75**	0.02	0.84**	0.09*	0.40**
NDVI[503,483]	0.34**	ns	0.37**	0.17**	0.61**	0.65**	0.05	0.04	0.20**
NDVI[565,533]	0.09*	0.12*	0.23**	0.06	0.61**	0.39**	0.07*	0.11*	0.24**
NDVI[1220,710]	0.31**	0.13*	0.26**	0.17*	0.70**	0.05	0.56**	0.02	0.31**
Combined index									
OSAVI	0.34**	0.20**	0.32**	0.22**	0.49**	0.25**	0.45**	0.01	0.34**
MCARI	0.20**	0.09*	0.17*	0.13*	0.41**	0.50**	0.02	0.27**	0.02
MCARI[705,750]	0.23**	0.21**	0.18*	0.27**	0.69**	0.07*	0.65**	ns	0.30**
TCARI	0.26**	ns	0.15*	0.03	0.48**	0.32**	ns	0.26**	ns
TCARI/OSAVI	0.05	ns	ns	0.12*	0.58**	0.02	0.26**	0.25**	0.20**
TCARI/OSAVI[705,750]	0.14*	0.29**	0.15*	0.26**	0.72**	ns	0.81**	0.04	0.32**

Analyses were performed using Pearson correlation. Symbols * and ** stand for significant at 0.05 and 0.01 levels, respectively; ns, no significance.

Overall, all the published spectral indices failed in explaining the variation in LNC in all three stage-divisions ($R^2 \leq 0.50$) and were very poorly correlated to PNC before heading ($R^2 \leq 0.30$). The spectral indices also had poor relationships with PNU after heading ($R^2 \leq 0.27$) and across all stages ($R^2 \leq 0.53$). Spectral indices provided good accuracy only in two cases that correlated closely with PNC after heading ($R^2 \geq 0.70$) and PNU before heading ($R^2 \geq 0.8$).

2.3.3 Identifying new 2-band vegetation indices using the lambda by lambda band-optimized algorithm

Since published VIs correlated well with LNC and PNC after heading, and were better associated with PNU before heading, it was decided to test the effects of growth stages on the performance of vegetation indices and optimum band combinations related to canopy N. We examined all the possible 2-band combinations from 400 to 1200 nm in the SR and NDI formulae and correlated them with LNC, PNC and PNU in the three stage-divisions. It is obvious that either linear or nonlinear relationships exist between VIs and the N status (Figure 2-3). Thus, both linear and nonlinear models were implemented for the lambda by lambda band-optimized algorithm. The lambda by lambda R^2 contour plots for nonlinear models are demonstrated in Figure 2-4 and Figure 2-5 by the total nine cases. The lambda by lambda R^2 contour plots for linear models are not presented because they showed almost the same patterns as the nonlinear models. Figure 2-4 and Figure 2-5 show that 2-band combinations for SR and NDI type indices both varied in three stage-divisions and for three N variables.

Similar to published vegetation indices, the best 2-band SRs and NDIs derived from lambda by lambda R^2 contour plots produced lower R^2 related to LNC. R^2 for SRs and NDIs relating to PNC and LNC after heading was higher than before heading (Figure 2-4 and Figure 2-5).

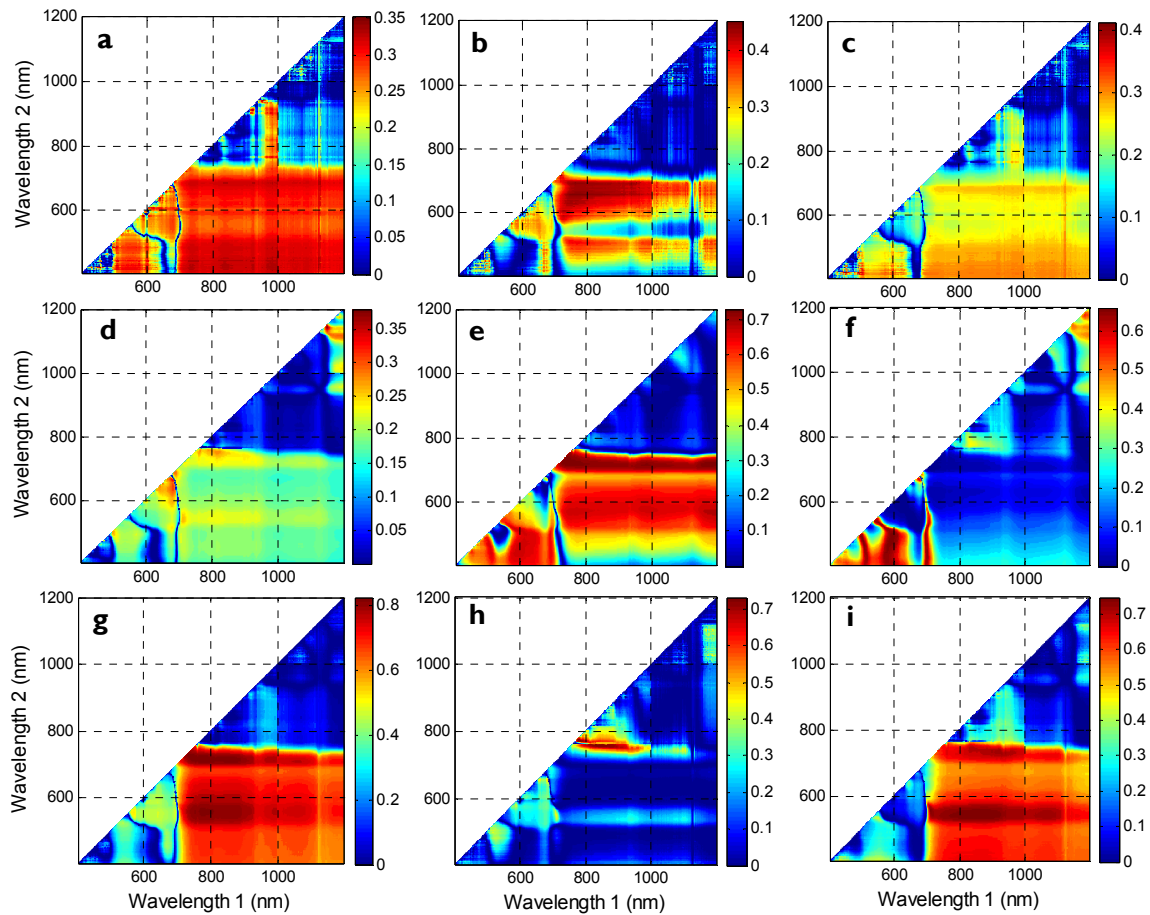
CHAPTER 2

Figure 2-4: Lambda by lambda R^2 Contour plots showing the coefficient of determination (R^2) for the exponential relationships between canopy N status and narrow band NDI calculated from all possible 2-band combinations in the range of 400-1200 nm for nine cases. The letters of a, b, c, d, e, f, g, h and i stand for each different case of: (a) Leaf N concentration before heading in 2007, (b) Leaf N concentration after heading in 2007, (c) All data for leaf N concentration in 2007, (d) Plant N concentration before heading in 2008, (e) Plant N concentration after heading in 2008, (f) All data for plant N concentration in 2008, (g) Plant N uptake before heading in 2007 and 2008, (h) Plant N uptake after heading in 2007 and 2008, (i) All data for plant N uptake in 2007 and 2008, respectively.

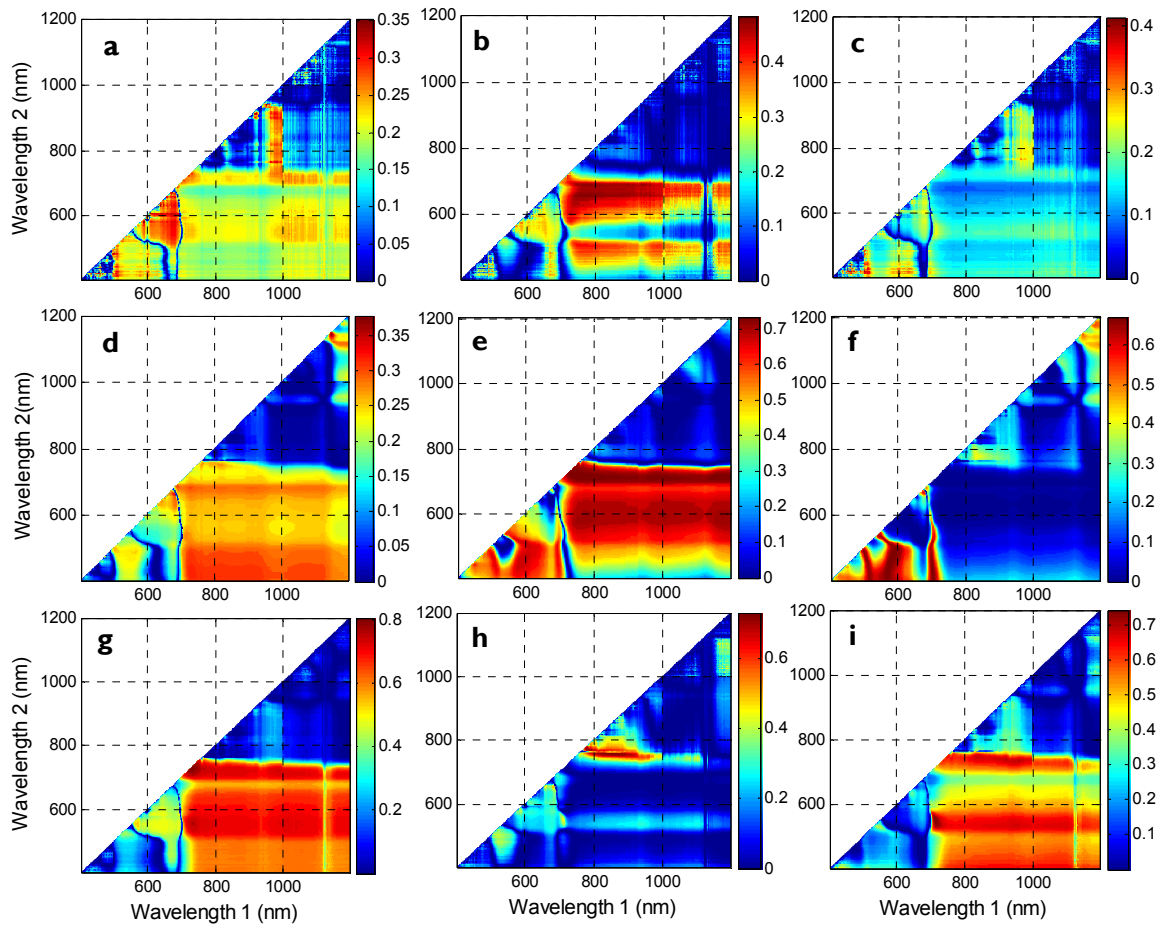


Figure 2-5: Lambda by lambda R^2 Contour plots showing the coefficient of determination (R^2) for the exponential relationships between canopy N status and narrow band SR calculated from all possible 2-band combinations in the range of 400-1200 nm for nine cases. The letters of a, b, c, d, e, f, g, h and i stand for each different case of: (a) Leaf N concentration before heading in 2007, (b) Leaf N concentration after heading in 2007, (c) All data for leaf N concentration in 2007, (d) Plant N concentration before heading in 2008, (e) Plant N concentration after heading in 2008, (f) All data for plant N concentration in 2008, (g) Plant N uptake before heading in 2007 and 2008, (h) Plant N uptake after heading in 2007 and 2008, (i) All data for plant N uptake in 2007 and 2008, respectively.

In agreement with the findings of *Xue et al. (2004)*, growth stages influenced the relationships between vegetation indices and leaf N concentration before heading. In comparison, the best SRs and NDIs relating to PNU were concentrated in: (i) the red-edge bands (700-760 nm) paired with the red-edge to NIR bands (700-1100 nm) and, (ii) green bands (500-590 nm) paired with red-edge to NIR bands (700-1100 nm) (Figures 2-4g, h, i and 2-5g, h, i). These two “hot zones” were also apparent for PNC after heading. However, the green bands were shifted to the bands centered on 600 nm (570-630 nm, Figures 2-4e and 2-5e). In addition, blue bands (450-495 nm) paired with shorter green bands (500 nm), longer green bands (580-600 nm) or red-edge bands (700-720 nm) (Figures 2-5e, f and 2-6e, f) also yielded highest R^2 for PNC. The highest R^2 for LNC were concentrated in the red-edge bands (700-760 nm) paired with the red-edge to NIR bands (700-1100 nm), followed by blue to green bands (450-520 nm) paired with red-edge to NIR bands (740-1000 nm) (Figures 2-4b and 2-5b).

Table 2-6 summarizes the best performing SRs and NDIs obtained from the lambda by lambda R^2 contour plots for both linear and nonlinear models. SRs and NDIs generally constitute the same band combinations and did not result in a significant difference in each individual case (Table 2-6). However, nonlinear exponential models yielded a significant increase in R^2 than linear models for PNU after heading and across all stages. The newly proposed 2-band indices SR (758,854, also the NDI with same bands) and SR (550,715) yielded a significant increase in R^2 by 48% and 23% respectively after heading and across all stages in modeling PNU (Table 2-6) compared with published indices. It is also worth noting that SR (730, 808) even performed better than the 3-band index MTCI, which is the best performing published index that we reviewed in this study. Figure 2-6 illustrates the above three newly proposed indices that had the best performance in modeling PNU respectively in the three stage-divisions. The SR (730, 808) was linearly related to PNU before heading, whereas SR (758, 854) and SR (550, 715) were exponentially related to PNU respectively after heading and across all stages.

Table 2-6: R² for the relationships between best selected 2-band indices from contour plots and N variables.

N variable	Tillering to heading						Heading to filling						All stages					
	Linear model			Nonlinear exponential model			Linear model			Nonlinear exponential model			Linear model			Nonlinear exponential model		
	Index	R ²		Index	R ²		Index	R ²		Index	R ²		Index	R ²		Index	R ²	
LNC	SR(580,592)	0.38		SR(580,592)	0.36		SR(656,772)	0.52		SR(656,766)	0.49		SR(420,458)	0.43		SR(420,458)	0.42	
	NDI(580,592)	0.38		NDI(580,592)	0.36		NDI(716,720)	0.47		NDI(716,720)	0.46		NDI(426,602)	0.44		NDI(420,458)	0.42	
	Percent increase over published indices	3			1			2			-1			7			5	
PNC	SR(1142,1150)	0.39		SR(1142,1150)	0.39		SR(712,758)	0.74		SR(718,744)	0.75		SR(424,706)	0.67		SR(462,580)	0.68	
	NDI(1142,1150)	0.39		NDI(1142,1150)	0.39		NDI(730,732)	0.72		NDI(724,738)	0.75		NDI(490,502)	0.66		NDI(478,506)	0.67	
	Percent increase over published indices	9			9			-1			0			2			3	
PNU	SR(730,808)	0.85		SR(730,732)	0.82		SR(774,780)	0.66		SR(758,854)	0.75		SR(752,840)	0.72		SR(550,715)	0.78	
	NDI(736,808)	0.83		NDI(718,772)	0.84		NDI(774,780)	0.66		NDI(758,854)	0.75		NDI(750,840)	0.72		NDI(538,874)	0.76	
	Percent increase over published indices	1			0			39			48			19			23	

CHAPTER 2

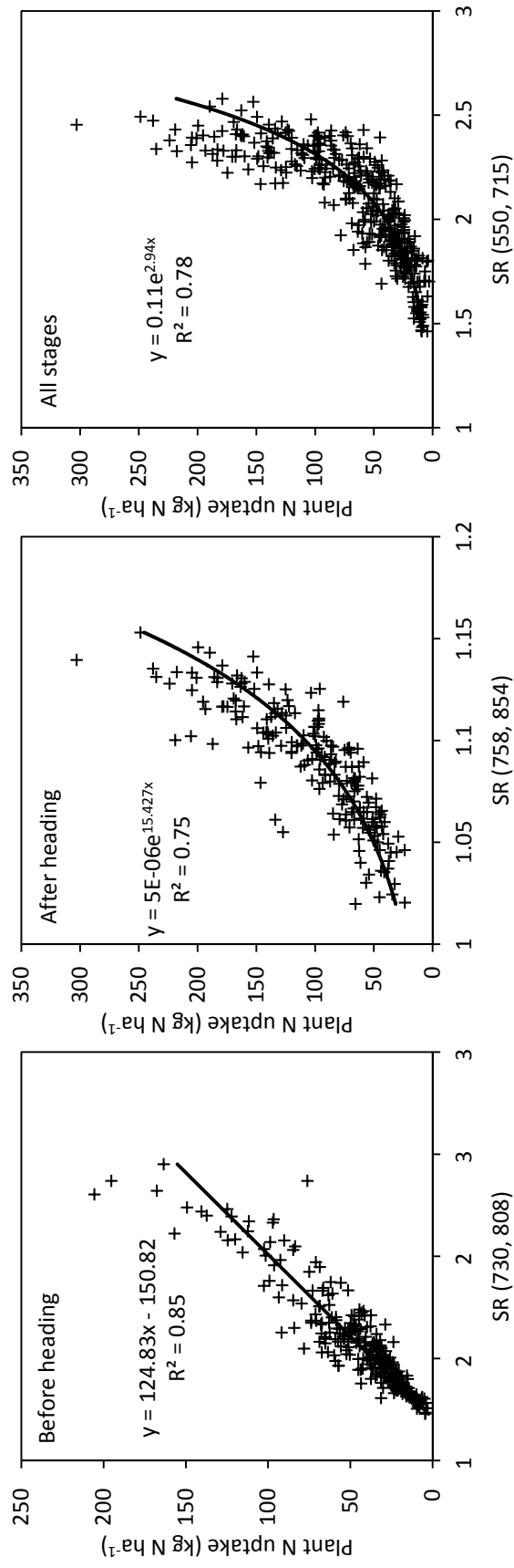


Figure 2-6: Best simple ratios (SRs) selected using the lambda by lambda band-optimized algorithm in relation to PNU before, after heading and across all stages.

2.3.4 Identifying the OMNBR models using multiple linear regression analysis

Both the optimum 2-band indices and published indices failed to explain a large proportion of the variation in LNC in all three stage-divisions ($R^2 \leq 0.52$, Tables 2-5 and 2-6) and PNC before heading ($R^2 \leq 0.39$). Therefore, a stepwise multi-variable selection technique was implemented to find multi-band combinations relating to canopy N status. The OMNBR indices were identified by selecting the best 1-band, 2-band, ..., n-band models with the multiple linear regression analysis implemented with MAXR in SAS (*SAS Institute Inc., 2008*). Results show that R^2 increases with the increase of the band count for the OMNBR models (Figure 2-7). For LNC the R^2 increased significantly until the sixth band was selected. Beyond six bands, the R^2 increase with the addition of each band was small (Figure 2-7a). For PNC after heading and across all stages, the R^2 increased significantly until the fourth band was used for the model. Beyond four bands, no significant improvement in R^2 was observed, except in the case across all stages where the 8-band model yielded a jump in R^2 (Figure 2-7b). For PNC before heading the R^2 increased significantly until nine bands, by which the 9-band model explained 67% of the variation (Figure 2-8d). The OMNBR models explained more variation in LNC and PNC with fewer band counts after heading than before heading or across all stages (Figure 2-7a, b). In contrast, the OMNBR models explained more variation in PNU with fewer band counts before heading and across all stages than after heading (Figure 2-7c). For PNU after heading the R^2 increased significantly until five bands were used for the OMNBR model. In comparison, the best 2-band model explained 80% of the variation in PNU before heading (Figure 2-7c). Overall, band counts of 4 to 6 are preferable for constructing OMNBR models with an ideal suppression effect on “over-fitting”, except in the case for PNC before heading where a 9-band model is more acceptable (Figure 2-7b). For demonstration, the best 1- to 6-band models and their corresponding bands are shown in Table 2-7.

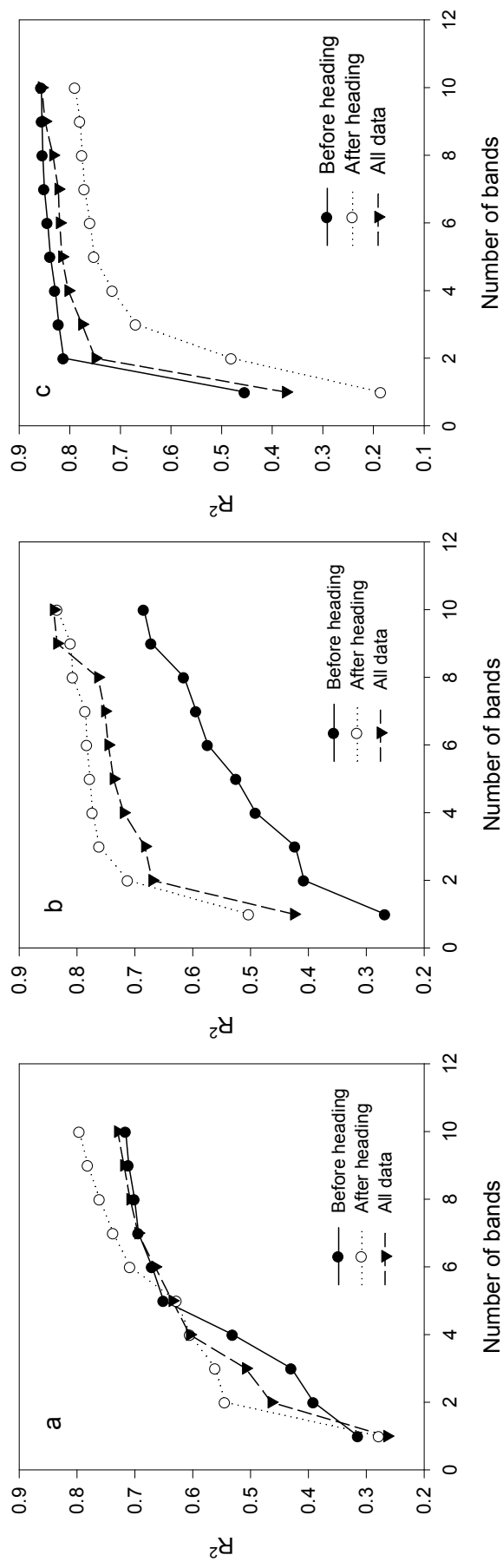


Figure 2-7: Plots of the band count for the best n -band ($n=1-10$) models versus R^2 values for every N variables, (a) Leaf N concentration, (b) Plant N concentration and (c) Plant N uptake.

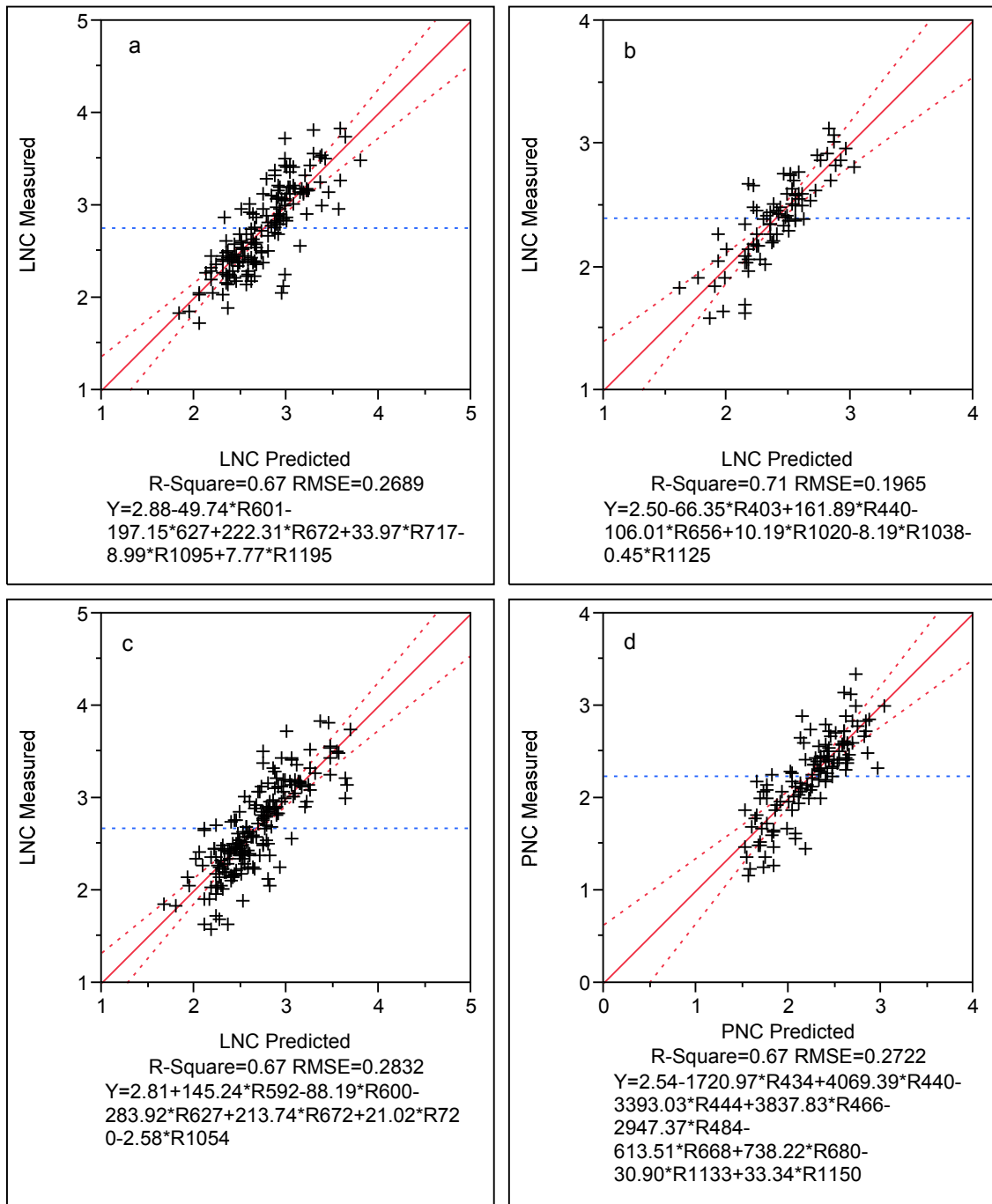


Figure 2-8: The best 6-band OMNBR models for LNC before heading (a), after heading (b) and across all stages (c) and the best 9-band OMNBR model for PNC before heading (d). Red and blue dash lines show the 95% confidence intervals and mean values, respectively. Letter Y denotes the dependent variable (LNC or PNC) in every multiple linear regression model. The units for LNC and PNC are percent (%).

CHAPTER 2**Table 2-7: Optimum multiple narrow band reflectance (OMNBR) models.**

Model	Leaf N Concentration (LNC)			Plant N Concentration (PNC)			Plant N Uptake (PNU)		
	Before Heading	After Heading	All Stages	Before Heading	After Heading	All Stages	Before Heading	After Heading	All Stages
Best 1-Band Model									
R ²	0.31	0.28	0.26	0.27	0.50	0.43	0.45	0.19	0.37
Band	R1008	R685	R414	R817	R703	R727	R690	R538	R403
Best 2-Band Model									
R ²	0.39	0.54	0.46	0.41	0.71	0.67	0.81	0.48	0.75
Band	R939	R419	R426	R1108	R735	R487	R731	R580	R758
	R967	R666	R601	R1197	R751	R619	R775	R586	R847
Best 3-Band Model									
R ²	0.43	0.56	0.51	0.42	0.76	0.68	0.82	0.67	0.78
Band	R420	R403	R426	R577	R536	R485	R731	R567	R406
	R937	R419	R602	R1108	R735	R487	R794	R582	R757
	R967	R669	R701	R1182	R737	R620	R1123	R952	R847
Best 4-Band Model									
R ²	0.53	0.60	0.61	0.49	0.77	0.72	0.83	0.72	0.80
Band	R483	R403	R591	R440	R400	R470	R731	R567	R406
	R602	R418	R632	R444	R732	R580	R807	R582	R446
	R937	R663	R671	R1108	R735	R1140	R1123	R680	R752
	R1033	R686	R706	R1167	R738	R1150	R1154	R901	R847
Best 5-Band Model									
R ²	0.65	0.63	0.64	0.52	0.78	0.74	0.84	0.75	0.82
Band	R627	R403	R593	R431	R400	R487	R732	R605	R406
	R671	R418	R601	R440	R405	R576	R806	R616	R446
	R717	R663	R632	R444	R732	R1121	R1010	R648	R756
	R1095	R686	R672	R1107	R735	R1139	R1109	R745	R845
	R1195	R942	R706	R1179	R738	R1150	R1123	R838	R921
Best 6-Band Model									
R ²	0.67	0.71	0.67	0.57	0.78	0.75	0.84	0.76	0.82
Band	R601	R403	R592	R440	R400	R486	R680	R605	R406
	R627	R440	R600	R444	R405	R487	R738	R616	R439
	R672	R656	R627	R672	R407	R576	R807	R648	R756
	R717	R1020	R672	R680	R732	R1121	R1010	R750	R845
	R1095	R1038	R720	R1116	R735	R1139	R1109	R834	R918
	R1195	R1125	R1054	R1167	R738	R1150	R1139	R903	R939
Percent increase over best SR and NDI									
	29	19	23	18	3	7	-1	1	4

The best n-band (n=1-10) OMNBR models were obtained using the MAXR algorithm in SAS software (SAS Institute Inc.). The best 1-band, ..., 6-band models and their corresponding reflectance (R) bands are presented. For models with same band count, bold values show the highest R² among three stage-divisions.

For LNC and PNC before heading, the first best band determined by the MAXR method were NIR bands at 1008 nm and 817 nm respectively, whereas after heading it selected a red (685 nm) and red-edge (703 nm) band (Table 2-7), indicating that growth stages influence the selection of sensitive bands. With addition of one red band (671 nm), the 5-band model increased the R^2 by 0.12 in modeling LNC before heading compared to the 4-band model, and the 4-band model for all stages increased the R^2 by 0.10 compared to the 3-band model. The adjacent red bands (660-690 nm) were always used in the OMNBR models for modeling LNC after heading (Table 2-7).

The violet bands (430-450 nm) were most frequently used for modeling PNC before heading, whereas the red-edge bands (700-740 nm) were predominant after heading. In comparison, the blue (470-480 nm) and green bands (570-580 nm) were always used for modeling PNC across all stages in the best 4- to 6-band models.

The center of red-edge (731 nm) and the early NIR (775-810 nm) were dominant in modeling PNU before heading, whereas the longer red-edge (750 nm) and the center of NIR (840-850 nm) were predominant for all stages. In comparison, green bands were more frequently used in modeling PNU after heading.

The best 6-band OMNBR models significantly improved the R^2 for modeling LNC before ($R^2 = 0.67$) and after heading ($R^2 = 0.71$) and across all stages ($R^2 = 0.67$) compared to 2-band SRs and NDIs and published indices. The 9-band model explained 67% the variation in PNC before heading (Figure 2-8, Table 2-7). They significantly increased the R^2 respectively by 29%, 19%, 23% and 28% respectively (Tables 2-5, 2-6 and 2-7).

2.4 Discussion

Growth stages significantly influence the performance of hyperspectral indices for estimating canopy N status of rice. As illustrated in Figure 2-3, two clusters of points were observed before and after heading when LNC and PNC were plotted versus investigated indices. The LNC and PNC were linearly related to spectral indices after the heading stage, when more variation in LNC and PNC could be explained by spectral indices compared to before the heading stage (Table 2-5). During the early stages in rice fields, canopy reflectance is often confused by soil (*Haboudane et al., 2002; Huete, 1988*) and water (*Shibayama et al., 1993*), which commonly results in poor association with canopy chlorophyll or N concentration. It was noted that the rate of the above-ground biomass production exceeds the rate of N uptake by plants before heading when the biomass dominates canopy reflectance (*Mistele & Schmidhalter, 2008*). In contrast, the increase in biomass becomes slower and the “dilution effect” ends after heading when plant N

dominates canopy reflectance. Thus, PNC is relatively easily evaluated using spectral indices following the heading stage. Consistent with previous results, *Li et al. (2010)* reported that PNC of winter wheat and spectral indices are more closely related at later growth stages ($R^2 = 57\%$) than at early stages ($R^2 = 43\%$). Results show a great potential for monitoring N concentration at later stages to improve the grain quality of rice, similar to *Ryu et al. (2011)* who reported on integrating remote sensing and GIS for estimating protein content of brown rice before harvest. However, yield is determined by crop condition at the earlier stages of growth, so it is also mandatory to provide farmers with N status before heading in order to supply appropriate rates of fertilizers based upon an accurate assessment of plant N requirements and deficiencies (*Haboudane et al., 2002*). The most encouraging result is that PNU was strongly linearly related to the hyperspectral indices before the heading stage, when 85% of the variation in PNU was explained by the best performing newly proposed SR(760, 808), followed by the published index MTCI ($R^2 = 0.84$) (Tables 2-5 and 2-6). Due to the contribution of biomass (Table 2-4) and canopy structure (Figure 2-2) before the heading stage and given that PNU is the combination of biomass and N concentration, PNU is more closely associated with hyperspectral indices before the heading stage. Our results suggest that, to monitor rice canopy N status for the entire growth stages, we could use hyperspectral indices to estimate canopy N uptake before heading and canopy N concentration after heading.

Interestingly, more variation in LNC than in PNC was explained before heading stage by the published hyperspectral indices (Table 2-5, Figure 2-3). This could have resulted from the inconsistency of the temporal rice canopy development pattern (*Bridhikitti & Overcamp, 2012*), and reveals again that growth stages have significant influences on the performance of hyperspectral indices for estimating N concentration, and especially larger influences on PNC. Before the heading stage, variation in biomass (CV= 81.7%) and canopy structure of whole plants is greater than that of individual leaves (CV = 56.6%, Table 2-4), especially the top canopy leaves because N can be remobilized from shaded leaves at the bottom of the canopy to leaves at the top (*Lemaire et al., 2008*). Thus, less variation in PNC was explained by the hyperspectral indices before heading compared to LNC. The influence of the N dilution effect makes it difficult to provide the maximum N-related physiological information with the use of only 2-band spectral indices. Therefore, multi-band indices are required to be used to provide the maximum information relating to PNC. It is apparent that the multi-band models significantly increased the R^2 in the comparison with the OMNBR models presented in Table 2-7. In addition, even with the same number of bands, 6-band models explained 10% more of the variation in LNC than that in PNC before heading, confirming that LNC is more easily captured than PNC by reflectance measures before heading. However, after the heading stage, when the canopy is closed, PNC

related information can be much more readily captured by the canopy hyperspectral characteristics than that before heading. The use of fewer bands may also provide the maximum N-related information. This is affirmed by our results that the best 2-band SR (Table 2-6) explained 75% of the variation in PNC after heading, only slightly lower than the best 3- to 6-band OMNBR models (76%-78% Table 2-7).

The main advantage of the use of the lambda by lambda band-optimized algorithm is that it can systematically search for the most sensitive 2-band combinations as SR- and NDI-like indices in relation to crop variables of interest. The band combinations of red-edge bands (700-750 nm) paired with “NIR shoulder” (780-940 nm) were mostly closely related to PNU and PNC. Therefore, published indices composed of reflectance at the shoulder of NIR (750nm) with reflectance at 700-710 nm (red edge) were most closely related to PNC after heading and PNU before heading. For instance, SR3 (*Zarco-Tejada et al., 2001*), SR4 (*Gitelson & Merzlyak, 1996*), MTCI (*Dash & Curran, 2004*), mSR705 (*Sims & Gamon, 2002*) and TCARI/OSAVI[705, 750] (*Wu et al., 2008*), which were all composed of reflectance at both 750 nm and 700-710 nm, performed better in deriving PNC and PNU than other indices. The results further confirm that the red bands (670-680 nm) substituted by red edge (700-750 nm) bands significantly improve the predictive power in deriving crop canopy N related parameters (*Tarpley et al., 2000; Wu et al., 2008*). The best SRs and NDIs relating to PNC after heading were exclusively composed of two red-edge bands, whereas across all stages they were exclusively the blue paired with green bands. This result suggests that red-edge bands are sensitive to PNC after heading, whereas the blue and green bands are sensitive to PNC across all stages. A recent study conducted before heading by *Stroppiana et al. (2009)* also found that the blue and green bands (483, 503 nm) provided the best performance for deriving PNC using the lambda by lambda band-optimized algorithm. Therefore, combinations of blue with green bands are very useful for estimating PNC. This is also in agreement with the OMNBR models that both the blue bands (470-490 nm) and green bands (570-580 nm) were used for the best 4- to 6-band models for modeling PNC across all stages (Table 2-7). Moreover, in the OMNBR models for PNC after heading, red-edge bands were used in every model with 50-100% proportion of total band count. In particular, the red-edge band at 735 nm was always used in the best 2- to 6-band models, indicating that the red-edge bands are very effective for estimating PNC after heading.

Although hyperspectral data have been widely used for rice N monitoring (*Nguyen et al., 2006; Stroppiana et al., 2009; Tian et al., 2011; Xue et al., 2004; Zhu et al., 2007*), research is still limited by our knowledge of how to use hyperspectral data to directly estimate the PNU of rice at specific growth periods. Newly selected 2-band SRs and NDIs significantly increase R^2 in relating to PNU as compared to published vegetation indices. Particularly, the indices composed of

red-edge at around 750 nm paired with NIR at around 850 nm (e.g. SR/NDI (758, 854), Table 2-6) yielded more than 40% increase in R^2 for modeling PNU after heading compared to published indices. This band combination was also the best combination for PNU across all stages in the linear model (Table 2-6), and was always used in the best 2- to 6-band OMNBR models for PNU across all stages and the 5- and 6-band OMNBR models after heading (Table 2-7). This indicates that the combinations of longer red-edge (750 nm) paired with the “center” of NIR shoulder (850 nm) are very efficient for modeling PNU after heading and across all stages. In comparison, the combinations of the “center” of red-edge (730 nm) paired with early NIR band (at around 800 nm) both yielded the best SR (Table 2-6) and the best 3- to 6-band OMNBR models (Table 2-7) for PNU before heading. Thus, the combinations of the center of red-edge paired with early NIR can provide high accuracy for modeling PNU at early growth stages. The best performances of 2-band SRs and NDIs were achieved by using nonlinear exponential models for the PNU after heading and across all stages (Table 2-6). This is consistent with the study in predicting LAI and biomass (Thenkabail *et al.*, 2000), indicating that the biomass variation dominates PNU and its relation to hyperspectral reflectance. Although the lambda by lambda band-optimized algorithm provides an insight on the selection of sensitive bands, results of contour plots sometimes may mislead us into selecting improper 2-band combinations and indices. The best 2-band combinations for PNC before the heading stage were determined as SR/NDI (1142, 1150) in the wavebands of far-NIR. However, these bands are dominated by water and organic compounds of which cellulose, lignin, starch and protein (van Der Meer & de Jong, 2001), are not correlated directly to N status, demonstrating that variation of canopy structure and N dilution effect constrains the band-optimized algorithm before heading. Thus, the indices composed of these 2-band combinations should not have consistent relationships with N status. Ignoring the exception in these bands (Figures 2-4d, f and 2-5d, f), it is clear that indices composed of reflectance at the shoulder of NIR with reflectance at red edge were closely correlated with canopy N status.

Although the best performing SRs and NDIs increased the R^2 compared to the published indices, limitation still exists when we used the 2-band SRs and NDIs for modeling LNC and PNC. This may be due to the use of only 2-band indices that constrain the regression analysis (Thenkabail *et al.*, 2000), and cannot overcome the N dilution effect to provide the maximum N-related information. Using stepwise multi-band selection algorithm to construct the OMNBR models, 67%-71% of the variation in LNC was explained with 6-band models for all three stage divisions. In agreement with the findings of Thenkabail *et al.* (2000; 2004), the stepwise multiple regression analysis is very effective for selecting multiple sensitive bands. It is worth noting that the red maximum absorption bands (671, 672, and 680 nm) were always used for modeling both LNC and PNC before heading (Table 2-7), whereas the red-edge bands were either not used or

“later and lesser” (SAS Institute Inc.) switched in models than the red bands. This confirms that for modeling LNC and PNC before heading the red bands are more efficient than red-edge bands (Kanke *et al.*, 2012). Moreover, with the addition of these N-related bands (671, 672, 680 nm, Table 2-7) the OMNBR models significantly increased the accuracy for modeling N, suggesting again that the N dilution effect significantly constrains the performance of 2-band SRs, NDIs and published indices before heading. Once these N-related bands were involved in the models, the N dilution effect can be overcome and N-related information can be maximized by the OMNBR models. Therefore, to overcome the influence by the N dilution effect, the stepwise multiple regression analysis based OMNBR models should be used. However, there is a likelihood of multi-band models being over-fitted (Blackburn, 1998). To avoid over-fitting the OMNBR models, Thenkabail *et al.* (2000) suggested a M/N evaluation criteria (M= band count, N= number of observations) in which this ratio should not exceed 0.15-0.20. In this study, all of the OMNBR models did not break the criteria with one to ten bands ($M/N < 0.12$). The band count used for modeling PNU before heading is in agreement with the study in predicting biomass (Thenkabail *et al.*, 2004) that using more than three or four bands only yielded an insignificant increase in modeling accuracy. This reaffirms the large impact of biomass on canopy reflectance before heading, since the minimum PNU is dependent on the maximum crop biomass (Lemaire *et al.*, 2008). The results reveal the importance of using multi-band models to overcome the negative influence of the N dilution effect especially, for specific growth periods and different agricultural crop variables.

Many studies aim to develop indices closely related to N or chlorophyll that are not influenced by canopy structure, LAI, biomass, soil background etc. (Baret & Guyot, 1991; Haboudane *et al.*, 2002; Huete, 1988; Qi *et al.*, 1994; Rondeaux *et al.*, 1996; Stroppiana *et al.*, 2009). However, almost no one index provides consistent predictive abilities under different conditions and limited studies have focused on how to improve their use for estimating N and chlorophyll at specific growth periods. Using 2-band hyperspectral indices before the heading stage, more than 80% of the variation in PNU was explained even by the leaf chlorophyll indices (SR3, TCARI/OSAVI [705, 750], MTCI and mSR705, Tables 2-5 and 2-6). This suggests not only that reflectance estimates for chlorophyll can be used to estimate the N status (Filella & Peñuelas, 1994; Peñuelas & Filella, 1998), but also the importance of improving our knowledge for better understanding both the physiological and biophysical characteristics of plants to benefit N management using hyperspectral measures. Although the 2-band indices have limitations, they are easy to use compared to the multi-band OMNBR models. It is feasible to choose the best SRs and NDIs for monitoring PNU at early stages and PNC at later stages. The OMNBR models should be used as a compensatory method when the SRs and NDIs cannot provide satisfactory accuracy under given conditions. The two techniques for band optimization can be integrated for precision

N management over the entire growth period.

2.5 Conclusions

In this study, hyperspectral narrow band reflectance measures were collected on paddy rice canopy across six critical growth stages in two growing seasons. Two techniques for band optimization were used to thoroughly examine all possible 2-band and multi-band models relating to N variables. Specifically, the lambda by lambda band-optimized algorithm was used to select the 2-band SRs and NDIs, and a stepwise multiple linear regression method was implemented to obtain the OMNBR models. The performances of both techniques were compared by always covering three growth stage-divisions and three N variables (LNC, PNC and PNU), totally nine cases. The most important conclusions that can be drawn from this study are as follows:

- (i) The N dilution effect negatively influences the selection of sensitive bands and their performance in modeling canopy N status.
- (ii) Best 2-band SRs or NDIs increased the R^2 significantly in modeling PNU ($R^2 \geq 0.75$). However, they still failed to explain the LNC ($R^2 \leq 0.52$) and PNC before heading ($R^2 \leq 0.39$).
- (iii) The OMNBR models significantly increased R^2 for modeling LNC and PNC compared to the best performing SRs and NDIs.
- (iv) Combinations of the center of Red-edge at 735 nm with other longer red-edge bands (730-760 nm) are very efficient for modeling PNC after heading, whereas the combinations of blue with green bands are more efficient across all stages.
- (v) Combinations of the center of red-edge (730-735nm) paired with early NIR bands (775-808 nm) are predominant in estimating PNU before heading, whereas longer red-edge (750 nm) paired with the center of NIR shoulder (840-850 nm) are dominant after heading and across all stages.
- (vi) Red absorption maximum bands (670-680 nm) are predominant in modeling LNC, whereas they are important before heading for estimating PNC.

To summarize, the N dilution effect dynamically influences two- and multi-band combinations in different ways for LNC, PNC and PNU. The lambda by lambda band-optimized algorithm is useful for identifying the best 2-band indices and can improve the performance for estimating canopy N. However, this method still has limitations because the N dilution effect makes it difficult to provide the maximum N-related information with the use of only 2-band hyperspectral indices, particularly for modeling LNC and PNC before heading. The multi-band OMNBR models provide significant improvement in modeling canopy N using multiple N related bands. However, the OMNBR models do not offer the simplicity of 2-band SR or NDI type models ([Thenkabail et](#)

al., 2000). Thus, a “lambda cubic” algorithm (or to say “lambda by lambda by lambda”) or even a higher dimensional band-optimized algorithm should be useful to identify new hyperspectral indices that involve multiple bands and are less dependent on the N dilution effect. Alternatively, new “stage-adjusted” hyperspectral vegetation indices may be developed to minimize the influence by growth stages. The primary results of the present study provide a useful reference base for further research on canopy N concentration and N uptake estimation, and remains to be validated in future studies.

Acknowledgements

The study was funded by China 973 Program (Grant No. 2009CB118606), the innovative group grant of the Natural Science Foundation of China (NSFC Grant No. 31121062) and the German Federal Ministry of Education and Research (BMBF, project No. CHN 08/051). We acknowledge the support of Jiansanjiang Branch Bureau. We thank Lei Gao, Guangming Zhao, Yinkun Yao, Shanyu Huang for their field work contribution and Prof. Tony Fuller for English language editing. The authors are very grateful for the critical comments of both anonymous reviewers, one suggested using the comprehensive multi-band-optimized method and the other one helped us to better explain the N dilution effect. We would also like to thank the editor for putting in extraordinary effort to catch grammatical errors in our manuscript.

References

- Baret, F., Guyot, G. 1991.** Potentials and limits of vegetation indices for LAI and APAR assessment. *Remote Sens. Environ.* **35**: 161-173.
- Barton, C.V.M. 2001.** A theoretical analysis of the influence of heterogeneity in chlorophyll distribution on leaf reflectance. *Tree Physiol.* **21**: 789-795.
- Blackburn, G.A. 1998.** Quantifying chlorophylls and carotenoids at leaf and canopy scales: An evaluation of some hyperspectral approaches. *Remote Sens. Environ.* **66**: 273-285.
- Bridhikitti, A., Overcamp, T.J. 2012.** Estimation of Southeast Asian rice paddy areas with different ecosystems from moderate-resolution satellite imagery. *Agric. Ecosyst. Environ.* **146**: 113-120.
- Ciganda, V., Gitelson, A., Schepers, J. 2009.** Non-destructive determination of maize leaf and canopy chlorophyll content. *J. Plant Physiol.* **166**: 157-167.
- Dash, J., Curran, P.J. 2004.** The MERIS terrestrial chlorophyll index. *Int. J. Remote Sens.* **25**: 5403-5413.

- Daughtry, C.S.T., Walthall, C.L., Kim, M.S., de Colstoun, E.B., McMurtrey III, J.E. 2000.** Estimating corn leaf chlorophyll concentration from leaf and canopy reflectance. *Remote Sens. Environ.* **74**: 229-239.
- Dobermann, A., Witt, C., Abdulrachman, S., Gines, H.C., Nagarajan, R., Son, T.T., Tan, P.S., Wang, G.H., Chien, N.V., Thoa, V.T.K., Phung, C.V., Stalin, P., Muthukrishnan, P., Ravi, V., Babu, M., Simbahan, G.C., Adviento, M.A.A., Bartolome, V. 2003.** Estimating indigenous nutrient supplies for site-specific nutrient management in irrigated rice. *Agron. J.* **95**: 924-935.
- Fageria, N.K. 2009.** *The use of nutrients in crop plants*. Boca Raton, Florida, USA: CRC Press, Taylor & Francis Group, LLC.
- Filella, I., Peñuelas, J. 1994.** The red edge position and shape as indicators of plant chlorophyll content, biomass and hydric status. *Int. J. Remote Sens.* **15**: 1459-1470.
- Flowers, M., Weisz, R., Heiniger, R. 2003.** Quantitative Approaches for Using Color Infrared Photography for Assessing In-Season Nitrogen Status in Winter Wheat. *Agron. J.* **95**: 1189-1200.
- Gitelson, A.A., Merzlyak, M.N. 1996.** Signature analysis of leaf reflectance spectra: Algorithm development for remote sensing of chlorophyll. *J. Plant Physiol.* **148**: 494-500.
- Haboudane, D., Miller, J.R., Tremblay, N., Zarco-Tejada, P.J., Dextraze, L. 2002.** Integrated narrow-band vegetation indices for prediction of crop chlorophyll content for application to precision agriculture. *Remote Sens. Environ.* **81**: 416-426.
- Hansen, P.M., Schjoerring, J.K. 2003.** Reflectance measurement of canopy biomass and nitrogen status in wheat crops using normalized difference vegetation indices and partial least squares regression. *Remote Sens. Environ.* **86**: 542-553.
- Huang, J., He, F., Cui, K., Buresh, R.J., Xu, B., Gong, W., Peng, S. 2008.** Determination of optimal nitrogen rate for rice varieties using a chlorophyll meter. *Field Crops Res.* **105**: 70-80.
- Huete, A.R. 1988.** A soil-adjusted vegetation index (SAVI). *Remote Sens. Environ.* **25**: 295-309.
- Jordan, C.F. 1969.** Derivation of leaf-area index from quality of light on the forest floor. *Ecology* **50**: 663-666.
- Kanke, Y., Raun, W., Solie, J., Stone, M., Taylor, R. 2012.** Red edge as a potential index for detecting differences in plant nitrogen status in winter wheat. *J. Plant Nutr.* **35**: 1526-1541.
- Lancashire, P.D., Bleiholder, H., Boom, T.V.D., Langelüddeke, P., Stauss, R., Weber, E., Witzemberger, A. 1991.** A uniform decimal code for growth stages of crops and weeds. *Ann. Appl. Biol.* **119**: 561-601.

- Lee, Y., Yang, C., Chang, K., Shen, Y. 2008.** A simple spectral index using reflectance of 735 nm to assess nitrogen status of rice canopy. *Agron. J.* **100**: 205-212.
- Lemaire, G., Jeuffroy, M., Gastal, F. 2008.** Diagnosis tool for plant and crop N status in vegetative stage: Theory and practices for crop N management. *Eur. J. Agron.* **28**: 614-624.
- Li, F., Miao, Y., Hennig, S., Gnyp, M., Chen, X., Jia, L., Bareth, G. 2010.** Evaluating hyperspectral vegetation indices for estimating nitrogen concentration of winter wheat at different growth stages. *Precis. Agric.* **11**: 335-357.
- Miao, Y., Stewart, B., Zhang, F. 2011.** Long-term experiments for sustainable nutrient management in China. A review. *Agron. Sustain. Dev.* **31**: 397-414.
- Mistele, B., Schmidhalter, U. 2008.** Estimating the nitrogen nutrition index using spectral canopy reflectance measurements. *Eur. J. Agron.* **29**: 184-190.
- Nguyen, H.T., Kim, J.H., Nguyen, A.T., Nguyen, L.T., Shin, J.C., Lee, B. 2006.** Using canopy reflectance and partial least squares regression to calculate within-field statistical variation in crop growth and nitrogen status of rice. *Precis. Agric.* **7**: 249-264.
- Nguyen, H.T., Lee, B. 2006.** Assessment of rice leaf growth and nitrogen status by hyperspectral canopy reflectance and partial least square regression. *Eur. J. Agron.* **24**: 349-356.
- Peng, S., Laza, M.R., Garcia, F.V., Cassman, K.G. 1995.** Chlorophyll meter estimates leaf area-based nitrogen concentration of rice. *Commun. Soil Sci. Plant Anal.* **26**: 927-935.
- Peñuelas, J., Filella, I. 1998.** Visible and near-infrared reflectance techniques for diagnosing plant physiological status. *Trends Plant Sci.* **3**: 151-156.
- Qi, J., Chehbouni, A., Huete, A.R., Kerr, Y.H., Sorooshian, S. 1994.** A modified soil adjusted vegetation index. *Remote Sens. Environ.* **48**: 119-126.
- Read, J.J., Tarpley, L., McKinion, J.M., Reddy, K.R. 2002.** Narrow-waveband reflectance ratios for remote estimation of nitrogen status in cotton. *J. Environ. Qual.* **31**: 1442-1452.
- Reyniers, M., Walvoort, D.J.J., De Baardemaaker, J. 2006.** A linear model to predict with a multi-spectral radiometer the amount of nitrogen in winter wheat. *Int. J. Remote Sens.* **27**: 4159-4179.
- Rondeaux, G., Steven, M., Baret, F. 1996.** Optimization of soil-adjusted vegetation indices. *Remote Sens. Environ.* **55**: 95-107.
- Russell, C.A., Dunn, B.W., Batten, G.D., Williams, R.L., Angus, J.F. 2006.** Soil tests to predict optimum fertilizer nitrogen rate for rice. *Field Crops Res.* **97**: 286-301.
- Ryu, C., Suguri, M., Iida, M., Umeda, M., Lee, C. 2011.** Integrating remote sensing and GIS for prediction of rice protein contents. *Precis. Agric.* **12**: 378-394.
- SAS Institute Inc. 2008.** SAS/STAT® 9.2 User's Guide. Cary, NC: SAS Institute Inc. In.

- Shibayama, M., Takahashi, W., Morinaga, S., Akiyama, T. 1993.** Canopy water deficit detection in paddy rice using a high resolution field spectroradiometer. *Remote Sens. Environ.* **45**: 117-126.
- Sims, D.A., Gamon, J.A. 2002.** Relationships between leaf pigment content and spectral reflectance across a wide range of species, leaf structures and developmental stages. *Remote Sens. Environ.* **81**: 337-354.
- Steele, M.R., Gitelson, A.A., Rundquist, D.C. 2008.** A comparison of two techniques for nondestructive measurement of chlorophyll content in grapevine leaves. *Agron. J.* **100**: 779-782.
- Stroppiana, D., Boschetti, M., Brivio, P.A., Bocchi, S. 2009.** Plant nitrogen concentration in paddy rice from field canopy hyperspectral radiometry. *Field Crops Res.* **111**: 119-129.
- Tarpley, L., Reddy, K.R., Sassenrath-Cole, G.F. 2000.** Reflectance indices with precision and accuracy in predicting cotton leaf nitrogen concentration. *Crop Sci.* **40**: 1814-1819.
- Thenkabail, P.S., Smith, R.B., De Pauw, E. 2000.** Hyperspectral vegetation indices and their relationships with agricultural crop characteristics. *Remote Sens. Environ.* **71**: 158-182.
- Thenkabail, P.S., Enclona, E.A., Ashton, M.S., Legg, C., De Dieu, M.J. 2004.** Hyperion, IKONOS, ALI, and ETM+ sensors in the study of African rainforests. *Remote Sens. Environ.* **90**: 23-43.
- Tian, Y.C., Yao, X., Yang, J., Cao, W.X., Hannaway, D.B., Zhu, Y. 2011.** Assessing newly developed and published vegetation indices for estimating rice leaf nitrogen concentration with ground- and space-based hyperspectral reflectance. *Field Crops Res.* **120**: 299-310.
- van Der Meer, F.D., de Jong, S.M. 2001.** *Imaging spectrometry: basic principles and prospective applications*. Dordrecht: Kluwer Academic Publishers.
- Wu, C., Niu, Z., Tang, Q., Huang, W. 2008.** Estimating chlorophyll content from hyperspectral vegetation indices: Modeling and validation. *Agric. For. Meteorol.* **148**: 1230-1241.
- Xue, L., Cao, W., Luo, W., Dai, T., Zhu, Y. 2004.** Monitoring leaf nitrogen status in rice with canopy spectral reflectance. *Agron. J.* **96**: 135-142.
- Yang, W., Peng, S., Huang, J., Sanico, A.L., Buresh, R.J., Witt, C. 2003.** Using leaf color charts to estimate leaf nitrogen status of rice. *Agron. J.* **95**: 212-217.
- Yi, Q., Huang, J., Wang, F., Wang, X., Liu, Z. 2007.** Monitoring rice nitrogen status using hyperspectral reflectance and artificial neural network. *Environ. Sci. Technol.* **41**: 6770-6775.
- Yoder, B.J., Pettigrew-Crosby, R.E. 1995.** Predicting nitrogen and chlorophyll content and concentrations from reflectance spectra (400-2500 nm) at leaf and canopy scales. *Remote Sens. Environ.* **53**: 199-211.

- Zarco-Tejada, P.J., Miller, J.R., Noland, T.L., Mohammed, G.H., Sampson, P.H. 2001.** Scaling-up and model inversion methods with narrowband optical indices for chlorophyll content estimation in closed forest canopies with hyperspectral data. *IEEE Trans. Geosci. Remote Sens.* **39**: 1491-1507.
- Zhu, Y., Zhou, D., Yao, X., Tian, Y., Cao, W. 2007.** Quantitative relationships of leaf nitrogen status to canopy spectral reflectance in rice. *Aust. J. Agric. Res.* **58**: 1077-1085.
- Zhu, Y., Yao, X., Tian, Y., Liu, X., Cao, W. 2008.** Analysis of common canopy vegetation indices for indicating leaf nitrogen accumulations in wheat and rice. *Int. J. Appl. Earth Obs. Geoinf.* **10**: 1-10.

CHAPTER 3**Estimate leaf chlorophyll content of rice using spectral indices and partial least squares (PLS) ***

* *This chapter is based on:*

Yu, K., Gnyp, M.L., Gao, L., Miao, Y., Chen, X., Bareth, G. 2014. Estimate Leaf Chlorophyll of Rice Using Reflectance Indices and Partial Least Squares. *Photogramm. Fernerkund. Geoinf.* **submitted.**

Summary

In this study field experiments were conducted to test the ability of optimized spectral indices and partial least squares (PLS) to estimate leaf chlorophyll (Chl) content of rice from non-destructive canopy reflectance measurements. We integrated techniques involving the optimization of narrow band spectral indices and the detection of red edge position to optimize one type of spectral indices: the Ratio of Reflectance Difference Index (RRDI) for the estimation of leaf Chl content. The optimized $RRDI = (R_{745} - R_{740}) / (R_{740} - R_{700})$ accounted for 62%-72% of the variation in leaf Chl content with RMSE of 4.59-4.89 $\mu\text{g}/\text{cm}^2$. Compared to spectral indices, PLS improved the estimation of leaf Chl content, yielding R^2 and RMSE of 0.85 and 3.22 $\mu\text{g}/\text{cm}^2$, respectively. Finally, the model based on RRDI and the PLS model were further validated by an independent dataset collected in farmer fields. RRDI and PLS models yielded acceptable accuracy with R^2 of 0.49 and 0.55, respectively, and RMSE of 5.47 and 5.13 $\mu\text{g}/\text{cm}^2$. Our results suggest the potential to optimize spectral indices and also the significance of PLS technique for mapping canopy biochemical variations.

Zusammenfassung

Abschätzung von Chlorophyll im Blatt von Reis mit Hilfe von Spektralindizes und Partial Least Squares. In dieser Studie wurden Feldversuche durchgeführt, um die Fähigkeit von optimierten Spektralindizes und Partial Least Squares (PLS) in der Abschätzung vom Chlorophyllgehalt im Blatt von Reis aus nicht destruktiven Reflexionsmessungen zu prüfen. Wir integrierten Techniken, die die Optimierung von Spektralindizes mit engen Bandbreiten und zur Detektion der Red-Edge Position involvieren, um einen Typ der Spektralindizes zu optimieren: Ratio of Reflectance Difference Index (RRDI) für die Abschätzung vom Chlorophyllgehalt im Blatt. Der optimierte $RRDI = (R_{745} - R_{740}) / (R_{740} - R_{700})$ erklärte 62%-72% von der Variabilität im Chlorophyllgehalt im Blatt mit einem RMSE von 4.59-4.89 $\mu\text{g}/\text{cm}^2$. Verglichen mit Spektralindizes verbesserte PLS die Abschätzung vom Chlorophyllgehalt im Blatt mit einem RMSE jeweils von 0.85 und 3.22 $\mu\text{g}/\text{cm}^2$. Letztendlich wurden das Model basierend auf RRDI und das PLS Model weiter mit einem unabhängigen Datensatz, der auf Feldern von Landwirten erhoben worden ist, validiert. RRDI und PLS Modelle erbrachten eine akzeptierbare Genauigkeit mit jeweils einem R^2 von 0.49 und 0.55 und einem RMSE von 5.47 und 5.13 $\mu\text{g}/\text{cm}^2$. Unsere Ergebnisse unterstreichen das Potential für die Optimierung von Spektralindizes aber auch die Bedeutung von PLS für die Bestandskartierung von biochemischen Variationen.

3.1 Introduction

Rice is one of the main agricultural crops in Northeast China. The Sanjiang Plain is well known for large scale farming in China and is becoming more and more important in supplying the food market with commercial rice of high quality (Yao *et al.*, 2012). For a high-yield and environment-friendly agricultural development, real-time monitoring of the growth status of rice is crucial to this region.

Remote sensing is increasingly being used in agricultural applications owing to its potential for noninvasively gathering information over larger areas (Atzberger, 2013; Mulla, 2013). Hyperspectral remote sensing of crop nutrient status is mainly based on the estimation of leaf chlorophyll (Chl), which absorbs and converts solar light to biochemical energy and thus often serves as an indicator of plant stresses (Filella & Peñuelas, 1994). Recent studies have shown great potential of hyperspectral remote sensing for the estimation of leaf chlorophyll (Zarco-Tejada *et al.*, 2001), plant nitrogen (N) (Yu *et al.*, 2013), leaf area index (LAI) (Darvishzadeh *et al.*, 2009), biomass (Gnyu *et al.*, 2013; 2014; Koppe *et al.*, 2012) and for disease detection (Delalieux *et al.*, 2009; Laudien & Bareth, 2006; Laudien *et al.*, 2006).

The red edge (ca. 680-750 nm) of spectra is of particular interest for estimating leaf chlorophyll content (Filella & Peñuelas, 1994; Main *et al.*, 2011). The red edge position (λ_{RE}) is defined as the wavelength of the peak (local maximum) on the first derivative reflectance spectra (Horler *et al.*, 1983). Generally, λ_{RE} shifts to longer wavelengths with the increase of Chl content (Filella & Peñuelas, 1994). Several studies have found that two or more peaks in red edge can be derived from the derivative spectra (Horler *et al.*, 1983; Zarco-Tejada *et al.*, 2002). Horler *et al.* (1983) suggested that the first peak at around 700 nm is determined mainly by chlorophyll content while the second peak at around 725 nm is governed more by scattering effects.

Recent studies have shown that optimized narrow band spectral indices perform better than broad band indices for the estimation of Chl and LAI (Darvishzadeh *et al.*, 2008; 2009). In most of these studies narrow band indices take the forms of Simple Ratio (SR) and Normalized Difference Vegetation Index (NDVI) to find the best band combinations. Yu *et al.* (2012) found that the optimized SR- and NDVI-like indices have similar sensitive bands and provide equal ability to estimate Chl.

The objective of this study is to estimate leaf Chl content of rice by optimizing spectral indices and using partial least squares (PLS).

3.2 Material and methods

3.2.1 Study area, experimental and farmer fields

The study area is located in the Sanjiang Plain, Heilongjiang Province, China. Sanjiang Plain was originally dominated by marshes and it was converted to agricultural production land since last six decades (Yao *et al.*, 2012). The climate in this region is cool-temperate subhumid continental monsoon, with very cold winters and warm summers. The climatic characteristics of Sanjiang Plain are suitable for rice, soybeans, wheat, and corn crops, and rice farming has become dominant land use in this region since last two decades. More information about the Sanjiang Plain has been described elsewhere (Gnyp *et al.*, 2013; Yao *et al.*, 2012; Yu *et al.*, 2013). In this study, two field experiments (Expt. 1 and Expt. 2) were conducted, and 14 farmer fields were selected for data collection.

Expt. 1: The N rate experiment was conducted at two sites: Qixing and Keyansuo experimental stations with a same experimental design in 2008. A randomized complete block design with four replications including five N rates (0, 35, 70, 105 and 140 kg N ha⁻¹ as urea) was applied at both stations, where a local rice cultivar *Kongyu 131* was planted. 60 kg ha⁻¹ P₂O₅ (as triple super-phosphate) and 75 kg ha⁻¹ K₂O (as potassium sulfate) were applied to ensure the supply of other nutrients. All plots had the same size of 100 m² (10 by 10 m).

Expt. 2: Similar design with Expt. 1, Expt. 2 was conducted under five N levels that used 70% of each of the five rates of Expt. 1, respectively. The same cultivar *Kongyu 131* and same amount of P- and K-fertilizers were used.

Farmer fields: In addition to the experimental fields, 14 farmer fields managed by two farmers were selected for data collection, which is to be used as the validation dataset. The same cultivar *Kongyu 131* was planted in those farmer fields.

3.2.2 Spectral measurement

Hyperspectral reflectance data was measured from a height of 30 cm above the rice canopy under clear sky conditions within 2 hours of solar noon, using the FieldSpec 3 spectroradiometer (Analytical Spectral Devices, Inc., Boulder, CO, USA) connected to a fiber foreoptic that has a 25 degree field-of-view. The FieldSpec 3 spectroradiometer operates in the 350–2500 nm spectral region and has a spectral resolution of 3 nm at 700 nm, 10 nm at 1400 and 2100 nm. The detailed description of FieldSpec 3 can be found in (Gnyp *et al.*, 2013). Hyperspectral reflectance data in 1 nm steps were automatically outputted by the spectroradiometer. We used the reflectance data of 350–900 nm in this study due to the specific interest in Chl.

3.2.3 Leaf chlorophyll measurement

On the same day of spectral measurements, leaf chlorophyll was measured using a SPAD-502 (Konica Minolta, Inc.) chlorophyll meter. In those spectroradiometer-scanned plants, a total of 10-15 newest fully expanded leaves were selected for recording SPAD values. For each leaf, 3 replicates were recorded in the middle of leaf base to tip and then averaged. Finally, SPAD values were transformed to the area based leaf chlorophyll content (Chl, $\mu\text{g}/\text{cm}^2$) using an empirically calibrated function commonly used in remote sensing studies (Atzberger et al., 2003; Darvishzadeh et al., 2008; Markwell et al., 1995).

3.2.4 Reflectance indices

A NDVI-like index: The Normalized reflectance difference index (NRDI, Eq. (3-1)) was optimized using a lambda-by-lambda band optimization method, which has been widely used in recent studies (Darvishzadeh et al., 2008; 2009; Yu et al., 2013).

$$NRDI = \frac{R_{\lambda_1} - R_{\lambda_2}}{R_{\lambda_1} + R_{\lambda_2}} \quad (3-1)$$

where R_λ is the reflectance at the wavelength λ .

To test whether we can further improve the robustness of optimized indices, we made a hypothesis, which assumes that R_c is the reflectance in response primarily to chlorophyll and is a function of the wavelength λ , i.e., $R_c = f(\lambda)$. However, due to effects of soil, water background and phenological development, measured canopy reflectance (R) can be further assumed as a function of R_c that has multiplicative and additive factors a and b across wavelengths, respectively (Eq. (3-2)).

$$R = a * f(\lambda) + b \quad (3-2)$$

Although such a linear hypothesis is rare in nature, we expect that it might reduce adverse effects. With measured reflectance, R_c could be calculated by eliminating the factors a and b following Eq. (3-3),

$$R_c = (R - b) / a \quad (3-3)$$

However, a and b are difficult to determine, an alternative approach to eliminate a and b is to use the ratio of reflectance difference as shown in Eq. (3-4),

$$\frac{R_{c,\lambda_1} - R_{c,\lambda_2}}{R_{c,\lambda_3} - R_{c,\lambda_4}} = \frac{R_{\lambda_1} - R_{\lambda_2}}{R_{\lambda_3} - R_{\lambda_4}} \quad (3-4)$$

Finally, we define the Ratio of Reflectance Difference Index (RRDI, Eq. (3-5)):

$$RRDI = \frac{R_{\lambda_1} - R_{\lambda_2}}{R_{\lambda_3} - R_{\lambda_4}} \quad (3-5)$$

, for which λ 1-4 are random wavelengths to be optimized for the estimation of Chl.

3.2.5 PLS model

In addition to the optimization of spectral indices, PLS was also used to estimate Chl in this study. PLS has the advantage that the precision of the model improves with the increasing number of variables and observations (Wold *et al.*, 2001). To optimize the number of factors (latent variables), leave-one-out cross validation was used to test the significance of the increase in the predicted residual sum of squares (PRESS) (van der Voet, 1994).

3.3 Results

3.3.1 NRDl optimization

All possible 2-band combinations of λ_1 and λ_2 were examined for the correlation with Chl. Figure 3-1A shows the lambda-by-lambda R^2 plot for the NRDIs. The highest R^2 values were yielded by the red edge bands paired with NIR bands.

Figure 3-1B shows the best NRDl with λ_1 and λ_2 respectively at 745 and 740 nm, which yielded the highest R^2 . The best NRDl = $(R_{745} - R_{740}) / (R_{745} + R_{740})$ accounted for 70% of the variation in Chl with RMSE of 4.8 $\mu\text{g}/\text{cm}^2$ (Figure 3-1B).

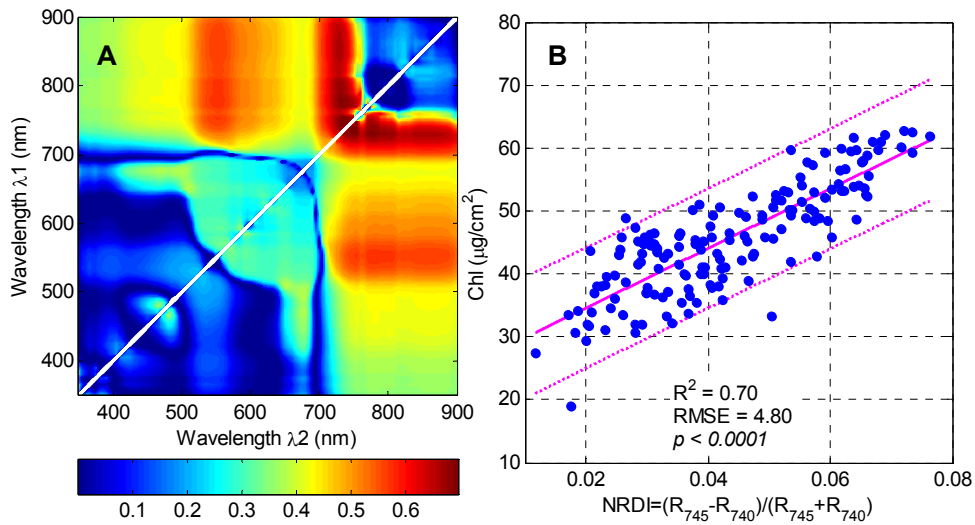


Figure 3-1: (A) Lambda-by-lambda R^2 plot showing the performance of different band combinations of λ_1 and λ_2 for the optimization of NRDI. (B) Scatter plot showing the relationship between Chl and the best 2-band combination of λ_1 and λ_2 derived from Figure 3-1A.

3.3.2 Red edge position

The red edge position (λ_{RE}) was determined as the maximum of the first derivative of the reflectance. Figure 3-2 shows that λ_{RE} ranged from 700 to 740 nm and yielded significant difference only when N rate was higher than 105 kg/ha. The N rates of 105 and 140 kg/ha led to the λ_{RE} shift to longer wavelengths and yielded higher values of λ_{RE} compared to the low-N rates.

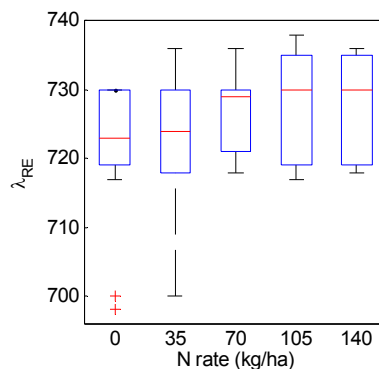


Figure 3-2: Boxplot showing the changes in red edge position (λ_{RE}) between different N rates.

To investigate the response of λ_{RE} to Chl variations, Chl was plotted as a function of λ_{RE} . Figure 3-3 shows that λ_{RE} was positively related to Chl. The highest value of λ_{RE} , ca. 740 (nm), corresponded to the highest Chl content that was 65 $\mu\text{g}/\text{cm}^2$ approximately.

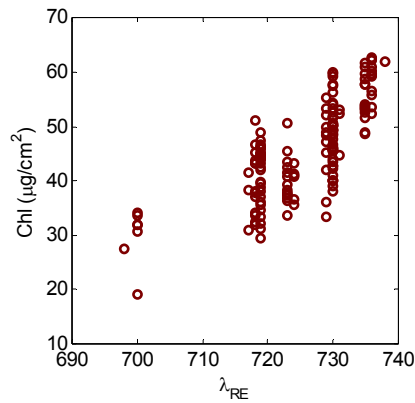


Figure 3-3: Leaf chlorophyll content (Chl, $\mu\text{g}/\text{cm}^2$) plotted as a function of the red edge position (λ_{RE}).

3.3.3 RRDI optimization

The RRDI was optimized based on the best λ_1 and λ_2 of NRDI. All possible combinations of λ_3 and λ_4 were further examined for the correlation with Chl. Figure 3-4 shows that RRDI generously increased the sensitivity to Chl across the whole wavelength range compared to NRDI (cf. Figure 3-1A).

One of the significantly hot zones for λ_3 vs. λ_4 locates in the wavelengths of 700-740 nm, which agrees well with the range of λ_{RE} (Figure 3-2 and Figure 3-3). Therefore, the λ_3 vs. λ_4 were determined as 740 and 700 nm, respectively, for the best RRDI.

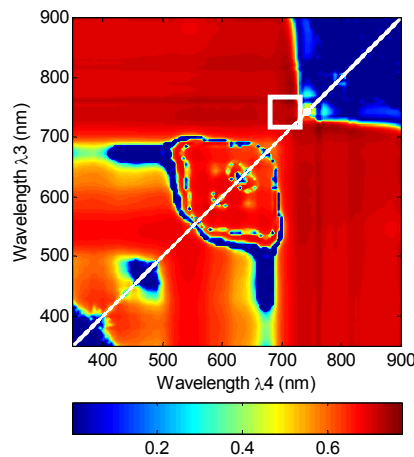


Figure 3-4: Lambda-by-lambda R^2 plot showing the performance of different band combinations of λ_3 vs. λ_4 for the RRDI. White rectangle highlights the red edge range of 700-740 nm.

The best RRDI = $(R_{745} - R_{740}) / (R_{740} - R_{700})$ accounted for 72% of the variation in Chl with RMSE of $4.59 \mu\text{g}/\text{cm}^2$ (Table 3-1).

Expt. 2 dataset was used to test the reliability of the best NRDI and RRDI for the estimation of Chl. Results show that NRDI and RRDI accounted for 60% and 62% of the variation in Chl, respectively, with RMSE of 4.77 and 4.63 $\mu\text{g}/\text{cm}^2$ (Table 3-1).

3.3.4 Chl estimation for farmer fields

Regression models based on RRDI and NRDI were calibrated using the pooled data of two experiments and were applied to farmer fields for the estimation of Chl.

Figure 3-5 shows the calibration results for RRDI and NRDI. RRDI and NRDI accounted for 65% and 62% of the variation in Chl of pooled data (Expt. 1+2), respectively.

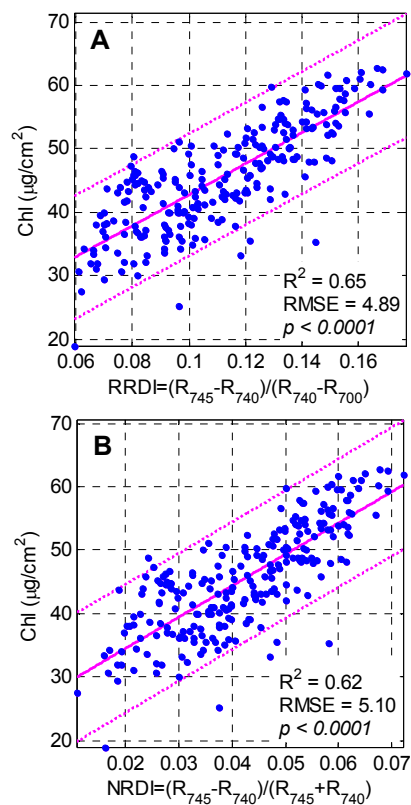


Figure 3-5: (A) RRDI model based on the pooled experimental data (Expt. 1+2). (B) NRDI model based on the pooled data.

Table 3-1 summarizes both the calibration and validation results for farmer fields. The R^2 for the predicted Chl by RRDI and NRDI against the measured Chl were 0.49 and 0.45, respectively, with RMSE of 5.47 and 5.68 $\mu\text{g}/\text{cm}^2$ (Figure 3-6A, B and Table 3-1).

3.3.5 Chl estimation for farmer fields using PLS model

PLS model was also calibrated using the pooled data of two experiments. Results showed that PLS model accounted for 85% of the variation in Chl (Table 3-1) with RMSE of 3.22 $\mu\text{g}/\text{cm}^2$.

The calibrated PLS model was further used to estimate the Chl of farmer fields. Figure 3-6C shows that R^2 for the predicted Chl by PLS against the measured Chl was 0.55 with RMSE of 5.13 $\mu\text{g}/\text{cm}^2$.

PLS model accounted for a larger portion of the variation in Chl of both experimental and farmer fields and yielded lower RMSE compared to the univariate regression models based on NRDI and RRDI (Table 3-1 and Figure 3-6).

Table 3-1: Results of R^2 and RMSE ($\mu\text{g}/\text{cm}^2$) for different datasets using NRDI= $(R_{745}-R_{740})/(R_{745}+R_{740})$, RRDI= $(R_{745}-R_{740})/(R_{740}-R_{700})$ and PLS model.

Dataset	Description	n	NRDI		RRDI		PLS	
			R^2	RMSE	R^2	RMSE	R^2	RMSE
Expt. 1	Optimize Indices	160	0.70	4.80	0.72	4.59		
Expt. 2	Test Indices	80	0.60	4.77	0.62	4.63		
Expt. 1+2	Model Calibration	240	0.62	5.10	0.65	4.89	0.85	3.22
Farmer fields	Model Validation	70	0.45	5.68	0.49	5.47	0.55	5.13

n, number of observations

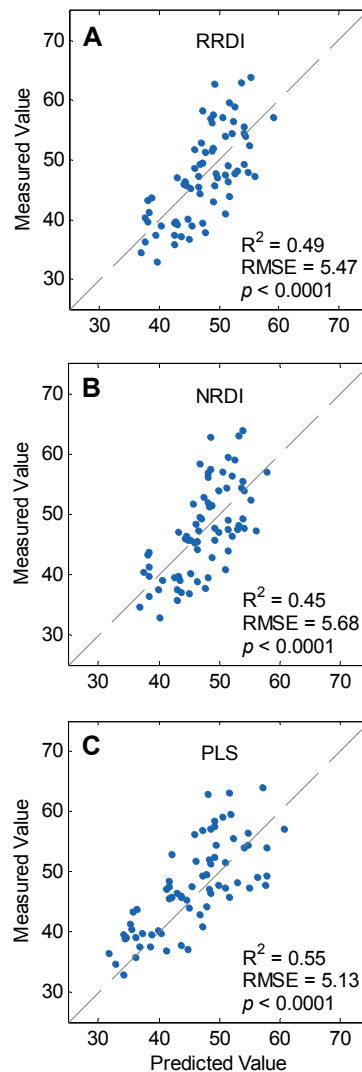


Figure 3-6: Scatter plots showing the measured by predicted values of Chl using (A) RRDI, (B) NRDI and (C) PLS models calibrated on the pooled data of two experiments (Expt. 1+2). Dashed line is the 1:1 line.

3.4 Discussion

The lambda-by-lambda band optimization method has been used to optimize NDVI- and SR-like indices for the estimation of canopy characteristics in different species (Darvishzadeh et al., 2008; 2009; Yu et al., 2012; 2013). However, the potential of linking red edge characteristics to the optimization of NDVI- or SR-like indices have not been fully explored. As shown in the lambda-by-lambda R^2 plots, the RRDI optimization increases the sensitivity over the entire wavelengths compared to NRDI (Figure 3-1 and Figure 3-4). In addition to the significant zone at red edge range, the range for NIR vs. red edge (e.g., 760-820 vs. 720 nm) also showed the best performance. However, the NIR range is governed primarily by LAI (Darvishzadeh et al., 2008), thus the red edge might be more appropriate for Chl estimation.

The best $RRDI = (R_{745} - R_{740}) / (R_{740} - R_{700})$ could be considered as the ratio of derivative of reflectance at 740 nm (i.e., $d\lambda_{740} = (\lambda_{745} - \lambda_{740})/5$) and the relative change in the red edge positions. Similarly, [Lee et al. \(2008\)](#) found that the derivative of reflectance at 735 nm could be used to estimate rice N. Soil background is one of the main factors that affect the hyperspectral remote sensing of leaf chlorophyll. [Darvishzadeh et al. \(2008\)](#) optimized the SAVI2 type indices to estimate Chl and found that it yielded equivalent accuracy in terms of RMSE compared to narrow band NDVI, i.e., NRDI in this study. However, the optimization of SAVI2 type indices requires the soil-line coefficients, which are difficult to determine for this study due to the flooding environment of rice field. Our results suggest that RRDI seems to be able to reduce to some extent the effects of soil, water background and phenological development compared to NRDI.

As expected, PLS outperformed both the optimized NRDI and RRDI and resulted in lower RMSE. Both NRDI and RRDI showed the underestimation of high Chl values compared to PLS model (Figure 3-6). This corroborates the suggestion to use PLS for the full spectrum analysis ([Atzberger et al., 2003](#)). However, the determination of sensitive bands and optimization of spectral indices might be useful as an early indicator of plant physiological status and potential stresses before a more precisely quantitative approach made by full spectrum analysis.

Considering that spectral indices serve simplicity and compatibility to different sensors having different resolutions or even a few discrete wavelength bands, the optimization of spectral indices still has practical value for applications of remote sensing in agriculture. Robust spectral indices will also contribute to the development of end-user-friendly crop sensors. Better development and validation of more complex, but more reliable, indices could be also achieved by integrating more rigorous cross-validation or bootstrap techniques ([Richter et al., 2012](#)).

3.5 Conclusions

The red edge plays a crucial role in the estimating chlorophyll (Chl), suggests potential to use red edge bands for the optimization of spectral indices. Two indices based on red edge: the Normalized Reflectance Difference Index ($NRDI = (R_{745} - R_{740}) / (R_{745} + R_{700})$) and the Ratio of Reflectance Difference Index ($RRDI = (R_{745} - R_{740}) / (R_{740} - R_{700})$) are robust indicators of leaf Chl content of rice ($R^2 = 0.60-0.72$, $RMSE = 4.59-5.1 \mu\text{g}/\text{cm}^2$) according to experimental data. They showed acceptable performance for mapping the Chl variation in farmer fields, yielding RMSE of 5.68 and 5.47 $\mu\text{g}/\text{cm}^2$, respectively, although the partial least squares (PLS) model delivered higher accuracy ($RMSE = 5.13 \mu\text{g}/\text{cm}^2$). The results show the potential of mapping canopy biochemical traits through the optimization of spectral indices and other feature reduction techniques such as PLS.

Acknowledgements

This study was supported by the China 973 Program (Grant No. 2009CBI18606), the innovative group grant of the Natural Science Foundation of China (NSFC Grant No. 31121062), German Federal Ministry of Education & Research (BMBF, Grant No. CHN 08/051) and the China Scholarship Council (CSC). We thank Y. YAO, S. HUANG, X. LI, E. DORNAUF, and J. WESKAMM for data collection; colleagues of Qixing and Keyansuo experimental stations for field management; and X. YU and J. MA for allowing the measurement in their fields.

References

- Atzberger, C., Jarmer, T., Schlerf, M., Kötz, B., Werner, W. 2003.** Spectroradiometric determination of wheat bio-physical variables. Comparison of different empirical-statistical approaches. In: R. Goossens (Ed.) *Remote Sensing in Transitions. Proc. 23rd EARSeL Symposium*. 2 – 5 June 2003. Belgium, pp. 463-470.
- Atzberger, C. 2013.** Advances in remote sensing of agriculture: Context description, existing operational monitoring systems and major information needs. *Remote Sens.* **5**: 949-981.
- Darvishzadeh, R., Skidmore, A., Schlerf, M., Atzberger, C., Corsi, F., Cho, M. 2008.** LAI and chlorophyll estimation for a heterogeneous grassland using hyperspectral measurements. *ISPRS J. Photogramm. Remote Sens.* **63**: 409-426.
- Darvishzadeh, R., Atzberger, C., Skidmore, A.K., Abkar, A.A. 2009.** Leaf Area Index derivation from hyperspectral vegetation indices and the red edge position. *Int. J. Remote Sens.* **30**: 6199-6218.
- Delalieux, S., Auwerkerken, A., Verstraeten, W., Somers, B., Valcke, R., Lhermitte, S., Keulemans, J., Coppin, P. 2009.** Hyperspectral reflectance and fluorescence imaging to detect scab induced stress in apple leaves. *Remote Sens.* **1**: 858-874.
- Filella, I., Peñuelas, J. 1994.** The red edge position and shape as indicators of plant chlorophyll content, biomass and hydric status. *Int. J. Remote Sens.* **15**: 1459-1470.
- Gnyp, M.L., Yu, K., Aasen, H., Yao, Y., Huang, S., Miao, Y., Bareth, G. 2013.** Analysis of crop reflectance for estimating biomass in rice canopies at different phenological stages. *Photogramm. Fernerkund. Geoinf.* **2013**: 351-365.
- Gnyp, M.L., Miao, Y., Yuan, F., Ustin, S.L., Yu, K., Yao, Y., Huang, S., Bareth, G. 2014.** Hyperspectral canopy sensing of paddy rice aboveground biomass at different growth stages. *Field Crops Res.* **155**: 42-55.
- Horler, D.N.H., Dockray, M., Barber, J. 1983.** The red edge of plant leaf reflectance. *Int. J. Remote Sens.* **4**: 273-288.

- Koppe, W., Gnyp, M.L., Hennig, S.D., Li, F., Miao, Y., Chen, X., Jia, L., Bareth, G. 2012.** Multi-temporal hyperspectral and radar remote sensing for estimating winter wheat biomass in the North China Plain. *Photogramm. Fernerkund. Geoinf.* **2012**: 281-298.
- Laudien, R., Bareth, G. 2006.** Multitemporal hyperspectral data analysis for regional detection of plant diseases by using a tractor-and an airborne-based spectrometer. *Photogramm. Fernerkund. Geoinf.* **2006**: 217-227.
- Laudien, R., Buercky, K., Doluschitz, R., Bareth, G. 2006.** Establishment of a web-based spectral database for the analysis of hyperspectral data from *Rhizoctonia solani*-inoculated sugarbeets. *Zuckerindustrie* **131**: 164-170.
- Lee, Y., Yang, C., Chang, K., Shen, Y. 2008.** A simple spectral index using reflectance of 735 nm to assess nitrogen status of rice canopy. *Agron. J.* **100**: 205-212.
- Main, R., Cho, M.A., Mathieu, R., O Kennedy, M.M., Ramoelo, A., Koch, S. 2011.** An investigation into robust spectral indices for leaf chlorophyll estimation. *ISPRS J. Photogramm. Remote Sens.* **66**: 751-761.
- Markwell, J., Osterman, J.C., Mitchell, J.L. 1995.** Calibration of the Minolta SPAD-502 leaf chlorophyll meter. *Photosynth. Res.* **46**: 467-472.
- Mulla, D.J. 2013.** Twenty five years of remote sensing in precision agriculture: Key advances and remaining knowledge gaps. *Biosyst. Eng.* **114**: 358-371.
- Richter, K., Atzberger, C., Hank, T.B., Mauser, W. 2012.** Derivation of biophysical variables from Earth observation data: validation and statistical measures. *J. Appl. Remote Sens.* **6**: 63551-63557.
- van der Voet, H. 1994.** Comparing the predictive accuracy of models using a simple randomization test. *Chemometr. Intell. Lab. Syst.* **25**: 313-323.
- Wold, S., Sjöström, M., Eriksson, L. 2001.** PLS-regression: a basic tool of chemometrics. *Chemometr. Intell. Lab. Syst.* **58**: 109-130.
- Yao, Y., Miao, Y., Huang, S., Gao, L., Ma, X., Zhao, G., Jiang, R., Chen, X., Zhang, F., Yu, K., Gnyp, M., Bareth, G., Liu, C., Zhao, L., Yang, W., Zhu, H. 2012.** Active canopy sensor-based precision N management strategy for rice. *Agron. Sustain. Dev.* **32**: 925-933.
- Yu, K., Lenz-Wiedemann, V., Leufen, G., Hunsche, M., Noga, G., Chen, X., Bareth, G. 2012.** Assessing hyperspectral vegetation indices for estimating leaf chlorophyll concentration of summer barley. *ISPRS Ann. Photogramm. Remote Sens. Spatial Inf. Sci.* **1-7**: 89-94.

CHAPTER 3

Yu, K., Li, F., Gnyp, M.L., Miao, Y., Bareth, G., Chen, X. 2013. Remotely detecting canopy nitrogen concentration and uptake of paddy rice in the Northeast China Plain. *ISPRS J. Photogramm. Remote Sens.* **78**: 102-115.

Zarco-Tejada, P.J., Miller, J.R., Noland, T.L., Mohammed, G.H., Sampson, P.H. 2001. Scaling-up and model inversion methods with narrowband optical indices for chlorophyll content estimation in closed forest canopies with hyperspectral data. *IEEE Trans. Geosci. Remote Sens.* **39**: 1491-1507.

Zarco-Tejada, P.J., Miller, J.R., Mohammed, G.H., Noland, T.L., Sampson, P.H. 2002. Vegetation stress detection through chlorophyll a+b estimation and fluorescence effects on hyperspectral imagery. *J. Environ. Qual.* **31**: 1433-1441.

Addresses of the Authors:

KANG YU, MARTIN LEON GNYP, Prof. Dr. GEORG BARETH, International Center for Agro-Informatics & Sustainable Development (www.icasd.org), Institute of Geography, GIS & RS Group, University of Cologne, D-50923 Köln, Tel.: +49-221-470-6551, Fax: +49-221-470-1638, e-mails: kyu@uni-koeln.de, mgnyp1@uni-koeln.de, g.bareth@uni-koeln.de

LEI GAO, Prof. Dr. YUXIN MIAO, Prof. Dr. XINPING CHEN, International Center for Agro-Informatics & Sustainable Development, Center for Resources, Environment & Food Security, College of Resources and Environmental Sciences, China Agricultural University, 100094 Beijing, Tel.: +86-10-62732865, Fax: +86-10-62731016, e-mails: jaypin@gmail.com, ymiao@cau.edu.cn, chenxp@cau.edu.cn

CHAPTER 4

Investigation of leaf diseases and estimation of chlorophyll concentration in seven barley varieties using fluorescence and hyperspectral indices^{*}

^{*} *This chapter is based on:*

Yu, K., Leufen, G., Hunsche, M., Noga, G., Chen, X., Bareth, G. 2014. Investigation of Leaf Diseases and Estimation of Chlorophyll Concentration in Seven Barley Varieties Using Fluorescence and Hyperspectral Indices. *Remote Sens.* **6**: 64-86.

Abstract

Leaf diseases, such as powdery mildew and leaf rust, frequently infect barley plants and severely affect the economic value of malting barley. Early detection of barley diseases would facilitate the timely application of fungicides. In a field experiment, we investigated the performance of fluorescence and reflectance indices on (1) detecting barley disease risks when no fungicide is applied and (2) estimating leaf chlorophyll concentration (LCC). Leaf fluorescence and canopy reflectance were weekly measured by a portable fluorescence sensor and spectroradiometer, respectively. Results showed that vegetation indices recorded at canopy level performed well for the early detection of slightly-diseased plants. The combined reflectance index, MCARI/TCARI, yielded the best discrimination between healthy and diseased plants across seven barley varieties. The blue to far-red fluorescence ratio (BFRR_UV) and OSAVI were the best fluorescence and reflectance indices for estimating LCC, respectively, yielding R^2 of 0.72 and 0.79. Partial least squares (PLS) and support vector machines (SVM) regression models further improved the use of fluorescence signals for the estimation of LCC, yielding R^2 of 0.81 and 0.84, respectively. Our results demonstrate that non-destructive spectral measurements are able to detect mild disease symptoms before significant losses in LCC due to diseases under natural conditions.

4.1 Introduction

Techniques for monitoring plant physiological and healthy status and their spatiotemporal variation will benefit more precise and target-oriented crop management. Cereal leaf diseases such as powdery mildew and leaf rust frequently infect barley plants and affect the economic value of malting barley. Chlorophyll plays a crucial role for the photosynthetic processes including light harvesting and energy conversion, and thus the content of chlorophyll is a potential indicator of a range of stresses (Zarco-Tejada *et al.*, 2002). Early detection of crop diseases and accurate assessment of chlorophyll variations are important to help crop managers to efficiently make applications of agrochemicals and fertilizers (Bürling *et al.*, 2010; Deldlieux *et al.*, 2007).

Active fluorescence techniques allow the sensing of plant physiological changes and are less affected by weather conditions than the passive ones (Chappelle *et al.*, 1984a; Tremblay *et al.*, 2012). The intensity of chlorophyll fluorescence emitted by plants is governed by both the photosynthetic activity and chlorophyll concentration (Chappelle *et al.*, 1984b). Red and far-red chlorophyll fluorescence and blue-green fluorescence (BGF) signals can be used for the detection of plant stresses as they often change before visible symptoms are detectable, for example water deficiency and heat stresses often lead to an increase in BGF and chlorophyll fluorescence, respectively (Lang *et al.*, 1996; Leufen *et al.*, 2013; Lichtenthaler, 1996).

Spectrally resolved fluorescence signals are typically expressed in the form of fluorescence ratios in order to be less dependent on instruments, on the intensity of exciting light and the distance of fluorescence detection (Buschmann, 2007; Lejealle *et al.*, 2010). The red/far-red chlorophyll fluorescence ratio (RF/FRF) is determined primarily by the *in vivo* chlorophyll content, of which the high amount has more reabsorption of RF while little effect on the FRF (Gitelson *et al.*, 1998; Lichtenthaler & Rinderle, 1988; Lichtenthaler & Babani, 2004). Hence, the decline in chlorophyll content caused by biotic or abiotic stresses often result in an increase of RF/FRF (Lichtenthaler & Miehé, 1997; Lichtenthaler & Babani, 2004). In contrast, Gitelson *et al.* (1999) suggested that the inverse form as far-red/red fluorescence ratio (FRF/RF) might be more precise for quantifying the chlorophyll in a wide range. Although fluorescence indices allow the non-invasive estimation of chlorophyll content, it is often unavoidable that they are nonlinearly related to chlorophyll content and lose the sensitivity when chlorophyll reaches a certain level (Babani & Lichtenthaler, 1996; Gitelson *et al.*, 1999; Lichtenthaler *et al.*, 2005). Therefore, comprehensive algorithms might be useful to improve the use of fluorescence signals in such situations. Partial least squares (PLS) (Wold *et al.*, 2001a) and support vector machines (SVM) (Vapnik, 1995) have been widely used in hyperspectral remote sensing studies (Hansen & Schjoerring, 2003; Plaza *et al.*, 2009). The partial least squares (PLS) method has the desirable

property that solves not only the problem of strong co-linearity but also the problem of regression singularity due to small sample size and high dimension of predictive variables (Wold *et al.*, 2001a). PLS is particularly relevant in the situation where modeling data consist of many predictors relative to the number of observations (Atzberger *et al.*, 2010). Atzberger *et al.* (2010) highlighted the advantage of PLS in dealing with multi-collinearity over stepwise multiple linear and principal component regressions, even when the number of observations was smaller than the number of predictive variables. The support vector machines (SVM) method has been widely used for classification problems (Mountrakis *et al.*, 2011; Plaza *et al.*, 2009; Römer *et al.*, 2011; Zheng *et al.*, 2010) and for retrieving biophysical parameters (Durbha *et al.*, 2007; Sun *et al.*, 2012). For non-linear problems in particular, the SVM transforms the nonlinearity into a linear regression via mapping the original input space to a high dimensional feature space (Vapnik, 1998).

Blue/red (BF/RF) and blue/far-red (BF/FRF) fluorescence ratios and combined fluorescence indices also allow to detect various stresses (Bürling *et al.*, 2011; Lang *et al.*, 1996) such as water (Leufen *et al.*, 2013) and nitrogen (N) deficiencies (Agati *et al.*, 2013; Lejealle *et al.*, 2010; Zhang *et al.*, 2012) and to monitor changes in chlorophyll and polyphenols (Cеровic *et al.*, 2008; Lejealle *et al.*, 2010). However, studies on detecting cereal diseases or estimating chlorophyll content of barley plants are scarce. Buschmann & Lichtenthaler (1998) reported that maize plants grown without nitrogen yield higher blue-green fluorescence and also the higher values of the fluorescence ratios BF/FRF and BF/RF. Langsdorf *et al.* (2000) also found that BF/RF and BF/FRF ratios are the most sensitive indicators to distinguish different N treatments. As aforementioned, fluorescence indices for chlorophyll are of potential for detecting diseases, as well as for estimating leaf N content since leaf chlorophyll is related to leaf N content (Cartelat *et al.*, 2005; Tremblay *et al.*, 2012). However, how early fluorescence indices can sense cereal diseases is not well known as diseases may precede significant losses in chlorophyll or N (Zarco-Tejada *et al.*, 2000). Furthermore, under natural conditions the changes in fluorescence signals/indices in response to foliar diseases are usually caused by cross infections.

Recent studies have made progress on detecting diseases and nutrient stresses by hyperspectral remote sensing (Agati *et al.*, 2013; Delalieux *et al.*, 2009a; 2009b; Miphokasap *et al.*, 2012). Reflectance indices have been suggested for detecting diseases such as apple leaf scab disease under well controlled conditions (Delalieux *et al.*, 2009a; 2009b). However, the discriminatory performances are often affected by plant phenological development (Delalieux *et al.*, 2009b). Therefore, comparisons between different hyperspectral indices are still needed to determine which method is most appropriate and which index is most reliable across phenological stages for the early detection of plant diseases, as well as between different fluorescence indices.

The objective of this study was (i) to investigate the performance of fluorescence and reflectance indices for detecting diseases in seven varieties of field grown barley and (ii) to estimate leaf chlorophyll concentration (LCC) using these indices, and PLS and SVM methods.

4.2 Materials and methods

4.2.1 Experimental design

The field experiment of barley (*Hordeum vulgare*) was conducted at the Institute of Crop Science and Resource Conservation (INRES-Horticultural Science, 50.7299 ° N, 7.0754 ° E; 70 m.a.s.l.), University of Bonn, Germany. The soil is sandy loam with the N_{\min} value of 20 kg N ha⁻¹. The annual average precipitation and temperature are 669 mm and 10.3 °C, respectively. The experiment was organized as a completely randomized block with three replications and a plot size of 6 m² (4 × 1.5 m) for each variety and fungicide treatment. Ten rows of barley plants sown with a density of 320 seeds per square meter were grown in each plot. The experimental design included seven barley varieties (Belana, Marthe, Scarlett, Iron, Sunshine, Barke and Bambina) and two fungicide variants (with fungicide and without fungicide).

For the treatment group with fungicide, plants were regularly sprayed with protective or curative fungicides over the entire experimental period, while for the treatment group without fungicide no fungicides were sprayed. The seven commercial varieties of malting barley were sown on March 24th 2010. All plots were fertilized immediately after sowing with ammonium nitrate (NH₄⁺-N) at the rate of 100 kg N ha⁻¹.

For the plants of without fungicide plots the infections were generally mild and showed only a few punctiform symptoms due to the unfavorable climatic conditions to pathogens at the study site in 2010.

4.2.2 Fluorescence measurements

Random plants were preselected and marked prior to the implementation of treatment design of fungicide. From these plants, six uppermost fully expanded flag leaves were randomly sampled, stored in a cold box and immediately transported into the lab for the fluorescence measurements. The fluorescence recordings were carried out at the beginning of June up to July at weekly intervals on five dates; June 9th (77 DAS, days after sowing), June 15th (83 DAS), June 22th (90 DAS), June 29th (97 DAS) and July 6th (104 DAS). A multi-parametric fluorescence sensor, Multiplex® 3 (Ben Ghozlen et al., 2010), was used in this study for the recording of fluorescence signals. Barley leaves were placed on a black anodized plate for measuring the fluorescence indices at room temperature

in the lab. The mean readings of the six leaves of each plot served as the representative of each plot. Table 4-1 presents the ten fluorescence indices that were investigated in this study.

Table 4-1: Fluorescence indices used in this study.

Index	Description	Formula
SFR_G	Simple Fluorescence Ratio (green excitation)	FRF_G / RF_G
SFR_R	Simple Fluorescence Ratio (red excitation)	FRF_R / RF_R
BFRR_UV	Blue-to-Far Red Fluorescence Ratio (UV excitation)	BGF_UV / FRF_UV
FER_RUV	Fluorescence Excitation Ratio (red & UV excitation)	FRF_R / FRF_UV
FLAV	Flavonols	$\log(FER_RUV)$
FER_RG	Fluorescence Excitation Ratio (red & green excitation)	FRF_R / FRF_G
ANTH	Anthocyanins	$\log(FER_RG)$
NBI_G	Nitrogen Balance Index (SFR_G / FER_RUV)	FRF_UV / RF_G
NBI_R	Nitrogen Balance Index (SFR_R / FER_RUV)	FRF_UV / RF_R
FERARI	Fluorescence Excitation Ratio Anthocyanin Relative Index	$\log(1/FRF_R)$

4.2.3 Hyperspectral reflectance measurements

Prior to leaf sampling, canopy reflectance was measured within two hours of solar noon using QualitySpec® Pro (June 9th, and June 15th) and FieldSpec® 3 (June 22th, June 29th and July 6th) spectrometers from a distance of 1 m above the canopy. The same white reference panel (Spectralon) was used for calibrations for both spectrometers before spectral measurement in the field. In addition, our unpublished results of cross calibration showed that the reflectance difference is negligible, especially for the wavelengths shorter than 1000 nm because both spectrometers were configured with the same type of detectors (ASD Inc.). The detailed configurations of the spectrometers were described elsewhere (Yu *et al.*, 2012). For each of the experiment plots, six reflectance spectra were measured at six random locations within the plot. Finally, reflectance data with 1 nm steps was output for further analysis. Table 4-2 shows the ten reflectance indices used in this study.

Table 4-2: Reflectance indices used in this study.

Index	Formula	Reference
PSSRa	R_{800} / R_{680}	<i>Blackburn (1998)</i>
ZM	R_{750} / R_{710}	<i>Zarco-Tejada et al. (2001)</i>
NPQI	$(R_{415} - R_{435}) / (R_{415} + R_{435})$	<i>Peñuelas et al. (1995)</i>
PRI	$(R_{531} - R_{570}) / (R_{531} + R_{570})$	<i>Gamon et al. (1992)</i>
MCARI	$[(R_{700} - R_{670}) - 0.2 * (R_{700} - R_{550})] * (R_{700} / R_{670})$	<i>Daughtry et al. (2000)</i>
TCARI	$3 * [(R_{700} - R_{670}) - 0.2 * (R_{700} - R_{550})] * (R_{700} / R_{670})$	<i>Haboudane et al. (2002)</i>
OSAVI	$(1 + 0.16) * (R_{800} - R_{670}) / (R_{800} + R_{670} + 0.16)$	<i>Rondeaux et al. (1996)</i>

MCARI/OSAVI	MCARI/OSAVI	<i>Daughtry et al. (2000)</i>
TCARI/OSAVI	TCARI/OSAVI	<i>Haboudane et al. (2002)</i>
MCARI/TCARI	MCARI/TCARI	Based on <i>Daughtry et al. (2000)</i> ; <i>Haboudane et al. (2002)</i>

4.2.4 Leaf sampling and chlorophyll determination

After the fluorescence recordings, the six leaf samples of each plot were immediately frozen, free-dried, grounded and stored in the dark at room temperature for the determination of their chlorophyll content. The total chlorophyll content of each sample was extracted from 50 mg lyophilized material by 5 ml methanol, which was then filled up to 25 ml. After extraction, the absorbance of the extracts was measured with a UV-VIS spectrophotometer (Perkin-Elmer, Lambda 5, Massachusetts, USA) and the leaf chlorophyll concentration (LCC) was finally determined.

4.2.5 Data analysis

4.2.5.1 Binary Logistic Regression

To detect diseases in the without-fungicide treatment group, binary classification with logistic regression was performed. This method was successfully used in previous studies for detecting scab disease in apple leaves (*Delalieux et al., 2007; 2009a*). Logistical regression was implemented to examine the ability of each of the fluorescence and reflectance indices (Tables 4-3 and 4-2) for detecting the event of interest (disease). Accordingly, the with- and without-fungicide treatment groups correspond respectively to 0 (healthy) and 1 (diseased) in the response variable that represents health status.

The *c*-statistic was used to evaluate the discriminatory performance of different indices. The *c*-value is equivalent to the area under the receiver-operating-characteristic (ROC) curve, and it ranges from 0.5 to 1. The minimum (0.5) and maximum (1) correspond to randomly guessing and perfectly discriminating the response, respectively. The general rule that considers: $0.7 \leq c < 0.8$ as acceptable discrimination; $0.8 \leq c < 0.9$ as excellent discrimination; and $c \geq 0.9$ as outstanding discrimination (*Hosmer & Lemeshow, 2000*) was used to evaluate the discriminatory performance.

4.2.5.2 Partial Least Squares Regression

The partial least squares (PLS) method was originally developed by the econometrician *Herman Wold (1966)*, for use in econometrics for modeling of multivariate time series (*Wold, 2001b*). The widely used PLS regression (PLSR), which is the simplest PLS approach for linear

multivariate modeling, has the advantage that the precision of the model improves with the increasing number of variables and observations (Wold et al., 2001a).

The predictive and response variables are considered as two blocks of variables in the PLSR method (Wold et al., 1989; 2001a). The key technique implemented in PLSR is to extract the latent variables (also called factors or components), which serve as new predictors and regress the response variables on these new predictors (Rosipal & Krämer, 2006). These new predictors (hereafter referred to as factors) are expected to explain the variation not only of the response variables but also the predictive variables. How much variation can be explained depends on how many factors are extracted. The more factors that are extracted the more variation can be explained. However, extracting too many factors increases the risk of model overfitting problem (i.e. tailoring the model too much to the training data, leading to the detriment of predicting future observations) (SAS Institute Inc., 2008). Cross validation is a powerful approach to determine the number of extracted factors through minimizing the prediction error (predicted residual sum of squares, PRESS). However, using the number of factors that yield the minimum in PRESS might also lead to some degree of overfitting (Haaland & Thomas, 1988). Although various cross validation methods are available, one goal is always preferred that not only a minimum number of factors be selected, but also the risk of overfitting is minimized. To achieve this goal, the statistical model comparison method proposed by van der Voet (1994) is implemented. The PLSR model implemented in this study was carried out using the SAS 9.2 software package (SAS Institute Inc.)

4.2.5.3 Support Vector Regression

The support vector machines (SVM) method is a universal theory of machine learning developed by Vapnik (1995). The main advantage of SVM is its ability to construct a linear function (e.g. classification/regression model) in a high dimensional feature space, where problems of non-linear relations of the training data in the original low dimensional space can be represented, transformed and solved. The support vector regression (SVR) is the implementation of SVM method for regression and function approximation (Smola & Schölkopf, 2004) and its standard concept and formulation are briefly described as follows:

Given a training set $\{(x_i, y_i), \dots, (x_l, y_l)\}$, where $x_i \in \mathbb{R}^n$ is a feature vector and $y \in \mathbb{R}$ is the target output (response variable). Assume that there is a linear function:

$$\hat{y} = f(x) = \omega \cdot x + b, \quad \omega \in \mathbb{R}^n, \quad b \in \mathbb{R} \quad (4-1)$$

where \hat{y} is the prediction of y_i , ω is the weight vector and b is the bias. We suppose in Eq. (4-1) the difference between \hat{y} and y is always extremely small in term of each x_i , i.e., the function $f(x)$

is powerful to predict y . Hence, in order to solve this linear problem of Eq. (4-1) SVR requires the solution of the following optimization problem:

$$\begin{aligned} & \text{minimize} \quad \frac{1}{2} \|\omega\|^2 \\ & \text{subject to} \quad \|y_i - (\omega \cdot x_i - b)\| \leq \varepsilon, \quad \varepsilon \geq 0 \end{aligned} \tag{4-2}$$

Note that the tacit assumption in Eq. (4-2) was that such a function $f(x)$ does actually exist and that $f(x)$ approximates all pairs (x_i, y_i) of the training set with the ε precision (Smola & Schölkopf, 2004). This optimization method using ε -insensitive loss function is the widely known ε -SVR (Vapnik, 1998), which is shown with a schematic in Figure 4-1. Only the points outside the shaded ε -insensitive tube are called support vectors, which are penalized, and will contribute to the optimization solution (Smola & Schölkopf, 2004).

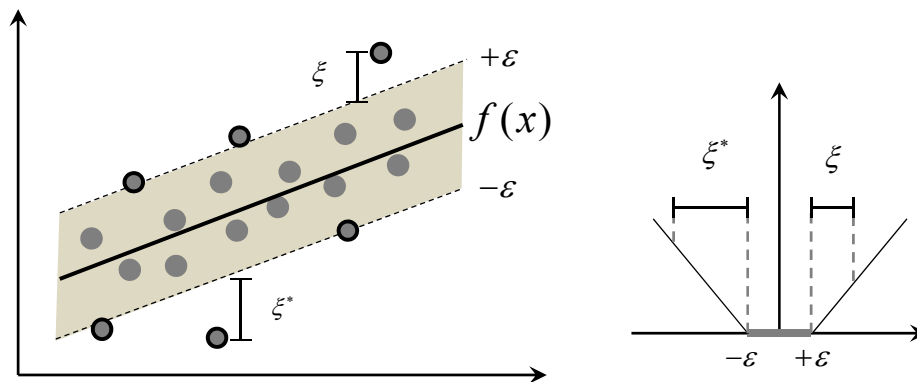


Figure 4-1: Schematic of linear support vector regression (SVR) and the ε -insensitive loss function (circles with black outline are support vectors).

Generally, when ε is under a reasonable range, the optimization problem is considered to be feasible. However, in practical application, it may not be feasible due to different kinds of noises and uncertainty. In this context, the slack variables ξ_i and ξ_i^* were introduced to permit an otherwise that some instances x_i being out of the ε precision, and then the optimization problem of Eq. (4-2) can be represented as the formulation of the standard form of SVR by Vapnik (1995) as follow:

$$\begin{aligned} & \text{minimize} \quad \frac{1}{2} \|\omega\|^2 + C \sum_{i=1}^l (\xi_i + \xi_i^*) \\ & \text{subject to} \quad \begin{cases} y_i - \omega \cdot x_i - b \leq \varepsilon + \xi_i \\ \omega \cdot x_i + b - y_i \leq \varepsilon + \xi_i^* \\ \xi_i, \xi_i^* \geq 0 \end{cases} \end{aligned} \quad (4-3)$$

where (x_i, y_i) has its corresponding ξ_i and ξ_i^* , respectively, which denotes the deviation of predicted value above $+\varepsilon$ and below $-\varepsilon$ (Figure 4-1). The parameter C is a constant to determine the tradeoff between the model complexity and the training errors (Yang et al., 2006). In addition to the ε -SVR, ν -SVR and some other kinds of SVRs, they vary in the optimization of the corresponding parameters.

Furthermore, based on kernel functions the training data will be mapped into feature space to apply the regression algorithm. Commonly used kernels include linear, polynomial, radial basis function (RBF) and sigmoid. In this study, the ε -SVR model was implemented in MATLAB R2010a (The MathWorks, Inc.) with the LIBSVM tool (Chang & Lin, 2011).

4.2.5.4 Model Validation

The performance of regression models for the estimation of LCC was evaluated by comparing the differences in the coefficients of determination (R^2) and root mean square error (RMSE) in predictions. The higher the R^2 and the lower the RMSE the higher the precision and accuracy of the model to predict LCC. The RMSE values were calculated according to Eq. (4-4),

$$RMSE = \sqrt{\frac{1}{n} \sum_{i=1}^n (y_i - \hat{y})^2} \quad (4-4)$$

where y_i and \hat{y} are the measured and the predicted values of LCC, respectively, and n is the number of samples.

4.3 Results

4.3.1 Leaf chlorophyll concentration (LCC)

Results of the repeated-measures ANOVA show that both fungicide and variety influenced LCC (Table 4-3). The effect of fungicide treatment on LCC was independent of barley variety ($p = 0.12$), and vice versa. Sampling date had a significant effect on LCC ($p < 0.0001$), as well as an interaction with fungicide treatment ($p < 0.01$). The interaction between the sampling date and

variety was not statistically significant ($p = 0.17$), and the interaction among sampling date, fungicide treatment and variety was not statistically significant ($p = 0.96$, Table 4-3).

Table 4-3: Results of repeated-measures ANOVA performed against the leaf chlorophyll concentration (LCC) of barley.

Source	DF	F	P
Fungicide	1	17.63	0.0002
Variety	6	17.10	<.0001
Fungicide × Variety	6	1.85	0.1244
Date	4	246.98	<.0001
Date × Fungicide	4	3.50	0.0099
Date × Variety	24	1.31	0.1731
Date × Fungicide × Variety	24	0.54	0.9588

As expected, LCC was higher on the first two sampling dates (77 and 83 DAS) and decreased as plants aged, irrespective of fungicide treatments (Figure 4-2). Across all varieties, LCC did not show significant differences between the with- and without-fungicide treatments until the last two sampling dates (97 and 104 DAS), where the LCC was lower in the without-fungicide treatment than the with-fungicide.

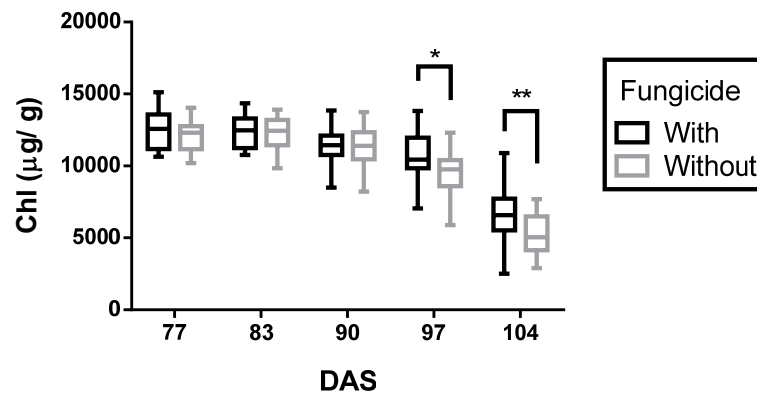


Figure 4-2: Box-and-whiskers plots showing the differences between the with- and without-fungicide treatments across varieties for each sampling date. Significant differences were observed at the last two sampling dates (*, $p < 0.05$; **, $p < 0.01$).

4.3.2 Discriminatory performances of fluorescence and hyperspectral indices

Table 4-4 shows the discriminatory performance of the ten fluorescence indices in discriminating between the with- and without-fungicide treatments. Only few indices performed acceptable ($c \geq 0.7$) discrimination for each variety on different sampling dates.

Table 4-4: The c statistic showing the performance of fluorescence indices in discriminating between the with- and without-fungicide treatments (bold font highlights c -values that are not less than 0.8).

DAS	Index	Belana	Marthe	Scarlett	Iron	Sunshine	Barke	Bambina	All
77	SFR_G	0.51	0.58	0.62	0.56	0.64	0.70	0.54	0.52
	SFR_R	0.56	0.61	0.60	0.52	0.61	0.67	0.50	0.50
	BFRR_UV	0.69	0.54	0.55	0.54	0.53	0.70	0.62	0.55
	FER_RUV	0.53	0.56	0.51	0.47	0.53	0.73	0.53	0.51
	FLAV	0.54	0.56	0.51	0.53	0.54	0.73	0.54	0.51
	FER_RG	0.57	0.54	0.54	0.54	0.52	0.63	0.57	0.52
	ANTH	0.56	0.54	0.54	0.55	0.52	0.62	0.57	0.53
	NBI_G	0.51	0.50	0.52	0.60	0.52	0.65	0.47	0.52
	NBI_R	0.51	0.52	0.50	0.57	0.52	0.68	0.47	0.52
FERARI	0.73	0.53	0.60	0.73	0.65	0.72	0.73	0.56	
83	SFR_G	0.55	0.65	0.58	0.83	0.55	0.65	0.52	0.61
	SFR_R	0.53	0.65	0.54	0.86	0.59	0.65	0.47	0.62
	BFRR_UV	0.52	0.57	0.62	0.81	0.58	0.67	0.72	0.59
	FER_RUV	0.62	0.58	0.57	0.87	0.54	0.53	0.64	0.55
	FLAV	0.63	0.58	0.57	0.87	0.55	0.53	0.64	0.55
	FER_RG	0.72	0.55	0.60	0.67	0.55	0.64	0.56	0.54
	ANTH	0.72	0.53	0.59	0.66	0.55	0.63	0.56	0.55
	NBI_G	0.64	0.68	0.61	0.70	0.49	0.50	0.60	0.49
	NBI_R	0.67	0.67	0.60	0.71	0.50	0.51	0.61	0.51
FERARI	0.70	0.54	0.71	0.52	0.68	0.70	0.75	0.58	
90	SFR_G	0.52	0.62	0.79	0.61	0.77	0.66	0.55	0.60
	SFR_R	0.54	0.60	0.81	0.60	0.76	0.67	0.51	0.61
	BFRR_UV	0.59	0.54	0.58	0.62	0.60	0.54	0.83	0.54
	FER_RUV	0.50	0.59	0.73	0.53	0.50	0.63	0.79	0.51
	FLAV	0.51	0.59	0.73	0.57	0.53	0.63	0.79	0.51
	FER_RG	0.82	0.68	0.68	0.61	0.62	0.70	0.46	0.62
	ANTH	0.81	0.68	0.67	0.60	0.62	0.71	0.48	0.62
	NBI_G	0.58	0.66	0.54	0.64	0.60	0.47	0.78	0.54
	NBI_R	0.53	0.66	0.56	0.62	0.61	0.55	0.78	0.53
FERARI	0.65	0.67	0.54	0.58	0.57	0.82	0.89	0.64	
97	SFR_G	0.63	0.54	0.65	0.55	0.63	0.67	0.69	0.61
	SFR_R	0.64	0.52	0.65	0.54	0.66	0.68	0.69	0.62
	BFRR_UV	0.82	0.71	0.55	0.65	0.64	0.66	0.88	0.65
	FER_RUV	0.61	0.64	0.68	0.68	0.62	0.58	0.72	0.56

	FLAV	0.61	0.64	0.68	0.68	0.62	0.58	0.72	0.56
	FER_RG	0.52	0.50	0.53	0.50	0.51	0.64	0.54	0.53
	ANTH	0.52	0.49	0.54	0.51	0.51	0.64	0.54	0.53
	NBI_G	0.65	0.61	0.57	0.67	0.60	0.70	0.79	0.60
	NBI_R	0.63	0.62	0.58	0.64	0.59	0.69	0.78	0.59
	FERARI	0.78	0.80	0.62	0.53	0.74	0.67	0.84	0.63
104	SFR_G	0.58	0.65	0.57	0.58	0.56	0.47	0.61	0.53
	SFR_R	0.56	0.63	0.55	0.56	0.53	0.54	0.63	0.51
	BFRR_UV	0.79	0.54	0.52	0.57	0.61	0.69	0.63	0.61
	FER_RUV	0.67	0.50	0.66	0.54	0.72	0.67	0.53	0.59
	FLAV	0.67	0.50	0.65	0.50	0.72	0.67	0.55	0.59
	FER_RG	0.65	0.55	0.49	0.54	0.60	0.70	0.67	0.57
	ANTH	0.65	0.55	0.48	0.54	0.60	0.70	0.67	0.57
	NBI_G	0.56	0.57	0.48	0.46	0.65	0.57	0.42	0.54
	NBI_R	0.62	0.58	0.51	0.45	0.67	0.62	0.61	0.55
	FERARI	0.66	0.54	0.52	0.52	0.61	0.59	0.69	0.57

Table 4-5 shows the performance of the ten hyperspectral indices in discriminating between the with- and without-fungicide treatments. In most cases, reflectance indices performed significant discrimination ($c \geq 0.8$), particularly at later stages. MCARI/TCARI performed best in early stages when across all varieties and yielded acceptable discrimination ($c = 0.73$) on the first sampling date (77 DAS).

Table 4-5: The c statistic showing the performance of hyperspectral indices in discriminating between the with- and without-fungicide treatments (bold font and shaded background highlight c -values that are not less than 0.8 for each variety and for all varieties, respectively).

DAS	Index	Belana	Marthe	Scarlett	Iron	Sunshine	Barke	Bambina	All
77	PSSRa	0.45	0.61	0.52	0.77	0.70	0.80	0.68	0.50
	ZM	0.60	0.72	0.55	0.71	0.67	0.84	0.80	0.57
	NPQI	0.76	0.62	0.72	0.69	0.67	0.79	0.82	0.68
	PRI	0.64	0.56	0.49	0.55	0.58	0.55	0.58	0.46
	MCARI	0.72	0.80	0.59	0.52	0.65	0.87	0.92	0.61
	TCARI	0.65	0.68	0.52	0.54	0.69	0.84	0.83	0.53
	OSAVI	0.72	0.56	0.54	0.63	0.54	0.68	0.45	0.52
	MCARI/OSAVI	0.74	0.81	0.59	0.44	0.65	0.86	0.90	0.62
	TCARI/OSAVI	0.59	0.69	0.51	0.60	0.70	0.84	0.82	0.54
	MCARI/TCARI	0.99	0.90	0.70	0.59	0.56	0.88	0.89	0.73
83	PSSRa	0.59	0.70	0.82	0.99	0.87	0.95	0.85	0.59
	ZM	0.49	0.80	0.77	0.98	0.80	0.94	0.70	0.53

CHAPTER 4

	NPQI	0.71	0.57	0.63	0.61	0.55	0.65	0.74	0.61
	PRI	0.63	0.49	0.82	0.86	0.90	0.75	0.86	0.69
	MCARI	0.85	0.68	0.68	0.54	0.65	0.93	0.79	0.66
	TCARI	0.71	0.49	0.58	0.57	0.68	0.98	0.58	0.55
	OSAVI	0.58	0.62	0.78	0.73	0.74	0.64	0.70	0.59
	MCARI/OSAVI	0.86	0.74	0.64	0.56	0.69	0.93	0.78	0.65
	TCARI/OSAVI	0.69	0.62	0.52	0.65	0.77	0.98	0.54	0.52
	MCARI/TCARI	1.00	0.88	0.95	0.73	0.51	0.81	0.96	0.80
90	PSSRa	0.82	0.51	0.98	1.00	1.00	0.73	1.00	0.77
	ZM	0.65	0.62	0.95	1.00	0.92	0.85	1.00	0.71
	NPQI	0.96	0.74	0.96	0.84	0.58	0.77	0.97	0.78
	PRI	0.86	0.70	0.98	1.00	1.00	0.65	1.00	0.86
	MCARI	1.00	0.75	0.98	0.71	0.55	0.89	0.70	0.80
	TCARI	0.92	0.70	0.84	0.55	0.65	0.90	0.55	0.66
	OSAVI	0.95	0.69	1.00	1.00	0.93	0.65	0.97	0.83
	MCARI/OSAVI	0.99	0.75	0.90	0.49	0.56	0.88	0.56	0.72
	TCARI/OSAVI	0.71	0.71	0.50	0.78	0.76	0.90	0.71	0.53
	MCARI/TCARI	1.00	0.81	1.00	0.90	0.80	0.77	1.00	0.83
97	PSSRa	0.82	0.85	1.00	0.95	0.93	0.97	0.99	0.88
	ZM	0.88	0.81	1.00	1.00	0.95	0.94	1.00	0.88
	NPQI	0.52	0.80	0.85	0.86	0.78	0.88	0.88	0.76
	PRI	0.73	0.88	0.94	0.96	0.96	0.89	0.98	0.89
	MCARI	0.51	0.65	0.90	0.74	1.00	0.84	0.71	0.73
	TCARI	0.77	0.59	0.67	0.63	0.93	0.51	0.50	0.54
	OSAVI	0.77	0.78	1.00	0.99	0.99	0.99	1.00	0.87
	MCARI/OSAVI	0.69	0.52	0.66	0.49	0.97	0.66	0.62	0.56
	TCARI/OSAVI	0.83	0.70	0.74	0.64	0.76	0.72	0.82	0.67
	MCARI/TCARI	0.76	0.86	1.00	0.74	0.77	0.97	0.93	0.82
104	PSSRa	0.77	0.93	1.00	0.99	0.86	0.98	0.96	0.90
	ZM	0.80	0.94	1.00	1.00	0.84	0.98	0.97	0.91
	NPQI	0.72	0.83	0.89	0.90	0.75	0.96	0.86	0.82
	PRI	0.85	0.84	0.62	0.94	0.84	0.90	0.87	0.78
	MCARI	0.78	0.91	1.00	0.94	0.99	0.97	0.93	0.88
	TCARI	0.79	0.88	1.00	0.87	0.96	0.89	0.86	0.85
	OSAVI	0.80	0.94	1.00	0.99	0.93	0.99	0.97	0.91
	MCARI/OSAVI	0.74	0.71	0.97	0.78	0.94	0.60	0.50	0.70
	TCARI/OSAVI	0.50	0.54	0.85	0.50	0.75	0.80	0.78	0.52
	MCARI/TCARI	0.73	0.91	1.00	0.98	0.83	0.98	0.96	0.88

On the first two sampling dates (77 and 83 DAS), SFR_R and MCARI/TCARI yielded the highest c -value compared to other fluorescence and reflectance indices, respectively. Figure 4-3 shows the ROC curves for the best performing fluorescence index (SFR_R) and reflectance index (MCARI/TCARI) on 83 DAS. MCARI/TCARI and SFR_R yielded the c -value of 0.80 and 0.62, respectively.

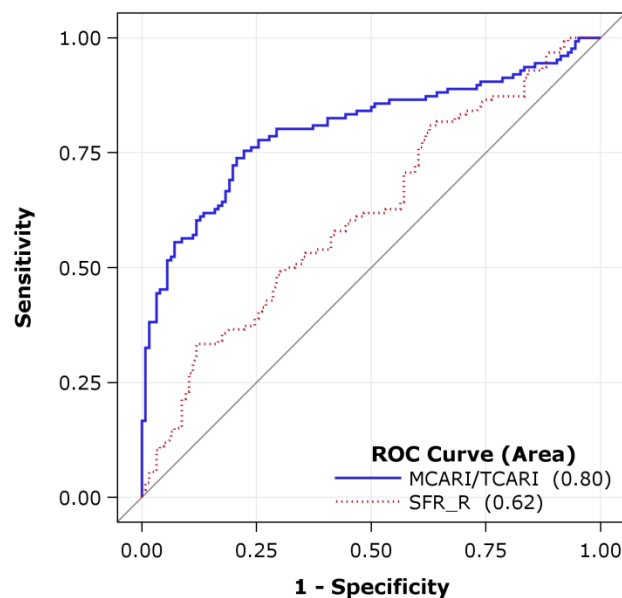


Figure 4-3: ROC plot shows the performances of MCARI/TCARI and SFR_R for the discriminating between the with- and without-fungicide treatments at the second sampling date (DAS 83). The area under ROC curves is 0.80 and 0.62 for MCARI/TCARI and SFR_R, respectively.

Figure 4-4 shows the performance of MCARI/TCARI on discriminating between the with- and without-fungicide treatments on each sampling date. The without-fungicide treatment yielded significant lower values of MCARI/TCARI than the with-fungicide treatment.

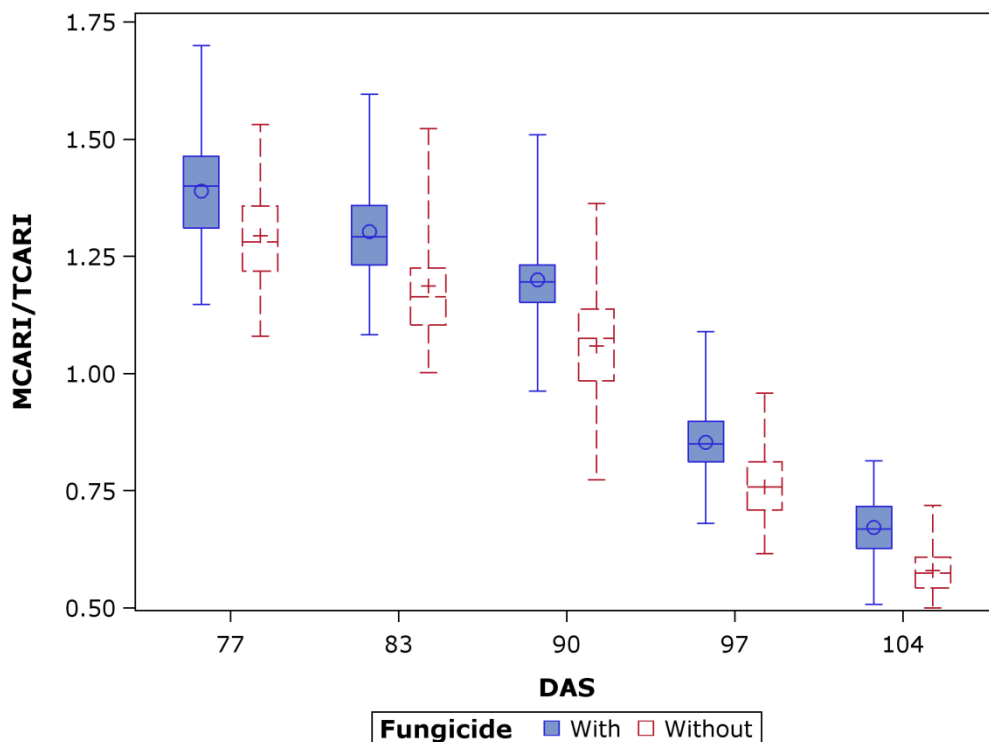


Figure 4-4: Box-and-whiskers plots showing the significant performance of MCARI/TCARI on discriminating between the with- and without-fungicide treatments. Significant ($p < 0.01$) differences between the with- and without-fungicide treatments were observed on each sampling date across all varieties (circle and plus signs show the means of the with- and without-fungicide treatments, respectively).

4.3.3 Relationships between LCC and fluorescence and hyperspectral indices

To compare the performance of different indices for estimating LCC, we divided the whole data into two parts: calibration data consisting of four varieties (Belana, Marthe, Scarlett and Iron) and validation data consisting of another three varieties (Sunshine, Barke and Bambina).

Based on the calibration data, correlation analysis was performed to examine the associations between LCC and the fluorescence and reflectance indices across all sampling dates. As shown in Figure 4-5, all the fluorescence indices were significantly correlated with the LCC across the sampling dates and varieties ($p < 0.0001$). The BFRR_UV, SFR_R and NBI_R were the best indices correlating with LCC (Figure 4-5c, b and i). All reflectance indices were significantly correlated with LCC, with the exception of TCARI ($p = 0.49$, Figure 4-5p) and MCARI/OSAVI ($p = 0.50$, Figure 4-5r).

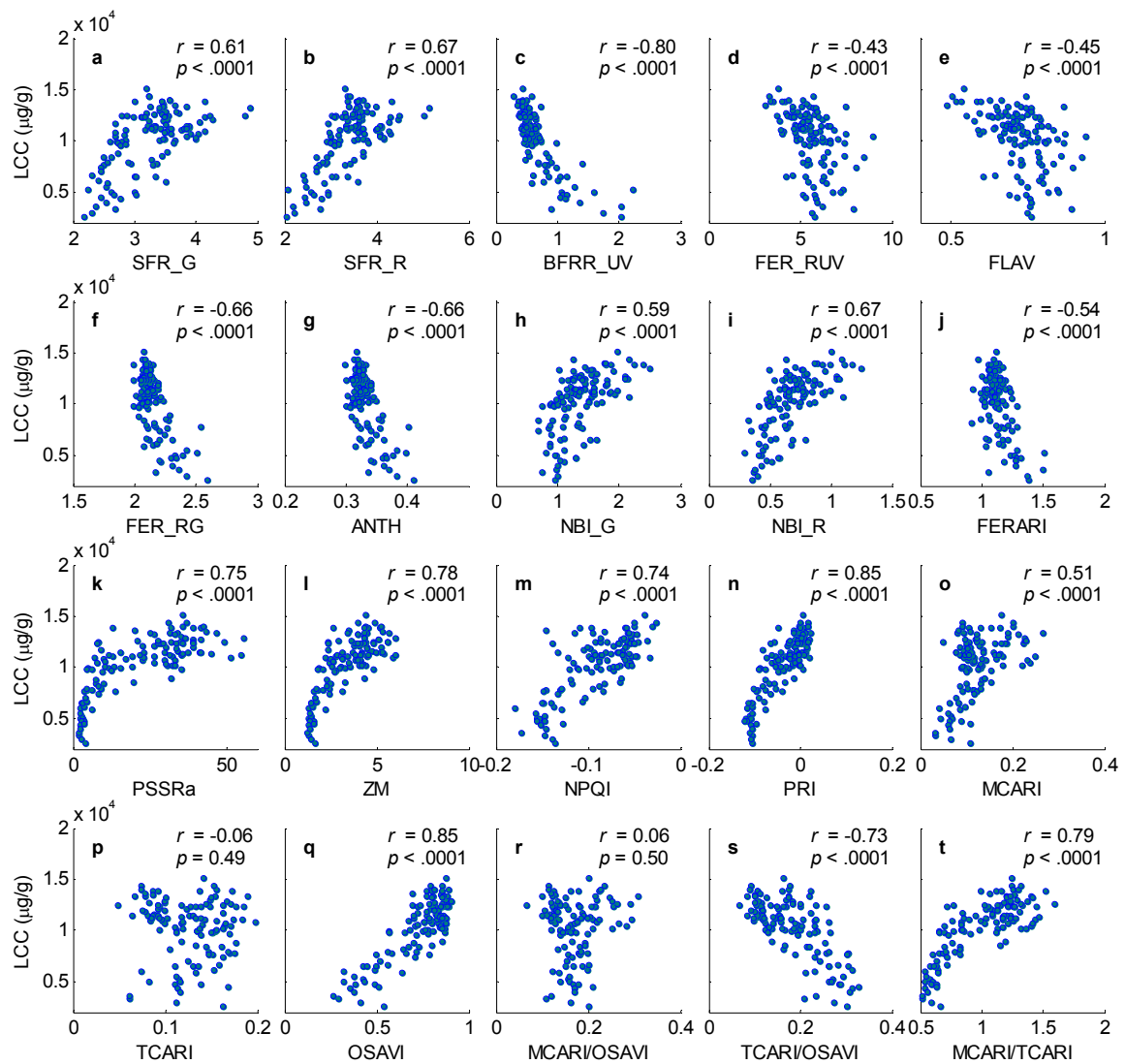


Figure 4-5: Scatter plots showing the relationships between LCC with (a-j) the ten fluorescence indices and (k-t) ten reflectance indices used in this study for the calibration data set.

4.3.4 Estimation of LCC

4.3.4.1 Polynomial Regression Model

Based on the trend of scatter points, second order polynomial regression was used to fit regression models for the three best fluorescence indices (Figure 4-6a-c) and three best reflectance indices (Figure 4-6d-f). The validation data set was used to examine the performance of the six indices in predicting LCC. Table 4-6 shows the results of the model calibration and validation for each index.

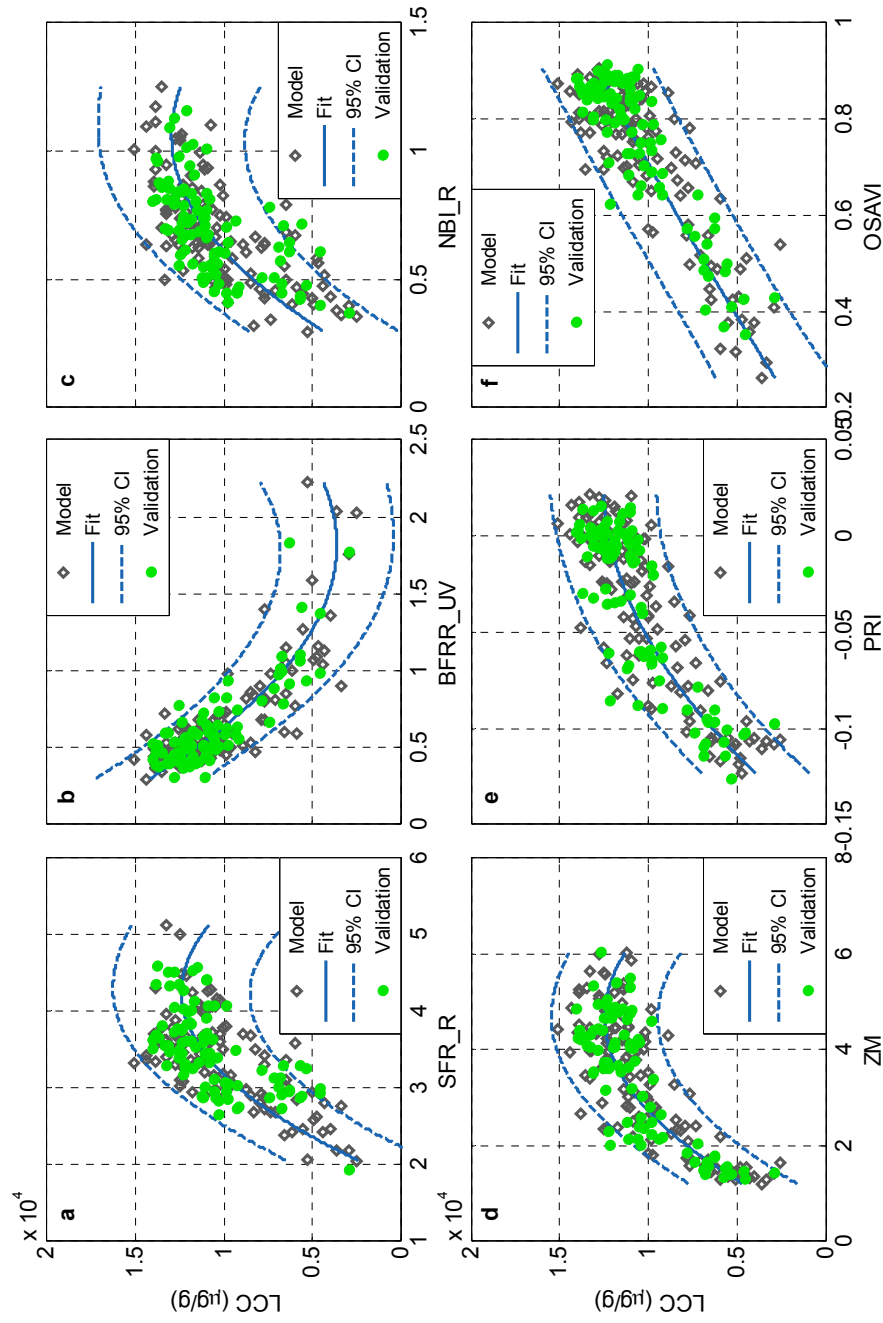


Figure 4-6: Fitting second order polynomial regression models to the calibration data for (a) SFR_R, (b) BFRR_UV, (c) NBI_R, (d) ZM, (e) PRI and (f) OSAVI and validating each of the indices for predicting LCC using the independent validation data.

For the calibration data set, SFR_R, BFRR_UV and NBI_R accounted for 57%, 73% and 52% of the variation in LCC, respectively (Table 4-6). ZM, PRI and OSAVI accounted for 74%, 75% and 72% of the variation in LCC, respectively.

For the validation data set, SFR_R, BFRR_UV and NBI_R models yielded the R² of 0.46, 0.72 and 0.42, respectively. ZM, PRI and OSAVI models yielded the R² of 0.76, 0.75 and 0.79, respectively. Figure 4-7 shows the comparison between the measured and predicted values of LCC using each of these six indices. BFRR_UV was the best fluorescence index for predicting LCC among the fluorescence indices (Figure 4-7b). OSAVI was the best reflectance index for predicting LCC among the reflectance indices (Figure 4-7f).

Table 4-6: Results of LCC estimations in calibration and validation data sets using SFR_R, BFRR_UV, NBI_R, ZM, PRI, OSAVI, partial least squares regression (PLSR) and support vector regression (SVR) (RMSE_c and RMSE_v represent root mean square errors for calibration and validation, respectively).

Model	Descriptions	Calibration		Validation	
		R ²	RMSE _c (µg/g)	R ²	RMSE _v (µg/g)
SFR_R	Polynomial	0.57	1927.3	0.46	1863.8
BFRR_UV	Polynomial	0.73	1524.0	0.72	1376.3
NBI_R	Polynomial	0.52	2040.6	0.42	1952.3
ZM	Polynomial	0.74	1500.9	0.76	1283.5
PRI	Polynomial	0.75	1471.8	0.75	1319.5
OSAVI	Polynomial	0.72	1549.0	0.79	1155.5
PLSR	6 Factors	0.84	1188.1	0.81	1111.0
SVR	RBF kernel	0.86	1094.9	0.84	1021.9

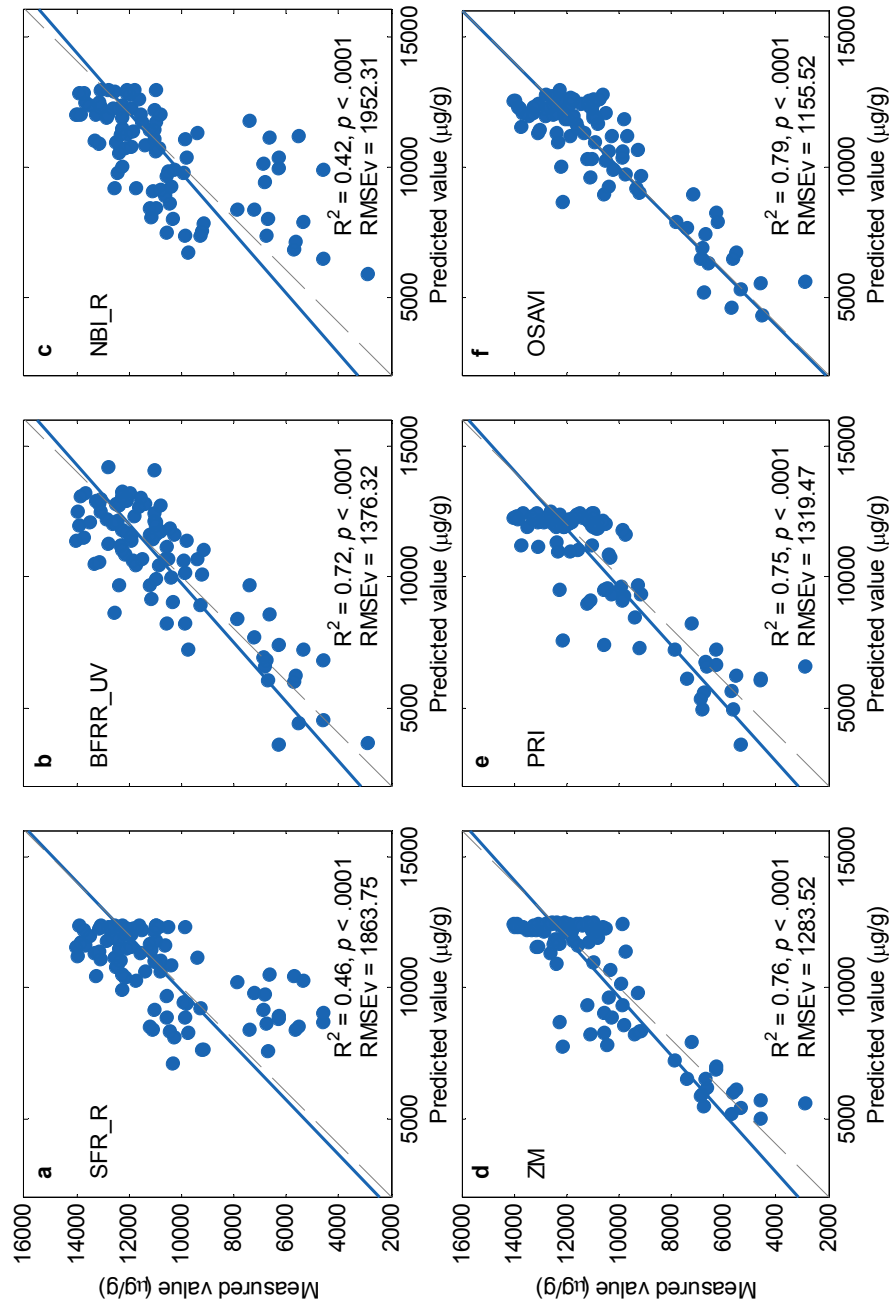


Figure 4-7: Measured-by-predicted values of LCC showing the validation results of (a) SFR_R, (b) BFRR_UV, (c) NBI_R, (d) ZM, (e) PRI and (f) OSAVI in predicting the LCC of the validation data set. Solid and dashed lines show the best linear fit and 1:1 lines, respectively.

4.3.4.2 PLSR and SVR models

Although fluorescence indices showed acceptable results, SFR_R and NBI_R still failed to account for a large portion ($R^2 < 0.5$) of the variation in LCC (Table 4-6). Therefore, multivariate regression methods were performed to improve the accuracy in estimating LCC using fluorescence signals.

PLSR and SVR models were constructed using all the available fluorescence signals/indices. They explained 84% and 86% of the variation in LCC of calibration data, respectively (Table 4-6). For the validation data, PLSR and SVR yielded R^2 of 0.81 and 0.84, respectively. Figure 4-8 shows that the consistencies between the measured and predicted values of LCC were very high and close to the 1:1 line. SVR slightly outperformed PLSR model for predicting LCC in the calibration and validation data sets. PLSR and SVR models were superior to the fluorescence and reflectance indices (Table 4-6).

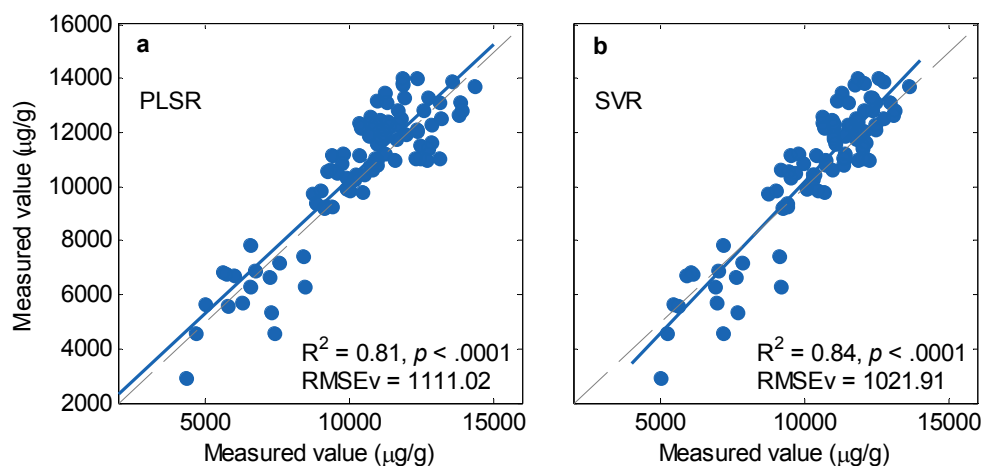


Figure 4-8: Measured-by-predicted values of LCC showing the validation results of (a) PLSR model and (b) SVR model in predicting the LCC of the validation data set. Solid and dashed lines show the best linear fit and 1:1 lines, respectively.

4.4 Discussion

4.4.1 Early detection of the risk of disease

Among the five sampling dates, LCC showed significant differences between the with- and without-fungicide treatments only on the last two dates, suggesting that there is a lag of LCC responding to diseases that were mild in this study. Some of the fluorescence indices (recorded on detached leaves) could distinguish between the with- and without-fungicide treatments on the first two sampling dates for some varieties individually, suggesting that fluorescence indices may observe chlorophyll functioning changes that precede significant losses of LCC (Zarco-Tejada *et al.*,

2000). Fluorescence indices did not show consistent performance for different varieties on different dates (Table 4-4), which is due not only to the effect of phenological development (Delalieux et al., 2009b) but also to variety variations and the mild disease symptoms. Reflectance indices generally showed good performance for distinguishing between the with- and without-fungicide plots (Tables 4-4 and 4-5). The difference might be related not only to the sensitivity of different indices but also to the measuring methods: while the fluorescence measurement was performed on individual leaves, the reflectance was done from the canopy and could have detected the infections in the leaves of lower layers.

MCARI/TCARI, which is the combination of the Modified Chlorophyll Absorption in Reflectance Index (MCARI) (Daughtry et al., 2000) and the Transformed Chlorophyll Absorption in Reflectance Index (TCARI) (Haboudane et al., 2002), showed promising performance for discrimination and differentiation between the with- and without-fungicide treatments (Table 4-5). MCARI was developed for minimizing effects of non-photosynthetic materials (Daughtry et al., 2000), based on which TCARI was proposed to counteract the effect of soil background on MCARI (Haboudane et al., 2002). Since diseases affect the absorbed photosynthetically active radiation and thus the radiation use efficiency by leaves, MCARI/TCARI is reasonably expected to detect physiological changes due to diseases, as well as the natural senescence of plant materials. The plants of without-fungicide treatment are also expected to accelerate the senescence process compared to the with-fungicide treatment.

BFRR_UV, as a blue/far-red fluorescence ratio (BF_UV/FRF_UV, Table 4-1) is considered as a robust indicator of plant stresses (Lichtenthaler & Miehe, 1997), however provided excellent ($c \geq 0.8$) discrimination for only one variety (Bambina) on the third and fourth sampling dates (90 and 97 DAS) (Table 4-4). Again, this might be due to that fluorescence measurements were performed on individual leaves rather than the canopy level, as well as for other fluorescence indices.

4.4.2 Estimation of LCC

Several studies have consistently shown that RF/FRF is a good inverse indicator of the chlorophyll content (Buschmann, 2007; Lichtenthaler et al., 2005; Ounis et al., 2001). However, our results show that BF/FRF (BFRR_UV) yielded the highest correlation with LCC (Figure 4-5c), suggesting that the BF/FRF (BFRR_UV) can serve as an indicator of the leaf chlorophyll. Similarly, Heisel et al. (1996) found that the BF/FRF (F440/F740) and BF/RF (F440/F690) were more sensitive to the growth conditions than the most frequently used chlorophyll fluorescence ratio RF/FRF (F690/F740).

SFR_G and SFR_R, the FRF/RF ratios that are suggested as chlorophyll indicators by Gitelson et al. (1999), were positively correlated to LCC (Figure 4-6a and b) but yielded lower correlation

coefficients as compared to BFRR_UV. This is probably due to (i) different varieties were served as model calibration and validation data sets, (ii) same amount of N fertilizer for each variety. The given conditions could have caused the inconsistency with the previous studies (Lejealle *et al.*, 2010; Zhang *et al.*, 2012). On the other hand, results are consistent to some degree with previous study that the reflectance indices comprised of blue-green and far-red wavelengths are efficient for estimating chlorophyll when across barley varieties (Yu *et al.*, 2012). Thus, results reveal that the blue to far-red fluorescence ratio (BF/FRF) might be more useful for modeling LCC across crop varieties. Far-red fluorescence excitation ratios FER_RG and ANTH were also closely related to LCC, which suggests the potential for simultaneously monitoring both chlorophylls and anthocyanins using chlorophyll fluorescence (Agati *et al.*, 2005).

PLS is known as an efficient tool to solve the collinear problems of multivariate statistical analysis (Hansen & Schjoerring, 2003; Wold *et al.*, 2001a). Apparently, the fluorescence indices are collinear since the fluorescence ratios are all derived from the measured fluorescence signals (Table 4-1). Results show that PLSR model provided higher prediction accuracy as compared to the best fluorescence index BFRR_UV (Table 4-6). Generally, calibration data is expected to have the minimum in predicted residual sum of squares (PRESS). However, a model with fewer factors is always preferred to alleviate the risk of over-fitting. Therefore, 6 factors were extracted for implementing the PLSR model because it satisfied not only the requirement of minimizing PRESS, but also the necessity of statistical tests for none significant increase in the PRESS (van der Voet, 1994).

SVM has theoretically the advantage for high dimensional data. Similar with previous study (Ben Ghazlen *et al.*, 2010), nonlinear problems of fluorescence indices also occurred in this study (Figure 4-6). However, it is critical to determine the proper kernel function in order to produce a good performance and also weaken the complexity of model selection. In this study, the RBF kernel was preferred because RBF kernel outperformed linear and polynomial kernels (*data not shown*). In addition, RBF kernel not only can handle the case when the relations between dependent variables and predictors are nonlinear but also has fewer numerical difficulties (Hsu *et al.*, 2003).

It is difficult to make a fair comparison between the SVM and the PLS methods. There are more factors and parameters to be carefully considered for the SVM and PLS models as compared to a simple regression method. In this study, SVR model only slightly outperformed PLSR model (Table 4-6 and Figure 4-8). Although the consistent result has also been addressed in other studies (Borin *et al.*, 2006; Thissen *et al.*, 2004; Yu *et al.*, 2008), this does not mean that SVR is always the best choice because SVR optimization is relatively slow and complicated compared to PLSR

(Thissen *et al.*, 2004). Overall, SVR and PLSR both seem to be powerful to improve the use of fluorescence signals in estimating LCC.

The relative error of estimation was about 10% for PLSR and SVR, which is low from the practical point of view. The polynomial models using the fluorescence index BFRR_UV was about 13%, which is applicable in practices. However, the multivariate models such as PLS and SVM might be more reliable for future scenarios, where which index is the best choice remains to be studied as shown in the preceding discussion. As the “full spectrum” methods, PLS and SVM not only can deal efficiently with the strong multi-collinearity problem but also consider covariance to the model response/dependent variable(s) (Atzberger *et al.*, 2010) when extracting regression factors and support vectors, respectively. Therefore, they are expected to be better adapted to deal with potential confounding factors compared to a simple index-based approach (Atzberger *et al.*, 2010).

4.5 Conclusions

There is a time lag between the occurrence of barley diseases and significant losses of leaf chlorophyll concentration (LCC). Hyperspectral reflectance indices showed good discrimination between healthy and slightly-diseased barley plants that precede significant losses in LCC. A combination of MCARI and TCARI (MCARI/TCARI) showed a promising performance on early detecting diseases across seven barley varieties. Reflectance indices generally showed good performance on predicting LCC ($R^2 = 0.75 - 0.79$). The blue to far-red fluorescence ratio, BFRR_UV, also performed well for predicting LCC ($R^2 = 0.72$) compared to other fluorescence indices. However, the BFRR_UV vs. LCC relationship was nonlinear, which still constrained the accuracy for LCC estimation. PLSR and SVR models overcome the nonlinear problem, significantly increased the accuracy in estimating LCC ($R^2 > 0.81$).

The possible shortage of this study is that fluorescence signals were measured on individual leaves while hyperspectral reflectance were measured on canopy level, thus a meaningful comparison between the fluorescence and reflectance indices is not possible. Future studies should consider performing canopy level fluorescence and hyperspectral measurements for cross comparisons, for example mounting the fluorescence sensor on a wheeled platform (Lejealle *et al.*, 2010).

Further studies on different species under different environmental conditions remain to be undertaken to explore the full potential of fluorescence and hyperspectral remote sensing for detecting and identifying crop diseases, which would facilitate the fungicide-specific management in precision agriculture.

Acknowledgments

This study has been supported in part by the German Federal Ministry of Education and Research (BMBF) funded CropSense.net project (www.cropsense.uni-bonn.de). We thank L. Schwager and I. Kurth for laboratory work. The authors also acknowledge the three anonymous reviewers and the editor for their very constructive comments.

Conflict of Interest

The authors declare no conflict of interest.

References

- Agati, G., Pinelli, P., Cortes Ebner, S., Romani, A., Cartelat, A., Cerovic, Z.G. 2005.** Nondestructive evaluation of anthocyanins in Olive (*Olea europaea*) fruits by *in situ* chlorophyll fluorescence spectroscopy. *J. Agric. Food Chem.* **53**: 1354-1363.
- Agati, G., Foschi, L., Grossi, N., Guglielminetti, L., Cerovic, Z.G., Volterrani, M. 2013.** Fluorescence-based versus reflectance proximal sensing of nitrogen content in *Paspalum vaginatum* and *Zoysia matrella* turfgrasses. *Eur. J. Agron.* **45**: 39-51.
- Atzberger, C., Guérif, M., Baret, F., Werner, W. 2010.** Comparative analysis of three chemometric techniques for the spectroradiometric assessment of canopy chlorophyll content in winter wheat. *Comput. Electron. Agric.* **73**: 165-173.
- Babani, F., Lichtenthaler, H.K. 1996.** Light-induced and age-dependent development of chloroplasts in etiolated barley leaves as visualized by determination of photosynthetic pigments, CO₂ assimilation rates and different kinds of chlorophyll fluorescence ratios. *J. Plant Physiol.* **148**: 555-566.
- Ben Ghazlen, N., Cerovic, Z.G., Germain, C., Toutain, S., Latouche, G. 2010.** Non-destructive optical monitoring of grape maturation by proximal sensing. *Sensors* **10**: 10040-10068.
- Blackburn, G.A. 1998.** Quantifying chlorophylls and carotenoids at leaf and canopy scales: An evaluation of some hyperspectral approaches. *Remote Sens. Environ.* **66**: 273-285.
- Borin, A., Ferrão, M.F., Mello, C., Maretto, D.A., Poppi, R.J. 2006.** Least-squares support vector machines and near infrared spectroscopy for quantification of common adulterants in powdered milk. *Anal. Chim. Acta* **579**: 25-32.
- Bürling, K., Hunsche, M., Noga, G. 2010.** Quantum yield of non-regulated energy dissipation in PSII (Y(NO)) for early detection of leaf rust (*Puccinia triticina*) infection in susceptible and resistant wheat (*Triticum aestivum* L.) cultivars. *Precis. Agric.* **11**: 703-716.

- Bürling, K., Hunsche, M., Noga, G. 2011.** Use of blue – green and chlorophyll fluorescence measurements for differentiation between nitrogen deficiency and pathogen infection in winter wheat. *J. Plant Physiol.* **168**: 1641-1648.
- Buschmann, C., Lichtenthaler, H.K. 1998.** Principles and characteristics of multi-colour fluorescence imaging of plants. *J. Plant Physiol.* **152**: 297-314.
- Buschmann, C. 2007.** Variability and application of the chlorophyll fluorescence emission ratio red/far-red of leaves. *Photosynth. Res.* **92**: 261-271.
- Cartelat, A., Cerovic, Z.G., Goulas, Y., Meyer, S., Lelarge, C., Prioul, J.L., Barbottin, A., Jeuffroy, M.H., Gate, P., Agati, G., Moya, I. 2005.** Optically assessed contents of leaf polyphenolics and chlorophyll as indicators of nitrogen deficiency in wheat (*Triticum aestivum* L.). *Field Crops Res.* **91**: 35-49.
- Cerovic, Z.G., Moise, N., Agati, G., Latouche, G., Ben Ghazlen, N., Meyer, S. 2008.** New portable optical sensors for the assessment of winegrape phenolic maturity based on berry fluorescence. *J. Food Compos. Anal.* **21**: 650-654.
- Chang, C., Lin, C. 2011.** LIBSVM: A library for support vector machines. *ACM Trans. Intell. Syst. Technol.* **2**: 1-27.
- Chappelle, E.W., Wood, F.M., McMurtrey III, J.E., Newcomb, W.W. 1984a.** Laser-induced fluorescence of green plants. 1: A technique for the remote detection of plant stress and species differentiation. *Appl. Opt.* **23**: 134-138.
- Chappelle, E.W., McMurtrey III, J.E., Wood, F.M., Newcomb, W.W. 1984b.** Laser-induced fluorescence of green plants. 2: LIF caused by nutrient deficiencies in corn. *Appl. Opt.* **23**: 139-142.
- Daughtry, C.S.T., Walthall, C.L., Kim, M.S., de Colstoun, E.B., McMurtrey III, J.E. 2000.** Estimating corn leaf chlorophyll concentration from leaf and canopy reflectance. *Remote Sens. Environ.* **74**: 229-239.
- Delalieux, S., van Aardt, J., Keulemans, W., Schrevens, E., Coppin, P. 2007.** Detection of biotic stress (*Venturia inaequalis*) in apple trees using hyperspectral data: Non-parametric statistical approaches and physiological implications. *Eur. J. Agron.* **27**: 130-143.
- Delalieux, S., Auwerkerken, A., Verstraeten, W., Somers, B., Valcke, R., Lhermitte, S., Keulemans, J., Coppin, P. 2009a.** Hyperspectral reflectance and fluorescence imaging to detect scab induced stress in apple leaves. *Remote Sens.* **1**: 858-874.
- Delalieux, S., Somers, B., Verstraeten, W.W., van Aardt, J.A.N., Keulemans, W., Coppin, P. 2009b.** Hyperspectral indices to diagnose leaf biotic stress of apple plants, considering leaf phenology. *Int. J. Remote Sens.* **30**: 1887-1912.

- Durbha, S.S., King, R.L., Younan, N.H. 2007.** Support vector machines regression for retrieval of leaf area index from multiangle imaging spectroradiometer. *Remote Sens. Environ.* **107**: 348-361.
- Gamon, J.A., Peñuelas, J., Field, C.B. 1992.** A narrow-waveband spectral index that tracks diurnal changes in photosynthetic efficiency. *Remote Sens. Environ.* **41**: 35-44.
- Gitelson, A.A., Buschmann, C., Lichtenthaler, H.K. 1998.** Leaf chlorophyll fluorescence corrected for re-absorption by means of absorption and reflectance measurements. *J. Plant Physiol.* **152**: 283-296.
- Gitelson, A.A., Buschmann, C., Lichtenthaler, H.K. 1999.** The chlorophyll fluorescence ratio F735/F700 as an accurate measure of the chlorophyll content in plants. *Remote Sens. Environ.* **69**: 296-302.
- Haaland, D.M., Thomas, E.V. 1988.** Partial least-squares methods for spectral analyses. I. Relation to other quantitative calibration methods and the extraction of qualitative information. *Anal. Chem.* **60**: 1193-1202.
- Haboudane, D., Miller, J.R., Tremblay, N., Zarco-Tejada, P.J., Dextraze, L. 2002.** Integrated narrow-band vegetation indices for prediction of crop chlorophyll content for application to precision agriculture. *Remote Sens. Environ.* **81**: 416-426.
- Hansen, P.M., Schjoerring, J.K. 2003.** Reflectance measurement of canopy biomass and nitrogen status in wheat crops using normalized difference vegetation indices and partial least squares regression. *Remote Sens. Environ.* **86**: 542-553.
- Heisel, F., Sowinska, M., Miehe, J.A., Lang, M., Lichtenthaler, H.K. 1996.** Detection of nutrient deficiencies of maize by laser induced fluorescence imaging. *J. Plant Physiol.* **148**: 622-631.
- Hosmer, D.W., Lemeshow, S. 2000.** *Applied logistic regression*. New York: John Wiley & Sons, Inc.
- Hsu, C.W., Chang, C.C., Lin, C.J. 2003.** A practical guide to support vector classification. Available online: <http://www.csie.ntu.edu.tw/~cjlin/papers/guide/guide.pdf>. (Accessed on 1 November 2013).
- Lang, M., Lichtenthaler, H.K., Sowinska, M., Heisel, F., Miehe, J.A. 1996.** Fluorescence imaging of water and temperature stress in plant leaves. *J. Plant Physiol.* **148**: 613-621.
- Langsdorf, G., Buschmann, C., Sowinska, M., Babani, F., Mokry, M., Timmermann, F., Lichtenthaler, H.K. 2000.** Multicolour fluorescence imaging of sugar beet leaves with different nitrogen status by flash lamp UV-excitation. *Photosynthetica* **38**: 539-551.

- Lejealle, S., Evain, S., Cerovic, Z.G.** 2010. Multiplex: A new diagnostic tool for management of nitrogen fertilization of turfgrass. In: *10th International Conference on Precision Agriculture*. 18-21 July, 2010. Denver, Colorado, USA.
- Leufen, G., Noga, G., Hunsche, M.** 2013. Physiological response of sugar beet (*Beta vulgaris*) genotypes to a temporary water deficit, as evaluated with a multiparameter fluorescence sensor. *Acta Physiol. Plant.* **35**: 1763-1774.
- Lichtenthaler, H.K., Rinderle, U.** 1988. The role of chlorophyll fluorescence in the detection of stress conditions in plants. *CRC Crit. Rev. Anal. Chem.* **19**: S29-S85.
- Lichtenthaler, H.K.** 1996. Vegetation stress: an introduction to the stress concept in plants. *J. Plant Physiol.* **148**: 4-14.
- Lichtenthaler, H.K., Miehé, J.A.** 1997. Fluorescence imaging as a diagnostic tool for plant stress. *Trends Plant Sci.* **2**: 316-320.
- Lichtenthaler, H.K., Babani, F.** 2004. Light adaptation and senescence of the photosynthetic apparatus. Changes in pigment composition, chlorophyll fluorescence parameters and photosynthetic activity. In: G. C. PapageorgiouGovindjee eds. *Chlorophyll a fluorescence: A signature of photosynthesis*. Dordrecht, The Netherlands: Springer, 713-736.
- Lichtenthaler, H.K., Langsdorf, G., Lenk, S., Buschmann, C.** 2005. Chlorophyll fluorescence imaging of photosynthetic activity with the flash-lamp fluorescence imaging system. *Photosynthetica* **43**: 355-369.
- Miphokasap, P., Honda, K., Vaiphasa, C., Souris, M., Nagai, M.** 2012. Estimating canopy nitrogen concentration in sugarcane using field imaging spectroscopy. *Remote Sens.* **4**: 1651-1670.
- Mountrakis, G., Im, J., Ogole, C.** 2011. Support vector machines in remote sensing: A review. *ISPRS J. Photogramm. Remote Sens.* **66**: 247-259.
- Ounis, A., Cerovic, Z.G., Briantais, J.M., Moya, I.** 2001. Dual-excitation FLIDAR for the estimation of epidermal UV absorption in leaves and canopies. *Remote Sens. Environ.* **76**: 33-48.
- Peñuelas, J., Filella, I., Lloret, P., Muñoz, F., Vilajeliu, M.** 1995. Reflectance assessment of mite effects on apple trees. *Int. J. Remote Sens.* **16**: 2727-2733.
- Plaza, A., Benediktsson, J.A., Boardman, J.W., Brazile, J., Bruzzone, L., Camps-Valls, G., Chanussot, J., Fauvel, M., Gamba, P., Gualtieri, A., Marconcini, M., Tilton, J.C., Trianni, G.** 2009. Recent advances in techniques for hyperspectral image processing. *Remote Sens. Environ.* **113**, Supplement 1: S110-S122.

- Römer, C., Bürling, K., Hunsche, M., Rumpf, T., Noga, G., Plümer, L. 2011.** Robust fitting of fluorescence spectra for pre-symptomatic wheat leaf rust detection with support vector machines. *Comput. Electron. Agric.* **79**: 180-188.
- Rondeaux, G., Steven, M., Baret, F. 1996.** Optimization of soil-adjusted vegetation indices. *Remote Sens. Environ.* **55**: 95-107.
- Rosipal, R., Krämer, N. 2006.** Overview and recent advances in partial least squares. In: C. Saunders, M. Grobelnik, S. Gunnj. Shawe-Taylor eds. *Subspace, Latent Structure and Feature Selection*. Berlin Heidelberg: Springer-Verlag, 34-51.
- SAS Institute Inc. 2008.** SAS/STAT® 9.2 User's Guide. In. Cary, NC: SAS Institute Inc.
- Smola, A.J., Schölkopf, B. 2004.** A tutorial on support vector regression. *Stat. Comput.* **14**: 199-222.
- Sun, D., Li, Y., Wang, Q., Le, C., Lv, H., Huang, C., Gong, S. 2012.** A novel support vector regression model to estimate the phycocyanin concentration in turbid inland waters from hyperspectral reflectance. *Hydrobiologia* **680**: 199-217.
- Thissen, U., Pepers, M., Üstün, B., Melssen, W.J., Buydens, L.M.C. 2004.** Comparing support vector machines to PLS for spectral regression applications. *Chemometr. Intell. Lab. Syst.* **73**: 169-179.
- Tremblay, N., Wang, Z., Cerovic, Z.G. 2012.** Sensing crop nitrogen status with fluorescence indicators. A review. *Agron. Sustain. Dev.* **32**: 451-464.
- van der Voet, H. 1994.** Comparing the predictive accuracy of models using a simple randomization test. *Chemometr. Intell. Lab. Syst.* **25**: 313-323.
- Vapnik, V.N. 1995.** *The nature of statistical learning theory*. New York: Springer-Verlag.
- Vapnik, V.N. 1998.** *Statistical learning theory*. New York: John Wiley & Sons, Inc.
- Wold, H. 1966.** Estimation of principal components and related models by iterative least squares. In: P. R. Krishnaiah ed. *Multivariate Analysis*. New York, USA: Academic Press, 391-420.
- Wold, S., Kettaneh-Wold, N., Skagerberg, B. 1989.** Nonlinear PLS modeling. *Chemometr. Intell. Lab. Syst.* **7**: 53-65.
- Wold, S., Sjöström, M., Eriksson, L. 2001a.** PLS-regression: a basic tool of chemometrics. *Chemometr. Intell. Lab. Syst.* **58**: 109-130.
- Wold, S. 2001b.** Personal memories of the early PLS development. *Chemometr. Intell. Lab. Syst.* **58**: 83-84.
- Yang, F., White, M.A., Michaelis, A.R., Ichii, K., Hashimoto, H., Votava, P., Zhu, A.X., Nemani, R.R. 2006.** Prediction of continental-scale evapotranspiration by combining MODIS and AmeriFlux data through support vector machine. *IEEE Trans. Geosci. Remote Sens.* **44**: 3452-3461.

- Yu, H., Lin, H., Xu, H., Ying, Y., Li, B., Pan, X. 2008.** Prediction of enological parameters and discrimination of rice wine age using least-squares support vector machines and near infrared spectroscopy. *J. Agric. Food Chem.* **56**: 307-313.
- Yu, K., Lenz-Wiedemann, V., Leufen, G., Hunsche, M., Noga, G., Chen, X., Bareth, G. 2012.** Assessing hyperspectral vegetation indices for estimating leaf chlorophyll concentration of summer barley. *ISPRS Ann. Photogramm. Remote Sens. Spatial Inf. Sci.* **1-7**: 89-94.
- Zarco-Tejada, P.J., Miller, J.R., Mohammed, G.H., Noland, T.L., Sampson, P.H. 2000.** Chlorophyll fluorescence effects on vegetation apparent reflectance: II. Laboratory and airborne canopy-level measurements with hyperspectral data. *Remote Sens. Environ.* **74**: 596-608.
- Zarco-Tejada, P.J., Miller, J.R., Noland, T.L., Mohammed, G.H., Sampson, P.H. 2001.** Scaling-up and model inversion methods with narrowband optical indices for chlorophyll content estimation in closed forest canopies with hyperspectral data. *IEEE Trans. Geosci. Remote Sens.* **39**: 1491-1507.
- Zarco-Tejada, P.J., Miller, J.R., Mohammed, G.H., Noland, T.L., Sampson, P.H. 2002.** Vegetation stress detection through chlorophyll a+b estimation and fluorescence effects on hyperspectral imagery. *J. Environ. Qual.* **31**: 1433-1441.
- Zhang, Y., Tremblay, N., Zhu, J. 2012.** A first comparison of Multiplex® for the assessment of corn nitrogen status. *J. Food. Agric. Environ.* **10**: 1008-1016.
- Zheng, H., Lu, H., Zheng, Y., Lou, H., Chen, C. 2010.** Automatic sorting of Chinese jujube (*Zizyphus jujuba* Mill. cv. 'hongxing') using chlorophyll fluorescence and support vector machine. *J. Food Eng.* **101**: 402-408.

CHAPTER 5

Optimizing spectral indices to reduce effects of soil background and canopy structure for the estimation of leaf chlorophyll of barley at different growth stages*

* *This chapter is based on:*

Yu, K., Chen, X., Lenz-Wiedemann, V., Bareth, G. 2014. Optimizing spectral indices to reduce effects of soil background and canopy structure for the estimation of leaf chlorophyll of barley at different growth stages. *ISPRS J. Photogramm. Remote Sens.* **submitted.**

Abstract

Monitoring in situ chlorophyll (Chl) content in agricultural crop leaves is of great importance for stress detection, nutritional state diagnosis, yield prediction and studying the mechanisms of plant and environment interaction. Numerous spectral indices have been developed for chlorophyll estimation from leaf- and canopy-level reflectance. However, in most cases, these indices are negatively affected by variations in canopy structure and soil background. The objective of this study was to develop spectral indices that can reduce the effects of varied canopy structure and growth stages for the estimation of leaf Chl. Hyperspectral reflectance data was obtained through simulation by a radiative transfer model, PROSAIL, and measurements from canopies of barley comprising different cultivars across growth stages using spectroradiometers. We applied a comprehensive band-optimization algorithm to explore five types of spectral indices: reflectance difference (RD), reflectance ratio (RR), normalized reflectance difference (NRD), difference of reflectance ratio (DRR) and ratio of reflectance difference (RRD). Indirectly using the multiple scatter correction (MSC) theory, we hypothesized that RRD can eliminate adverse effects of soil background, canopy structure and multiple scattering. Published indices and multivariate models such as optimum multiple band regression (OMBR), partial least squares regression (PLSR) and support vector machines for regression (SVR) were also employed. Results showed that the ratio of reflectance difference index (RRDI) optimized for simulated data significantly improved the correlation with Chl ($R^2 = 0.98$, $p < 0.0001$) and was insensitive to LAI variations (1-8), compared to widely used indices such as MCARI/OSAVI ($R^2 = 0.64$, $p < 0.0001$) and TCARI/OSAVI ($R^2 = 0.74$, $p < 0.0001$). The RRDI optimized for barley explained 76% of the variation in Chl and outperformed multivariate models. However, the accuracy decreased when employing the indices for individual growth stages ($R^2 < 0.59$). Accordingly, RRDIs optimized for open and closed canopies improved the estimations of Chl for individual stages before and after canopy closure, respectively, with R^2 of 0.65 ($p < 0.0001$) and 0.78 ($p < 0.0001$). This study shows that RRDI can efficiently eliminate the effects of structural properties on canopy reflectance response to canopy biochemistry.

5.1 Introduction

The chlorophylls, chlorophyll *a* and *b*, are the most important antenna pigments of photosynthesis, enabling plants to power the biosphere via the oxygenic conversion of light energy to chemical energy (Richardson *et al.*, 2002). From the perspective of precision agriculture, leaf chlorophyll content is of significant interest because chlorophyll content can be directly related to plant stresses and senescence (Gitelson & Merzlyak, 1994a; Merzlyak *et al.*, 1999; Peñuelas & Filella, 1998) and leaf nitrogen (N) status (Cartelat *et al.*, 2005; Moran *et al.*, 2000). For example, plant stresses that involve N or water deficiencies often lead to adverse effects on the amount of chlorophyll plants produce (Schlemmer *et al.*, 2005). Therefore, determination of chlorophyll content can provide important information about plant stress, nutritional state and relationships between plants and their environment, and consequently will be of great importance in agricultural field management (Zarco-Tejada *et al.*, 2004).

Wet chemical methods have long been used as a standard technique for chlorophyll determination, although it is relatively time consuming and requires destructive sampling, and thus does not permit measurement of changes in pigments over time for the same leaves. The use of portable chlorophyll meters (e.g., SPAD) has been proposed as a non-destructive technique for leaf chlorophyll determination and is widely used in agricultural studies (Cartelat *et al.*, 2005; Filella *et al.*, 1995; Martínez & Guiamet, 2004; Miao *et al.*, 2009; Steele *et al.*, 2008; Takebe *et al.*, 1990). However, most commercially available chlorophyll meters only measure a small leaf spot (point measurement) and might lose sensitivity at high chlorophyll levels (Ciganda *et al.*, 2009; Steele *et al.*, 2008). Therefore, both wet chemical and chlorophyll meter methods present problems for achieving the purpose of in-time measurement of chlorophyll on regional and global scales.

Advances in remote sensing technology offer the potential for linking remote sensing measurements to leaf and canopy biochemical characteristics in a reliable and operational way on a large scale. Spectral indices are considered as quantitative measurements indicating the vigor of vegetation (Bannari *et al.*, 1995). For decades, hyperspectral remote sensing applications described in the literature succeed in deriving the relationships between leaf-level reflectance and crop variables of interest (e.g., chlorophyll, water and N) by identifying spectral indices (Blackburn, 1998a; Datt, 1998; Gitelson *et al.*, 2003; 2006; Peñuelas *et al.*, 1995a; Sims & Gamon, 2002). Although spectral indices derived from leaf-level hyperspectral measurements in the laboratory have shown the strong link to chlorophyll, the relationships are frequently lower in precision and accuracy when these indices are used for canopy-level studies (Asner & Martin, 2008; Zarco-Tejada *et al.*, 2004). For agricultural canopies at early growth stages, soil background and variations in canopy structure have a large effect on canopy reflectance signals (Daughtry *et al.*, 2000;

Haboudane et al., 2002; Zarco-Tejada et al., 2005). Existing chlorophyll indices developed from leaf level or closed canopies might not be appropriate for open canopies at early growth stages. However, the crop vegetative growth phase accompanying with lower LAI is the critical stage for fertilization for high yield. Therefore, understanding the capability of existing spectral indices for estimating chlorophyll of agricultural crops at early growth stages is essential for the operational utility of remote sensing in precision agriculture, which will also benefit the design of new vegetation indices in such a context.

Reflectance signals are responsive to both structural and biochemical properties and often respond inseparably to biochemical and structural variations in a given ecosystem due to co-variation (*Haboudane et al., 2008; Jacquemoud et al., 2009; Ustin et al., 2009*), which complicates the remote retrieval of biochemical information when structural properties vary. Previous studies have shown special efforts on developing pigment sensitive indices at leaf and canopy levels, respectively. At the leaf level, multiple scattering induced by leaf internal and surface structures interferes with the retrieval of leaf chemistry, for which special efforts have been put into developing leaf pigment indices that can eliminate the leaf structural effects. Among those, *Peñuelas et al. (1995a)* developed the structure insensitive pigment index (SIPI) that minimizes the confounding effects of leaf surface and internal structure for the estimation of the ratio of carotenoids and chlorophyll *a* concentrations. *Datt (1998; 1999a)* used a semi-empirical method, multiple scatter correction (MSC), to eliminate multiple scattering effects, and consequently improved the estimation of chlorophyll. Similarly, incorporating an additional reference band into indices such as reflectance simple ratio or normalized difference vegetation index (NDVI), also allows the elimination of leaf structure effect, and improves the estimation of leaf chlorophyll (*Gitelson et al., 2003; Sims & Gamon, 2002*). In contrast, at the canopy level, special efforts have been put into developing indices by incorporating the soil line concept (*Huete, 1988; Rondeaux et al., 1996*) and taking into account non-photosynthesis materials (*Daughtry et al., 2000; Kim et al., 1994*). These indices aim to minimize effects of soil background and non-photosynthesis materials, e.g., modified chlorophyll absorption in reflectance index (MCARI) developed by *Daughtry et al. (2000)* and its variant form as transformed chlorophyll absorption in reflectance index (TCARI) proposed by *Haboudane et al. (2002)*. Further, *Haboudane et al. (2002; 2008)* combined the soil-line index OSAVI (*Rondeaux et al., 1996*) with TCARI to form TCARI/OSAVI that aims to increase the sensitivity to chlorophyll and resist LAI variations. Despite significant improvements on the estimation of pigments, soil-line and combined indices are still sensitive to some degree to soil background and LAI variations as indicated in recent studies, particularly when LAI is lower than 3 (*Haboudane et al., 2008; Zarco-Tejada et al., 2005*). Notably, the two focus areas for developing indices at both leaf and canopy levels are in consensus at the one point that aims to

maximize the sensitivity to biochemistry while minimizing structural effects. Insights from these studies, at the leaf level that eliminate within-leaf multiple scattering effects and at the canopy level that minimizes effects of soil background and LAI variations, might be integrated to design indices that are conceptually insensitive to the confounding effects of soil background, canopy 3-D structure and multiple scattering within leaves as well as between multiple leaf layers, from canopy opening to canopy closure (*Baret et al., 1992; Jacquemoud et al., 2009; Ustin et al., 2009*). Given the essential demand for simplicity when applying remote sensing in agriculture, such a simple approach that can eliminate confounding effects of those structural properties have great practical merit. Thus, whether existing indices can efficiently reduce the structural effects, and to what extent those effects can be eliminated by designing a spectral index remains to be further studied.

Previous studies have made progress in hyperspectral remote sensing of leaf chlorophyll and N in agricultural crops (*Daughtry et al., 2000; Haboudane et al., 2002; 2004; Hansen & Schjoerring, 2003; Inoue et al., 2012; Mutanga et al., 2003*) and many of them were performed on the canopy level. However, these studies were mainly undertaken in controlled conditions of varied N rates that are very different from farmer field management conditions and environments. It is evident that, unlike that for N rate experiments, farmers must not deliberately apply varied N rates in their fields, especially an obviously deficient rate like that in many studies. Spectral indices generally can account for a large portion of the variation in chlorophyll for leaves having large chlorophyll variations owing to distinct N gradients. However, considering that the aim of precision agriculture is to detect and minimize subtle variations within the field, these indices might not be able to account for the same portion of the variation in chlorophyll for the leaves having small chlorophyll variations for which N is evenly applied. Recently, *Haboudane et al. (2008)* found that wheat leaf chlorophyll with a narrow range (41.92–69.68 $\mu\text{g}/\text{cm}^2$) was not able to be accurately accounted for by the spectral index TCARI/OSAVI, yielding a R^2 of 0.29, whereas the R^2 was 0.73 for corn leaf chlorophyll with a wide range (24.00–63.78 $\mu\text{g}/\text{cm}^2$). Hence, here is not a critique on remote sensing studies that employ N rate experiments. On the contrary, this uncertainty leads to an important yet unanswered question that under more natural conditions without artificial nutrient deficiency levels, how can leaf chlorophyll be remotely estimated as consistently well as that in N rate experiments by canopy reflectance? It is particularly critical in the context of varied cultivars and different growth stages that generate changing canopy structure and ground coverage conditions, which might mask to some degree the spectral differences responding to subtle variation in canopy biochemistry.

Our objective was to develop spectral indices for the estimation of leaf chlorophyll that are insensitive to variations of canopy structure and soil background as well as multiple scattering

using canopy-level hyperspectral data. In this paper, new and published indices (Table 5-1) are examined using simulated data, by radiative transfer models, and field measured data at different growth stages. The performances of spectral indices in predicting chlorophyll are also compared with those commonly used multivariate techniques, i.e., multiple linear regression (MLR), partial least squares (PLS) and support vector machines (SVM).

5.2 Materials and methods

We describe in this section the datasets (barley and synthetic), methods for data collection/simulation and analysis, published spectral indices (Table 5-1), hypothesis and method for optimizing spectral indices and, the multivariate regressions used in this study.

5.2.1 Barley dataset

5.2.1.1 Study site and experimental design

The study area of barley experiment is located at the Institute of Crop Science and Resource Conservation (INRES-Horticultural Science, latitude 50.72999 °, longitude 7.0754 °; 70 m.a.s.l.; sandy loam soil; soil N_{min} value of 20 kg N ha⁻¹; annual average precipitation of 669 mm, average temperature of 10.3 °C), University of Bonn, Germany. The field experiment with seven commercial barley (*Hordeum vulgare* L.) cultivars (Belana, Marthe, Scarlett, Iron, Sunshine, Barke and Bambina) was conducted from March to July 2010. These cultivars have significantly different leaf geometrical characteristics, as well as canopy structure. The experiment was organized as a completely randomized block design with six replications and a plot size of 6 m² (1.5 × 4 m) for each cultivar. All barley cultivars were sown with a density of 320 seeds per square meter. All plots were fertilized directly after sowing with ammonium nitrate (NH₄-N) at the same rate of 100 kg N ha⁻¹.

5.2.1.2 Canopy spectral measurements

Canopy reflectance was measured with QualitySpec® Pro and FieldSpec® 3 spectroradiometers (Analytical Spectral Devices Inc., Boulder, CO, USA). QualitySpec® Pro and FieldSpec® 3 were used for the 1st to 4th measuring dates and the 5th to 7th measuring dates, respectively. The measurements were always carried out between 10:00 and 14:00 local time (GMT+1) under clear sky conditions throughout the growing season, with a distance of 1 m above the canopy and a field-of-view (FOV) of 25°.

Table 5-1: Hyperspectral reflectance indices investigated in this study.

Type	Formula	Published index		Reference
		Short	Name	
RDI	$R_i - R_k$	RDI	Reflectance difference	Tucker (1979)
		RD2	Reflectance difference	le Maire et al. (2008)
RRI	R_i / R_k	PSSR _a	Pigment specific simple ratio	Blackburn (1998b)
		RR ₇₁₀	Red edge reflectance ratio	Zarco-Tejada et al. (2001)
		RR ₇₂₀	Red edge reflectance ratio	Vogelmann et al. (1993)
NRDI	$(R_i - R_k)/(R_i + R_k)$	NDVI	Normalized difference vegetation index	Blackburn (1998b); Rouse et al. (1974)
		ND ₇₀₅	Normalized difference red edge	Gitelson & Merzlyak (1994b)
DRRI	$(R_i - R_k)/R_i$	PRI	Photochemical reflectance index	Gamon et al. (1992); Peñuelas et al. (1995b)
		PSRI	Plant senescence reflectance index	Merzlyak et al. (1999)
³ RRDI	$(R_i - R_k)/(R_i - R_k)$	CI _{red edge}	Chlorophyll index red edge	Gitelson et al. (2003)
		CI _{green}	Chlorophyll index green	Gitelson et al. (2003)
⁴ RRDI	$(R_i - R_k)/(R_i - R_k)$	SIPI [†]	Structure insensitive pigment index	Peñuelas et al. (1995a)
		EPI [†]	Eucalyptus pigment index	Datt (1999a; 1999b)
Hybrid	$(R_i - R_k)/(R_i - R_k)$	mSR705	Modified simple ratio	Sims & Gamon (2002)
		MTCI ^b	MERIS terrestrial chlorophyll index	Dash & Curran (2004)
REIP	Red edge inflection point	CARI	Chlorophyll absorption ratio index	Guyot & Baret (1988)
		MCARI	Modified CARI	Kim et al. (1994)
TCARI	Transformed CARI	OSAVI	Optimized SAVI	Daughtry et al. (2000)
		MCARI/OSAVI	MCARI/OSAVI	Haboudane et al. (2002)
TCARI/OSAVI	TCARI/OSAVI	TCARI/OSAVI	TCARI/OSAVI	Rondeaux et al. (1996)
		TCARI/OSAVI	TCARI/OSAVI	Haboudane et al. (2008)

* RDI: Reflectance difference index; RRI: Reflectance ratio index; NRDI: Normalized reflectance difference index; DRRI: Difference of reflectance ratio index. DRRI= $(R_i - R_k)/R_i$ was named "difference of reflectance ratio index" because it equals to $(R_i/R_i - R_k/R_k)$; RRDI: Ratio of reflectance difference index; ³RRDI: 3-band RRDI; ⁴RRDI: 4-band RRDI. [†] 3-band RRDI is a special case in which h is equal to k for Eq. (5-4), and $(R_i - R_k)/(R_i - R_k)$ is equivalent to $(R_k - R_i)/(R_k - R_i)$ and $-(R_i - R_k)/(R_k - R_i)$.

The QualitySpec® Pro spectroradiometer was configured with a spectral range of 350-1800 nm and a sampling interval of 1.4 nm for 350-1050 nm and 2 nm for 1000-1800 nm with a resolution of 3 nm and 10 nm at 700 nm and 1400 nm, respectively. Slightly different, the FieldSpec® 3 spectroradiometer was configured with a spectral range for 350 nm to 2500 nm, a sampling interval of 1.4 nm for 350-1050 nm and 2 nm for 1000-2500 nm, and with a spectral resolution of 3 nm at 700 nm and 10 nm at 1400 and 2100 nm. Both instruments automatically provide reflectance data with complete wavelength-channels (1 nm steps) using a cubic interpolation method (Analytical Spectral Devices Inc.). Prior to barley canopy reflectance measurements, a white Spectralon (Labsphere, Inc.) reference panel was used for baseline (white reference) measurement, allowing the ASD software to adjust instrument gain for optimal performance and also to determine dark-offsets for automatic subtraction from reflectance calculations (Analytical Spectral Devices Inc.). White references were collected approximately every 15 minutes. Six locations per plot were measured and then averaged as a mean spectrum for each plot. In this study, we used reflectance data in the wavelength range of 350-900 nm with a re-sampling interval of 5 nm (i.e., 350, 355, 360, ..., through to 900 nm).

5.2.1.3 Leaf chlorophyll measurements

From the spectroradiometer-scanned locations of each plot, ten intact “newest fully expanded leaves” (i.e., flag leaves when flag leaf was fully expanded) were randomly collected on 18 May, 27 May, 9 June (since then flag leaf was sampled), 15 June, 22 June, 29 June and 6 July, at the BBCH growth stages ([Lancashire et al., 1991](#)) 32, 39, 51, 55, 61, 73, and 83, respectively, and were lyophilized immediately after collection, then grounded and stored in the dark at room temperature. The 1st to 7th measuring dates were in those growth stages as follows: stem elongation (BBCH 32, 39), beginning and middle of heading (BBCH 51, 55) that has the highest degree of canopy closure, beginning of flowering (BBCH 61), early milk (BBCH 73) and early dough (BBCH 83) stages, respectively. The newest fully expanded leaf/ flag leaf, is the most powerful green tissue that captures light and contributes significantly to grain filling, thus it is critically important in determining grain yield and quality. Also, the newest fully expanded leaf is more likely to represent plant nutrient status, since N can be remobilized from old leaves to new leaves ([Lemaire et al., 2008](#)). Therefore, the newest fully expanded leaves were sampled at each measuring date.

Chlorophyll content for each plot was extracted from 50 mg lyophilized material of the ten leaves with 5 ml methanol and filled up to 25 ml. After extraction, the absorbance of extracts was measured with a UV-VIS spectrophotometer (Perkin-Elmer, Lambda 5, Massachusetts, USA) and

then chlorophyll was determined and presented on a dry biomass basis as the total chlorophyll concentration (Chl, $\mu\text{g/g}$).

For further analyses, we divided the barley dataset into two subsets that comprise completely different barley cultivars: the barley #1 subset of four cultivars (Belana, Marthe, Scarlett and Iron, $n=168$) and the barley #2 subset of three cultivars (Sunshine, Barke and Bambina, $n=126$).

5.2.2 Synthetic dataset

A synthetic dataset was generated by forward running the PROSAIL model (Jacquemoud *et al.*, 2009), which is a coupling of the leaf radiative transfer model PROSPECT (Jacquemoud & Baret, 1990) and the canopy model SAIL (Verhoef, 1984). PROSAIL simulates canopy reflectance for a wavelength range of 400-2500 nm with 1 nm steps. In this study, the synthetic dataset was simulated using the latest version of the PROSAIL model, PROSPECT-5 (Feret *et al.*, 2008) + 4SAIL (Verhoef *et al.*, 2007), with a range of input parameters as listed in Table 5-2. Finally, 43200 spectra were simulated by covering all possible combinations of the input parameters. Similarly to the measured spectra, simulated reflectance data ranging from 400 nm to 900 nm with a re-sampling interval of 5 nm were used for further analyses.

Table 5-2: PROSAIL model parameters that were used in this study to simulate the 43200 canopy reflectance spectra for the synthetic dataset (other six fixed parameters are: solar zenith angle=30°; view zenith angle=0°; view azimuth angle=0°; spherical leaf angel; hot spot size=0.15; fraction of diffuse incident radiation is 0.23 for clear sky based on François *et al.* (2002)).

Parameter	Minimum	Maximum	Step
Cab ($\mu\text{g}/\text{cm}^2$)	10	100	10
N	1.1	1.9	0.2
EWT (cm)	0.004	0.024	0.004
LMA (g/cm^2)	0.002	0.012	0.002
LAI (m^2/m^2)	1	8	1
P_{soil}	0	1	0.5

Cab, leaf chlorophyll content
 N, leaf structure parameter
 EWT, equivalent water thickness
 LMA, leaf mass per area
 LAI, leaf area index
 P_{soil} , soil moisture parameter

5.2.3 Data analysis

In this section we present the descriptive statistics analysis to show the variation in chlorophyll (hereafter referred to as Chl followed by the unit for each dataset) in different

growth stages (Table 5-3), and describe the theoretical and hypothetical basis for developing spectral indices that are conceptually insensitive to effects of canopy structure, soil background and multiple scattering. Descriptions of multivariate methods are also included.

Table 5-3: Descriptive statistics for leaf chlorophyll (Chl) of barley at each growth stage indicated with BBCH codes, and for the synthetic dataset simulated by the PROSAIL model using the input parameters described in Table 5-2.

Dataset	BBCH	n	Minimum	Maximum	Range	Mean	SD	CV
<u>Barley: Chl (µg/g)</u>	All	294	2512.23	15128.02	12615.79	10862.51	2541.52	23.40
	32	42	11133.64	14563.31	3429.66	13077.71	774.29	5.92
	39	42	9822.90	11929.36	2106.46	11058.69	516.26	4.67
	51	42	10191.50	15128.02	4936.52	12326.47	1228.61	9.97
	55	42	9848.23	14365.16	4516.93	12296.85	1077.00	8.76
	61	42	8208.50	13859.44	5650.94	11373.66	1255.45	11.04
	73	42	5897.46	13831.37	7933.91	10052.99	1585.66	15.77
	83	42	2512.23	10899.70	8387.47	5903.91	1736.62	29.41
<u>Synthetic: Chl (µg/cm²)</u>	All	43200	10.00	100.00	90.00	55.00	28.72	52.22

n, number of samples/simulations
 SD, standard deviation
 CV, coefficient of variation

5.2.3.1 Theoretical background and hypothesis

The theory of the multiple scatter correction (MSC, also called multiple signal correction) (Geladi et al., 1985; Martens & Naes, 1989), originally developed for NIR data, is a widely used transformation method that compensates for additive and/or multiplicative scatter effects in spectral data. The MSC method assumes that the light scatter and the chemical information can be mathematically differentiated, and the scatter for each sample is considered as a linear deviation from an ideal or a “standard” sample (Isaksson & Kowalski, 1993). For each individual spectrum, or sample, the MSC model can be expressed as,

$$x_{ml} = a_m + b_m \bar{x}_l + e_{ml} \quad (m = 1, \dots, N; l = 1, \dots, W) \tag{5-1}$$

where m is the measured sample number and l is the wavelength number. The constant a_m and b_m respectively represent the additive and multiplicative effects for the sample m . The \bar{x}_l is the “standard” value at l wavelength and, e_{ml} is the residual corresponding to all other effects in the spectrum that cannot be modeled by an additive and multiplicative constant (Næs et al., 2002). After simple operations, the scatter corrected spectrum will have the general form,

$$x_{ml, corrected} = (x_{ml} - a_m) / b_m \quad (5-2)$$

i.e., most of the variation due to the scatter is eliminated from the spectra, where $x_{ml, corrected}$ then remains only the variation representing the chemical information. It must be noted that, most often, the mean spectra are used as the “standard” values by averaging over the samples at the l th wavelength as follows,

$$\bar{x}_l = \frac{1}{N} \sum_{m=1}^N x_{ml} \quad (5-3)$$

However, in reality, the ideally “standard” sample does not exist, and hence that MSC would deliver different results even for the same spectrum if the MSC model was calibrated using different datasets (Datt, 1999a; Maleki et al., 2007).

Thus, in this study, we would neither perform the transformation of Eq. (5-2) nor use the mean spectra as Eq. (5-3) to correct the canopy multiple scattering, whereas it is obvious from Eqs. (5-1) and (5-2) that a formation of a ratio of reflectance difference (RRD) as Eq. (5-4) will also eliminate the scatter factors a and b , without knowing the exact values of a and b , and thus it has the advantage of being independent of the \bar{x}_l of calibration datasets,

$$RRD = \frac{R_j - R_k}{R_i - R_h} = \frac{R_{j, corrected} - R_{k, corrected}}{R_{i, corrected} - R_{h, corrected}} \quad (h \neq i; j \neq k) \quad (5-4)$$

where h , i , j , and k represent random wavelength bands over the full spectral range. Similarly, at leaf level, Peñuelas et al. (1995a) proposed the structure insensitive pigment index SIPI = $(R_{800} - R_{445}) / (R_{800} - R_{680})$ as a function of the relative composition of carotenoid and chlorophyll a , which used the same formula as Eq. (5-4). Also, a 3-band index $(R_{850} - R_{710}) / (R_{850} - R_{680})$ was developed by Datt (1999a; 1999b) for predicting leaf chlorophyll content, which provides equally a best performance in both scatter corrected and uncorrected spectra measuring from leaf stacks. Therefore, at the canopy level in this study, we hypothesized that a RRD type spectral index would be a better indicator of chlorophyll and is less sensitive to the confounding effects of soil background, canopy structure and multiple scattering. It should be noted that the RRD type indices proposed in previous studies employ three bands only, thus the use of four bands might increase the sensitivity to chlorophyll since Eq. (5-4) does not necessarily limit the use to only three bands.

5.2.3.2 Exploring the optimal indices

With the hypothesis that RRD eliminates the confounding effects of soil background, canopy structure and multiple scattering, we used a “lambda-by-lambda” band-optimization (LLBO) algorithm increasingly used for optimization of spectral indices (Darvishzadeh et al., 2008; Hansen & Schjoerring, 2003; le Maire et al., 2008; Peñuelas et al., 1995a; Thenkabail et al., 2000; 2004; Yu et al., 2013) to determine the best band combinations for RRD type indices. To date, reflectance simple-ratios and NDVI-like indices are mostly used in remote sensing. Reflectance ratios were calculated by dividing the reflectance in a reference band insensitive to pigment content to the reflectance in a band highly sensitive to pigment content (Datt, 1998; Sims & Gamon, 2002), or vice versa, wherein NDVI subtracts rather than divides (Sims & Gamon, 2002). Similarly, to explore the best band combinations for RRD, we would determine first two reference bands, and then another two bands using the LLBO algorithm. In addition, another four types of spectra indices that are often used in remote sensing would likewise be studied. To distinguish the new NDVI-like indices from the commonly used forms of NDVI, we designated these indices as normalized reflectance difference index (NRDI) in this paper, and finally optimized the following five types of reflectance-based indices,

- 1) Reflectance difference index (RDI);
- 2) Reflectance ratio index (RRI);
- 3) Normalized reflectance difference index (NRDI);
- 4) Difference of reflectance ratio index (DRRI);
- 5) Ratio of reflectance difference index (RRDI).

Names of the five types of indices were given mathematically, and the formulae are shown in Table 5-1, including some previously developed indices that have analogous forms, as well as several combined indices in hybrid forms (Table 5-1).

5.2.3.3 Optimum multiple band regression (OMBR)

The optimum multiple band regression (OMBR) model (Thenkabail *et al.*, 2000; 2002), uses a piecewise band-optimized method, the maximum R² improvement technique (SAS Institute Inc., 2008), to select the “best” one-variable model, the “best” two-variable model, and so forth, which takes the form:

$$Y = \sum_{j=1}^N a_j R_j + C \quad (5-5)$$

where Y is the dependent variable in the OMBR model, i.e., leaf Chl in this study; R_j is the reflectance at wavelength j ; a_j is the coefficient for reflectance at wavelength j ; C is the constant term. The OMBR model was run in SAS software package using the MAXR procedure (SAS Institute Inc.). The MAXR procedure begins by finding the one-band model that produces the highest R². Then another band, the one that yields the largest increase in R², is added. Once the two-band model is obtained, each of the bands in the model is compared to each band not in the model. This process continues comparing all possible switches until no switch can increase the R² and considers the switch that produces the highest R² as the “best” two-band model. Another band is then added to the model, and the comparing-and-switching process is repeated to find the “best” three-band model, and so forth (SAS Institute Inc., 2008). It should be noted that the MAXR method differs from that generally referred to as the “stepwise” method in that many more models are evaluated with MAXR, which considers all switches before making any switch (SAS Institute Inc., 2008).

5.2.3.4 Partial least squares regression (PLSR)

The partial least squares regression (PLSR) method has the advantage that the precision of the model improves with an increasing number of variables and observations (Wold *et al.*, 2001). The PLSR reduces full-spectrum data to a small set of independent latent variables, or factors, which serve as new predictors and regresses the response variables on these new predictors (Rosipal & Krämer, 2006). To determine the number of factors used in the PLSR model, leave-one-out cross validation was used to compute the predicted residual error sum of squares (PRESS), and the T-square test (van der Voet, 1994) was applied for testing the significance of incremental changes in PRESS. PLSR implemented in this study was carried out using the SAS 9.2 software package (SAS Institute Inc.)

5.2.3.5 Support vector regression (SVR)

The support vector machines (SVM) technique is a universal theory of machine learning developed by *Vapnik (1995)* originally for pattern recognition and classification (*Vapnik, 1998*). Support vector regression (SVR) is the implementation of the SVM method for regression and function approximation (*Smola & Schölkopf, 2004*). In this study, SVR models were implemented using the LIBSVM toolbox (*Chang & Lin, 2011*).

5.2.3.6 Model accuracy

The performances of the different spectral indices and multivariate models were evaluated by comparing the differences in the coefficients of determination (R^2) and root mean square error (RMSE) in predictions. The higher the R^2 and the lower the RMSE, the better the precision and accuracy the index or model provides. The RMSE values were calculated as follow:

$$RMSE = \sqrt{\frac{1}{n} \sum_{m=1}^n (y_m - \hat{y}_m)^2} \quad (5-6)$$

where y and \hat{y} are the measured and the predicated values of Chl, respectively, and n is the number of samples.

5.3 Results

In the section 5.3.1, general purpose models that do not take account of the effect of growth stage are described. In contrast, growth stage specific models concerning the effect of growth stage are described in the section 5.3.2. Since the synthetic dataset includes no growth stage information, section 5.3.2 focuses mainly on the barley dataset.

5.3.1 General purpose models

For the synthetic dataset, the optimization of RRDI was an automatic routine running without a priori knowledge of wavelengths. The best bands i and j determined in optimizing RRI (R_i and R_j) were used directly for the optimization of RRDI as the link in formulae (Table 5-1) and computational efficiency, which also demonstrates that the results are reproducible when using PROSAIL simulated data.

One might have expected the automatic routine to be consistent with the prior knowledge of wavelengths of field measured spectra. Hence, to verify whether the automatic routine agrees with a prior knowledge, we manually selected the reference bands h and k based on the prior

knowledge of canopy reflectance characteristics (section 5.3.1.3) for which the barley #1 dataset was used.

Finally, the barley #2 dataset were used to validate the best indices determined by synthetic and barley #1 datasets. Multivariate methods were used as a reference for assessing the performances of spectral indices based on the barley (barley #1 and 2) dataset.

5.3.1.1 *Published indices*

Results of correlation and regression analyses for relationships between published indices (Table 5-1) and Chl for synthetic and barley #1 datasets are shown in Table 5-4. The performances of published indices were different for synthetic and barley #1 datasets. The best 4 indices for synthetic dataset were REIP, TCARI, MTCI and EPI, which explained 76%, 78%, 78% and 80% of the variation in Chl ($\mu\text{g}/\text{cm}^2$), respectively. The best 4 indices for barley #1 dataset were PRI, PSRI, ND705 and NDVI, which explained 69%, 70%, 70% and 73% of the variation in Chl ($\mu\text{g}/\text{g}$), respectively. The widely used TCARI/ OSAVI accounted for 74% of the variation in Chl ($\mu\text{g}/\text{cm}^2$) for synthetic dataset, whereas it was not correlated significantly with Chl ($\mu\text{g}/\text{g}$) for barley #1 dataset ($R^2 = 0.003$, $p = 0.52$). Similarly, TCARI, OSAVI, NDVI and PSRI also showed very large discrepancies of accuracy between synthetic and barley #1 datasets Table 5-4.

5.3.1.2 *Optimization of indices for synthetic dataset without prior knowledge*

The LLBO algorithm was used to determine the best band combinations for the five types of indices (Table 5-1). The sensitivity of different band combinations was indicated according to the values of R^2 of Pearson Correlation. Figure 5-1 shows the lambda-by-lambda R^2 contour (LLRC) plots for different types of indices, for which the best band combinations are shown in Table 5-5. As expected, the best bands for RRI and NRDI were identical due to their inherent relationships, $\text{NRDI} = (\text{RRI} - 1) / (\text{RRI} + 1)$ or $\text{NRDI} = (1 - \text{RRI}) / (1 + \text{RRI})$. They explained 91% and 88% of the variation in Chl ($\mu\text{g}/\text{cm}^2$), respectively.

CHAPTER 5

Table 5-4: Results of regression analysis for relationships between published indices (Table 5-1) and leaf chlorophyll (Chl). Chl is presented on the bases of area ($\mu\text{g}/\text{cm}^2$) and dry mass ($\mu\text{g}/\text{g}$) for Synthetic and Barley #1 datasets, respectively.

Type	Index	Synthetic			Barley #1		
		R^2	RMSE ($\mu\text{g}/\text{cm}^2$)	p -value	R^2	RMSE ($\mu\text{g}/\text{g}$)	p -value
RD	$R_{800}-R_{680}$	0.003	28.67	<.0001	0.39	2126.8	<.0001
	$R_{705}-R_{505}$	0.74	14.74	<.0001	0.51	1914.0	<.0001
RR	PSSR_a	0.14	26.59	<.0001	0.47	1979.0	<.0001
	R_{750}/R_{710}	0.63	17.51	<.0001	0.52	1892.1	<.0001
	R_{740}/R_{720}	0.68	16.34	<.0001	0.57	1777.2	<.0001
NRD	NDVI	0.06	27.88	<.0001	0.73	1407.1	<.0001
	ND_{705}	0.58	18.66	<.0001	0.70	1501.0	<.0001
	PRI	0.68	16.17	<.0001	0.69	1510.3	<.0001
DRR	PSRI	0.07	27.65	<.0001	0.70	1499.5	<.0001
	$\text{CI}_{\text{red edge}}$	0.65	17.08	<.0001	0.40	2106.8	<.0001
	CI_{green}	0.57	18.79	<.0001	0.43	2055.3	<.0001
RRD	SIPI	0.14	26.62	<.0001	0.64	1641.8	<.0001
	EPI	0.80	12.99	<.0001	0.53	1859.0	<.0001
	mSR705	0.61	17.99	<.0001	0.51	1899.3	<.0001
	MTCI	0.78	13.60	<.0001	0.47	1980.8	<.0001
Hybrid	REIP	0.76	13.99	<.0001	0.44	2043.3	<.0001
	CARI	0.72	15.14	<.0001	0.21	2423.6	<.0001
	MCARI	0.70	15.83	<.0001	0.24	2372.5	<.0001
	TCARI	0.78	13.44	<.0001	0.003	2717.2	0.52
	OSAVI	0.03	28.30	<.0001	0.67	1567.3	<.0001
	MCARI/OSAVI	0.64	17.24	<.0001	0.57	1786.6	<.0001
	TCARI /OSAVI	0.74	14.64	<.0001	0.05	2650.4	0.003

Bold font indicates the indices yielding the highest correlations.

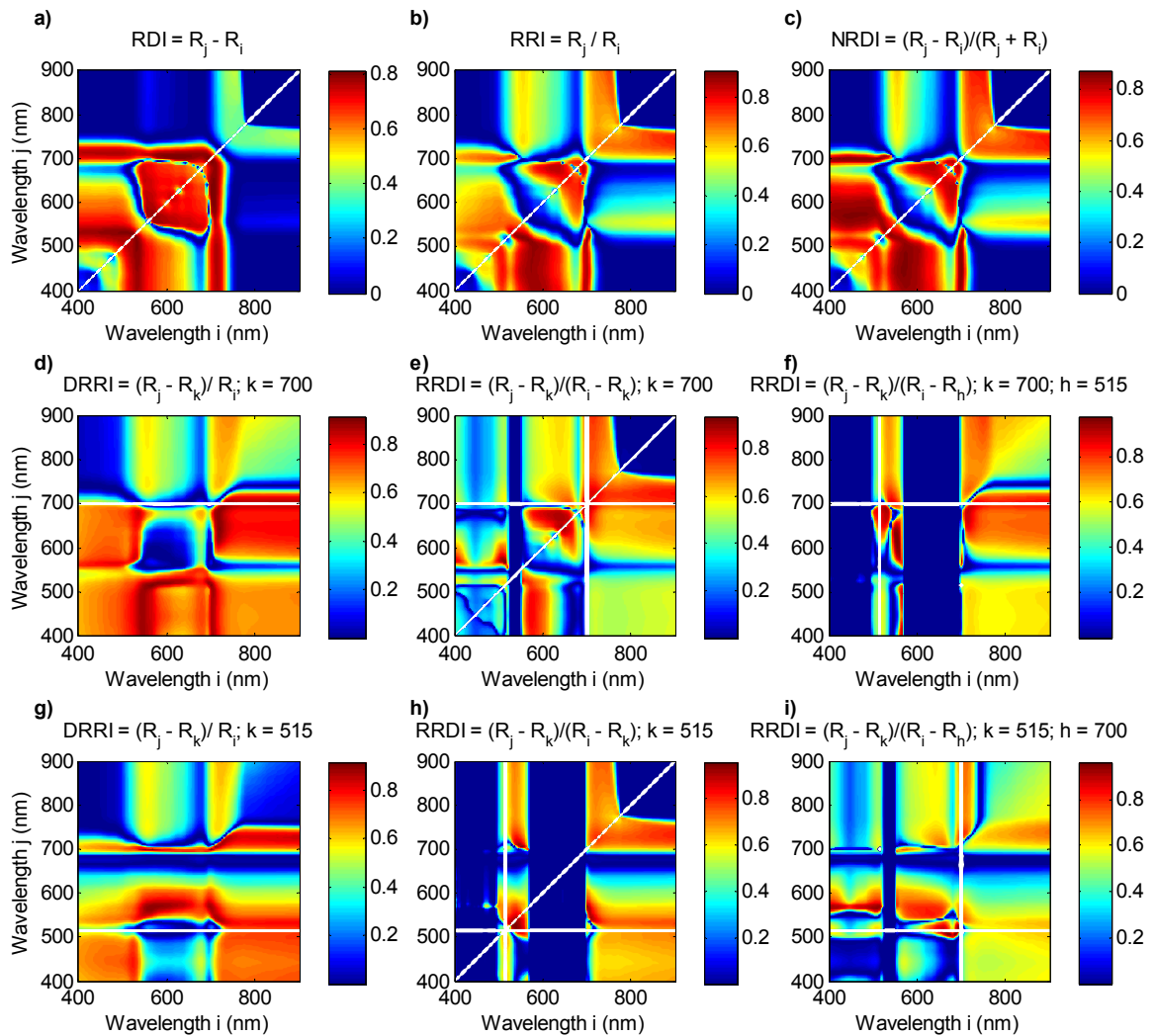


Figure 5-1: Lambda-by-lambda R^2 contour plots show the sensitivity of different band combinations to Chl ($\mu\text{g}/\text{cm}^2$) for the synthetic dataset ($n= 43200$). Subplots a, b and c show the sensitivity for RDI, RRI and NRDI, respectively. Subplots d, e and f show the sensitivity for DRRi, 3-band RRDI and 4-band RRDI, respectively, using reference bands k at 700 nm and h at 515 nm. Subplots g, h and i show the sensitivity for DRRi, 3-band RRDI and 4-band RRDI, respectively, using reference bands k at 515 nm and h at 700 nm. The synthetic dataset was generated by PROSAIL simulation (Table 5-2). Color scale bars are different between subplots.

Table 5-5: Best band combinations for each type of indices determined for synthetic and barley #1 datasets as indicated in Figure 5-1 and Figure 5-3, respectively, using the lambda-by-lambda band-optimization algorithm.

Index	Band count	Synthetic					Barley #1						
		k	h	Optimized Form	R ²	RMSE (µg/cm ²)	p-value	k	h	Optimized Form	R ²	RMSE (µg/g)	p-value
RDI	2	~	~	$R_{705} - R_{615}$	0.81	12.4	<.0001	~	~	$R_{485} - R_{450}$	0.74	1383.3	<.0001
		~	~	$R_{615} - R_{705}$	0.81	12.4	<.0001	~	~	$R_{450} - R_{485}$	0.74	1383.3	<.0001
RRI	2	~	~	R_{515} / R_{700}	0.91	8.5	<.0001	~	~	R_{640} / R_{725}	0.75	1372.0	<.0001
NIRDI	2	~	~	$(R_{700} - R_{515}) / (R_{700} + R_{515})$	0.88	10.0	<.0001	~	~	$(R_{735} - R_{660}) / (R_{735} + R_{660})$	0.75	1372.8	<.0001
		~	~	$(R_{515} - R_{700}) / (R_{515} + R_{700})$	0.88	10.0	<.0001	~	~	$(R_{660} - R_{735}) / (R_{660} + R_{735})$			
DRRI	3	700	~	$(R_{515} - R_{700}) / R_{565}$	0.92	8.4	<.0001	730	~	$(R_{725} - R_{730}) / R_{765}$	0.76	1337.8	<.0001
		515	~	$(R_{700} - R_{515}) / R_{565}$	0.92	8.4	<.0001	540	~	$(R_{570} - R_{540}) / R_{730}$	0.76	1345.3	<.0001
RRDI	3	700	~	$(R_{570} - R_{700}) / (R_{515} - R_{700})$	0.94	7.2	<.0001	730	~	$(R_{555} - R_{730}) / (R_{550} - R_{730})$	0.75	1348.2	<.0001
		515	~	$(R_{525} - R_{515}) / (R_{535} - R_{515})$	0.96	5.9	<.0001	540	~	$(R_{570} - R_{540}) / (R_{725} - R_{540})$	0.76	1345.9	<.0001
	4	700	515	$(R_{615} - R_{700}) / (R_{555} - R_{515})$	0.98	4.0	<.0001	730	540	$(R_{735} - R_{730}) / (R_{785} - R_{540})$	0.76	1327.2	<.0001
		515	700	$(R_{505} - R_{515}) / (R_{675} - R_{700})$	0.96	5.5	<.0001	540	730	$(R_{570} - R_{540}) / (R_{395} - R_{730})$	0.76	1342.7	<.0001

Tilde symbols indicate the absence of reference bands k and/or h in certain types of indices. Bold font highlights the best correlations.

The best bands i and j inherited from RRI were further used to determine the best RRD_I, as well as DRRI. As expected, optimized RRD_Is were the best indices to correlate with Chl ($\mu\text{g}/\text{cm}^2$) and accounted for 94-98% of the variation in Chl ($\mu\text{g}/\text{cm}^2$) for the synthetic dataset (Table 5-5). Figure 5-2 shows the scatterplots of Chl ($\mu\text{g}/\text{cm}^2$) with three widely used chlorophyll indices, $\text{CI}_{\text{red-edge}}$, MCARI/OSAVI and TCARI/OSAVI, as well as the best RDI, RRI, NRDI, DRRI and RRD_I. Apparently, $\text{CI}_{\text{red-edge}}$ was very sensitive to LAI variations as Figure 5-2a shows a highly scattered relationship. MCARI/OSAVI and TCARI/OSAVI relatively resisted LAI variations and yielded nonlinear relationships (Figure 5-2b and c), which still scatter (point span) to some degree at each LAI level and show saturations for middle-to-high Chl (40-100 $\mu\text{g}/\text{cm}^2$). The best RDI, RRI, NRDI and DRRI yielded robust correlations with Chl ($\mu\text{g}/\text{cm}^2$), with R^2 of 0.81 ($p < 0.0001$), 0.91 ($p < 0.0001$), 0.88 ($p < 0.0001$), and 0.92 ($p < 0.0001$), respectively (Table 5-5), but the relationships still slightly scatter at each LAI level (Figure 5-2d-g). The best RRD_I = $(R_{615} - R_{700}) / (R_{555} - R_{515})$ was most robustly and linearly related to Chl ($\mu\text{g}/\text{cm}^2$) with R^2 of 0.98 ($p < 0.0001$) and was most insensitive to LAI variations (Table 5-5 and Figure 5-2h).

5.3.1.3 Canopy reflectance characteristics of barley (“prior knowledge”)

Canopy reflectance varied over the spectral range from visible to NIR (Figure 5-3a) and showed both additive and multiplicative effects (Figure 5-3b), suggesting the confounding effects of soil background, canopy structure and multiple scattering on canopy reflectance data across the seven growth stages. Coefficient of variation (CV) is considered as a good means of comparing the variation among different variables (e.g. wavelengths). The CV curve shows that canopy reflectance at 660-680 nm yielded the highest CV, followed by reflectance at 490-500 nm (Figure 5-3c). In contrast, wavelength range for red edge to NIR showed lower CV. This result agrees well with a previous canopy-level (airborne) survey that the red edge to NIR range yielded lower CV than visible bands (Collins, 1978), despite the fact that visible bands showed lower standard deviations (Figure 5-3d). Reflectance at red edge (730 nm) showed the lowest CV, followed by reflectance at 530-550 nm of green, which yielded a broad “trough” in the CV curve. The two “troughs” at around 540 and 730 nm were also noticed in the canopy-level study by Collins (1978). In contrast, reflectance measured on leaf stacks yielded a local peak of CV near 550 nm, while was a trough near 680 nm (Datt, 1999a). This inconsistency suggests that the variation in canopy reflectance over wavelengths measured in the field differs from that of reflectance measured on leaf stacks, again highlighting the effects of soil background, canopy structure and multiple scattering on canopy-level reflectance.

CHAPTER 5

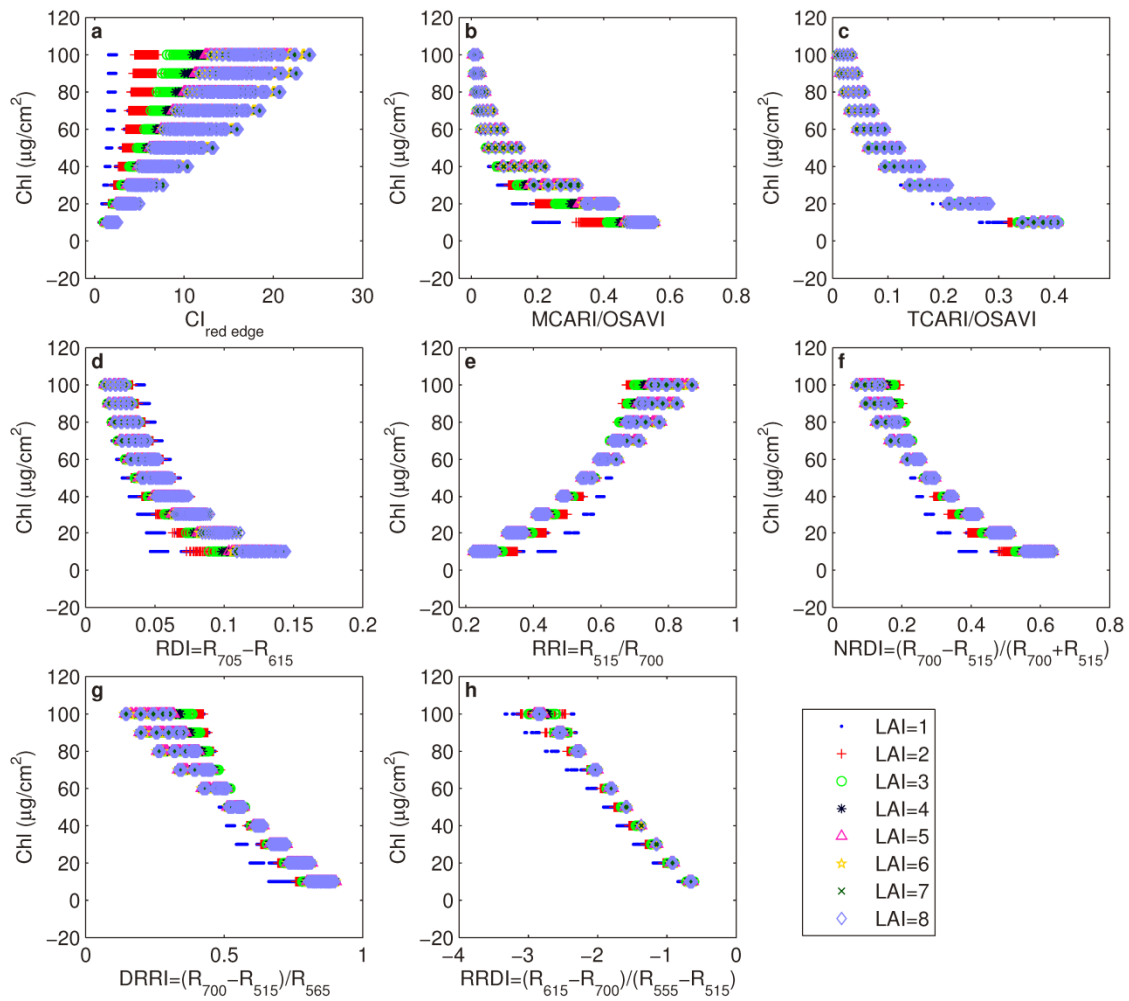


Figure 5-2: Leaf chlorophyll (Chl, $\mu\text{g}/\text{cm}^2$) plotted as a function of three published chlorophyll indices, (a) $CI_{\text{red edge}}$, (b) $MCARI/OSAVI$ and (c) $TCARI/OSAVI$ and (d-h) the best RDI , RRI , $NRDI$, $DRRI$ and $RRDI$ determined for the synthetic dataset, where canopy reflectance spectra were simulated by the PROSAIL model with LAI ranging from 1 to 8 by 1 at each step.

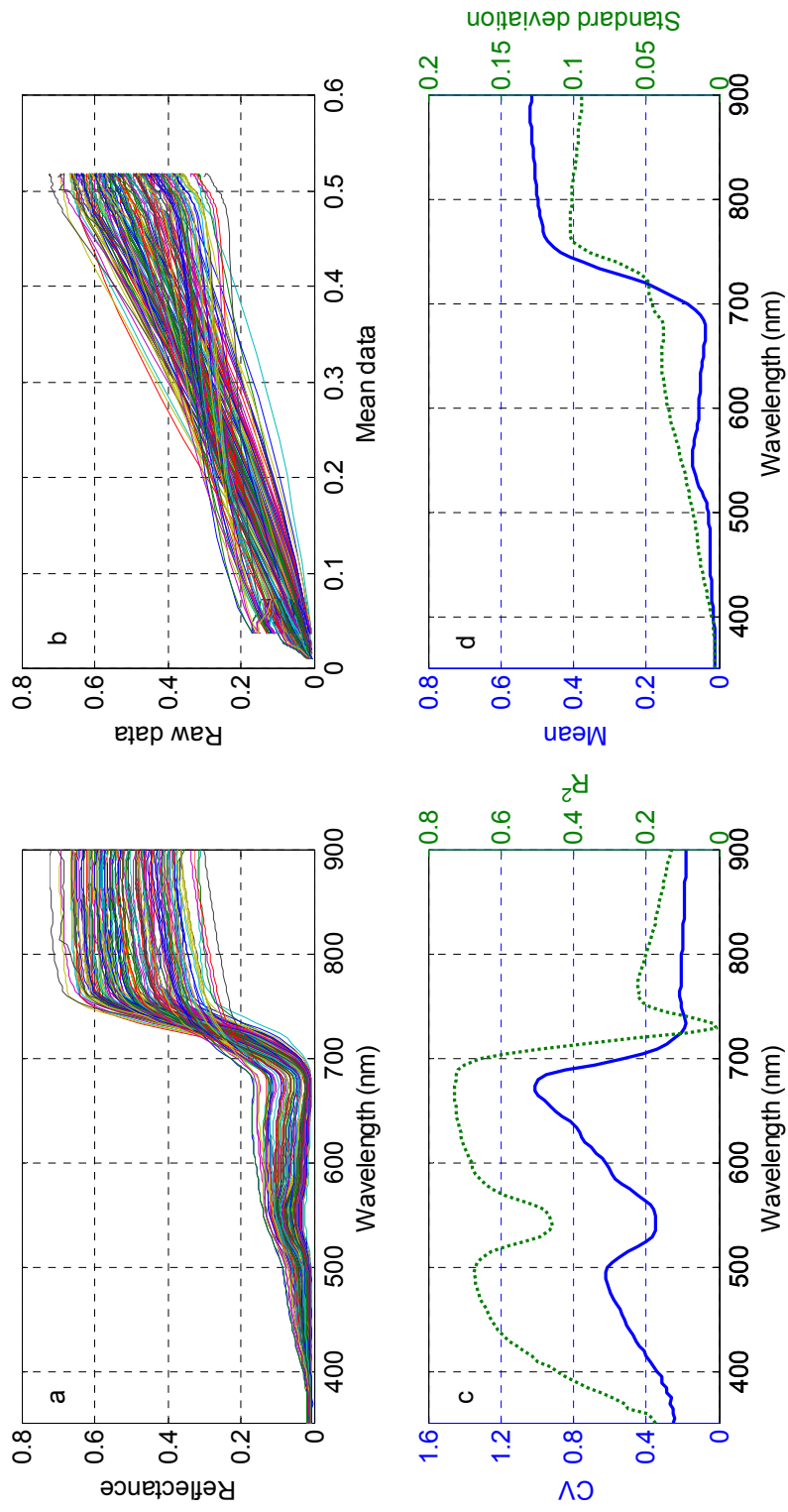


Figure 5-3: Measured canopy reflectance data (a), relationships of measured reflectance (raw data) as a function of mean data derived from Eq. (5-3) (b), R^2 curve (dot line) for canopy reflectance vs. leaf Chl ($\mu\text{g/g}$) and coefficient of variation (CV) curve (solid line) (c) and, mean (solid line) and standard deviation (dot line) (d) over the wavelength range for 350-900 nm. Results were generated using the barley #1 dataset ($n=168$).

Correlation analysis was performed by sequentially correlating the value of reflectance at each wavelength against Chl ($\mu\text{g/g}$) and plotting the R^2 against all wavelengths. The R^2 curve shows a very similar pattern with the CV curve in which reflectance at 660-680 nm of red showed maximum sensitivity to Chl ($\mu\text{g/g}$), followed by reflectance at 490-500 nm of blue (Figure 5-3c). Reflectance at 730 nm yielded the lowest R^2 and showed a deep trough in the R^2 curve, while reflectance at 530-550 nm of green bands also showed a dip. This result agrees with previous study using canopy-level reflectance (Blackburn, 1998b).

5.3.1.4 Optimization of indices for barley dataset with the “prior knowledge”

Figure 5-4 shows the LLRC plots for Chl ($\mu\text{g/g}$) vs. RD, RR, NDR, DRR and RRD type indices based on barley #1 dataset, which generated broader “hot zones” relative to the synthetic dataset (Figure 5-1). Notably, for synthetic and barley #1 datasets, LLRC plots for RDI and NRDI both show diagonally symmetrical patterns (Figure 5-1a and c and Figure 5-4a and c), whereas RRI produced asymmetrical patterns (Figure 5-1b and Figure 5-4b). The asymmetrical pattern for RRI indirectly agrees with previous studies that reciprocal reflectance at certain wavelengths could be very useful for chlorophyll quantification (Gitelson *et al.*, 1996; 2003), since an RRI and its reciprocal (i.e., two symmetric points above and below the diagonal) could yield significantly different values of R^2 (Figure 5-1b and Figure 5-4b).

Across all growth stages, higher CV suggests the higher degree of variation in reflectance at certain wavelengths, which are more likely to co-vary with changing ground coverage and structural properties. Accordingly, wavelengths at 730 nm and 540 nm that yielded the local minima of CV were used as the reference bands k and h for the optimizations of DRR and RRD. As expected, LLRC plots for DRR and RRD that used the reference band k at 540 nm (Figure 5-4g) show significantly different patterns from the use of k at 730 nm (Figure 5-4d), as well as for reference band h . Table 5-5 summarizes the best band combinations derived from all of the LLRC plots in Figure 5-4.

Optimized RD, RR, NRD, DRR and RRD type indices slightly improved the correlation and yielded smaller RMSEs compared to published indices that have analogous forms (Table 5-4 and Table 5-5). Among these, the 4-band RRD $= (R_{735} - R_{730}) / (R_{785} - R_{540})$ yielded the highest correlation ($R^2 = 0.76$, $p < 0.0001$) with Chl ($\mu\text{g/g}$). Figure 5-5 shows the relationships between the Chl ($\mu\text{g/g}$) and best RRDs and DRRs for the barley #1 dataset.

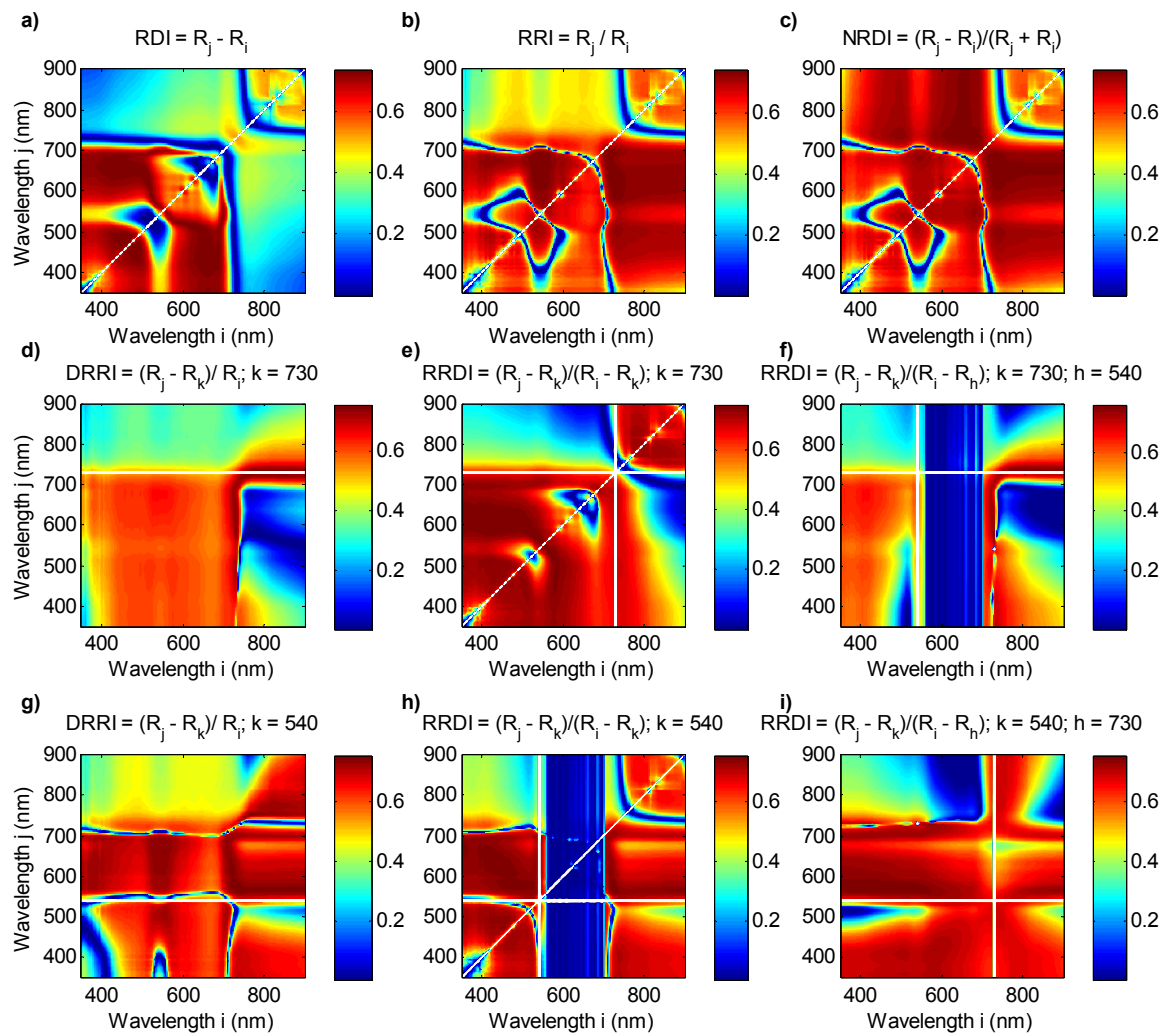


Figure 5-4: Lambda-by-lambda R^2 contour plots showing the sensitivity of different band combinations to leaf Chl ($\mu\text{g/g}$) of barley. Subplots a, b and c show the sensitivity for RDI, RRI and NRDI, respectively. Subplots d, e and f show the sensitivity DRRI, 3-band RRD1 and 4-band RRD1, respectively, using reference bands k at 730 nm and h at 540nm. Subplots g, h and i show the sensitivity for DRRI, 3-band RRD1 and 4-band RRD1, respectively, with reference bands k at 540 nm and h at 730 nm. Results were generated using the barley #1 dataset ($n=168$). Color scale bars are different between subplots.

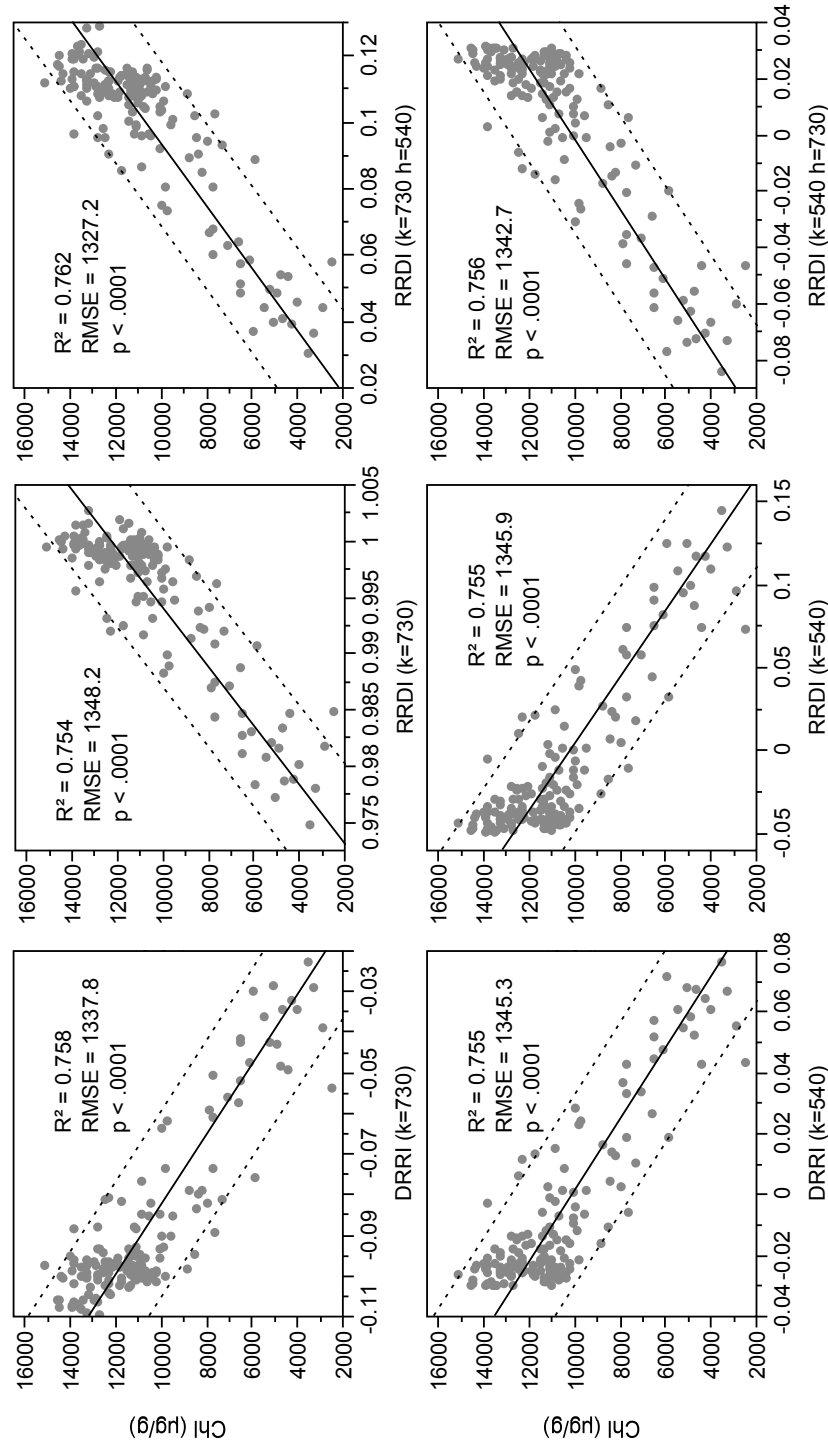


Figure 5-5: Scatter plots showing best DRRIs and RRDI s derived from Figure 5-4 as a function of leaf Chl (µg/g) for the barley #1 (calibration) dataset (n=168). Solid and dash lines indicate the linear fit and 95% confidence intervals of prediction, respectively.

Interestingly, the three best indices: the DRRI= $(R_{570}-R_{540})/R_{730}$, the 3-band RRDI= $(R_{570}-R_{540})/(R_{725}-R_{540})$ and the 4-band RRDI= $(R_{570}-R_{540})/(R_{395}-R_{730})$ showed remarkable consistency in band combinations (Table 5-5 and Figure 5-5), which are very close to the form of photochemical reflectance index (PRI= $(R_{531}-R_{570})/(R_{531}+R_{570})$) (Gamon et al., 1992; Peñuelas et al., 1995b). Although PRI was originally proposed for the assessment of photosynthetic light use efficiency (LUE), recent studies have shown that PRI is also significantly related to leaf total chlorophyll (Moran et al., 2000; Nakaji et al., 2006; Weng et al., 2009), especially when PRI is measured over a long time span or across species (reviewed by Ustin et al., 2009). Accordingly, we incorporated one additional reference band at 730 nm into PRI to be a PRI-like 3-band RRDI= $(R_{531}-R_{570})/(R_{531}-R_{730})$ and, found that this 3-band RRDI improved the correlation ($R^2 = 0.75$, $p < 0.0001$) with Chl ($\mu\text{g/g}$) and lowered the RMSE (1356.7 $\mu\text{g/g}$) compared to PRI ($R^2 = 0.69$, $p < 0.0001$, RMSE=1510.3 $\mu\text{g/g}$) (Figure 5-6 and Table 5-4). This further confirms our hypothesis and also suggests the usefulness of prior knowledge of wavelengths. Clearly, structural differences of the canopies and background effects (soil color, moisture, shadows etc.) still preclude the operational use of PRI at the canopy scale (Peñuelas et al., 2011). The PRI-like 3-band RRDI used here might not ensure the success of assessment of LUE, but the method is expected to apply to the optimization of spectral indices for LUE assessment.

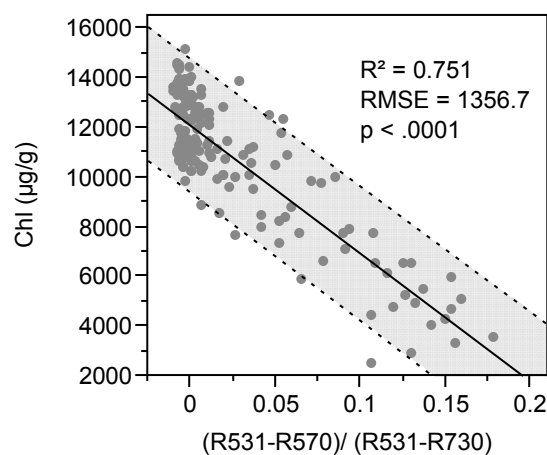


Figure 5-6: Plot of the PRI-like RRDI= $(R_{531}-R_{570})/(R_{531}-R_{730})$ as a function of leaf Chl ($\mu\text{g/g}$) based on the barley #1 (calibration) dataset ($n=168$). Solid and dash lines indicate the linear fit and 95% confidence intervals of prediction, respectively.

Given the fact that both additive and multiplicative effects existed in canopy-level reflectance and that reflectance for each sample was approximately linear with the empirically assumed “standard” as Eq. (5-3) (Figure 5-3b), the RRDI was thus expected to eliminate both additive and multiplicative effects according to our hypothesis.

5.3.1.5 Cross validation of spectral indices

The top ranked 4 published indices for synthetic (REIP, TCARI, MTCI and EPI) and barley #1 (PRI, PSRI, ND705 and NDVI) datasets (Table 5-4) and top ranked 4 optimized indices for each dataset (Table 5-5) were cross-validated and further evaluated by the barley #2 dataset. Cross validation between synthetic and barley #1 datasets showed that accuracy generally decreased for the validation (Table 5-6). Results also showed that the best index calibrated by barley #1 ($RRDI = (R_{735} - R_{730}) / (R_{785} - R_{540})$) performed better in predicting Chl ($\mu\text{g/g}$) for barley #2 than the index calibrated by the synthetic dataset ($RRDI = (R_{615} - R_{700}) / (R_{555} - R_{515})$), the former and the latter accounted for 76% and 45% of the variation in Chl ($\mu\text{g/g}$) for barley #2 dataset, respectively (Table 5-6).

5.3.1.6 Multivariate models

OMBR models

We constructed best 1- to 4-band OMBR models to compare with spectral indices. For the calibration step using the barley #1 dataset, 1- to 4-band OMBR models explained 72-77% of the variation in Chl ($\mu\text{g/g}$) for the barley #1 dataset. The more band counts used in an OMBR model, the more of the variation in Chl ($\mu\text{g/g}$) was explained by the model (Table 5-7). The 4-band OMBR model only marginally increased the R^2 by 0.01 compared with the best 4-band RRDI (Table 5-5 and Table 5-7). For the validation step using barley #2 dataset, the 2-band OMBR model provided the best performance in predicting Chl ($\mu\text{g/g}$) with R^2 of 0.74 ($p < 0.0001$) and RMSE of 1184.8 $\mu\text{g/g}$, whereas the 4-band OMBR model provided relatively lower accuracy with R^2 of 0.69 ($p < 0.0001$) and RMSE of 1292.2 $\mu\text{g/g}$ (Table 5-7). Clearly, the 4-band OMBR model was over-fitted. This suggests that uncertainty remains for an OMBR model that has higher calibration accuracy when it is used for independent observations. Our results showed that the 2-band OMBR model was preferred in terms of validation accuracy.

Table 5-6: Cross validations of top ranked 4 published and 4 best indices determined in Synthetic and Barley #1 datasets respectively for the estimation of leaf chlorophyll (Chl) in independent datasets.

Validation	Synthetic			Barley #1			Barley #2		
	R ²	RMSE (µg/cm ²)	p-value	R ²	RMSE (µg/g)	p-value	R ²	RMSE (µg/g)	p-value
<u>Calibration: Synthetic</u>									
Published									
EPI	~	~	~	0.53	1859.0	<.0001	0.61	1443.4	<.0001
MTCI	~	~	~	0.47	1980.8	<.0001	0.51	1621.8	<.0001
REIP	~	~	~	0.44	2043.3	<.0001	0.52	1592.9	<.0001
TCARI	~	~	~	0.00	2717.2	0.52	0.00	2305.9	0.72
This study	~	~	~	0.58	1764.6	<.0001	0.58	1488.7	<.0001
				0.12	2552.8	<.0001	0.13	2149.5	<.0001
				0.45	2012.9	<.0001	0.45	1715.1	<.0001
				0.06	2643.5	0.002	0.24	2016.9	<.0001
<u>Calibration: Barley #1</u>									
Published									
NDVI	0.06	27.9	<.0001	~	~	~	0.75	1253.7	<.0001
ND ₇₀₅	0.58	18.7	<.0001	~	~	~	0.71	1248.7	<.0001
PRI	0.68	16.2	<.0001	~	~	~	0.64	1377.4	<.0001
PSRI	0.07	27.7	<.0001	~	~	~	0.74	1172.1	<.0001
This study	0.43	21.7	<.0001	~	~	~	0.75	1142.6	<.0001
	0.40	22.2	<.0001	~	~	~	0.73	1189.8	<.0001
	0.56	19.1	<.0001	~	~	~	0.76	1141.5	<.0001
	0.41	22.0	<.0001	~	~	~	0.74	1186.3	<.0001

Tilde symbols replace unnecessary self-validations.

Bold font highlights the indices with best performance for each validation dataset.

CHAPTER 5*PLSR models*

We applied leave-one-out cross validation to determine the optimal number of factors to be used in PLSR models. Results showed that 7 factors yielded the minimum of the prediction error (PRESS). Generally, the number of factors that yields the minimum PRESS is used to calibrate a PLSR model. However, using the number of factors which yields the minimum in PRESS can also lead to some overfitting (Haaland & Thomas, 1988). Therefore, we implemented the T-square test (van der Voet, 1994) and found that use of no less than 3 factors did not significantly increase the PRESS (Figure 5-7). Consequently, we constructed two PLSR models for Chl ($\mu\text{g/g}$) prediction with 3 and 7 factors, respectively. They explained 73% and 78% of the variation in Chl ($\mu\text{g/g}$) for the barley # 1 dataset, respectively (Table 5-7). However, for the validation step using the barley #2 dataset, the PLSR model with 3 factors explained more of the variation in Chl ($\mu\text{g/g}$) ($R^2= 0.73$, $p < 0.0001$) and yielded lower RMSE (1195.1 $\mu\text{g/g}$) than the model with 7 factors ($R^2= 0.68$, $p < 0.0001$, RMSE= 1297.5 $\mu\text{g/g}$), highlighting that using the number of factors which produces the minimum PRESS to calibrate a PLSR model might lead to some decrease in accuracy when used for predicting future observations. Clearly, in this study, 3 factors was a better choice to calibrate the PLSR model.

Table 5-7: Optimum multiple band regression (OMBR), partial least squares regression (PLSR) and support vector regression (SVR) models for the predictions of Chl ($\mu\text{g/g}$) for Barley #1 (calibration) and Barley #2 (validation) datasets.

Model	Barley #1 dataset ($n=168$)			Barley #2 dataset ($n=126$)			
	R^2	RMSE ($\mu\text{g/g}$)	p -value	R^2	RMSE ($\mu\text{g/g}$)	p -value	
OMBR	Band count						
	1	0.72	1420.8	<.0001	0.71	1231.9	<.0001
	2	0.74	1385.0	<.0001	0.74	1184.8	<.0001
	3	0.76	1342.3	<.0001	0.68	1301.9	<.0001
	4	0.77	1312.7	<.0001	0.69	1292.2	<.0001
PLSR	Factors						
	3	0.73	1410.8	<.0001	0.73	1195.1	<.0001
	7	0.78	1267.7	<.0001	0.68	1297.5	<.0001
SVR	Kernel						
	RBF	0.76	1233.7	<.0001	0.73	1197.6	<.0001
	Linear	0.81	1176.4	<.0001	0.67	1330.0	<.0001
	Polynomial	0.72	1435.5	<.0001	0.68	1311.9	<.0001

n , number of samples

Bold font indicates the best performance for each type of model in terms of model validation.

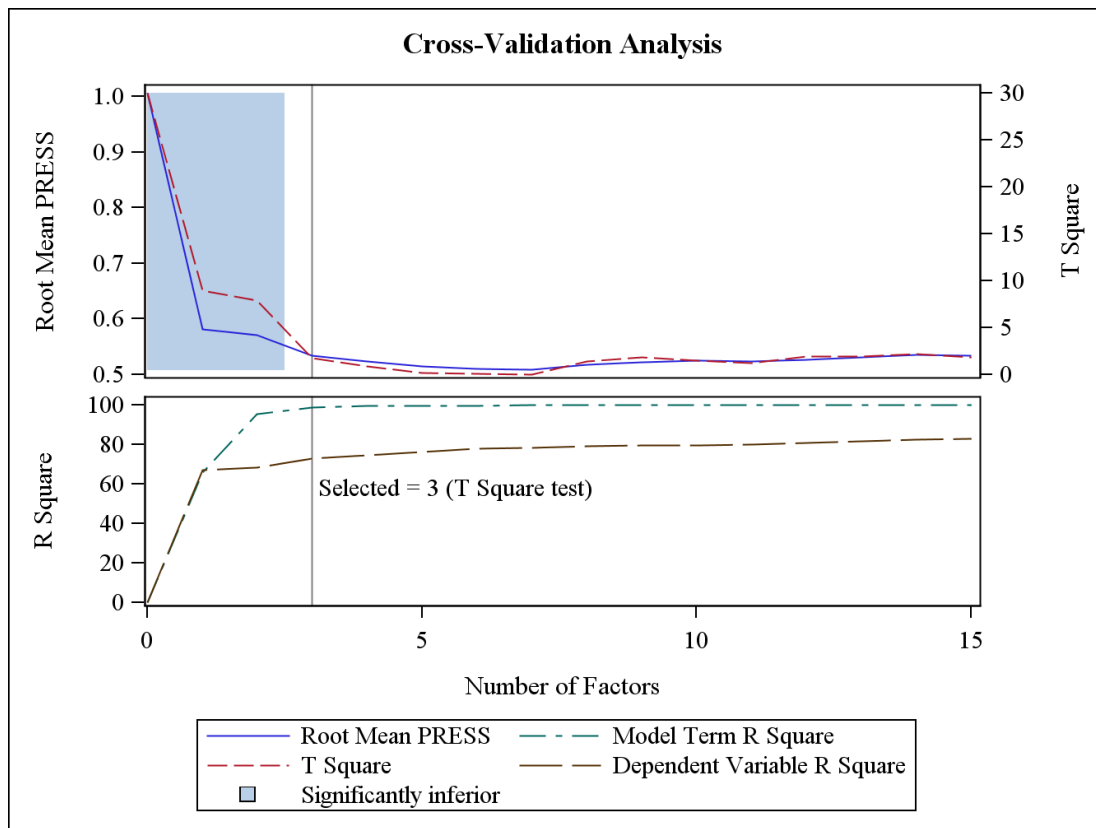


Figure 5-7: Results of Leave-One-Out Cross-Validation (LOOCV) and T-square significance test showing the optimal number of factors for constructing the PLSR model.

SVR models

In this study, we constructed three SVR models, one with a radial basis function (RBF), a linear and a polynomial kernel respectively. Generally, the RBF kernel is preferred for SVR, because it can handle the case where the relations between dependent variables and predictors are nonlinear, and it also has fewer numerical difficulties (Hsu et al., 2003). By the “grid search” on C and γ using cross validation (Figure 5-8), the SVR model with RBF kernel was optimized for Chl ($\mu\text{g/g}$) prediction. Results showed that RBF-, linear- and polynomial-SVR models explained 76%, 81% and 72% of the variation in Chl ($\mu\text{g/g}$), respectively, with RMSEs of 1233.7, 1176.4 and 1435.5 $\mu\text{g/g}$ for the calibration step using the barley #1 dataset (Table 5-7). Although the linear-SVR model explained relatively more of the variation in Chl ($\mu\text{g/g}$) than the other two SVR models, for the validation step using the barley #2 dataset RBF-SVR model outperformed the linear and polynomial models and explained 73% of the variation in Chl ($\mu\text{g/g}$) with the lowest RMSE (1197.6 $\mu\text{g/g}$). Therefore, RBF-SVR was the best model in terms of accuracy for both the calibration (barley #1) and validation (barley #2) datasets in this research.

was closer to the distribution of destructively measured values of Chl ($\mu\text{g/g}$) than was the distribution of Chl ($\mu\text{g/g}$) predicted by multivariate models (histograms in Figure 5-9).

Figure 5-10 shows the scatterplots of RREDI predicted Chl ($\mu\text{g/g}$) as a function of OMBR, PLSR and SVR predicted Chl ($\mu\text{g/g}$) for barley #2 dataset. RREDI predicted Chl ($\mu\text{g/g}$) values agreed very well with the Chl ($\mu\text{g/g}$) values predicted by the three multivariate models, suggesting the reliability of RREDI in predicting Chl. In terms of consistency, SVR was the best, followed by PLSR and OMBR models (Figure 5-10). Therefore, multivariate models are also powerful to verify the robustness of univariate models based on spectral indices. In addition, multivariate models have the advantage of using one calibration model to estimate multiple dependent variables such as canopy chemicals (e.g., *Asner & Martin, 2008*).

5.3.2 Growth stage specific models

In section 5.3.1, optimized indices for the synthetic dataset showed robust relationships with Chl ($\mu\text{g/cm}^2$) (Figure 5-2). However, the scatterplots for the barley dataset show relatively large variability despite the high correlations (Figure 5-5, Figure 5-6 and Figure 5-9), suggesting the poor predictive ability for individual stages. Therefore, indices were optimized for each growth stage and different stage spans.

5.3.2.1 Published indices vs. Chl in each growth stage

Regression analysis for published indices with barley Chl ($\mu\text{g/g}$) was performed for each growth stage. Results showed that all published indices failed to account for the variation in Chl ($\mu\text{g/g}$) for individual stages such as BBCH 32, 39, 51, 55, 61 and 73 ($R^2 \leq 0.27$), with the exception of BBCH 83 stage where R_{740}/R_{720} explained 55% of the variation in Chl ($\mu\text{g/g}$) (Table 5-8).

CHAPTER 5

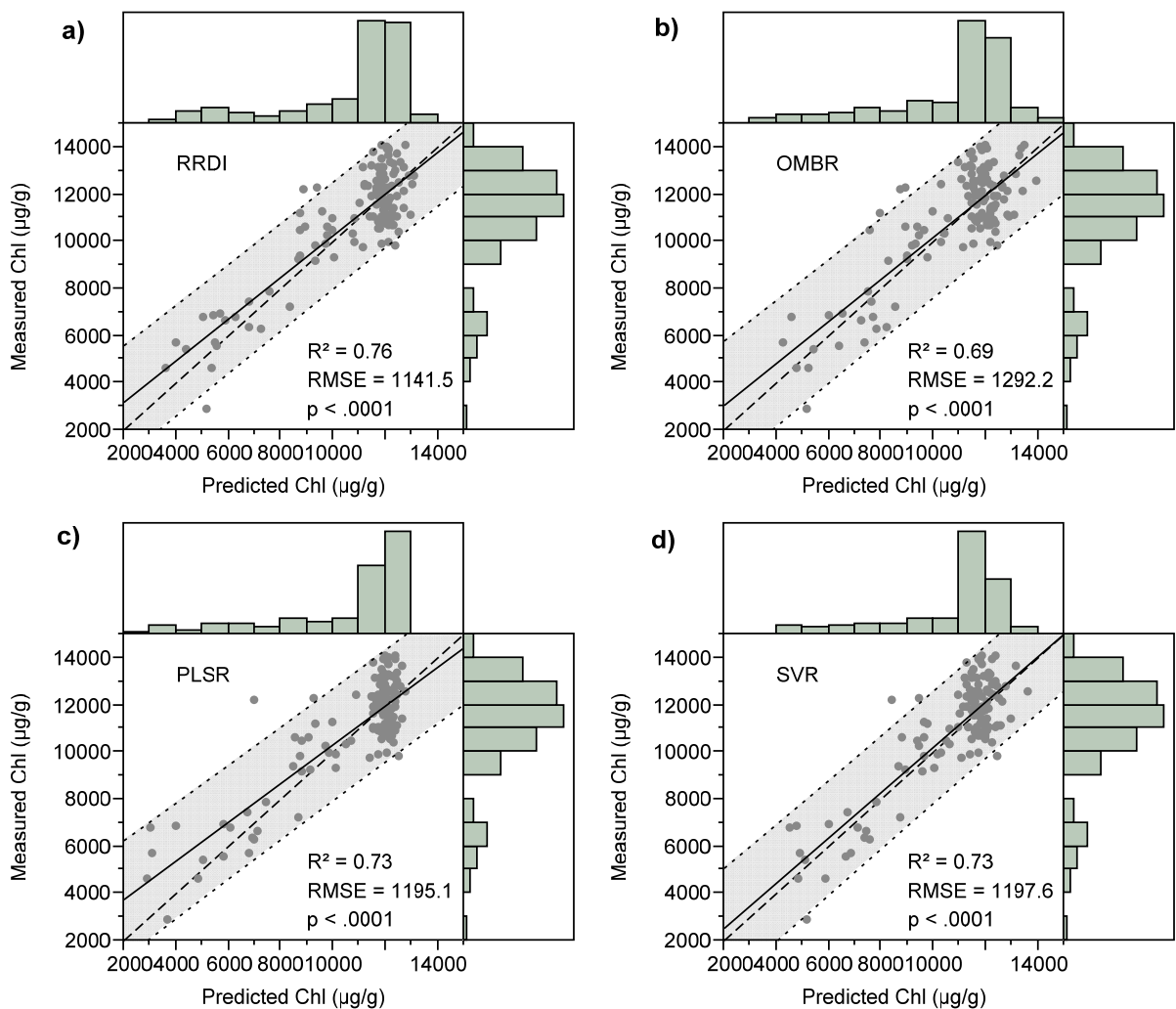


Figure 5-9: Scatter and histogram plots showing the measured leaf Chl (µg/g) as a function of predicted Chl by (a) RRDI= $(R_{735}-R_{730}) / (R_{785}-R_{540})$, (b) OMBR, (c) PLSR and (d) SVR models and distributions of both measured and predicted values for the barley #2 (validation) dataset (n=126). Solid, dash and dotted lines indicate linear fits, 1:1 lines and confidence intervals of prediction, respectively.

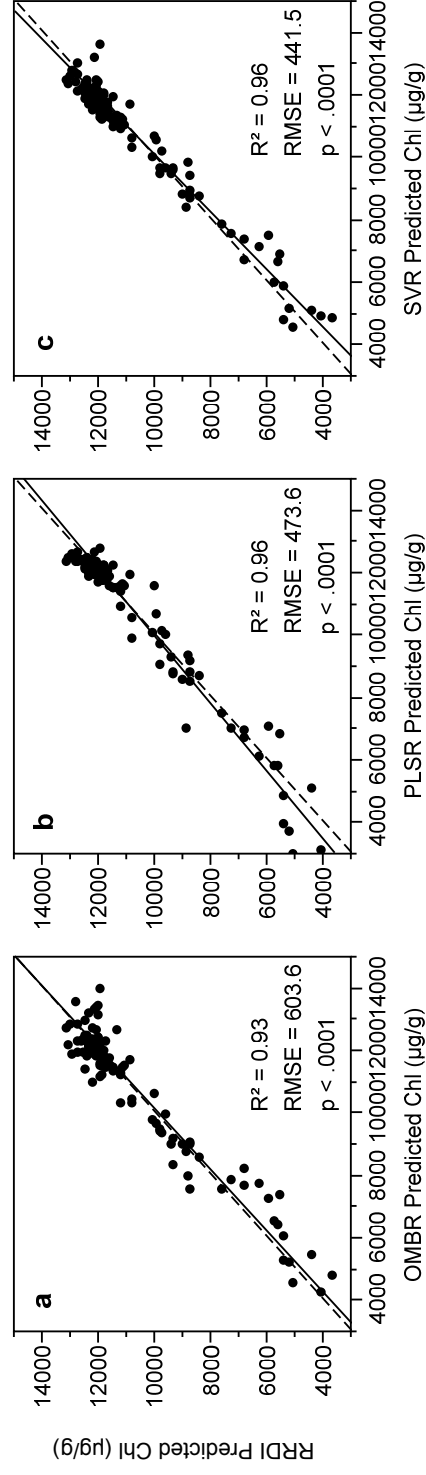


Figure 5-10: Scatter plots show $RRDI = (R_{735} - R_{730}) / (R_{785} - R_{540})$ predicted Chl ($\mu\text{g/g}$) as a function of (a) OMBR, (b) PLSR and (c) SVR predicted Chl ($\mu\text{g/g}$) based on the barley #1 dataset ($n=126$). Solid and dash lines indicate linear fits and 1:1 lines, respectively.

5.3.2.2 Optimization of indices for specific growth stages

The best RRI and RRDI were determined for each single stage using the LLBO algorithm. Table 5-9 shows the best band combinations and corresponding R^2 values. The optimized RRIs yielded moderate correlations in BBCH 32, 39, and 83 with R^2 of 0.45, 0.41 ($p < 0.0001$) and 0.59, respectively, whereas the correlations were very poor for other stages ($R^2 \leq 0.32$, Table 5-9). With the automatic optimization routine for RRDI optimization (described in section 5.3.1), best RRDI improved the R^2 for each growth stage compared to RRIs (Figure 5-11a). Notably, the correlations were still poor in BBCH 39, 55, 61 and 73 stages ($R^2 \leq 0.40$) (Table 5-9). However, BBCH 39 is the critical stage for fertilization for high yield, BBCH 55 and 61 are the middle heading and early flowering stages, where a small amount of fertilizer is often applied to regulate within-field variations.

To improve the estimation of Chl ($\mu\text{g/g}$) in these stages, we optimized indices for all possible cases of growth stage spans respectively in the forward- and backward-cumulative ways (see also descriptions in Table 5-9). Similarly to single stage, the best RRI and RRDI were determined for each of the stage spans using the LLBO algorithm. The R^2 and the best band combinations for RR and RRD are shown in Table 5-9. The forward-cumulative (BBCH 32-39) method significantly improved the correlations before BBCH 51. Optimized RRI and RRDI yielded an increase of R^2 by 0.24 and 0.43, respectively, relative to the single stage (BBCH 39) method (Figure 5-11b and Table 5-9). Figure 5-12a shows the relationship between Chl ($\mu\text{g/g}$) and the RRDI optimized for BBCH 32-39 ($R^2 = 0.65$, $p < 0.0001$). Notably, RRDI outperformed RRI with an increase of R^2 by 0.24 (Figure 5-11b and Table 5-9). In contrast, the backward-cumulative method improved the correlations more significantly after BBCH 51. Optimized RRIs and RRDI yielded an increase of R^2 by 0.43-0.63 relative to the single stage method for BBCH 55, 61 and 73 (Table 5-9).

Table 5-8: Results of regression analysis for relationships between published indices (Table 5-1) and leaf chlorophyll (Chl, $\mu\text{g/g}$) for barley dataset in each growth stage.

Index	Barley_BBCH32			Barley_BBCH39			Barley_BBCH51			Barley_BBCH55			Barley_BBCH61			Barley_BBCH73			Barley_BBCH83		
	R^2	RMSE ($\mu\text{g/g}$)	p-value	R^2	RMSE ($\mu\text{g/g}$)	p-value	R^2	RMSE ($\mu\text{g/g}$)	p-value	R^2	RMSE ($\mu\text{g/g}$)	p-value	R^2	RMSE ($\mu\text{g/g}$)	p-value	R^2	RMSE ($\mu\text{g/g}$)	p-value	R^2	RMSE ($\mu\text{g/g}$)	p-value
$R_{800}-R_{680}$	0.27	669.0	0.001	0.06	506.8	0.119	0.00	1243.7	0.927	0.00	1088.3	0.696	0.03	1251.3	0.265	0.10	1526.4	0.046	0.44	1318.6	<0.0001
$R_{705}-R_{505}$	0.09	748.2	0.057	0.01	519.7	0.500	0.02	1229.9	0.344	0.01	1084.3	0.507	0.22	1121.5	0.002	0.02	1587.8	0.352	0.05	1712.0	0.147
PSSR _s	0.09	747.6	0.055	0.00	520.7	0.588	0.01	1239.2	0.585	0.01	1086.0	0.572	0.13	1184.7	0.018	0.03	1578.6	0.249	0.53	1207.1	<0.0001
R_{750}/R_{710}	0.09	748.3	0.058	0.00	522.0	0.746	0.02	1231.8	0.379	0.00	1089.0	0.747	0.16	1165.9	0.009	0.01	1595.7	0.490	0.54	1197.2	<0.0001
R_{740}/R_{720}	0.08	750.1	0.065	0.00	522.1	0.779	0.02	1232.2	0.389	0.01	1086.8	0.613	0.17	1156.6	0.006	0.01	1597.7	0.538	0.55	1184.2	<0.0001
NDVI	0.08	752.3	0.074	0.00	521.5	0.673	0.01	1239.8	0.611	0.03	1076.1	0.308	0.20	1139.8	0.003	0.06	1559.3	0.130	0.47	1276.3	<0.0001
ND ₇₀₅	0.08	750.7	0.067	0.00	522.4	0.851	0.01	1235.0	0.451	0.01	1084.7	0.522	0.19	1143.0	0.004	0.02	1586.2	0.330	0.52	1216.7	<0.0001
PRI	0.12	734.2	0.024	0.00	522.6	0.933	0.05	1213.0	0.159	0.06	1054.8	0.106	0.14	1175.8	0.013	0.02	1588.0	0.355	0.31	1462.1	<0.0001
PSRI	0.00	783.9	0.870	0.00	522.6	0.932	0.02	1228.8	0.326	0.02	1078.6	0.353	0.16	1163.6	0.008	0.07	151.0	0.099	0.43	1326.0	<0.0001
$CI_{\text{red edge}}$	0.10	744.7	0.046	0.01	521.2	0.633	0.04	1218.9	0.206	0.00	1089.1	0.765	0.17	1155.6	0.006	0.00	1604.9	0.882	0.52	1217.1	<0.0001
CI_{green}	0.12	733.7	0.024	0.01	519.7	0.501	0.01	1235.0	0.451	0.01	1087.5	0.650	0.15	1169.8	0.010	0.01	1593.7	0.448	0.54	1191.7	<0.0001
SIPI	0.02	777.6	0.423	0.00	522.7	0.980	0.01	1237.8	0.533	0.03	1076.2	0.309	0.18	1152.0	0.005	0.07	1551.9	0.102	0.38	1380.9	<0.0001
EPI	0.09	748.2	0.057	0.00	522.4	0.827	0.02	1228.9	0.328	0.00	1088.2	0.690	0.20	1140.0	0.003	0.00	1604.5	0.835	0.27	1505.2	0.001
mSR705	0.08	752.7	0.076	0.00	522.2	0.780	0.02	1231.1	0.366	0.00	1089.4	0.790	0.15	1169.9	0.011	0.01	1597.3	0.528	0.54	1198.8	<0.0001
MTCI	0.09	749.0	0.060	0.00	522.1	0.773	0.02	1229.9	0.345	0.00	1089.7	0.818	0.16	1165.8	0.009	0.00	1604.8	0.864	0.51	1230.1	<0.0001
REIP	0.09	747.0	0.053	0.01	521.3	0.654	0.05	1213.0	0.159	0.00	1089.6	0.812	0.19	1145.9	0.004	0.00	1603.9	0.788	0.43	1322.0	<0.0001
CARI	0.09	747.5	0.055	0.01	519.3	0.474	0.02	1230.2	0.350	0.00	1089.1	0.759	0.12	1193.1	0.025	0.06	1552.8	0.105	0.04	1718.5	0.179
MCARI	0.10	742.8	0.041	0.02	518.7	0.437	0.03	1227.7	0.309	0.00	1090.3	0.929	0.01	1268.0	0.662	0.25	1392.3	0.001	0.33	1442.7	<0.0001
TCARI	0.10	744.8	0.046	0.01	521.0	0.616	0.01	1234.7	0.444	0.01	1084.6	0.519	0.09	1209.8	0.048	0.15	1483.9	0.012	0.23	1538.4	0.001
OSAVI	0.26	675.5	0.001	0.05	509.2	0.152	0.00	1243.3	0.846	0.00	1089.9	0.859	0.10	1205.5	0.041	0.07	1544.7	0.081	0.48	1269.7	<0.0001
MCARI/OSAVI	0.02	774.4	0.325	0.04	512.5	0.214	0.04	1219.8	0.214	0.05	1062.4	0.152	0.07	1228.3	0.100	0.11	1517.3	0.035	0.43	1332.3	<0.0001
TCARI/OSAVI	0.05	766.3	0.182	0.01	520.0	0.528	0.03	1226.7	0.294	0.00	1090.4	0.969	0.03	1251.2	0.265	0.25	1392.3	0.001	0.06	1701.8	0.108

Bold font and shaded background highlights best index and statistically significant correlations in each growth stage, respectively.

Table 5-9: Best band combinations of RR and RRD type indices determined for the barley dataset using the lambda-by-lambda band-optimization algorithm. The optimization of RRD is based on the bands i and j determined in the optimization of RR. Best RRI and RRDs were determined respectively in three ways: 1) for each single BBCH stage; 2) forward-cumulative method that uses data from BBCH 32 through to different BBCH stages (i.e., BBCH 32-?); and 3) backward-cumulative method that uses data from any one BBCH stage through to the BBCH 83 (i.e., BBCH ?-83). To avoid redundancy, lambda-by-lambda R² contour plots for the optimizations are not shown.

Method	Single stage			Forward cumulative stage			Backward cumulative stage					
	BBCH	n	RRI	RRDI	BBCH	n	RRI	RRDI	BBCH	n	RRI	RRDI
R^2	32	42	0.453 ^{****}	0.500 ^{****}	32-32	42	0.453 ^{****}	0.500 ^{****}	32-83	294	0.744 ^{****}	0.753 ^{****}
	39	42	0.177 ^{**}	0.225 ^{**}	32-39	84	0.422^{****}	0.655^{****}	39-83	252	0.755 ^{****}	0.746 ^{****}
	51	42	0.408^{****}	0.495^{****}	32-51	126	0.191 ^{****}	0.315^{****}	51-83	210	0.776 ^{****}	0.772^{****}
	55	42	0.155 ^{**}	0.211 ^{**}	32-55	168	0.067 ^{****}	0.172 ^{****}	55-83	168	0.780^{****}	0.782^{****}
	61	42	0.321 ^{****}	0.399 ^{****}	32-61	210	0.129 ^{****}	0.212 ^{****}	61-83	126	0.750 ^{****}	0.749 ^{****}
	73	42	0.141 [*]	0.258 ^{****}	32-73	252	0.328 ^{****}	0.342 ^{****}	73-83	84	0.680 ^{****}	0.670 ^{****}
	83	42	0.590 ^{****}	0.645^{****}	32-83	294	0.744 ^{****}	0.753^{****}	83-83	42	0.590 ^{****}	0.645^{****}
	<u>Band</u>			i, j	h, k			i, j	h, k			i, j
	32	42	445; 455	435; 425	32-32	42	445; 455	435; 425	32-83	294	665; 740	780; 720
	39	42	425; 430	815; 425	32-39	84	385; 395	545; 535	39-83	252	685; 880	880; 680
	51	42	370; 375	480; 485	32-51	126	455; 450	540; 535	51-83	210	660; 750	815; 710
	55	42	460; 465	535; 540	32-55	168	600; 605	575; 565	55-83	168	660; 755	765; 705
	61	42	890; 895	385; 350	32-61	210	600; 610	575; 545	61-83	126	680; 875	895; 690
	73	42	755; 800	770; 715	32-73	252	600; 610	425; 415	73-83	84	690; 875	875; 675
	83	42	805; 810	510; 505	32-83	294	665; 740	780; 720	83-83	42	805; 810	510; 505

n , number of samples

* , $p < 0.01$; ** , $p < 0.01$; *** , $p < 0.001$; **** , $p < 0.0001$

Shaded background indicates BBCH 51 which is the start of heading stage.

Bold font highlights the best indices for open (BBCH < 51) and closed canopy (BBCH > 51), respectively.

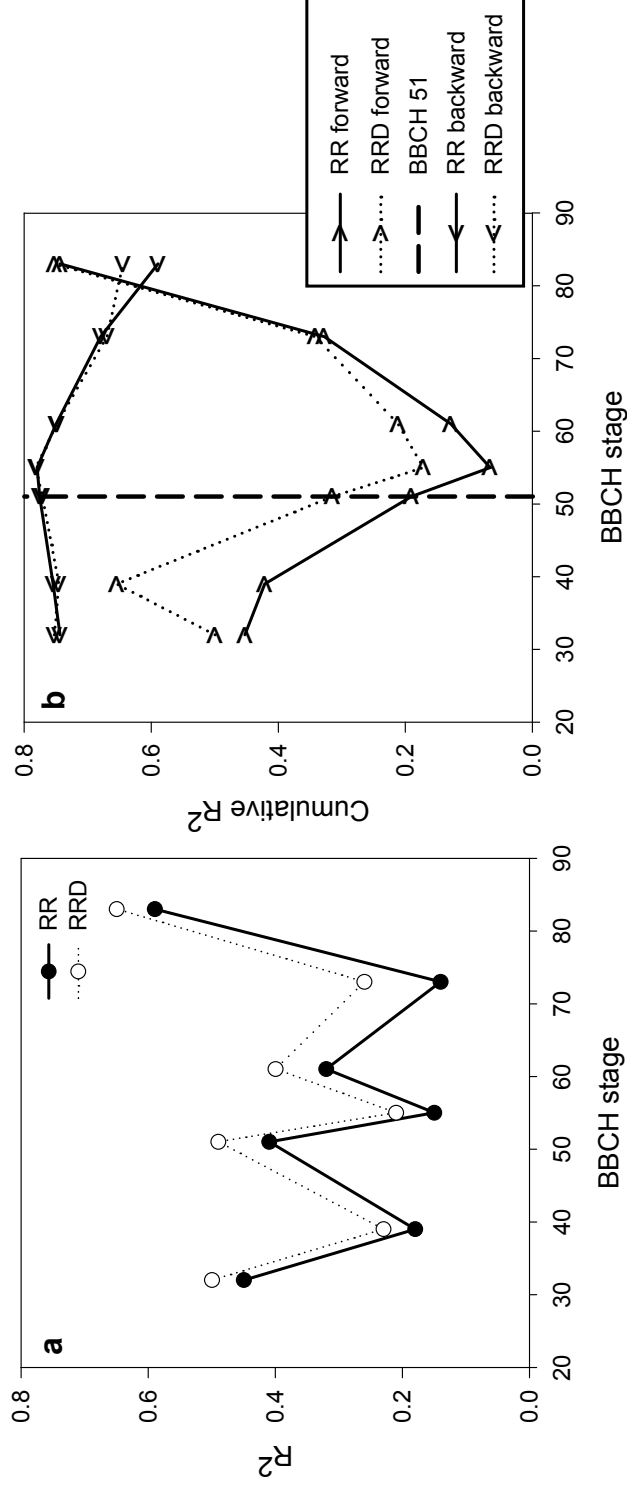


Figure 5-11: R^2 for the best RR and RRD type indices correlating with Chl ($\mu\text{g/g}$) for (a) each growth stage individually, and for (b) forward-cumulative (rightwards arrow) stage/stages beginning with BBCH 32 and backward-cumulative (leftwards arrow) stage/stages ending with BBCH 83 (see more detailed descriptions of Table 5-9). Solid and dotted lines highlight the RR and RRD, respectively. The dash line indicates the BBCH 51 stage.

Interestingly, the correlations always decreased when BBCH 51 was included in the forward- and backward-cumulative methods (Figure 5-11b), which suggests that emerged spikelets have a large effect on the behavior of canopy reflectance since the BBCH 51 stage is the beginning of the heading stage (Appendix A, Figure 5-A1). Figure 5-12b shows the relationship between Chl ($\mu\text{g/g}$) and the RRDl optimized for BBCH 55-83 ($R^2 = 0.78, p < 0.0001$). Notably, the optimized RRDl only slightly improved the R^2 relative to the optimized RRI when using the backward-cumulative method (Figure 5-11b), suggesting the improvement of RRD relative to RR might become smaller after canopy closure (BBCH > 50).

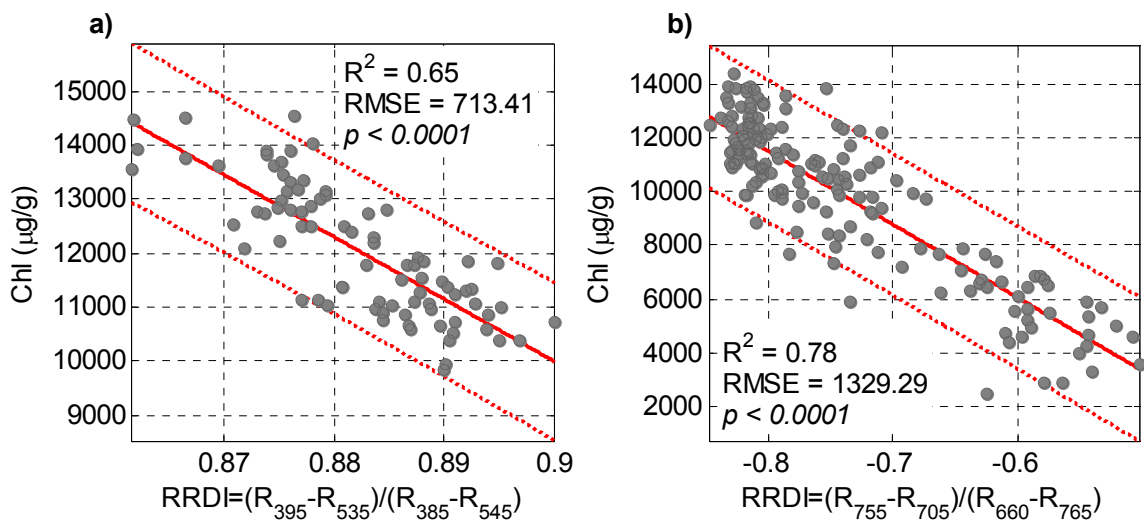


Figure 5-12: Relationships for leaf Chl ($\mu\text{g/g}$) vs. best RRDIs determined for (a) BBCH 32-39 and (b) BBCH 55-83 for the barley dataset using the lambda-by-lambda band-optimization algorithm. Solid and dotted lines indicate the linear fit and 95% confidence intervals of prediction, respectively.

5.4 Discussion

5.4.1 Confounding effects of soil background, canopy structure and multiple scattering

Canopy reflectance is a response to the integrated canopy information including soil background, canopy structure and leaf/ plant biochemistry. Although multiple scattering can be positively interpreted as enhancing the reflectance signals responding to leaf biochemical information (e.g. Asner, 1998; Asner & Martin, 2008), it can also be considered as the noise source since scattering of light by plant or leaf layers is highly anisotropic (e.g. Li et al., 1995). Like the latter, we considered the confounding effects of soil background, canopy structure and multiple scattering as the noise source that affects the way canopy reflectance responds to biochemical information, i.e. Chl in this study. Empirically, the noise shows both additive and multiplicative

effects across cultivars over growth stages (Figure 5-3b), and thus it can be eliminated by optimizing the RRD type indices based on the MSC theory. Theoretically, the apparent canopy reflectance might not be a simple linear function of the ideal “standard” as described in Eq. (5-1). However, a nonlinear hypothesis seems to be too complicated to determine since an ideally standard sample that allows reflectance to respond purely to the variation in canopy biochemistry is not measurable in reality. Therefore, we assumed that a large proportion of the confounding effects due to the structural properties are linearly eliminable. Apparently, such a linear hypothesis is simple, and it works in simulated and measured spectral data, suggesting that the hypothesis and method used here could be applied to other canopies.

5.4.2 Band optimization: green and red edge bands

In optimizing RRDI for the synthetic dataset with the automatic routine, reference bands at red edge (700 nm) and green (515 nm) wavelengths were determined for the best RRI and were further used for optimizing RRDI. Interestingly, for the barley dataset, reference bands at 730 nm and 540 nm were used according to variation analysis as described in section 5.3.1.3, suggesting a certain degree of consistency in wavelengths between the automatic routine and the use of a prior knowledge. Reflectance at 730 nm showed not only lower CV than visible bands (Figure 5-3c), but also a lower standard deviation than the NIR plateau (Figure 5-3d), suggesting that reflectance at 730 nm might be less affected by canopy structural variations across barley cultivars over growth stages. In previous studies, it has also been noted that spectral bands at around 730 nm often result in minimum reflectance differences between varied N rates at both leaf (*Daughtry et al., 2000*) and canopy levels (*Bajwa et al., 2010*). In addition, reflectance at around 730 nm also has a more consistent crop-to-soil ratio at different growth stages than other wavelength bands as shown in *Thenkabail et al. (2000)*. These results suggest that red edge bands have a low degree of co-variation relative to other wavelengths under different conditions when structural properties vary. On the other hand, the spectral band at around 540 nm, which has been long known as the absorption minima of chlorophylls and carotenoids (*reviewed in Ustin et al., 2009*), also showed significantly different characteristics with other wavelength bands in this study, yielding local minima of CV in reflectance (Figure 5-3c). Moreover, *Gitelson et al. (2006)* found that the optimum position of spectral band (λ_1) that is maximally sensitive to absorption by the total chlorophyll in the $[R(\lambda_1)^{-1} - R(\lambda_2)^{-1}] \times R(\lambda_3)$ model (*Gitelson et al., 2003*) was in either the green (530-540 nm) or red edge (700-730 nm) ranges. Collectively, both previous studies and our results suggest the usefulness of green and red edge bands in designing spectral indices as they respond to Chl variations while they co-vary less with structural variations.

5.4.3 Improvement of RRD type indices relative to other types of indices

Results of different types of indices optimized for the synthetic dataset revealed that RRDI significantly improved the correlation with Chl ($\mu\text{g}/\text{cm}^2$) relative to other types of indices (Table 5-5 and Figure 5-2). According to our hypothesis, RDI and RRI solely eliminate additive and multiplicative effects, respectively. Although NRDI eliminated the multiplicative effect, the additive effect was strengthened by the “normalized” transformation from RDI to NRDI. To balance out the strengthening of the additive effect in the denominator of NRDI, the most significant hot zones shifted to red edge and NIR range (Figure 5-4c), where the lowest CVs were produced (Figure 5-3c), when optimizing the NRDI.

Although optimized RDI, RRI, NRDI and DRRI all yielded high correlations with Chl, they only partially eliminated the additive and/or multiplicative effects (i.e., a and b in Eq.(5-1)) compared to RRDI (see also formulae in Table 5-1). The relationships with Chl ($\mu\text{g}/\text{cm}^2$) still scatter to different degrees at different LAI levels (Figure 5-2). In contrast, RRDI yielded a more robust relationship that subtly scatters only when LAI= 1 (Figure 5-2h). At the leaf level, *Sims & Gamon (2002)* modified the RR and NRD type indices to reduce leaf surface (specular) effect by subtracting a reference band at 445 nm (mSR705, see Table 5-1). At the canopy level, *le Maire et al. (2008)* also optimized the mSR type (RRD) indices with a very similar blue band at 450 nm although they found no improvement relative to NRD and RR. This might be due to the inappropriate use of R_{450} in mSR (RRD) when scaling-up to canopy level as suggested by our results where R_{450} did not yield local minimum of CV compared to red edge and green bands (Figure 5-3c). In contrast, the use of red edge and green bands showed improvement relative to RRI or NRDI (Table 5-5 and Figure 5-2), highlighting that the structural effects at leaf and canopy levels affect leaf- and canopy-level reflectance in different ways over wavelengths.

5.4.4 Connections with previous studies

The optimized indices showed interesting characteristics of wavelengths. For the barley data, $\text{RRDI} = (R_{735} - R_{730}) / (R_{785} - R_{540})$ was the best index for the estimation of Chl ($\mu\text{g}/\text{g}$). One could have noticed that the numerator ($R_{735} - R_{730}$) can be considered as the numerator of a backward first-difference transformation as $D_{735} = (R_{735} - R_{730}) / \Delta\lambda$ (*Dawson & Curran, 1998*). Similarly, *Zhao et al. (2005)* found that leaf Chl was highly and linearly correlated with the first derivative ($dR/d\lambda$) at 730 or 740 nm. Also, the first derivative of canopy reflectance at 735 nm was found to be a good indicator of plant N concentration of rice (*Lee et al., 2008*). More recently, a ratio of first derivatives of reflectance at 740 and 522 nm (D_{740}/D_{522}) also showed improvement in mapping canopy N of rice (*Inoue et al., 2012*). Based on laboratory leaf reflectance data, *Vogelmann et al. (1993)* also found that a ratio of the first derivative at 705 and 715 nm (D_{715}/D_{705}) was highly

correlated with total chlorophyll content while it was much less affected by leaf biomass and background condition than NDVI or simple ratio indices (RR). Therefore, our results indirectly agree well with previous studies that a ratio of reflectance first-derivatives can also eliminate both additive and multiplicative effects, and is thus closely related to Chl and is insensitive to the effects of soil background and structural variations.

The hypothesis and method used here indirectly elucidate the mechanisms for the successful application of derivative-transformed spectral indices in previous studies. In addition, our method is not limited to the sensors measuring continuous wavelengths compared to the derivative analysis method. RRD type indices eliminate the additive effect without employing derivative transformation and they reduce both additive and multiplicative effects without applying the MSC, suggesting that RRDI optimization has the advantage of simplicity in hyperspectral remote sensing of canopy biochemistry.

5.4.5 Effects of crop type, growth stage and the range of variation in Chl

Published and optimized indices calibrated by the synthetic dataset failed to account for a large portion of the variation in Chl of barley, suggesting there is a large effect of crop type on spectral indices. This is consistent with the study on corn and wheat by *Haboudane et al. (2008)* at a local scale. However, on a large regional scale, a dataset comprising several crop types might also increase the convergence of canopy reflectance/ indices responding to Chl (e.g. *Houborg & Boegh, 2008*), suggesting the effect of crop type is also dependent on the scale of specific studies. The negative effect of crop type might be expected to be negligible when a dataset is large and general enough such as at large ecosystem scales (*Ollinger, 2011*).

Optimization for each single stage was not able to account for a large portion of the variation in Chl for some of the growth stages individually, which suggests the large effect of growth stage. Furthermore, the decrease in accuracy when heading stage (BBCH 51) was included in the forward- and backward-cumulative methods suggests, more particularly, the effect of canopy closure and ear emerging in the heading stage (BBCH 50-60). Supposing open and closed canopies are two functional types that are optically distinguishable (*Ustin & Gamon, 2010*), forward- and backward-cumulative methods are able to improve the accuracy for Chl estimation for growth stages before and after canopy closure (heading stage), respectively. This fits well into agricultural practices before and after heading for “yield dressing” and “quality dressing” purposes, respectively. Particularly, the improvement seems to be more useful before canopy closure where the effect of soil background is more pronounced (Figure 5-11b).

On the other hand, decreased accuracy for each single stage is due not only to the effect of growth stage, but also to the small range of variation in Chl for individual stages (Table 5-3). As

also shown in our results, the larger the variation in Chl for a dataset, the more of the variation in Chl of the dataset is accounted for (Table 5-3, Table 5-4, and Table 5-5); and the larger the variation in Chl within a single stage, the more of the variation in Chl of the single stage is accounted for (Table 5-8 and Table 5-9), suggesting the challenge to remote detection and estimation of the subtle variation in Chl in the context of precision agriculture ([Haboudane et al., 2008](#)).

Effects of growth stage, crop type and the range of variation in Chl should be taken into account when applying remote sensing in precision agriculture. Canopy reflectance responds to narrow and wide ranges of variation in Chl differently over wavelengths, which is still not fully explored due to the complexity of canopy structural properties in respond to environmental changes. In addition, confounding effects of the structural properties co-vary in different ways with Chl at different growth stages (Appendix A), which might mask to some extent the subtle variation in canopy biochemistry that should have been expressed in canopy reflectance signals. Therefore, methods used here still need to be improved to uncover those aspects for remote sensing that apply to precision agriculture.

5.5 Conclusions

Monitoring in situ the variation in chlorophyll is of great importance for stress detection, yield and grain quality prediction in the context of precision agriculture. In this study, we aimed to optimize spectral indices that are insensitive to structural effects for the estimation of leaf chlorophyll (Chl). Canopy reflectance data were obtained through model simulation (PROSAIL) and spectral measurement from barley canopies. We proposed a comprehensive band-optimization method to explore the best spectral indices for estimating Chl, and compared them with published indices and multivariate methods (i.e., OMBR, PLSR and SVR).

The findings of this study support our hypothesis that the ratio of reflectance difference (RRD) type indices eliminate both additive and multiplicative effects owing to canopy structural properties, i.e., soil background, canopy structure and multiple scattering, thus improves the estimation of Chl. For example, under varying LAIs (1-8), optimized $RRDI = (R_{615} - R_{700}) / (R_{555} - R_{515})$ for simulated data yielded a very strong correlation with Chl with R^2 of 0.98 ($p < 0.0001$), suggesting the potential to apply RRD type indices to canopies with low LAI.

Importantly, the growth stage negatively affects the accuracy of spectral indices that account for the variation in Chl. Thus, a general purpose model for the entire growing season might not be able to accurately account for the variation in Chl for individual, but critical, stages. However, we found that RRDIs optimized for the stage-spans covering individual stages before and after

canopy closure (i.e. heading stage), respectively, improved the accuracy with R^2 of 0.65 ($p < 0.0001$) and 0.78 ($p < 0.0001$). It is of practical merit to optimize the open-canopy model for “yield dressing” and the closed-canopy model for “quality dressing” in precision agriculture.

Our results might provide support for future studies into the remote estimation of canopy biochemistry. These studies might have different focuses of, 1) monitoring nutrient cycling at the ecosystem scale by optimizing a general model based on RRD type indices; 2) monitoring canopy Chl or N in precision agriculture by classifying open and closed canopies into two “optical types” (Ustin & Gamon, 2010) and optimizing yield-dressing and quality-dressing RRD models, respectively. The main criticism of the methods developed here is that the wavelengths optimized for RRDs are still crop/species specific. Thus, the exact wavelengths determined here might not ensure accuracy when applied to other crops under different conditions. However, the methods are expected to apply, since precision agriculture prefers crop- and site-specific nutrient managements. Therefore, further studies on more crop or vegetation species, for different purposes and at different scales, will be of great importance for evaluating and improving the methods developed here.

Acknowledgements

Part of this study was supported by the BMBF funded CropSense project (www.cropsense.de). The authors gratefully acknowledge G. Leufen, Dr. M. Hunsche and Prof. G. Noga (INRES-Horticultural Science of the University of Bonn) for the enthusiastic collaboration. We thank T. Schuhmacher, C. Jekel, C. Hütt, L. Schwager and I. Kurth for their contributions to field and laboratory work. This work would not have been possible without a scholarship to K.Y. from the China Scholarship Council (CSC), which is gratefully acknowledged. K.Y. also wishes to thank Dr. S. Wang (Department of Statistics, University of Oxford) for giving suggestions on how to name spectral indices, and Prof. T. Fuller for grammar corrections.

References

- Asner, G.P. 1998.** Biophysical and biochemical sources of variability in canopy reflectance. *Remote Sens. Environ.* **64**: 234-253.
- Asner, G.P., Martin, R.E. 2008.** Spectral and chemical analysis of tropical forests: Scaling from leaf to canopy levels. *Remote Sens. Environ.* **112**: 3958-3970.
- Bajwa, S.G., Mishra, A.R., Norman, R.J. 2010.** Canopy reflectance response to plant nitrogen accumulation in rice. *Precis. Agric.* **11**: 488-506.
- Bannari, A., Morin, D., Bonn, F., Huete, A.R. 1995.** A review of vegetation indices. *Remote Sens. Rev.* **13**: 95-120.

CHAPTER 5

- Baret, F., Jacquemoud, S., Guyot, G., Leprieur, C. 1992.** Modeled analysis of the biophysical nature of spectral shifts and comparison with information content of broad bands. *Remote Sens. Environ.* **41**: 133-142.
- Blackburn, G.A. 1998a.** Spectral indices for estimating photosynthetic pigment concentrations: A test using senescent tree leaves. *Int. J. Remote Sens.* **19**: 657-675.
- Blackburn, G.A. 1998b.** Quantifying chlorophylls and carotenoids at leaf and canopy scales: An evaluation of some hyperspectral approaches. *Remote Sens. Environ.* **66**: 273-285.
- Cartelat, A., Cerovic, Z.G., Goulas, Y., Meyer, S., Lelarge, C., Prioul, J.L., Barbottin, A., Jeuffroy, M.H., Gate, P., Agati, G., Moya, I. 2005.** Optically assessed contents of leaf polyphenolics and chlorophyll as indicators of nitrogen deficiency in wheat (*Triticum aestivum* L.). *Field Crops Res.* **91**: 35-49.
- Chang, C., Lin, C. 2011.** LIBSVM: A library for support vector machines. *ACM Trans. Intell. Syst. Technol.* **2**: 1-27.
- Ciganda, V., Gitelson, A., Schepers, J. 2009.** Non-destructive determination of maize leaf and canopy chlorophyll content. *J. Plant Physiol.* **166**: 157-167.
- Collins, W. 1978.** Remote sensing of crop type and maturity. *Photogramm. Eng. Remote Sensing* **44**: 43-45.
- Darvishzadeh, R., Skidmore, A., Schlerf, M., Atzberger, C., Corsi, F., Cho, M. 2008.** LAI and chlorophyll estimation for a heterogeneous grassland using hyperspectral measurements. *ISPRS J. Photogramm. Remote Sens.* **63**: 409-426.
- Dash, J., Curran, P.J. 2004.** The MERIS terrestrial chlorophyll index. *Int. J. Remote Sens.* **25**: 5403-5413.
- Datt, B. 1998.** Remote sensing of chlorophyll a, chlorophyll b, chlorophyll a+b, and total carotenoid content in eucalyptus leaves. *Remote Sens. Environ.* **66**: 111-121.
- Datt, B. 1999a.** Visible/near infrared reflectance and chlorophyll content in Eucalyptus leaves. *Int. J. Remote Sens.* **20**: 2741-2759.
- Datt, B. 1999b.** A new reflectance index for remote sensing of chlorophyll content in higher plants: Tests using eucalyptus leaves. *J. Plant Physiol.* **154**: 30-36.
- Daughtry, C.S.T., Walthall, C.L., Kim, M.S., de Colstoun, E.B., McMurtrey III, J.E. 2000.** Estimating corn leaf chlorophyll concentration from leaf and canopy reflectance. *Remote Sens. Environ.* **74**: 229-239.
- Dawson, T.P., Curran, P.J. 1998.** A new technique for interpolating the reflectance red edge position. *Int. J. Remote Sens.* **19**: 2133-2139.
- Feret, J., François, C., Asner, G.P., Gitelson, A.A., Martin, R.E., Bidet, L.P.R., Ustin, S.L., le Maire, G., Jacquemoud, S. 2008.** PROSPECT-4 and 5: Advances in the leaf

- optical properties model separating photosynthetic pigments. *Remote Sens. Environ.* **112**: 3030-3043.
- Filella, I., Serrano, L., Serra, J., Peñuelas, J. 1995.** Evaluating wheat nitrogen status with canopy reflectance indices and discriminant analysis. *Crop Sci.* **35**: 1400-1405.
- François, C., Ottlé, C., Oliosio, A., Prévot, L., Bruguier, N., Ducros, Y. 2002.** Conversion of 400-1100 nm vegetation albedo measurements into total shortwave broadband albedo using a canopy radiative transfer model. *Agronomie* **22**: 611-618.
- Gamon, J.A., Peñuelas, J., Field, C.B. 1992.** A narrow-waveband spectral index that tracks diurnal changes in photosynthetic efficiency. *Remote Sens. Environ.* **41**: 35-44.
- Geladi, P., MacDougall, D., Martens, H. 1985.** Linearization and scatter-correction for near-infrared reflectance spectra of meat. *Appl. Spectrosc.* **39**: 491-500.
- Gitelson, A., Merzlyak, M.N. 1994a.** Spectral reflectance changes associated with autumn senescence of *Aesculus hippocastanum* L. and *Acer platanoides* L. leaves. Spectral features and relation to chlorophyll estimation. *J. Plant Physiol.* **143**: 286-292.
- Gitelson, A., Merzlyak, M.N. 1994b.** Quantitative estimation of chlorophyll-a using reflectance spectra: Experiments with autumn chestnut and maple leaves. *J. Photochem. Photobiol. B: Biol.* **22**: 247-252.
- Gitelson, A.A., Kaufman, Y.J., Merzlyak, M.N. 1996.** Use of a green channel in remote sensing of global vegetation from EOS-MODIS. *Remote Sens. Environ.* **58**: 289-298.
- Gitelson, A.A., Gritz, Y., Merzlyak, M.N. 2003.** Relationships between leaf chlorophyll content and spectral reflectance and algorithms for non-destructive chlorophyll assessment in higher plant leaves. *J. Plant Physiol.* **160**: 271-282.
- Gitelson, A.A., Keydan, G.P., Merzlyak, M.N. 2006.** Three-band model for noninvasive estimation of chlorophyll, carotenoids, and anthocyanin contents in higher plant leaves. *Geophys. Res. Lett.* **33**: L11402.
- Guyot, G., Baret, F. 1988.** Utilisation de la haute resolution spectrale pour suivre l'etat des couverts vegetaux. In: *Spectral Signatures of Objects in Remote Sensing*. 18-22 January 1988. Aussois, France.
- Haaland, D.M., Thomas, E.V. 1988.** Partial least-squares methods for spectral analyses. I. Relation to other quantitative calibration methods and the extraction of qualitative information. *Anal. Chem.* **60**: 1193-1202.
- Haboudane, D., Miller, J.R., Tremblay, N., Zarco-Tejada, P.J., Dextraze, L. 2002.** Integrated narrow-band vegetation indices for prediction of crop chlorophyll content for application to precision agriculture. *Remote Sens. Environ.* **81**: 416-426.

CHAPTER 5

- Haboudane, D., Miller, J.R., Pattey, E., Zarco-Tejada, P.J., Strachan, I.B. 2004.** Hyperspectral vegetation indices and novel algorithms for predicting green LAI of crop canopies: Modeling and validation in the context of precision agriculture. *Remote Sens. Environ.* **90**: 337-352.
- Haboudane, D., Tremblay, N., Miller, J.R., Vigneault, P. 2008.** Remote estimation of crop chlorophyll content using spectral indices derived from hyperspectral data. *IEEE Trans. Geosci. Remote Sens.* **46**: 423-437.
- Hansen, P.M., Schjoerring, J.K. 2003.** Reflectance measurement of canopy biomass and nitrogen status in wheat crops using normalized difference vegetation indices and partial least squares regression. *Remote Sens. Environ.* **86**: 542-553.
- Houborg, R., Boegh, E. 2008.** Mapping leaf chlorophyll and leaf area index using inverse and forward canopy reflectance modeling and SPOT reflectance data. *Remote Sens. Environ.* **112**: 186-202.
- Hsu, C.W., Chang, C.C., Lin, C.J. 2003.** A practical guide to support vector classification. Available online: <http://www.csie.ntu.edu.tw/~cjlin/papers/guide/guide.pdf>. (Accessed on 1 November 2013)
- Huete, A.R. 1988.** A soil-adjusted vegetation index (SAVI). *Remote Sens. Environ.* **25**: 295-309.
- Inoue, Y., Sakaiya, E., Zhu, Y., Takahashi, W. 2012.** Diagnostic mapping of canopy nitrogen content in rice based on hyperspectral measurements. *Remote Sens. Environ.* **126**: 210-221.
- Isaksson, T., Kowalski, B. 1993.** Piece-wise multiplicative scatter correction applied to near-infrared diffuse transmittance data from meat products. *Appl. Spectrosc.* **47**: 702-709.
- Jacquemoud, S., Baret, F. 1990.** PROSPECT: A model of leaf optical properties spectra. *Remote Sens. Environ.* **34**: 75-91.
- Jacquemoud, S., Verhoef, W., Baret, F., Bacour, C., Zarco-Tejada, P.J., Asner, G.P., François, C., Ustin, S.L. 2009.** PROSPECT + SAIL models: A review of use for vegetation characterization. *Remote Sens. Environ.* **113**: S56-S66.
- Kim, M.S., Daughtry, C.S.T., Chappelle, E.W., McMurtrey, J.E., Walthall, C.L. 1994.** The use of high spectral resolution bands for estimating absorbed photosynthetically active radiation (APAR). In: Proceedings of 6th International Symposium on Physical Measurements and Signatures in Remote Sensing. 17-21 January 1994. Val D'Isere, France: CNES, pp. 299-306.
- Lancashire, P.D., Bleiholder, H., Boom, T.V.D., Langelüddeke, P., Stauss, R., Weber, E., Witzemberger, A. 1991.** A uniform decimal code for growth stages of crops and weeds. *Ann. Appl. Biol.* **119**: 561-601.

- le Maire, G., François, C., Soudani, K., Berveiller, D., Pontailier, J., Bréda, N., Genet, H., Davi, H., Dufrêne, E. 2008.** Calibration and validation of hyperspectral indices for the estimation of broadleaved forest leaf chlorophyll content, leaf mass per area, leaf area index and leaf canopy biomass. *Remote Sens. Environ.* **112**: 3846-3864.
- Lee, Y., Yang, C., Chang, K., Shen, Y. 2008.** A simple spectral index using reflectance of 735 nm to assess nitrogen status of rice canopy. *Agron. J.* **100**: 205-212.
- Lemaire, G., Jeuffroy, M., Gastal, F. 2008.** Diagnosis tool for plant and crop N status in vegetative stage: Theory and practices for crop N management. *Eur. J. Agron.* **28**: 614-624.
- Li, X., Strahler, A.H., Woodcock, C.E. 1995.** A hybrid geometric optical-radiative transfer approach for modeling albedo and directional reflectance of discontinuous canopies. *IEEE Trans. Geosci. Remote Sens.* **33**: 466-480.
- Maleki, M.R., Mouazen, A.M., Ramon, H., De Baerdemaeker, J. 2007.** Multiplicative scatter correction during on-line measurement with near infrared spectroscopy. *Biosyst. Eng.* **96**: 427-433.
- Martens, H., Naes, T. 1989.** *Multivariate calibration*. New York: John Wiley & Sons.
- Martínez, D.E., Guiamet, J.J. 2004.** Distortion of the SPAD 502 chlorophyll meter readings by changes in irradiance and leaf water status. *Agronomie* **24**: 41-46.
- Merzlyak, M.N., Gitelson, A.A., Chivkunova, O.B., Rakitin, V.Y. 1999.** Non-destructive optical detection of pigment changes during leaf senescence and fruit ripening. *Physiol. Plantarum* **106**: 135-141.
- Miao, Y., Mulla, D., Randall, G., Vetsch, J., Vintila, R. 2009.** Combining chlorophyll meter readings and high spatial resolution remote sensing images for in-season site-specific nitrogen management of corn. *Precis. Agric.* **10**: 45-62.
- Moran, J.A., Mitchell, A.K., Goodmanson, G., Stockburger, K.A. 2000.** Differentiation among effects of nitrogen fertilization treatments on conifer seedlings by foliar reflectance: a comparison of methods. *Tree Physiol.* **20**: 1113-1120.
- Mutanga, O., Skidmore, A.K., van Wieren, S. 2003.** Discriminating tropical grass (*Cenchrus ciliaris*) canopies grown under different nitrogen treatments using spectroradiometry. *ISPRS J. Photogramm. Remote Sens.* **57**: 263-272.
- Næs, T., Isaksson, T., Fearn, T., Davies, T. 2002.** *A User-Friendly Guide to Multivariate Calibration and Classification*. Chichester, UK: NIR Publications.
- Nakaji, T., Oguma, H., Fujinuma, Y. 2006.** Seasonal changes in the relationship between photochemical reflectance index and photosynthetic light use efficiency of Japanese larch needles. *Int. J. Remote Sens.* **27**: 493-509.

CHAPTER 5

- Ollinger, S.V. 2011.** Sources of variability in canopy reflectance and the convergent properties of plants. *New Phytol.* **189**: 375-394.
- Peñuelas, J., Baret, F., Filella, I. 1995a.** Semi-empirical indices to assess carotenoids/chlorophyll-a ratio from leaf spectral reflectance. *Photosynthetica* **31**: 221-230.
- Peñuelas, J., Filella, I., Gamon, J.A. 1995b.** Assessment of photosynthetic radiation-use efficiency with spectral reflectance. *New Phytol.* **131**: 291-296.
- Peñuelas, J., Filella, I. 1998.** Visible and near-infrared reflectance techniques for diagnosing plant physiological status. *Trends Plant Sci.* **3**: 151-156.
- Peñuelas, J., Garbulsky, M.F., Filella, I. 2011.** Photochemical reflectance index (PRI) and remote sensing of plant CO₂ uptake. *New Phytol.* **191**: 596-599.
- Richardson, A.D., Duigan, S.P., Berlyn, G.P. 2002.** An evaluation of noninvasive methods to estimate foliar chlorophyll content. *New Phytol.* **153**: 185-194.
- Rondeaux, G., Steven, M., Baret, F. 1996.** Optimization of soil-adjusted vegetation indices. *Remote Sens. Environ.* **55**: 95-107.
- Rosipal, R., Krämer, N. 2006.** Overview and recent advances in partial least squares. In: C. Saunders, M. Grobelnik, S. Gunnj. Shawe-Taylor eds. *Subspace, Latent Structure and Feature Selection*. Berlin Heidelberg: Springer-Verlag, 34-51.
- Rouse, J.W., Haas, R.H., Deering, D.W., Schell, J.A., Harlan, J.C. 1974.** Monitoring the vernal advancement and retrogradation (green wave effect) of natural vegetation. In. Type III Final Report, Greenbelt, MD, USA.: NASA/GSFC.
- SAS Institute Inc. 2008.** SAS/STAT® 9.2 User's Guide. In. Cary, NC: SAS Institute Inc.
- Schlemmer, M.R., Francis, D.D., Shanahan, J.F., Schepers, J.S. 2005.** Remotely measuring chlorophyll content in corn leaves with differing nitrogen levels and relative water content. *Agron. J.* **97**: 106-112.
- Sims, D.A., Gamon, J.A. 2002.** Relationships between leaf pigment content and spectral reflectance across a wide range of species, leaf structures and developmental stages. *Remote Sens. Environ.* **81**: 337-354.
- Smola, A.J., Schölkopf, B. 2004.** A tutorial on support vector regression. *Stat. Comput.* **14**: 199-222.
- Steele, M.R., Gitelson, A.A., Rundquist, D.C. 2008.** A comparison of two techniques for nondestructive measurement of chlorophyll content in grapevine leaves. *Agron. J.* **100**: 779-782.
- Takebe, M., Yoneyama, T., Inada, K., Murakami, T. 1990.** Spectral reflectance ratio of rice canopy for estimating crop nitrogen status. *Plant Soil* **122**: 295-297.

- Thenkabail, P.S., Smith, R.B., De Pauw, E. 2000.** Hyperspectral vegetation indices and their relationships with agricultural crop characteristics. *Remote Sens. Environ.* **71**: 158-182.
- Thenkabail, P.S., Smith, R.B., De Pauw, E. 2002.** Evaluation of narrowband and broadband vegetation indices for determining optimal hyperspectral wavebands for agricultural crop characterization. *Photogramm. Eng. Remote Sensing* **68**: 607-621.
- Thenkabail, P.S., Enclona, E.A., Ashton, M.S., Legg, C., De Dieu, M.J. 2004.** Hyperion, IKONOS, ALI, and ETM+ sensors in the study of African rainforests. *Remote Sens. Environ.* **90**: 23-43.
- Tucker, C.J. 1979.** Red and photographic infrared linear combinations for monitoring vegetation. *Remote Sens. Environ.* **8**: 127-150.
- Ustin, S.L., Gitelson, A.A., Jacquemoud, S., Schaepman, M., Asner, G.P., Gamon, J.A., Zarco-Tejada, P. 2009.** Retrieval of foliar information about plant pigment systems from high resolution spectroscopy. *Remote Sens. Environ.* **113**: S67-S77.
- Ustin, S.L., Gamon, J.A. 2010.** Remote sensing of plant functional types. *New Phytol.* **186**: 795-816.
- van der Voet, H. 1994.** Comparing the predictive accuracy of models using a simple randomization test. *Chemometr. Intell. Lab. Syst.* **25**: 313-323.
- Vapnik, V.N. 1995.** *The nature of statistical learning theory.* New York: Springer-Verlag.
- Vapnik, V.N. 1998.** *Statistical learning theory.* New York: John Wiley & Sons, Inc.
- Verhoef, W. 1984.** Light scattering by leaf layers with application to canopy reflectance modeling: The SAIL model. *Remote Sens. Environ.* **16**: 125-141.
- Verhoef, W., Jia, L., Qing, X., Su, Z. 2007.** Unified Optical-Thermal Four-Stream Radiative Transfer Theory for Homogeneous Vegetation Canopies. *IEEE Trans. Geosci. Remote Sens.* **45**: 1808-1822.
- Vogelmann, J.E., Rock, B.N., Moss, D.M. 1993.** Red edge spectral measurements from sugar maple leaves. *Int. J. Remote Sens.* **14**: 1563-1575.
- Weng, J., Lai, K., Liao, T., Hwang, M., Chen, Y. 2009.** Relationships of photosynthetic capacity to PSII efficiency and to photochemical reflectance index of *Pinus taiwanensis* through different seasons at high and low elevations of sub-tropical Taiwan. *Trees-Struct. Funct.* **23**: 347-356.
- Wold, S., Sjöström, M., Eriksson, L. 2001.** PLS-regression: a basic tool of chemometrics. *Chemometr. Intell. Lab. Syst.* **58**: 109-130.
- Yu, K., Li, F., Gnyp, M.L., Miao, Y., Bareth, G., Chen, X. 2013.** Remotely detecting canopy nitrogen concentration and uptake of paddy rice in the Northeast China Plain. *ISPRS J. Photogramm. Remote Sens.* **78**: 102-115.

Zarco-Tejada, P.J., Miller, J.R., Noland, T.L., Mohammed, G.H., Sampson, P.H. 2001.

Scaling-up and model inversion methods with narrowband optical indices for chlorophyll content estimation in closed forest canopies with hyperspectral data. *IEEE Trans. Geosci. Remote Sens.* **39**: 1491-1507.

Zarco-Tejada, P.J., Miller, J.R., Morales, A., Berjón, A., Agüera, J. 2004.

Hyperspectral indices and model simulation for chlorophyll estimation in open-canopy tree crops. *Remote Sens. Environ.* **90**: 463-476.

Zarco-Tejada, P.J., Berjón, A., López-Lozano, R., Miller, J.R., Martín, P., Cachorro, V.,

González, M.R., de Frutos, A. 2005. Assessing vineyard condition with hyperspectral indices: Leaf and canopy reflectance simulation in a row-structured discontinuous canopy. *Remote Sens. Environ.* **99**: 271-287.

Zhao, D., Reddy, K.R., Kakani, V.G., Reddy, V.R. 2005.

Nitrogen deficiency effects on plant growth, leaf photosynthesis, and hyperspectral reflectance properties of sorghum. *Eur. J. Agron.* **22**: 391-403.

Appendix A. Temporal changes in canopy reflectance

Figure 5-A1a-g shows the changes in canopy reflectance over seven growth stages for each barley cultivar, respectively. All cultivars showed similar trends across the entire growing season. Across growth stages, NIR reflectance generally increased until BBCH 51 and then decreased, whereas green reflectance decreased until BBCH 55 and then increased, suggesting the effect of the heading stage (BBCH 50-60) on canopy reflectance. Figure 5-A1h-n shows reflectance differences between seven barley cultivars at each growth stage, respectively. The range of reflectance differences between cultivars varied at different growth stages. The differences between cultivars were more pronounced in NIR than in other wavelengths. Notably, before BBCH 51 differences were more pronounced in green bands than in red, (Figure 5-A1h-j), whereas after BBCH 55 they were more pronounced in red bands than in green (Figure 5-A1l-n).

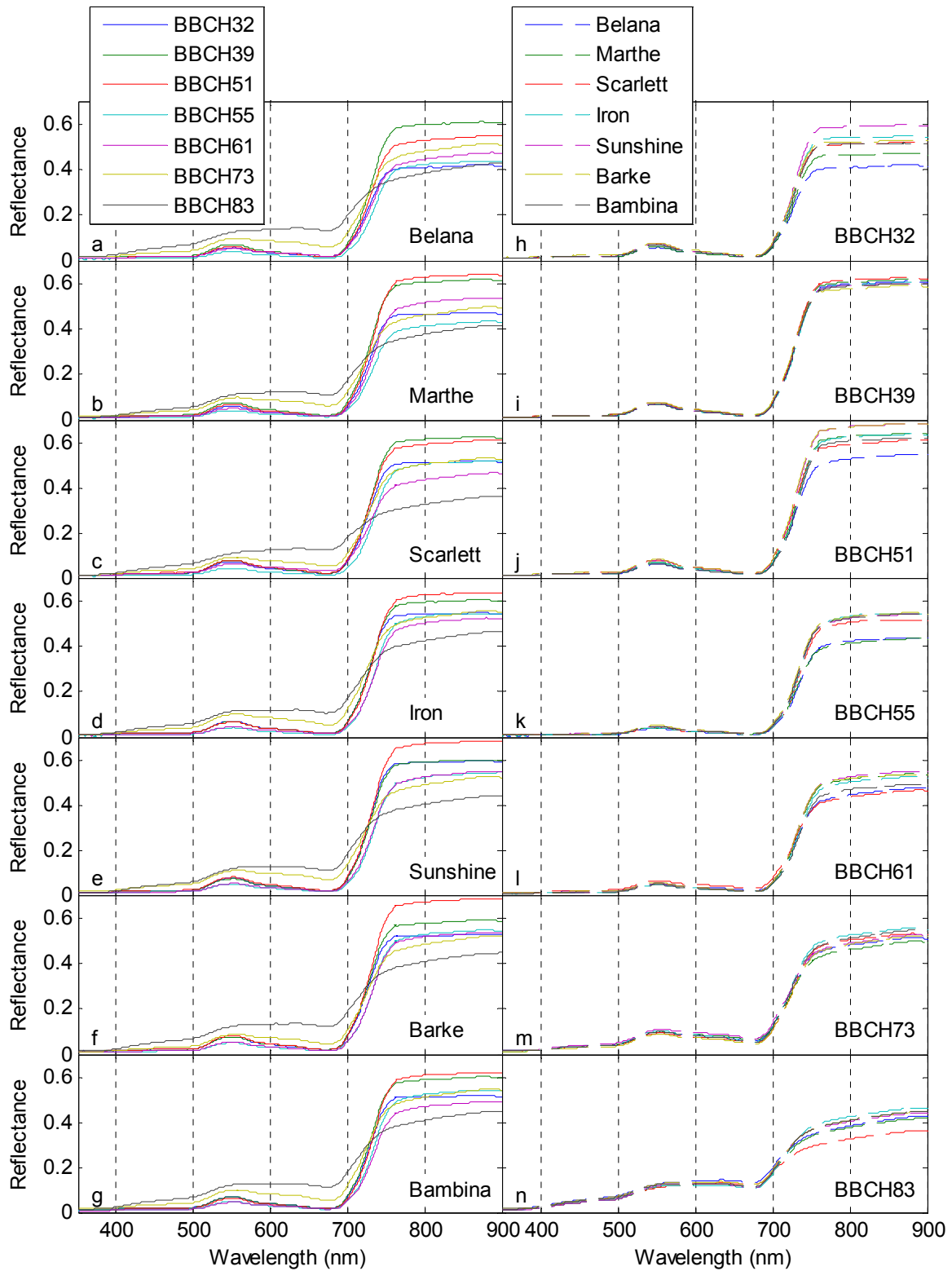


Figure 5-A1: Temporal changes in canopy reflectance of barley across seven growth stages for each cultivar (a-g) and reflectance differences between seven cultivars at each growth stage (h-n).

CHAPTER 6

Validation of N dilution effect and developed vegetation index (RRDI) and evaluation of crop responses to diseases*

Summary

Chapter 6 presents additional data from the barley experiments to evaluate and validate the results of the early phases of this study. This chapter focuses on (1) validating the effect of growth stages on the remote estimation of chlorophyll (Chl) and nitrogen (N) concentrations, (2) evaluating the performance of the Ratio of Reflectance Difference Index (RRDI) in the red edge (RRDI_{re}) for estimating Chl and N, and (3) verifying the efficiency of the vegetation indices based on water absorption bands in discriminating plant diseases compared to indices based on Chl absorption bands.

The results confirmed that the N dilution effect that occurs along with barley plant growth has a significant impact on the correlations between the vegetation indices and canopy N, which was highlighted in CHAPTER 2 and based on rice data. RRDI_{re}, which was developed in this study based on the rice dataset (CHAPTER 3), provided the best performance for estimating Chl and N of barley plants and suggested the promising potential of capturing canopy Chl and N variations across different crop types and cultivars. The results also showed the effectiveness of vegetation indices based on water absorption bands in discriminating diseased plants, which highlighted the importance of water absorption bands for the remote detection of crop diseases.

* This chapter provides addition results to (1) evaluate the results of the previous chapters and (2) validate the new vegetation index, Ratio of Reflectance Difference Index (RRDI), developed in this study.

6.1 Materials and methods

6.1.1 Experimental design and descriptions of disease symptom

Field experiments were conducted in 2011 and 2012 at the Institute of Crop Science and Resource Conservation (INRES-Horticulture), University of Bonn, Germany. The experiments were arranged in a randomized block design with four replications and had a plot size of 10.5 m² (7*1.5). The treatments were combinations of two factors: fungicide application and barley cultivar. There were two fungicide treatments (“with-fungicide” and “without-fungicide”) and four cultivar treatments (Belana, Marthe, Conchita and Tocada). Barley seeds were sown on March 23 and April 3 for the experiments in 2011 and 2012, respectively, with a density of 320 seeds m⁻². Figure 6-1 shows all of the field measurement activities on different days after sowing (DAS) in 2011 and 2012.

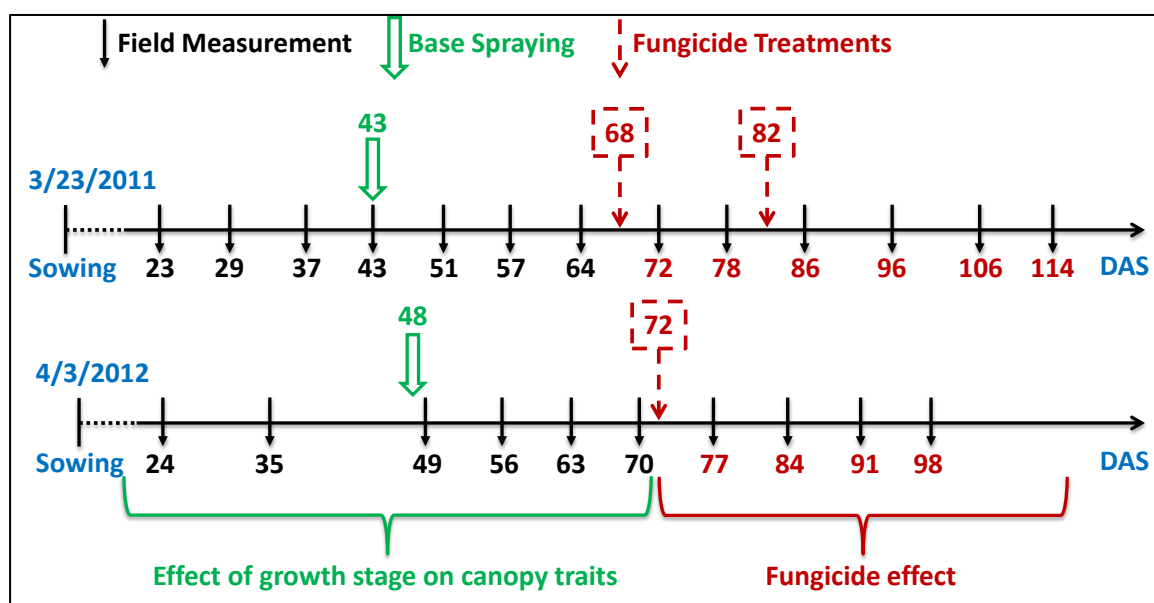


Figure 6-1: Time table shows the field activities of canopy spectral measurements and fungicide applications in 2011 and 2012. A basal spraying of fungicide on all of the experiment plots was performed to establish a baseline for studying the effect of fungicide applications. The measurements in the early phase (days after sowing (DAS) < 70) were performed to understand the effects of growth stages and cultivars on the canopy biological traits, whereas the effect of fungicide was studied in the late growth phase (DAS > 70).

Considering the favorable time period for pathogen infection, the effect of the fungicide factor was studied mainly in the late growth phase (DAS > 70). For the early growth phase, the growth stage and cultivar variability were assumed to be the primary agents affecting the experiments. Therefore, the relationships between different biophysical and biochemical traits of barley crop were studied along with correlations with the optical properties (mainly vegetation indices).

As observed in this study, plant diseases infections were not prominent in the field experiments under natural conditions. Figure 6-2 shows that the leaves of the without-fungicide treatment were moderately infected, whereas the with-fungicide treatment controlled the disease infections.

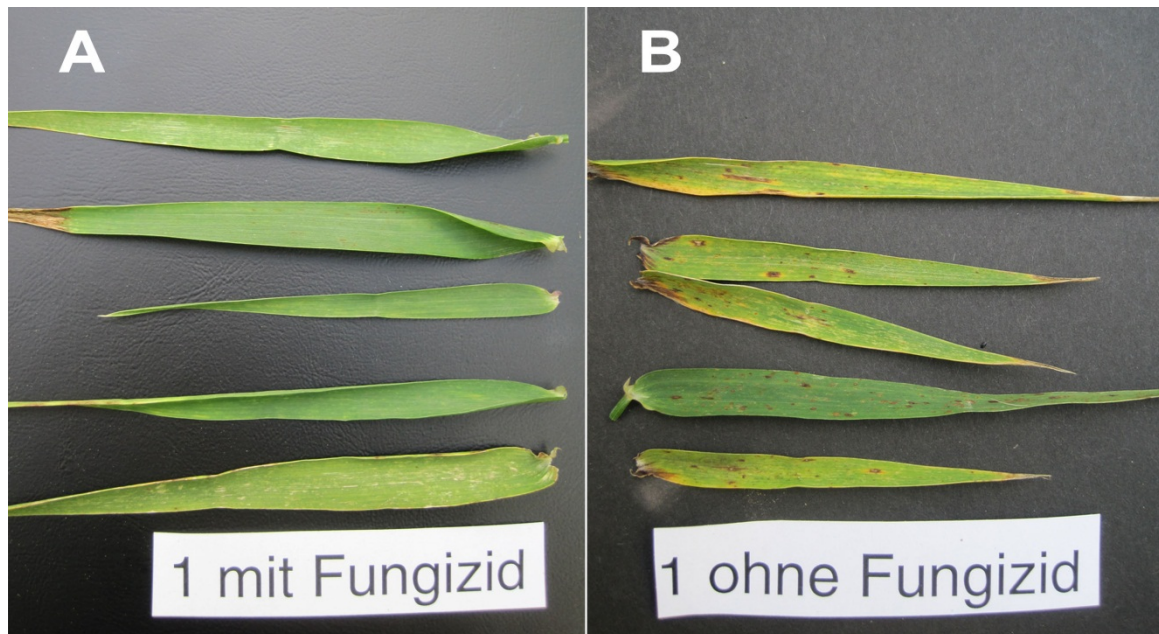


Figure 6-2: Photographs show barley leaves with fungicide spraying (A) compared with the leaves without fungicide spraying (B). The leaves in the without-fungicide plots showed visual symptoms of infections at a mild/moderate level.

6.1.2 Canopy spectral measurement and plant sampling

Canopy reflectance was measured with an ASD FieldSpec® 3 spectrometer (Analytical Spectral Devices Inc., Boulder, CO, USA) from a distance of 1 m above the canopy and within two hours of solar noon. The configuration of the FieldSpec® 3 has been detailed in previous chapters (see CHAPTER 2). The spectrometer was calibrated every 15 min using a white reference panel (Spectralon®). For each plot, six spectra were collected at six random locations within the plot.

After the spectral measurement, the above ground parts of the barley plants within an area of 400 cm² (20*20) were sampled from each plot. For the experiment in 2011, plant samples were cut 50-cm from the top (upper part) when the plants were higher than 50 cm, and the remainder (lower part) was processed separately for further analysis. This approach was used to examine the Chl vs. N relationships in different parts/organs of a plant and was not used for comparison purposes in the 2012 experiments. After cutting, the plant samples were stored in a cool box and transported to the laboratory where the samples were weighed for fresh weight and then lyophilized to determine the Chl concentration. Thereafter, the plant samples were free-dried

CHAPTER 6

until a constant weight and then ground before determining the N concentration (%) was determined. The Chl concentration ($\mu\text{g/g}$) was determined by the spectrophotometric method described in CHAPTER 3. The N concentration (%) was determined using a C/N elemental analyzer.

6.1.3 Selected vegetation indices for sensitivity comparison with the new index RRDI

To study the response of vegetation indices to different variables, i.e., Chl, N and biomass, nine vegetation indices were selected by considering their band combinations and applications that focused mainly on canopy biochemical traits (Chl and N). The new Ratio of Reflectance Difference Index (RRDI) in the red edge (RRDI_{re}), was included to compare its performance with other vegetation indices. Table 6-1 provides the nine vegetation indices and their formulae.

Table 6-1: Selected vegetation indices for sensitivity comparison.

Index	Formula	Reference
Clg	$(R_{750}-R_{550})/R_{550}$	<i>Gitelson et al. (2003b)</i>
Clre	$(R_{750}-R_{700})/R_{700}$	<i>Gitelson et al. (2003b)</i>
EVI	$2.5 * (R_{800}-R_{670}) / (R_{800} + 6 * R_{670} - 7.5 * R_{470} + 1)$	<i>Huete et al. (2002)</i>
NDVI	$(R_{800}-R_{680}) / (R_{800} + R_{680})$	<i>Blackburn (1998b)</i>
ND705	$(R_{750}-R_{705}) / (R_{750} + R_{705})$	<i>Sims & Gamon (2002)</i>
PRI	$(R_{531}-R_{570}) / (R_{531} + R_{570})$	<i>Gamon et al. (1992)</i>
REIP	$700 + 40 * ((R_{670} + R_{780}) / 2 - R_{700}) / (R_{740} - R_{700})$	<i>Guyot & Baret (1988)</i>
RRDI _{re}	$(R_{745}-R_{740}) / (R_{740}-R_{700})$	<i>Yu et al. (2014a)</i>
TCARI/OSAVI	TCARI/OSAVI	<i>Haboudane et al. (2002)</i>

The formulae for TCARI and OSAVI are provided in Table I-1.

6.2 Results

6.2.1 Relationships between Chl and N in different parts of a plant

One of the main objectives of the 2011 experiments was to examine the relationships between N and Chl. Thus, the plant samples were divided into two parts (upper and lower) by cutting at a length of 50 cm from the top when the barley plants were well developed (height > 50 cm). The results of the regression analysis showed that Chl increased as N increased in both the upper and lower parts of the barley plant and the whole plant when the plant height was less than 50 cm (Figure 6-3). The regression models for the different parts differed, although a robust correlation was observed between Chl and N across all of the data of the different parts.

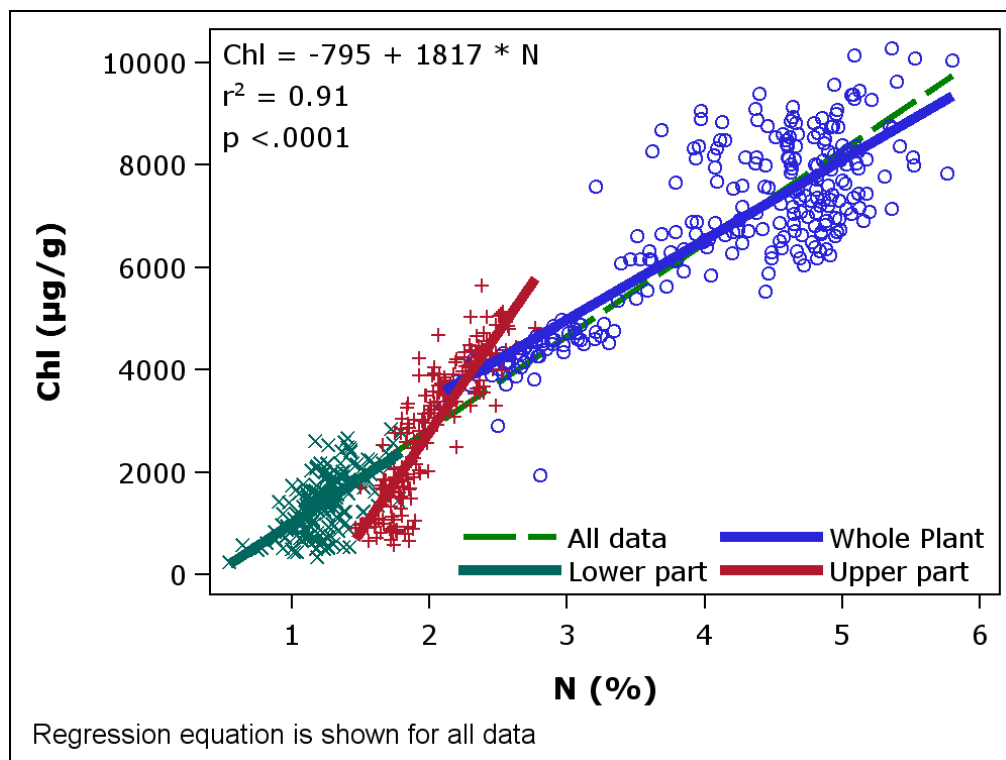


Figure 6-3: Relationships between chlorophyll concentration (Chl, $\mu\text{g/g}$) and nitrogen concentration (N, %) as observed in the whole plant and upper and lower parts of the barley plants. The results were obtained from the 2011 experiment. The upper and lower parts denote the upper 50 cm and remaining parts of the whole plant, respectively.

6.2.2 Relationships between Chl and N at different growth stages as observed in different cultivars of barley

Across the data of the two experiments in 2011 and 2012, Figure 6-4 shows that Chl increased as N increased in the four different barley cultivars at four different growth stages. The Chl vs. N relationships at individual growth stages were similar for the different cultivars and yielded almost identical slopes of regression (Figure 6-4). By contrast, the relationships in different growth stages differed significantly from each other, with no exception found in the cultivars studied in the two experiments. Compared to the cultivars, the growth stages have shown a significant effect on the correlation between Chl and N concentrations of the whole plants.

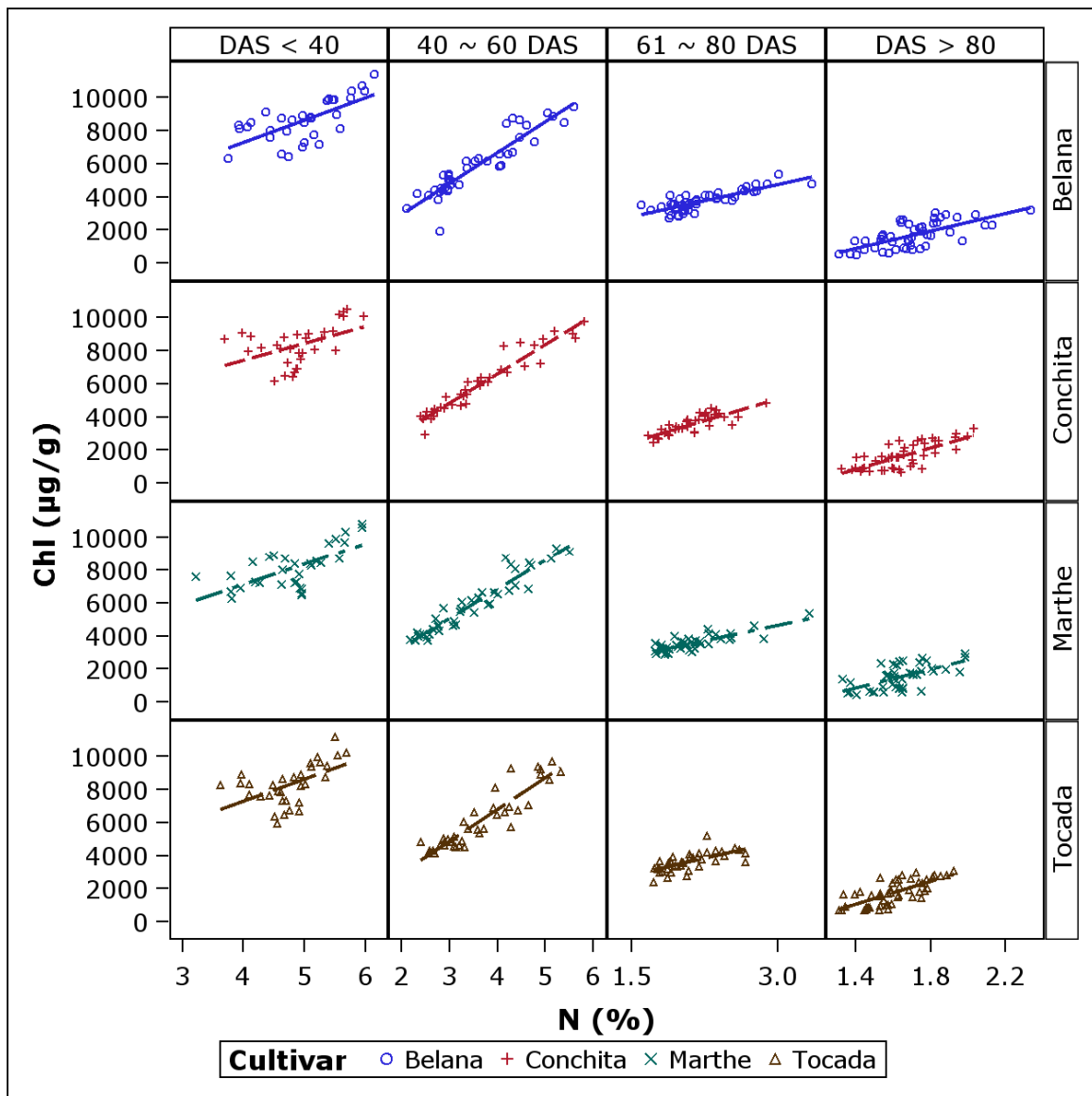


Figure 6-4: Relationships between chlorophyll concentration (Chl, µg/g) and nitrogen concentration (N, %) at different growth stages (days after sowing, DAS) as observed in the whole plants of different barley cultivars. The results were obtained from the field experiments in 2011 and 2012.

6.2.3 Relationships between Chl and vegetation indices (VIs)

To find the most robust indicator of Chl, all data from the two experiments in 2011 and 2012 were used to study the correlations between Chl and different VIs (Table 6-1). Figure 6-5 shows the relationships between Chl and the nine selected vegetation indices by different growth stages. They showed reverse relationships at the very early (DAS < 40) and vary late stages (DAS >80), which confirms the previous results observed in rice experiments (CHAPTER 2).

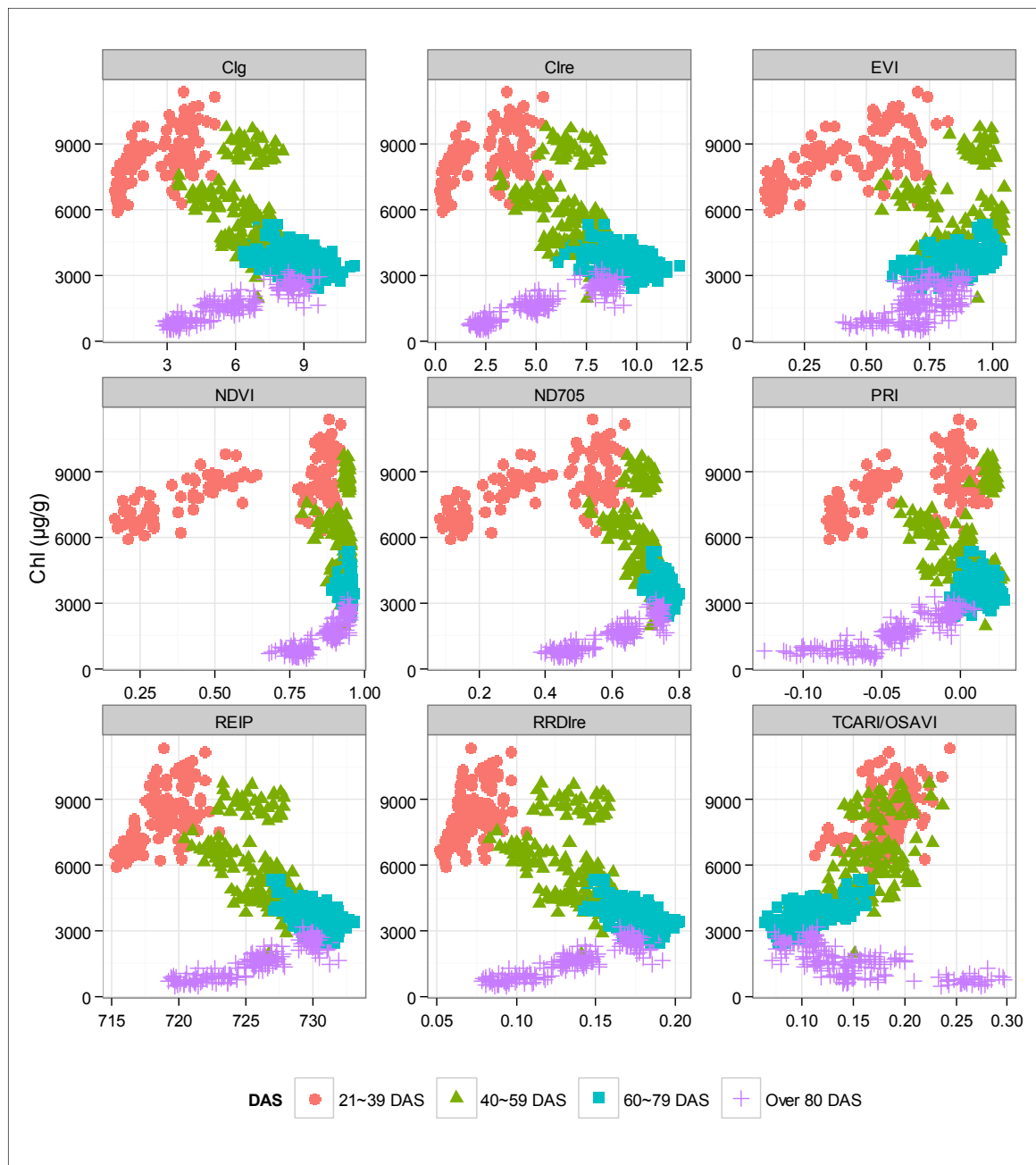


Figure 6-5: Scatterplots showing the chlorophyll concentration (Chl, $\mu\text{g/g}$) plotted as a function of the nine vegetation indices (Clg, Clre, EVI, NDVI, ND705, PRI, REIP, RRDlre and TCARI/OSAVI, see Table 6-1).

Accordingly, the data for DAS > 80 were excluded from the regression analysis because the correlation showed an opposite trend compared to other stages (Figure 6-5). Figure 6-6 shows the performances of the nine VIs when accounting for the variation in Chl. The performances of the EVI, NDVI, ND705 and PRI appeared to be too poor to explain the variation in Chl and yielded an $r^2 < 0.35$. Both Clg and Clre explained 57% of the variation in Chl. The most robust

indices were REIP, RRDI_{re} and TCARI/OSAVI, which yielded r^2 of 0.65, 0.66 and 0.68, respectively.

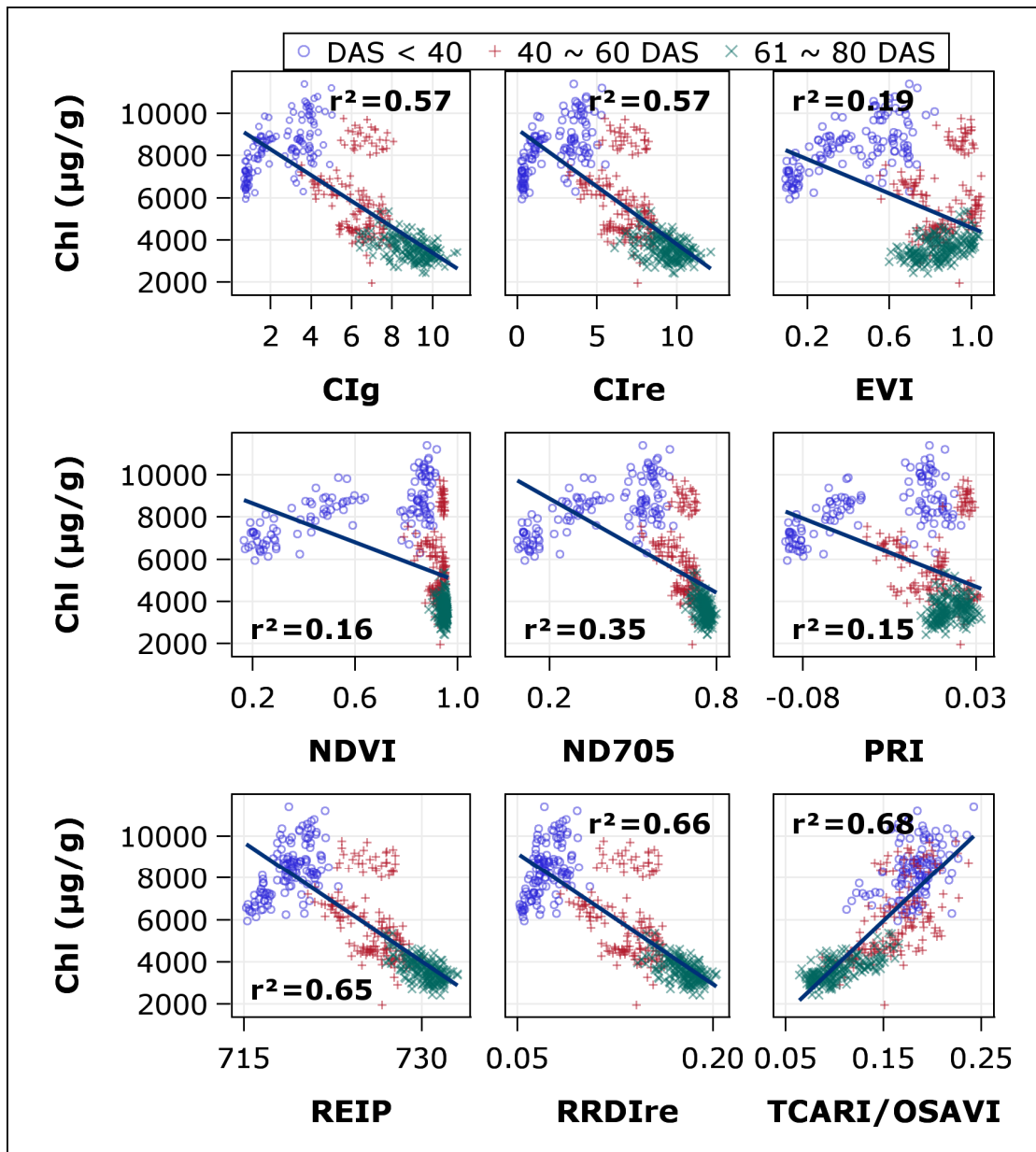


Figure 6-6: The results of the linear regression analyses show the extent of the variation in chlorophyll concentration (Chl, $\mu\text{g/g}$) that was explained by the different vegetation indices. Data for days after sowing (DAS) > 80 were excluded from the analysis.

6.2.4 Relationships between N, biomass and VIs

To study whether the robust indicators of Chl are also related to N and biomass, the relationships between N and the nine VIs were also studied by excluding the data for DAS > 80. Figure 6-7 shows the performances of the nine VIs when accounting for the variation in N. Similarly, the performances of the EVI, NDVI, ND705 and PRI were relatively poor in explaining

the variation in N compared to the other indices and yielded $r^2 < 0.48$. By contrast, Clg, Clre and TCARI/OSAVI explained 67%, 67% and 69%, respectively, of the variation in N. The most robust indicators were the two red edge vegetation indices, REIP and RRDIre, which both yielded an r^2 of 0.76.

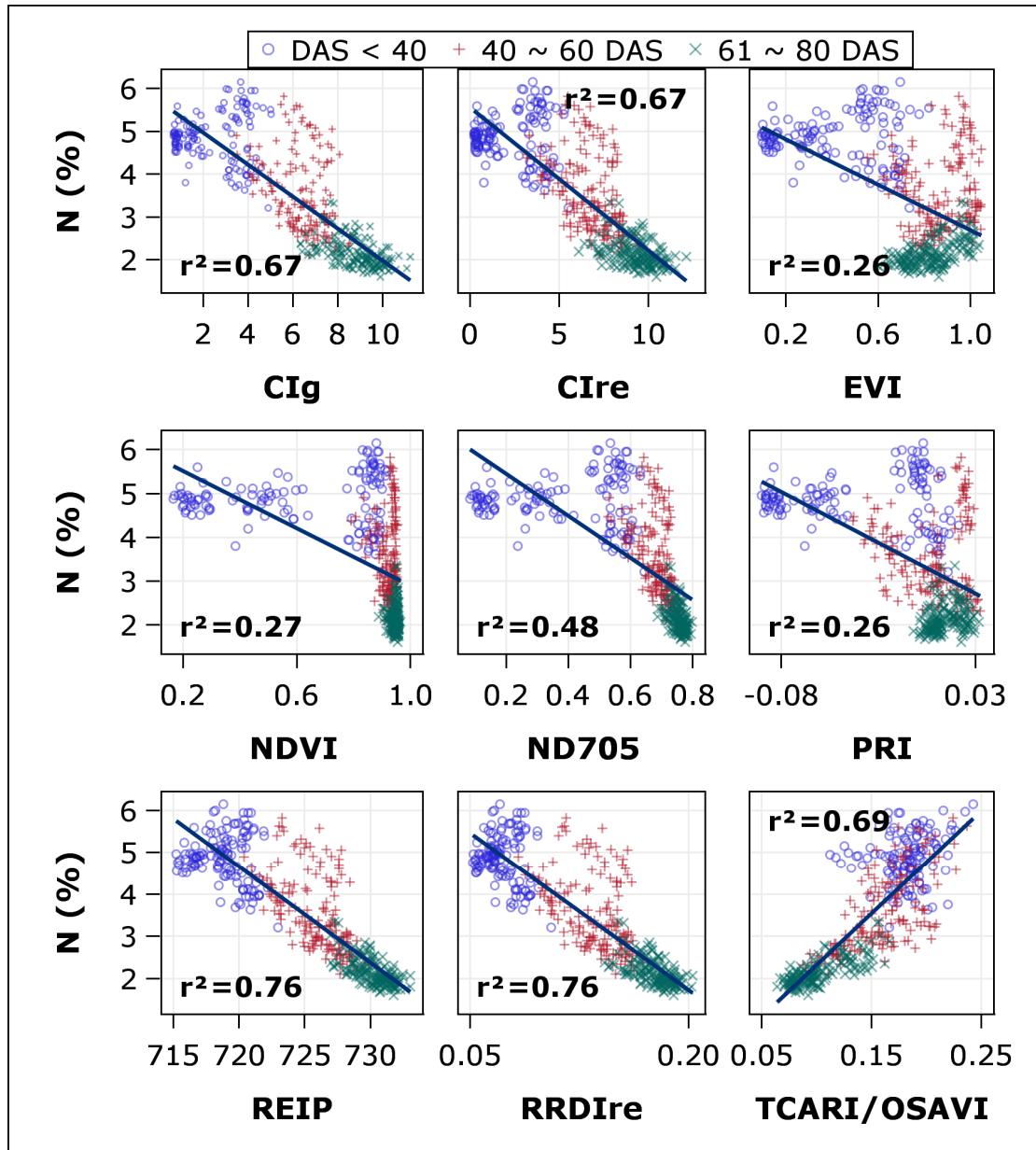


Figure 6-7: The results of linear regression analyses show the extent of the variation in nitrogen concentration (N, %) that was explained by different vegetation indices. Data for days after sowing (DAS) > 80 were excluded from the analysis.

Figure 6-8 shows that the correlations between biomass dry weight (BDW) and EVI, NDVI, ND705 and PRI became saturated as BDW increased, which indicated relatively poor performances of these indices for explaining the variation in BDW ($r^2 < 0.54$). By contrast, Clg,

CI_{re} and TCARI/OSAVI explained 77%, 76% and 64%, respectively, of the variation in BDW. Similar to the relationships with N, the most robust indicators for BDW were also found to be the two red edge indices, REIP and RRDI_{re}, which yielded r^2 of 0.81 and 0.82, respectively.

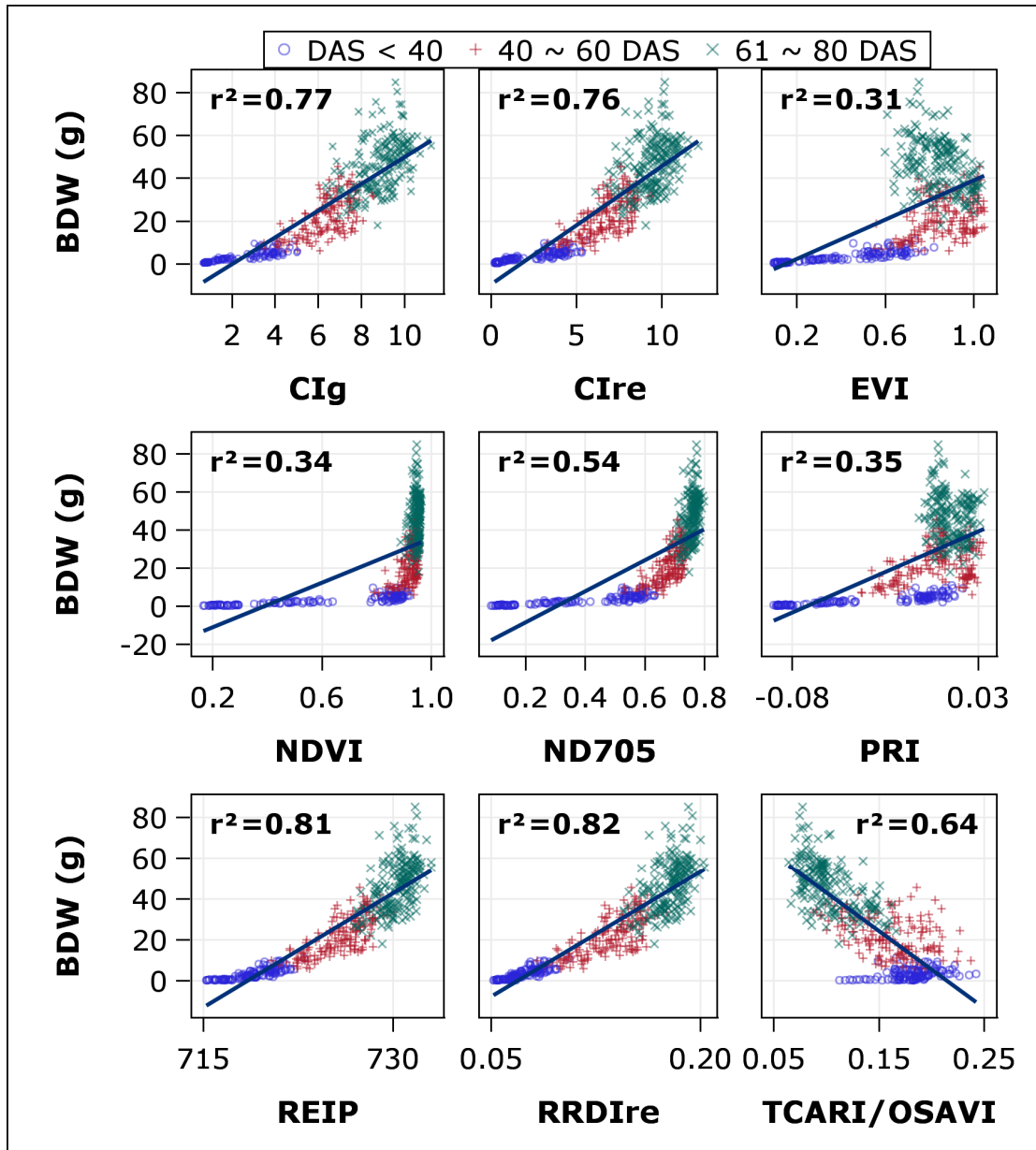


Figure 6-8: The results of linear regression analyses show the extent of the variation in biomass dry weight (BDW) that was explained by different vegetation indices. Data for days after sowing (DAS) > 80 were excluded from the analysis.

Briefly, according to the results of the barley experiments, the REIP and RRDI_{re} appeared to be robust indicators of Chl and N concentrations and BDW.

6.2.5 Responses of BDW, Chl and N to fungicide treatments

The effect of fungicide application and responses of barley biochemical and biophysical traits to fungicide treatments were studied mainly in the late growth phase (DAS > 70). Figure 6-9 shows that the with-fungicide treatment yielded a significantly higher amount of BDW than the without-fungicide treatment after the fungicide applications on 68 DAS and 72 DAS in 2011 and 2012, respectively. Although the second application on 82 DAS did not yield significantly higher BDW in the following days, it enabled the with-fungicide treatment to maintain a relatively high amount of BDW compared to the without-fungicide treatment (Figure 6-9).

It was observed that the with-fungicide treatment in 2012 always maintained a higher amount of BDW than the without-fungicide treatment on different days.

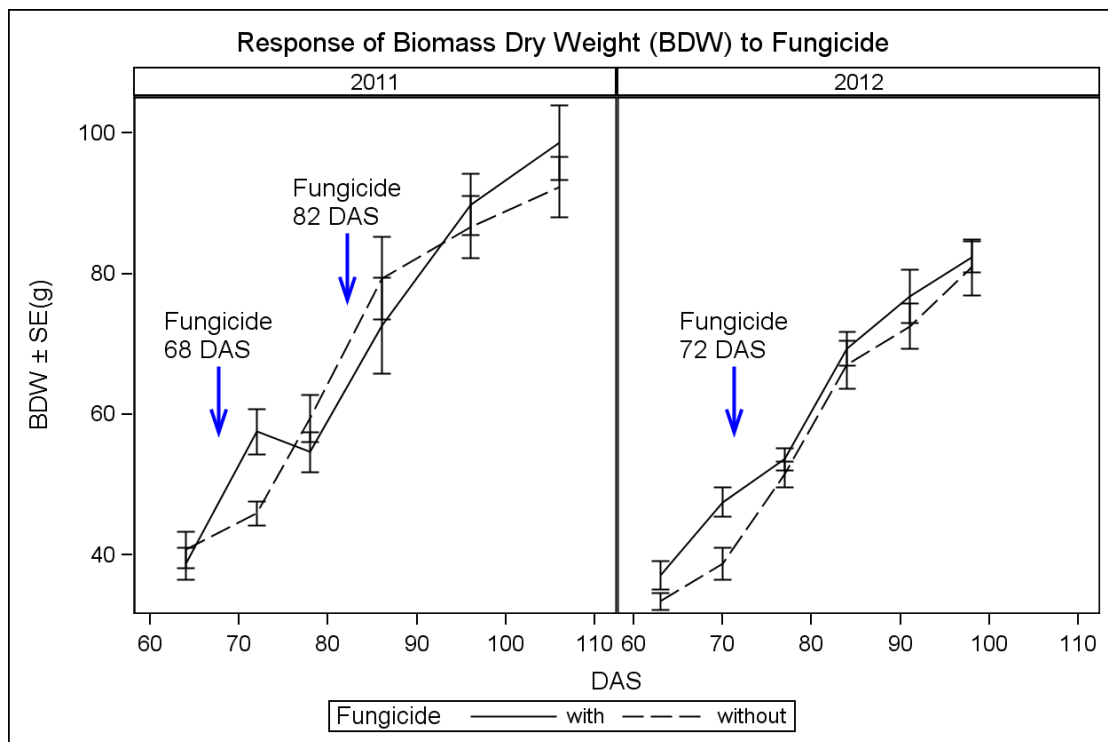


Figure 6-9: Response of biomass dry weight (BDW) to the two treatments of fungicide (with- and without-fungicide) observed on different days after sowing (DAS) in 2011 and 2012. BDW is shown by the mean \pm SE (standard error).

The responses of Chl concentration to the two different fungicide treatments for different years are shown in Figure 6-10. The with-fungicide treatment yielded relatively higher Chl in 2011, whereas it yielded lower Chl in 2012. Figure 6-10 also shows that the with-fungicide treatment did not yield a significantly higher Chl than the without-fungicide treatment after the application of fungicide in 2011 and 2012. However, it is obvious that the with-fungicide treatment closed the gap with Chl relative to the without-fungicide treatment after the fungicide application on 72 DAS

CHAPTER 6

in 2012, which enabled the with-fungicide treatment to maintain a high amount of Chl concentration even when the BDW was at a relatively high level (cf. Figure 6-10 and Figure 6-9). Therefore, it can be deduced that the application of fungicide in 2012 inhibited the pathogen infections in the with-fungicide plots.

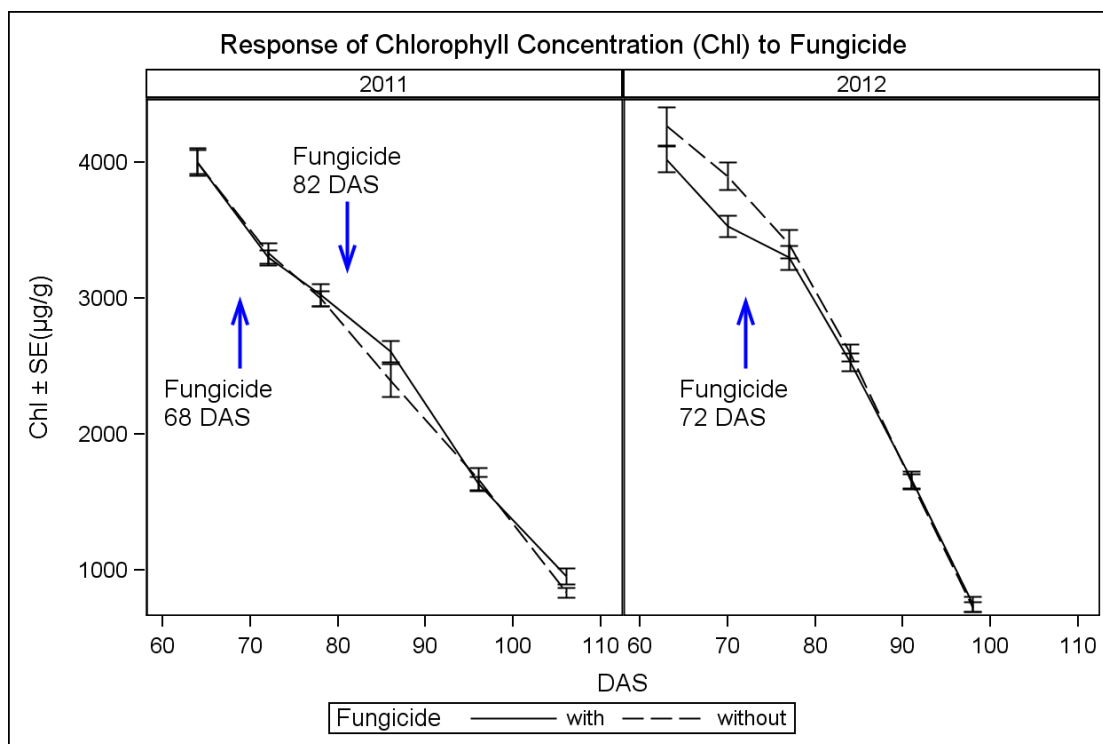


Figure 6-10: Response of chlorophyll concentration (Chl) to the two treatments of fungicide (with- and without-fungicide) observed on different days after sowing (DAS) in 2011 and 2012. Chl is shown by the mean \pm SE.

The responses of N concentration to the two different fungicide treatments for different years are shown in Figure 6-11. The with-fungicide treatment did not yield higher N concentration than the without-fungicide treatment after the application of fungicide in 2011 and 2012.

The results appear to indicate that the fungicide application did not have an effect on the N concentration. However, according to the results of the BDW variations, the variation in N concentration was clearly dominated by the variation in BDW (cf. Figure 6-11 and Figure 6-9). Therefore, the plant N concentration might not be a reliable indicator of crop disease stress, particularly when the infections are mild, as observed in this study. The results also highlighted that the N concentrations are dominated by the plant biomass as discussed in Chapter 2. Therefore, the with-fungicide treatment showed a relatively lower N than the without-fungicide treatment as a result of the high BDW.

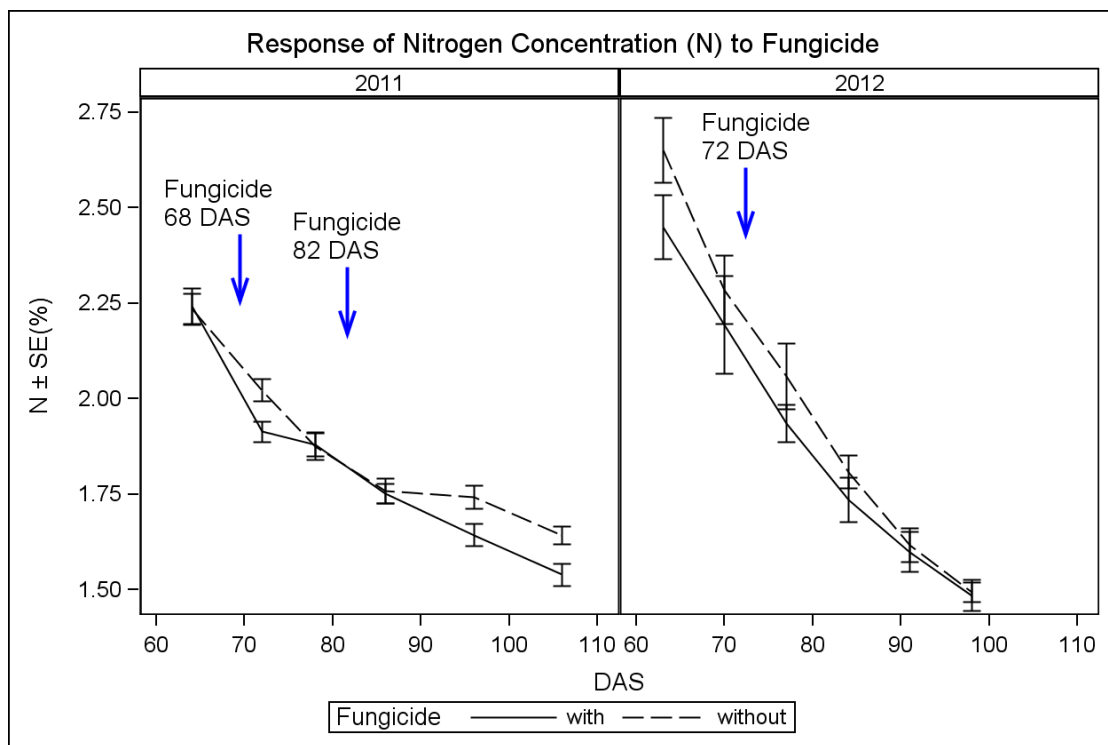


Figure 6-11: Response of N concentration (N, %) to the two treatments of fungicide (with- and without-fungicide) observed on different days after sowing (DAS) in 2011 and 2012. N is shown by the mean \pm SE.

6.2.6 Yield response to diseases

The infections were at a mild/moderate level and did not show significantly severe disease symptoms (cf. Figure 6-2). To study the effect of pathogen infections developed under natural conditions on the final yield, the grain yield was determined for each plot and treatment after harvest.

The responses of yield to the two different fungicide treatments for different years are provided in Figure 6-12. Generally, the with-fungicide treatment produced relatively high yield compared to the without-fungicide treatment in both years. Further, an ANOVA analysis was performed and the results showed that the with-fungicide treatment produced a significantly higher ($p < 0.01$) yield than the without-fungicide treatment in 2011 (Figure 6-12A). In 2012, however, the difference between the with- and without-fungicide treatments was not statistically significant ($p = 0.27$, Figure 6-12B).

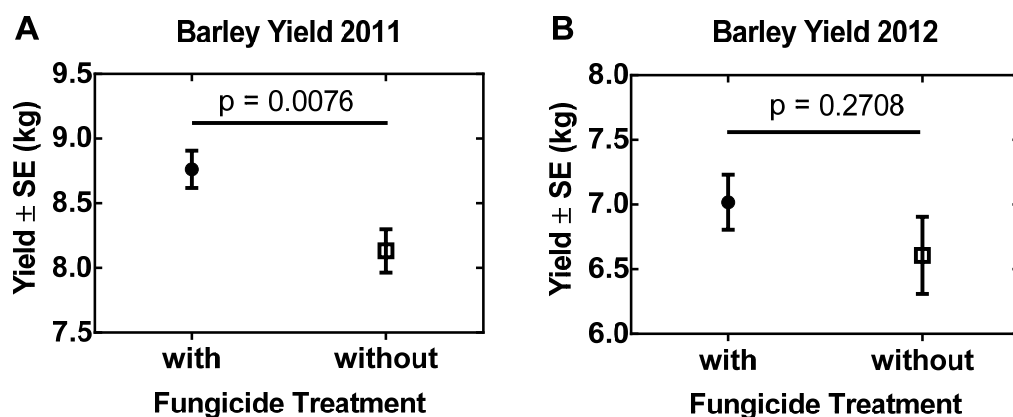


Figure 6-12: Response of barley yield to the two treatments of fungicide (with- and without-fungicide) observed in the experiments in 2011 (A) and 2012 (B), respectively. Yield is shown by the mean \pm SE.

6.2.7 Responses of VIs to diseases

The results from CHAPTER 4 that were based on earlier experiments suggested that the MCARI and MCARI/TCARI were capable of indicating plants grown under disease stresses. Therefore, the two indices were examined for their ability to discriminate the with- and without-fungicide treatments on different DAS for each cultivar in 2011 and 2012. Additionally, diseases may have had specific effects on the spectral traits of the water absorption bands compared to the chlorophyll absorption bands. Thus, the two vegetation indices based on water absorption bands, WBI and NDWI (see CHAPTER 1, Table 1-1), were also employed for the discrimination of different treatments of fungicide.

Figure 6-13 shows that the MCARI/TCARI values were higher in the with-fungicide treatment than in the without-fungicide treatment for the cultivar Belana in 2011 (DAS 72-96). Following the fungicide applications in both 2011 and 2012, the with-fungicide treatment showed a positive response by closing the gap relative to the without-fungicide treatment.

Figure 6-14 shows that the MCARI yielded higher values in the with-fungicide treatment than in the without-fungicide treatment for the cultivars Belana and Tocada in 2011. By contrast, there appeared to be no significant differences between the two treatments for each cultivar in 2012. Following the fungicide application days, the with-fungicide treatment showed a positive response by closing the gap relative to the without-fungicide treatment.

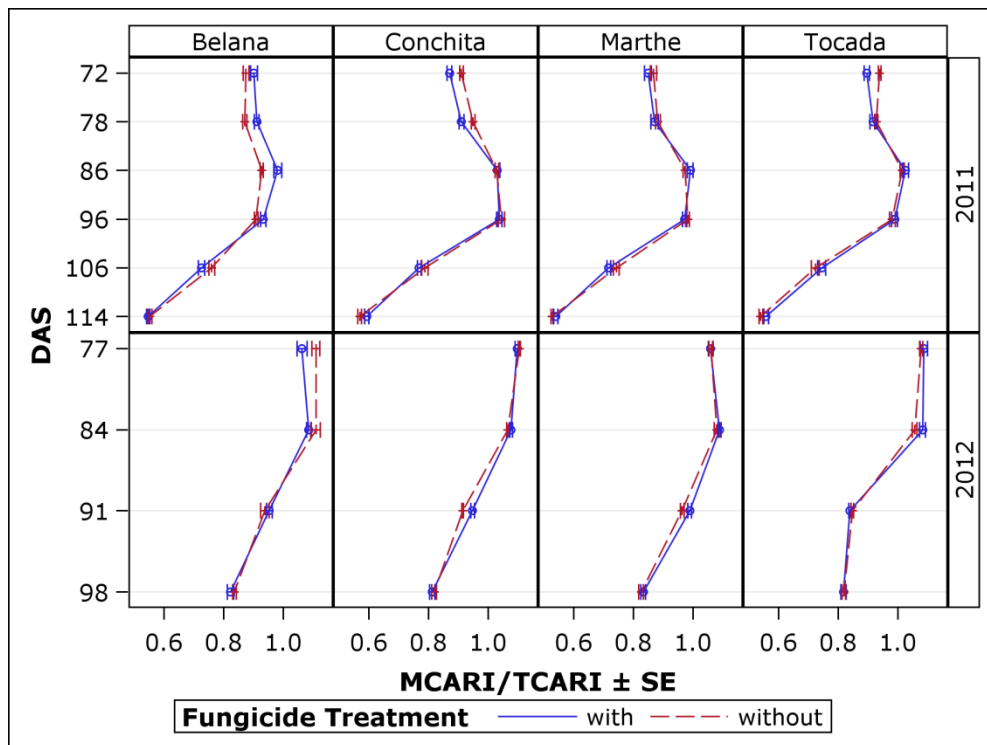


Figure 6-13: MCARI/TCARI response to the two treatments of fungicide (with- and without-fungicide) observed on different days after sowing (DAS), for different cultivars and years. MCARI/TCARI is shown by the mean \pm SE.

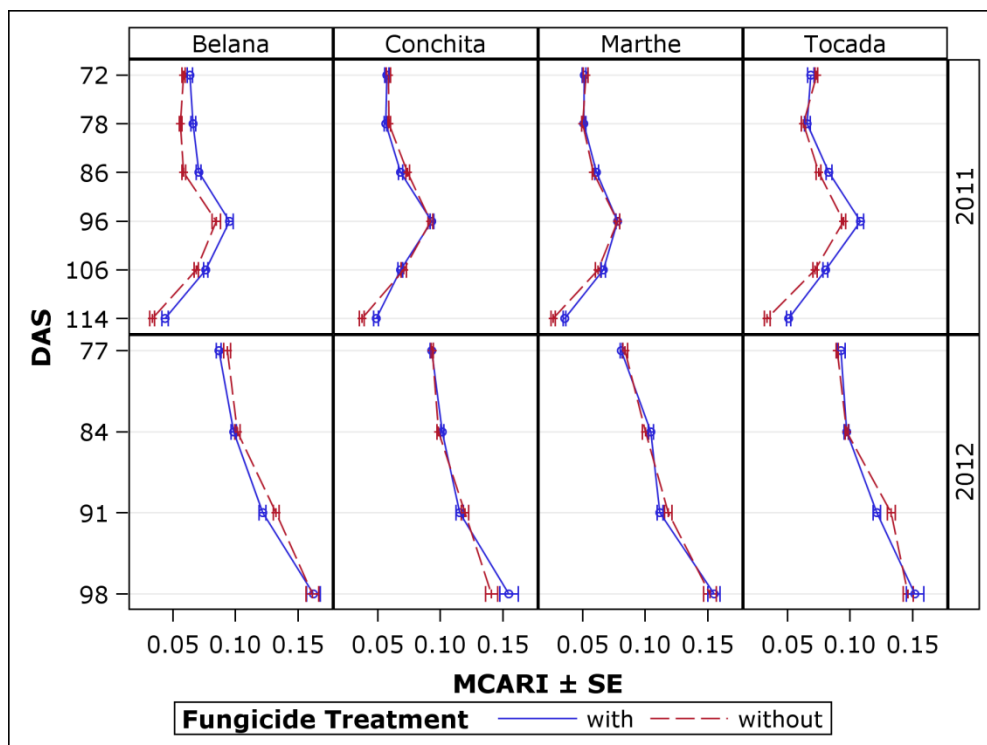


Figure 6-14: MCARI response to the two treatments of fungicide (with- and without-fungicide) observed on different days after sowing (DAS), for different cultivars and years. MCARI is shown by the mean \pm SE.

CHAPTER 6

The responses of the WBI to the two different treatments for each cultivar and year are shown in Figure 6-15. It is obvious that the WBI generally yielded higher values in the with-fungicide treatment than in the without-fungicide treatment, particularly in 2011. By contrast, there were almost no significant differences between the two treatments for the cultivars Belana and Tocada in 2012 (Figure 6-15). Overall, the WBI provided significant separability and showed the ability to discriminate diseased plants that yielded lower WBI values.

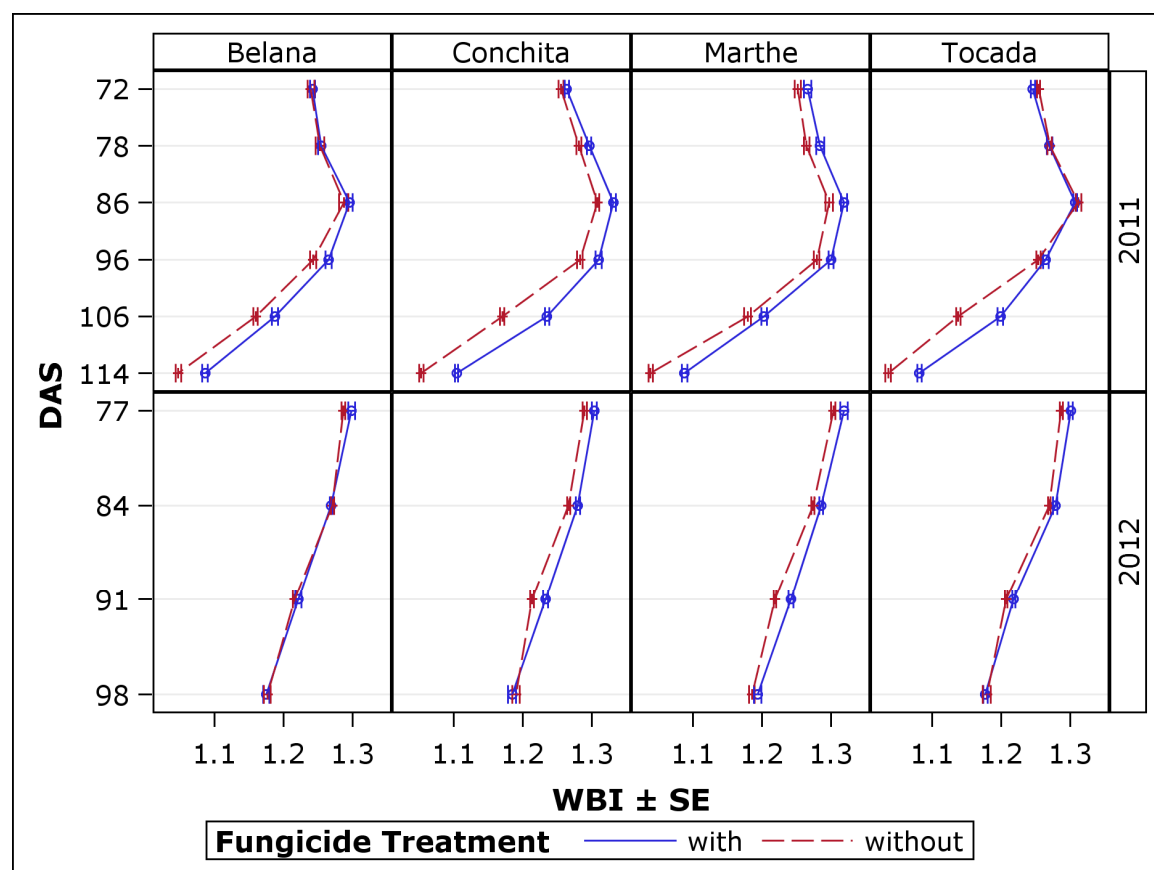


Figure 6-15: WBI response to the two treatments of fungicide (with- and without-fungicide) observed on different days after sowing (DAS), for different cultivars and years. WBI is shown by the mean \pm SE.

The responses of the NDWI to the two different treatments for each cultivar and year are shown in Figure 6-16. Similarly, the NDWI also yielded higher values in the with-fungicide treatment than in the without-fungicide treatment in 2011. The NDWI also provided significant separability and showed an ability to discriminate diseased plants that yielded lower values in the NDWI. However, there appeared to be no significant differences between the two treatments for 2012.

Compared to the MCARI/TCARI and MCARI, the WBI and NDWI provided a significantly positive performance for discriminating the with- and without-fungicide treatments, suggesting

the potential of using water absorption bands to remotely detect crop diseases. The relatively weak performance in 2012 was expected as the yield difference was not significantly different.

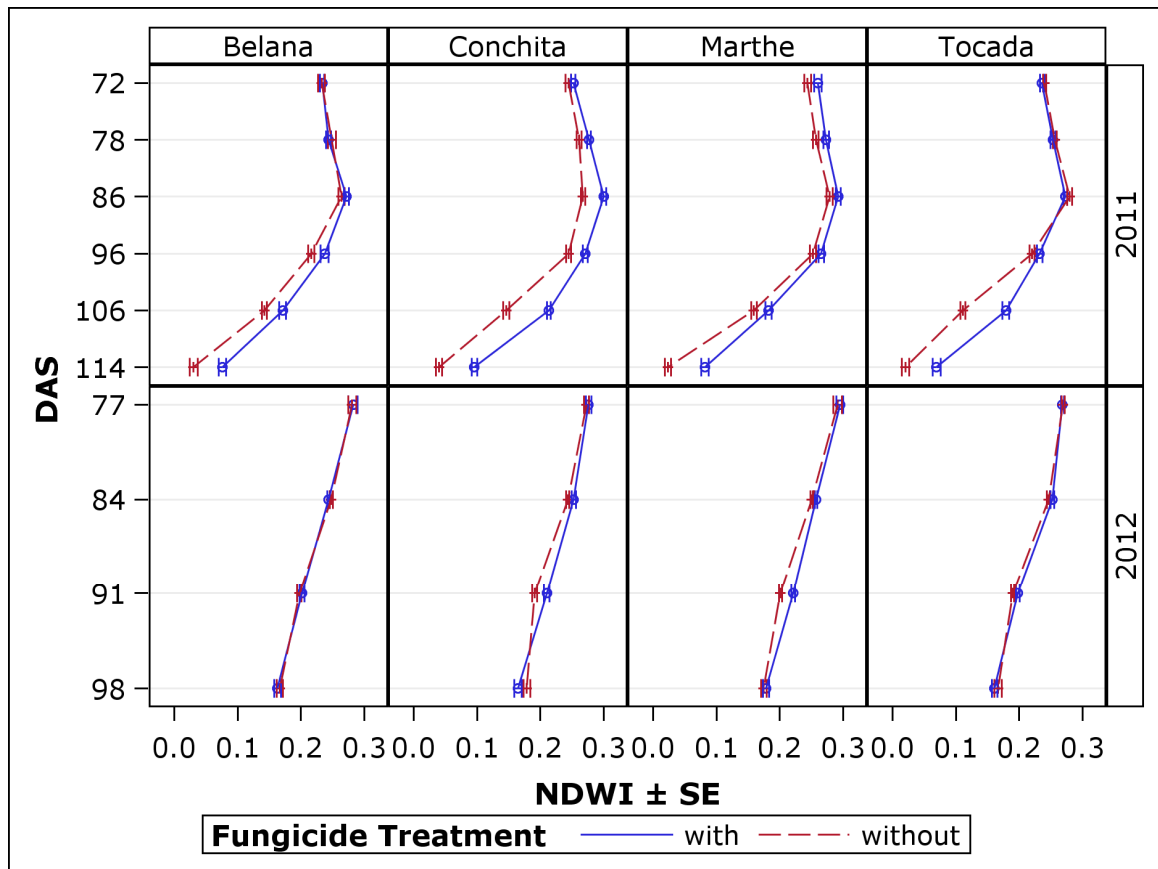


Figure 6-16: NDWI response to the two treatments of fungicide (with- and without-fungicide) observed on different days after sowing (DAS), for different cultivars and years. NDWI is shown by the mean \pm SE.

CHAPTER 7

General discussion and conclusions

7.1 Remote sensing of canopy N

There remains some dispute about the ability of remote sensing to detect the canopy N status, particularly when using the NIR spectral range (*Knyazikhin et al., 2013; Ollinger et al., 2013; Townsend et al., 2013*). The previously observed correlation between NIR spectral and N concentration was deemed a consequence of canopy structural variations rather than of N (*Knyazikhin et al., 2013*). However, other researchers have argued that the lack of a direct link between N and NIR spectra does not necessarily mean that NIR reflectance does not contain useful information for inferring the N variability (*Ollinger et al., 2013; Townsend et al., 2013*) and the indirect link indicates that NIR spectra are correlated with the functional associations between canopy N and leaf/canopy structural traits. The co-variations of biochemical and biophysical traits across plant functional types may allow for the prediction and mapping of canopy biochemical variations that could be used to understand the N cycling in vegetation canopies (*Ollinger et al., 2008; Townsend et al., 2013*).

Although the previous studies were conducted on forest canopies, they provide positive implications for remote sensing of the crop canopy N status. Similarly, NIR bands have been found to be efficient in estimating crop N status using near-ground multispectral (*Gianquinto et al., 2011*) and hyperspectral data (*Li et al., 2008; 2014*), airborne multispectral data (*Lee et al., 2008; Tilling et al., 2007*) and satellite images (*Martin et al., 2008; Shou et al., 2007*). Based on hyperspectral narrow band data collected on rice canopies, *Yu et al. (2013b)* also showed that NIR reflectance plays a key role in optimizing the best 2-band combinations, which follow the formulae of simple ratio (SR) and NDVI (see CHAPTER 2). In addition, the optimum multiple narrow band reflectance (OMNBR) models also required the use of NIR bands to improve model accuracy, particular for modeling N uptake — the product of plant dry biomass and N concentration (CHAPTER 2). Together, these studies based on hyperspectral narrow bands and multispectral broad bands, through near-ground to space platforms, scaling from experimental fields to larger ecosystems, have shown consistent results that NIR bands can be used to remotely sense canopy N (*Gianquinto et al., 2011; Li et al., 2008; Martin et al., 2008; Ollinger et al., 2008; Shou et al., 2007; Tilling et al., 2007; Yu et al., 2013b*). However, as observed in powdered samples of dried leaf materials, the most abundant nitrogen-bearing compound in green leaves has

absorption features mainly in the SWIR bands (1500, 1680, 1740, 1940, 2050, 2170, 2290 and 2470 nm) instead of NIR bands (Elvidge, 1990), which appears to be a contradiction — NIR bands are important in estimate canopy N, but they are not directly linked to N — with the large number of observed results as mentioned previously.

From the perspective of the effect of N supply, Heege *et al.* (2008) argued that N has two effects on the reflectance of a plant canopy: (1) the first effect occurs only in the visible (VIS) bands and is known as the photosynthetically active radiation (PAR). This effect is due to that N supply increases the chlorophyll per unit area in the leaves, causing that more light is absorbed and that reflectance is very low in VIS region; and (2) the second effect is a very pronounced effect on canopy reflectance and occurs in the NIR region (known as the “NIR shoulder”), which is due to that N supply increases the growth of plant mass and green leaf area. Theoretically, the larger the green leaf area, the more incident solar radiation should be scattered back by the canopy instead of the soil (Heege *et al.*, 2008). These authors clarified the indirect link between N supply and VIS-NIR reflectance of crop canopies by comparing with the “control canopy” that has no N supply, which contradicts the view that N is not related to NIR reflectance. The results observed by Yu *et al.* (2013b) also support this explanation by demonstrating an indirect link between VIS-NIR reflectance and N uptake (see CHAPTER 2).

To date, by assuming that N in fresh leaves does not alter their absorption bands, RS community tacitly accepts the explanation that the absorption of nitrogen-bearing compounds in fresh leaves is not strong and is generally masked by water absorption in the SWIR bands (Kumar *et al.*, 2001). However, there are still no definitive answers to (1) how the *in-vivo* N in green leaves affects the light absorption, transmittance and reflectance of a canopy over the full wavelengths, since the absorption of N-bearing compounds is difficult to be measured in fresh leaves; and (2) whether the *in-vivo* N in fresh leaves have different absorption features relative to those absorption bands (SWIR) that are observed in powdered samples of dry leaf materials. The answers to these questions might uncover the role of the *in-vivo* N in determining the canopy reflectance. Additionally, these different arguments suggest the need to improve our understanding on the underlying mechanisms that can link canopy reflectance with N status/variability. For this purpose, a means of physical explanation is needed, despite that currently available radiative transfer models appear to be unable to fully represent the linkages (Townsend *et al.*, 2013).

As a result of the importance of the N status of the whole plants in determining the grain production (Qiao *et al.*, 2013), this study focuses mainly on N estimation of the whole plants. The canopy sensing of N requires us to consider that the distribution of *in vivo* N and chlorophyll

(chlorophyll is also a N-bearing compound) within individual leaves may be heterogeneous and the N element is mobile between different leaves of a plant (Barton, 2001; Gastal & Lemaire, 2002). Under N deficiency, plants have developed relatively elaborate mechanisms to improve N use efficiency by remobilizing N element from older leaves that are generally at the bottom of the plant and transporting it to younger leavers at the top of the canopy (Lemaire et al., 2008; Yu et al., 2013b) (see Figure 7-1). Short-term N stress may not significantly change the top canopy properties — both biological and optical properties — compared to healthy plants with sufficient N supply except a possible yellowing of the older leaves (Fageria, 2009) (Figure 7-1). In contrast, long-term N stress may produce leaves and stems that are light green, yellow and spindly and lead to significant structural differences, such as the production of smaller plants, compared to the healthy plants with sufficient N supply (Figure 7-1). These differences are readily captured by canopy spectra and often yield low reflectance in NIR region and green bands of VIS but reflectance increase in blue and red regions (Yu et al., 2013a) (Figure 7-2).

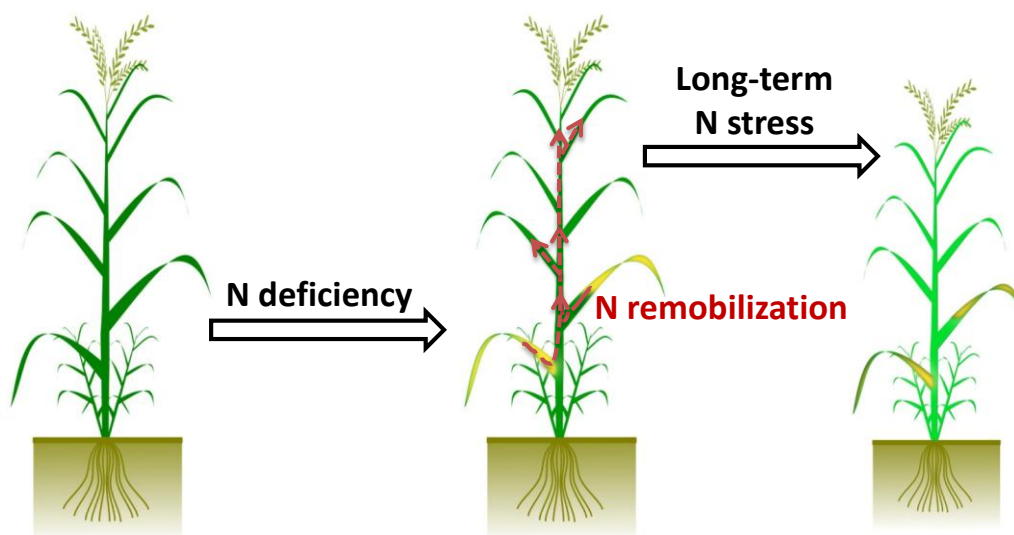


Figure 7-1: A schematic diagram shows the responses of plants to N deficiency. Plants perceive N deficiency and improve N use efficiency by remobilizing N element from older leaves and transporting it to younger leavers at the top of the canopy.

Accordingly, the best time to remotely capture crop N deficiency is right after the plants perceive a signal of N deficiency and start N remobilization (Figure 7-1). However, individual leaves of the top canopy may not adequately represent the N state of the whole plant (Yu et al., 2013b) (see CHAPTER 2); therefore, it is not recommended to assess canopy N status by leaf level spectral measurements. With long-term N stress or significant N deficiencies, robust correlations are often observed in leaf level spectral measurements because top canopy leaves have undergone significant changes (Xue et al., 2004); however, the appearance and detection of

these changes after the excessive “N hunger” is often too late to guide the crop N management. Thus, important uncertainties remain when N statuses are estimated by spectral measurements of individual leaves rather than the canopy.

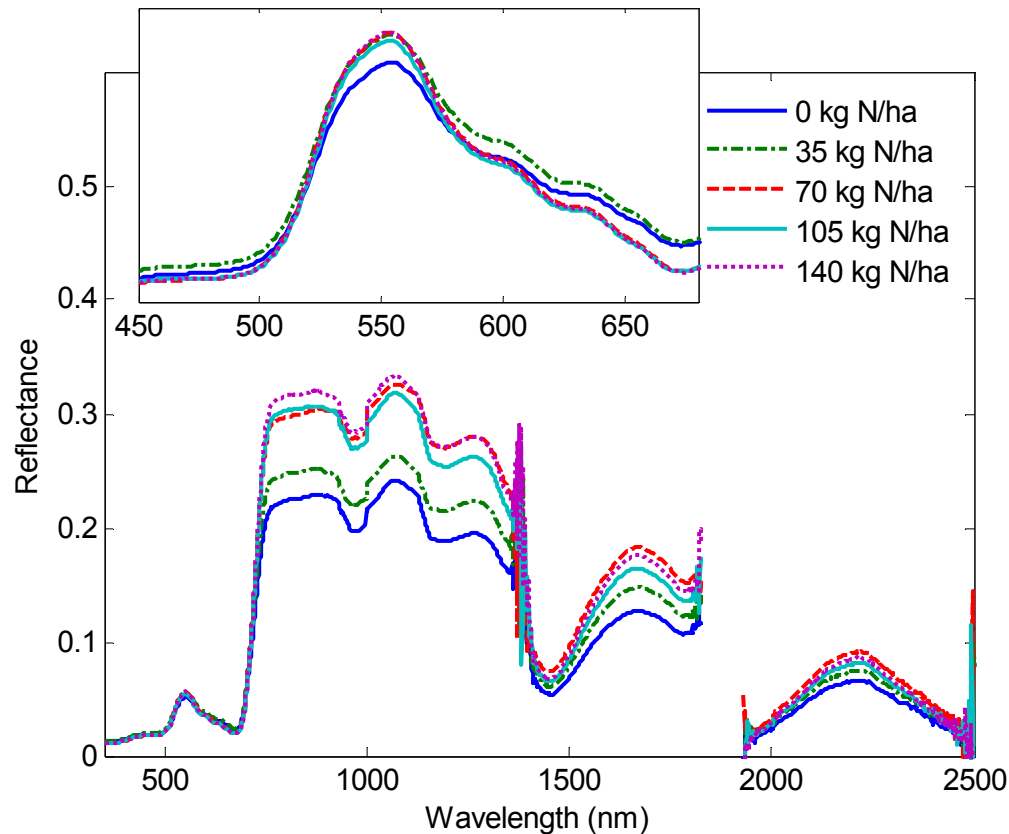


Figure 7-2: Canopy reflectance observed on rice canopies with different nitrogen supply at the booting stage. Inset highlights the reflectance variation in the 450-680 nm range (adapted from Yu *et al.* (2013a)).

7.2 Growth stage and N dilution effect

The effect of growth stage on the remote sensing of canopy traits is not as simple as a change in ground coverage and has not sufficiently studied in the past. Different trends of the correlations between plant N concentration and vegetation indices in different growth stages have been reported in rice (Yu *et al.*, 2013b) (see CHAPTER 2) and wheat crops (Li *et al.*, 2010b). In this study, the results of the barley experiments also showed the distinct trends in the correlations between vegetation indices and plant N concentration, as well as chlorophyll concentration (CHAPTER 6, Figure 6-5), which implies that the limitations of vegetation indices due to the influence of growth stages are not crop-species-specific responses and might be unavoidable in the currently existing vegetation indices. Yu *et al.* (2014b) observed the temporal changes in canopy reflectance collected on seven barley cultivars across seven growth stages (see

CHAPTER 5). They found that NIR reflectance generally increased until the heading stage and then decreased, whereas green reflectance decreased until the heading stage and then increased (CHAPTER 5, Appendix A, Figure 5-A1), suggesting that canopy reflectance at different wavelengths change in different ways across growth stages. This may explain the distinct trends of vegetation indices in response to canopy nitrogen in different stages (Li et al., 2010b).

With the advance of growth stage, plant growth rate is much faster than the rate at which N is accumulated in the plant mass until the stage of full heading, which results in the decrease of N concentration (Figure 7-3) and yields the N dilution effect (Justes et al., 1994; Yu et al., 2013b). The N dilution effect causes the crop canopy structural variations (mainly biomass) to be the dominant factor that determines the canopy spectral signatures before the canopy closure, particularly in the NIR and SWIR regions (Heege et al., 2008; Mistele & Schmidhalter, 2008). Similarly, the results of this study also showed that barley canopy N concentration decreased as plant biomass increased (Figure 7-3). As shown in the N dilution curves in both experiments in 2011 and 2012, the dilution effect has faded from 75 days after sowing (DAS). This corresponds with the trends that were observed in the correlations of vegetation indices and canopy chlorophyll concentration (CHAPTER 6, Figure 6-5). Following the DAS 75-80, the growth rate of plant biomass became very low compared to the early growth stages (DAS < 75), and crop canopy reached closure. Theoretically, after the canopy closure, biomass variations might not be sufficiently captured by canopy reflectance, because two dense canopies with significant difference in biomass might not produce significant difference in their canopy reflectance or vegetation indices. This might explain the well-known “saturation effect” of traditional vegetation indices (e.g., NDVI) when they are used to estimate green leaf area (Kimura et al., 2004; Sims & Gamon, 2003). Also, the saturation phenomena of traditional vegetation indices (e.g., NDVI) that have been found in biomass estimation are attributed to the effect of growth stages (Gnyp et al., 2014a; Li et al., 2010a). In contrast, after canopy closure, the effect of canopy biochemical variations (e.g., Chl, N, water etc.) on canopy reflectance might become prominent compared to the effect of biomass variations, thus cause the significantly different trends of correlations for DAS > 80 (CHAPTER 6, cf. Figure 6-5 and Figure 7-3). These biochemical variations might be due to various factors, for example variation in chlorophyll, N or even variations caused by senescence (Merzlyak et al., 1999; Viña & Gitelson, 2011) and other factors. Therefore, in a closed canopy*, biochemical variations might be one of the dominant factors that produce canopy spectral variations.

* Closed canopies denote maximal ground coverage (closure).

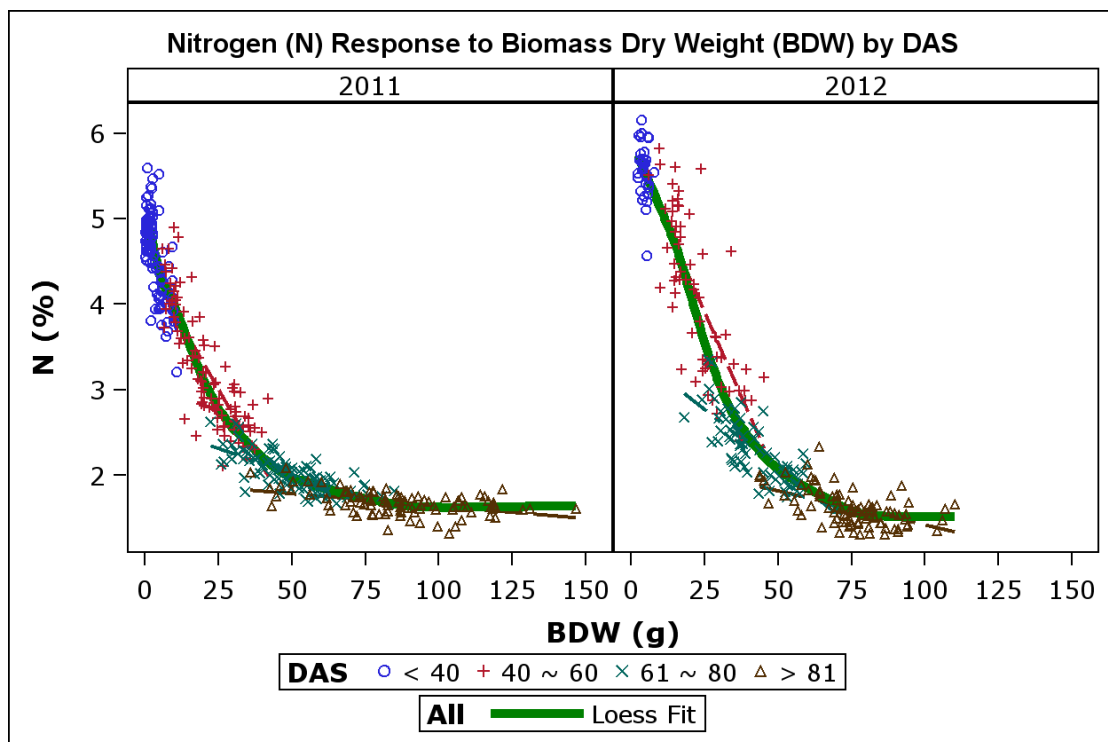


Figure 7-3: Response of nitrogen concentration (N, %) to biomass dry weight (BDW) observed along with the growth stages of the barley experiments in 2011 and 2012. Loess fit shows the N dilution curves for each year.

7.3 Relating Chl to N

There are a number of studies have consistently shown that chlorophyll (Chl) is related to N (Fageria, 2009; Filella et al., 1995; Fridgen & Varco, 2004). As expected, the correlations were relatively robust for individual stages (Figure 6-4), although the relationships appeared to be more variable across growth stages (Figure 7-4). Therefore, using one variable of the Chl vs. N relationship to infer another one makes it difficult to obtain a high precision for all growth stages. Importantly, the results also indicate that growth stages have a relatively significant effect on the Chl vs. N relationship compared to the differences between cultivars (Figure 6-4).

The results based on the barley experiments showed that the nine selected vegetation indices (see Table 6-1) explained more variation in N concentration than the Chl (cf. Figure 6-6 and Figure 6-7), suggesting that using spectrally modeled Chl to estimate the N concentration might result in significant errors compared to using proper vegetation indices to estimate N directly. Consequently, one of the questions concerned in this study — why most of the investigations do not use the spectrally modeled Chl and a Chl vs. N model to indirectly model N, instead, they use canopy spectra directly to estimate N (CHAPTER 1, section 1.4) — becomes clear.

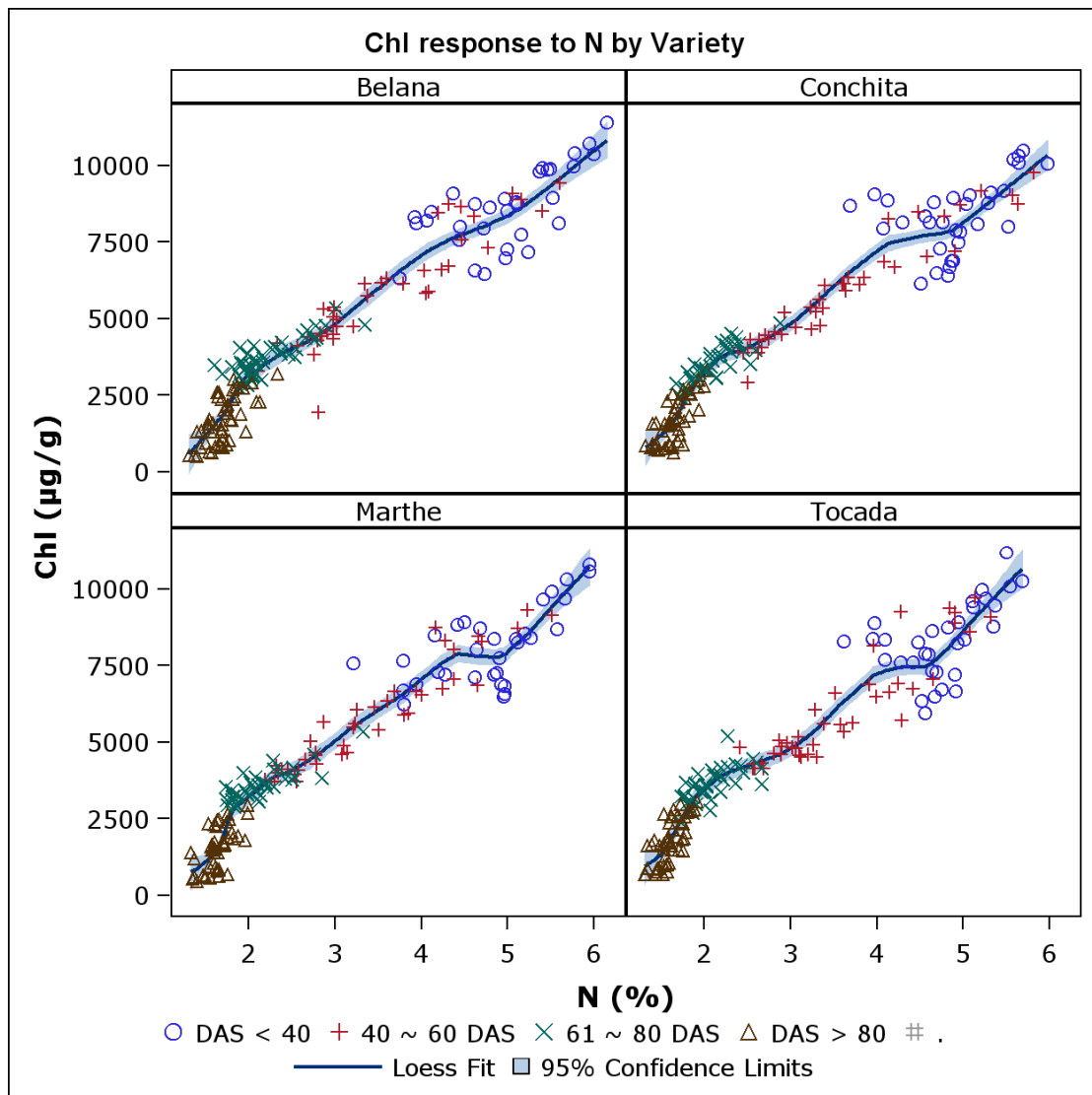


Figure 7-4: Response of chlorophyll concentration (Chl, $\mu\text{g/g}$) to nitrogen concentration (N, %) observed in each barley cultivar.

As discussed in previously section, N variation causes variation in both biomass and chlorophyll, which has significant effects on canopy reflectance in both VIS and NIR regions (Heege *et al.*, 2008). These indirect effects on the VIS and NIR bands were also been highlighted by (Yu *et al.*, 2013a) in rice canopies (Figure 7-2). Therefore, a direct estimation of N concentration from canopy hyperspectral data appears to be more effective compared to modeling N from spectrally modeled chlorophyll.

7.4 Decoupling of biochemical and biophysical traits

In this study, we explored the possibility of decoupling the contributions of biochemical and biophysical traits to canopy spectra by introducing a new method to optimize vegetation indices (Yu *et al.*, 2014a; 2014b) that employs a transformed “reflectance unit” comprising the Ratio of

Reflectance Difference (RRD) (see CHAPTER 3 and CHAPTER 5). Canopy structural variations (e.g., biomass, LAI, soil background) cause a confounding effect on the analysis of canopy spectra for the estimation of biochemical parameters, and it has been hypothesized that the confounding effect is partially linearly eliminable (Figure 7-5, see also CHAPTER 3 and CHAPTER 5). Based on this hypothesis, the confounding effect of multiple scattering, soil/water backgrounds and their interactions within the canopy can be weakened and eliminated from the measured canopy reflectance by defining the Ratio of Reflectance Difference Index (RRDI) and optimizing its corresponding bands ($\lambda 1-4$, Figure 7-5). This hypothesis proved to have an inherent relation with the multiple scatter correction (MSC) theory as interpreted in *Yu et al. (2014b)* (see CHAPTER 5).

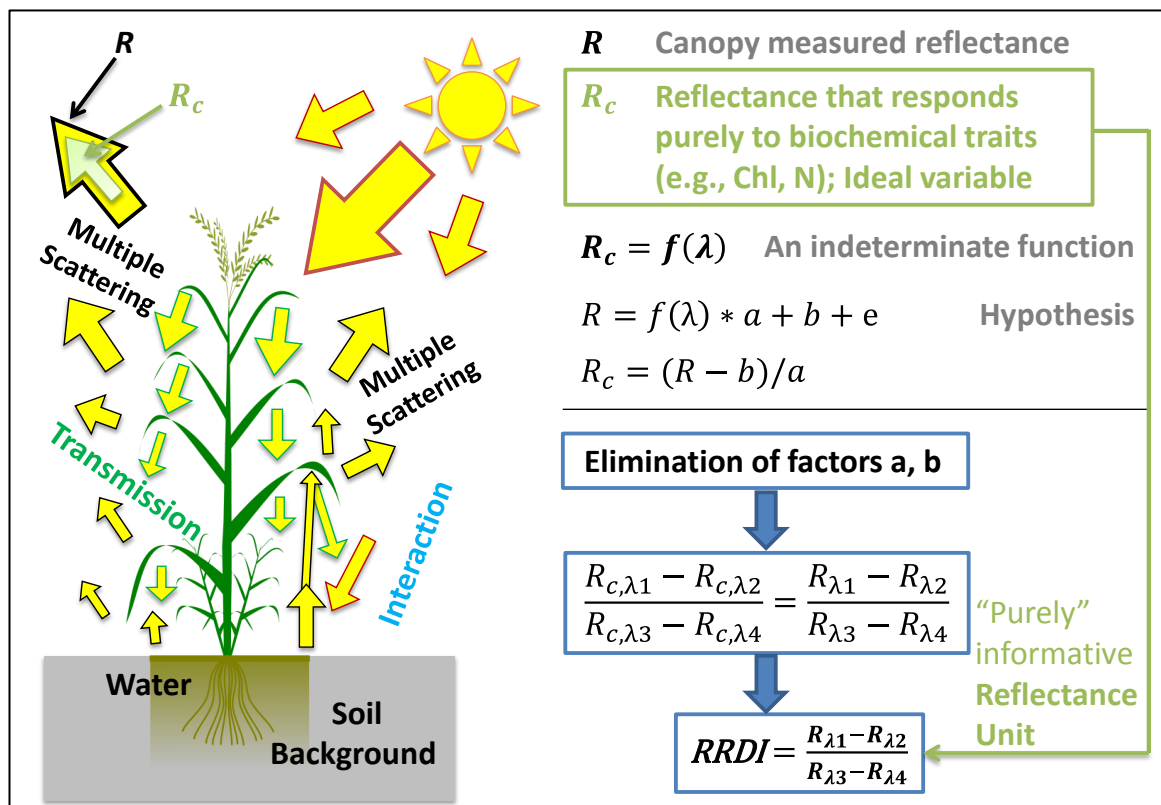


Figure 7-5: A schematic diagram illustrates the hypothesis for developing a reflectance unit that attempts to cancel out the effects of canopy confounding factors when correlating the biochemical traits and canopy spectra. It is named the Ratio of Reflectance Difference Index (RRDI), and the bands can be optimized by a lambda-by-lambda band optimization algorithm (CHAPTER 3 and CHAPTER 5). The RRDI is based on the linear hypothesis that the confounding effect of multiple scattering, soil/water backgrounds and their interactions induces multiplicative (a) and additive (b) contributions to the measured canopy reflectance with the error term e.

The red edge index, REIP, showed comparable performance to RRDIre for the estimation of Chl and N concentrations. *Darvishzadeh et al. (2009)* suggested that REIP was not a reliable indicator of LAI because it was insensitive to LAI variations. Similar results were also found by

Boegh *et al.* (2002), who reported that REIP was relatively insensitive to structural variations and REIP proved to be good indicator of Chl, suggesting that using the red edge range for Chl estimation is less affected by structural variations. Accordingly, the RRDl in the red edge — $RRDI_{re} = (R_{745} - R_{740}) / (R_{740} - R_{700})$ — was developed for the estimation of the canopy Chl content* of rice (Yu *et al.*, 2014a) (see CHAPTER 3). This index showed a comparable performance to the partial least squares regression (PLSR) when it was employed to estimate the Chl content of farmer fields (Yu *et al.*, 2014a). In the subsequent barley experiments, the RRDl_{re} also showed a promising performance on estimating the canopy Chl concentration† (Figure 6-6) and N concentration (Figure 6-7) of barley plants and explained 66% and 76% of the variation in Chl and N, respectively. These results suggest that the RRDl_{re} has the promising potential to model canopy Chl and N across different crop types.

At the canopy level, Chl per unit area is of interest because of its important role in linking with photosynthesis capacity relative to the Chl per unit mass (van der Meer & de Jong, 2001; Yoder & Waring, 1994). Generally, a thicker leaf with similar Chl per unit area would have a lower Chl per unit mass; therefore, the Chl per unit mass might be less related to the photosynthesis capacity than is the Chl per unit area. At the leaf level, two leaves that have the same Chl per unit area should have a similar spectral reflectance. However, the degree of the similarity of reflectance might decrease when scaling-up to canopy level (Zarco-Tejada *et al.*, 2005). At the canopy level, a thicker leaf will be more likely to prevent light from penetrating inside the canopy to deeper leaf layers than a thinner leaf with similar Chl per unit area. Additionally, a thinner or narrower leaf might be more likely to enable light to encounter soils or non-photosynthesis materials compared to a thicker or wider leaf with similar Chl per unit area. Therefore, at the canopy level, remote sensing of Chl per unit area appears to be more readily affected by soil background and canopy structures (Yu *et al.*, 2014b) (see CHAPTER 5). This was confirmed by the results that showed that the optimized RRDl significantly improved the correlation with Chl per unit area (Cab) based on the PROSAIL simulation ($r^2 = 0.98$) compared to Chl per unit mass of barley leaves (Figure 5-2, CHAPTER 5), which suggests that the method developed in this study can be applied to both Chl per unit mass and Chl per unit area estimations; however, it might be more applicable to the area-based Chl content.

In addition, this method has the potential to reduce background signals similar to the derivative-transformed spectral indices (Gnyp *et al.*, 2014a; Yu *et al.*, 2014a; Zhao *et al.*, 2005) (see CHAPTER 3 and CHAPTER 5); however, it may not be limited to the sensors measuring continuous wavelengths compared to derivative analyses. Therefore, the RRDl eliminates the additive effect

* Content uses the area-based unit $\mu\text{g cm}^{-2}$.

† Concentration uses the dry-mass based unit $\mu\text{g/g}$.

without employing derivative transformation and reduces both the additive and multiplicative effects without having to apply the MSC (Yu *et al.*, 2014b), which indicated that RRDl optimization has the advantage of simplicity in hyperspectral remote sensing of canopy biochemistry. However, in addition to Chl and N, the main biochemicals found in plants also include cellulose, hemicellulose, lignin, protein, starch and water (Kumar *et al.*, 2001) for which this method still need to be evaluated.

7.5 General model and growth-stage-specific model

As previously discussed, growth stages have a dominant effect on the remote estimation of crop canopy N and Chl concentrations. Therefore, one vegetation index or general model covering all of the growth stages may not be able to capture precise information about crop growth status. It has been recommended that different vegetation indices should be used for different crop parameters at different growth stages (Hatfield & Prueger, 2010). This is consistent with our results wherein the optimized vegetation indices for N uptake and N concentration are used in the early and late growth stages, respectively (Yu *et al.*, 2013b) (CHAPTER 2). To design a general method to overcome the effect of growth stages on vegetation indices, Yu *et al.* (2014b) suggested to classify crop canopies into two types — open and closed canopies* — based on the concept “optical types” proposed by Ustin & Gamon (2010), and select the best vegetation indices/models for open and closed canopies, respectively (CHAPTER 5). A pre-screening method based on a threshold value of NDVI has been used (0.8) to ensure that the canopy biochemical traits of forest canopies that only have high-LAI are analyzed (Asner & Martin, 2008). Similar methods for classifying the degree of canopy closure may be applied to crop canopies by selecting the proper vegetation indices. Based on prior knowledge on the growth stages, Yu *et al.* (2013b; 2014b) used the BBCH scales (Lancashire *et al.*, 1991) to distinguish the canopy closure (open or closed canopies) in rice and barley canopies, respectively, and this method proved to be able to improve the estimation of canopy N and Chl for both open and closed canopies (CHAPTER 2 and CHAPTER 5). In addition, the results also indicate that different narrow bands and band combinations must be used at different growth stages and that the use of additional bands, such as NIR-SWIR bands (Koppe *et al.*, 2010; Yu *et al.*, 2013b).

Compared to vegetation indices, multivariate methods offers the potential of the calibration of a general model for the estimation of multiple variables such as biomass, Chl, LAI, N and other canopy biochemical and biophysical parameters (Asner & Martin, 2008; Atzberger *et al.*, 2010; Hansen & Schjoerring, 2003; Yu *et al.*, 2013a; 2013b; 2014a; 2014b; 2014c). Yu *et al.* (2013a)

* Open and closed canopies denote before and after reaching the maximal ground coverage (closure), respectively.

suggested the use of both biochemical (N) and biophysical (biomass) variables to calibrated a partial least squares regression (PLS) model to take the co-variations of both variables into account, which proved to be able to improve the estimations of both biomass and N variations. Therefore, to use canopy reflectance for the N estimation at different growth stages, this study suggests two approaches: (1) use the two-step method that first classifies the degree of canopy closure into two classes (open and closed canopies) and selects the proper vegetation indices and optimizes the open- and closed-canopy models, respectively; and (2) calibration of multivariate methods.

Currently available radiative transfer (RT) models are still not able to account for the effect of crop growth stages. Although LAI variations might be able to indicate to some extent the variations due to phenological stage development, they are not able to fully represent the linkages between different factors that co-vary in reality, e.g., biomass, LAI, N and Chl ([Jacquemoud et al., 2009](#); [Townsend et al., 2013](#)). Some studies have suggested that the ill-posed problems — different variable combinations may produce almost identical spectra — should be taken into account when using RT models ([Atzberger, 2004](#); [Richter et al., 2011](#)). Concerning the effect of growth stage, ill-posed problems might occur in the form that different growth stages might produce almost identical spectra, which further increases uncertainties in estimating crop characteristics.

7.6 Canopy sensing of plant diseases

Comparisons between vegetation indices derived from chlorophyll and water absorption bands are rarely conducted ([Apan et al., 2004](#); [Delalieux et al., 2009](#)); therefore, the methods by which plant diseases impact chlorophyll functional change and water absorption are not well understood. According to the results of the barley experiments, water band indices (WBI, NDWI) appeared to be superior to chlorophyll band indices in the tests in this study (cf. Figure 6-13, Figure 6-14, Figure 6-15 and Figure 6-16), which suggests that the response of canopy spectra to plant diseases might be dominant in water absorption bands compared to the chlorophyll absorption bands. Recent studies have shown that water absorption bands are also useful for the estimation of plant biomass ([Gnyp et al., 2014b](#); [Koppe et al., 2010](#)), which suggests that significant higher values of the WBI and NDWI might be due to the higher amount of biomass. However, according to the results of this study, the with-fungicide treatment did not yield significant high amount of biomass compared to the without-fungicide treatment (see Figure 6-9) on those days that the with-fungicide treatment yielded significant higher WBI and NDWI (Figure 6-15 and Figure 6-16). The possible explanation is that the disease infections were mild as observed in this study (Figure 6-2). The vegetation indices derived from the chlorophyll absorption bands and water absorption bands failed to distinguish the fungicide treatments in 2012, which is in

accordance with the yield response in 2012 in which no significant difference was observed between the two fungicide treatments (Figure 6-12). Finally, our results suggest that spectral features in the NIR-SWIR range might be more efficient for detecting crop diseases compared to those in the VIS range.

Plant height has an effect on the vertical expansion of diseases; therefore, infection symptoms may appear earlier on the upper parts of dwarf cultivars than on the leaves of taller cultivars (Gröll, 2008). Therefore, compared to the leaf level proximal sensing, hyperspectral canopy sensing provides the potential to detect the infection symptoms in a relatively low layer of the canopy. This is confirmed by the results of the barley experiment (see CHAPTER 4) in which the hyperspectral vegetation indices detected the diseased plants even when the upper-most flag leaves did not show obvious infection symptoms (Yu *et al.*, 2014c).

Canopy remote sensing of crop diseases has the potential to provide site-specific applications of agricultural chemicals (Cao *et al.*, 2013; Delalieux *et al.*, 2007). However, the successful implementation depends on both spatial and spectral resolution of the detecting sensors (Gröll, 2008; Laudien & Bareth, 2006). A low spatial resolution sensor system might be not able to detect the unevenly spread diseases compared to a high spatial resolution system (Figure 7-6).

It is well known that the severity and occurrence of diseases are affected by the weather and climate conditions (Barkley *et al.*, 2014), which is why disease infections often appear to be mild under natural conditions. Additionally, mild symptoms of diseases and disease symptoms in the lower leaf layers might not be detectable by high spatial resolution systems with a low spectral resolution or limited disease-insensitive bands (Figure 7-6). In these cases, mild symptoms might be masked by other variations of the canopy, and a sensor with a low spectral resolution is more likely to capture canopy spectra that are primarily dominated by other factors other than the disease symptoms. Therefore, the detection of mild symptoms of diseases requires both high spatial and high spectral resolution sensors and the sensors should have the sensitive bands, for example the NIR-SWIR bands as highlighted in this study.

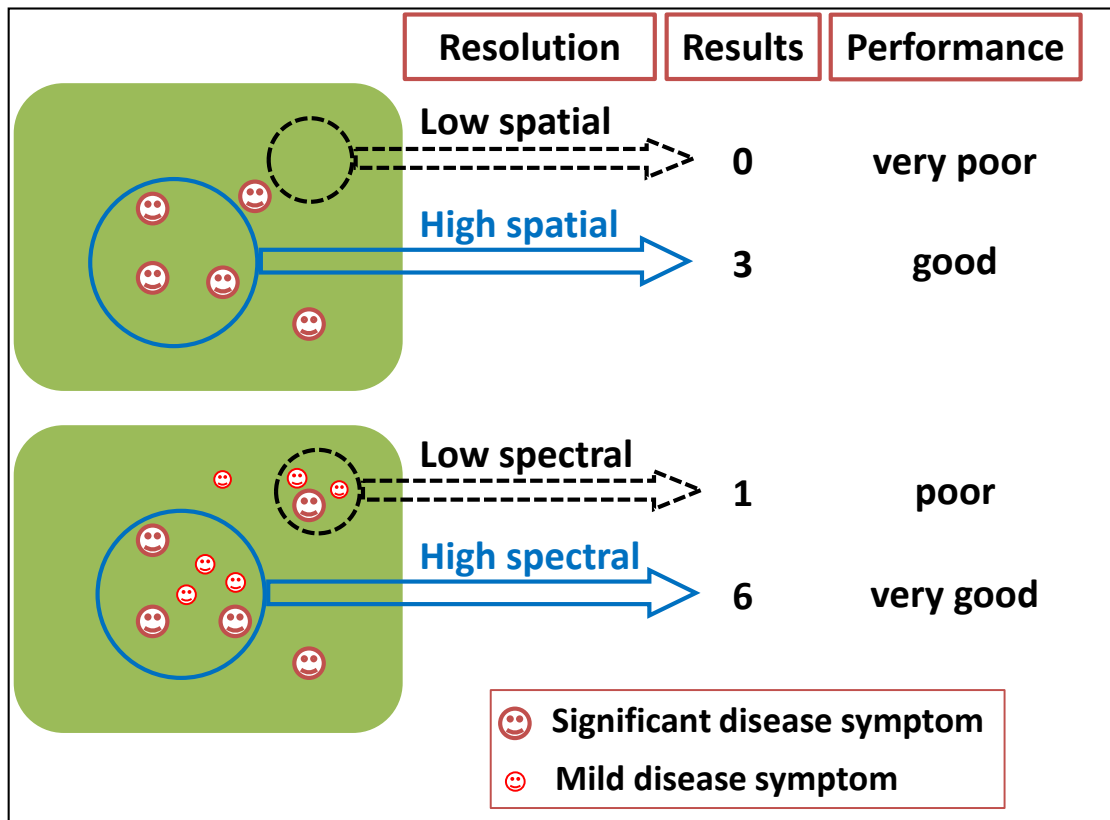


Figure 7-6: A schematic diagram illustrates the effect of spatial and spectral resolutions of canopy sensors on the detection of plant diseases.

7.7 Near-ground remote sensing for PA

Compared to the wide spectrum of remote sensing (RS) applications, the scope of this dissertation is very narrow and focuses mainly on understanding and estimating the variability of chlorophyll (Chl) and nitrogen (N) in crop canopies. Over the last 40 decades, remote sensing has proved to be a valuable tool for agronomic management (Gausman & Cardenas, 1968; Hatfield et al., 2008). High spatial resolution RS data collected by sensors on most available airborne or satellite platforms have low spectral resolution and a limited number of bands, which prohibits the capturing of rich information about the variation in crop biological characteristics (Zhang & Kovacs, 2012). Although satellite hyperspectral images (e.g., Hyperion (EO-1)) provide greater spectral resolution, they have very low spatial resolution that cannot sufficiently represent the within-field subtle variability (Thenkabail et al., 2012). Hyperspectral remote sensing based on near-ground platforms allows for studying the sensitivity of hyperspectral narrow bands to various plant biochemical and biophysical characteristics (e.g., biomass, Chl, N, water) with low costs. By combining with ground truth data, near-ground hyperspectral remote sensing allows for the investigation of how to efficiently use the high dimensional RS data to interpret variability of

crop growth and yield. Consequently, it also enables the development of new methods and products that can be applied to PA, as well as airborne or satellite platforms.

With the enlargement of intensive production and mechanization of site-specific fertilization and pest managements, near-ground remote sensing also plays a key role in facilitating the development of crop sensors, tractor-based sensing system and low-cost UAV systems for precision crop management (Heege *et al.*, 2008; Hunt *et al.*, 2010; Yao *et al.*, 2012; Zhang & Kovacs, 2012).

7.8 Mains findings and conclusions

Growth stages have a dominant impact on the remote sensing of crop canopy biochemical and biophysical traits and variations, which suggests that different vegetation indices must be used for open (early stage) and closed (late stage) canopies. Multivariate models such as multiple linear regression (MLR) analysis, partial least squares (PLS) and support vector machines (SVM) are relatively resistant to the effect of growth stage by employing more spectral bands or a full-spectrum analysis.

The ratio of reflectance difference index (RRDI) removes the confounding effects of canopy structures, multiple scattering and soil background as well as their interactions, which improves the estimation of canopy biochemical traits (e.g., Chl and N) compared to traditional vegetation indices such as the normalized difference vegetation index (NDVI) and simple ratios (SR). As an example, the RRDI in the red edge (RRDI_{re}) shows a promising performance in estimating canopy chlorophyll and N across the different cultivars of barley and rice crops.

Canopy hyperspectral measurements are able to detect disease stresses before significant losses in Chl and N concentrations are observed. The MCARI and its variants are useful for the detection of disease symptoms because they are sensitive to Chl functional change. However, vegetation indices based on water absorption bands, such as the WBI and NDWI, offer a superior ability in discriminating diseased plants compared to the vegetation indices based on Chl absorption bands. Thus, water absorption bands might be more useful for crop disease detection at the canopy level.

7.9 Limitations and outlook

The possible limitations of this study are that (1) method developed here is not able to completely decouple the contribution of canopy biochemical and biophysical properties to canopy spectra data by optimizing the newly proposed vegetation index (RRDI); (2) underlying hypothesis is not comprehensive enough to account for the nonlinear factors of the confounding effect that result from the canopy structures, soil background and their interactions; and (3) lack

of validations using satellite and airborne sensors, despite the specific spectral bands detailed in this study being absent on the sensors of these platforms. Therefore, the method should be improved in the future work to verify whether validation is achievable through the hyperspectral imaging sensors mounted on unmanned aerial vehicles (UAVs).

Despite important progress has been made on the remote sensing of canopy N, there is a need to understand the underlying mechanisms and causality principles that generate the observed consistencies. The distribution of the *in vivo* N and its dynamic response to phenological stages, biotic and abiotic stresses make it difficult to fully represent canopy N variability using remote sensing; therefore, integration with vertical N distribution models might be able to improve the quantitative modeling of canopy N (Li *et al.*, 2013). Crop growth and soil fertility within a field or at a regional scale are both spatially and temporally variable (Cao, Q *et al.*, 2012; Dobermann *et al.*, 2004; Moran *et al.*, 1997); therefore, the challenge for precision agriculture techniques is to provide the precise information on the within-field spatial variability. To achieve this goal, remote sensing must allow for the timely determination of the source and extent of the variability, differentiation between the yield-limiting factors and identification of the specific crop stresses.

Despite the various limitations to understanding the links between canopy optical and biological traits, remote sensing will become an irreplaceable tool for understanding the links and studying the carbon and nitrogen cycles from leaf to global levels in agricultural and ecological applications. Future work for agricultural remote sensing should be highly integrated through sensor and data fusion.

General references *

- Aase, J.K., Siddoway, F.H. 1981.** Assessing winter wheat dry matter production via spectral reflectance measurements. *Remote Sens. Environ.* **11**: 267-277.
- Apan, A., Held, A., Phinn, S., Markley, J. 2004.** Detecting sugarcane 'orange rust' disease using EO-1 Hyperion hyperspectral imagery. *Int. J. Remote Sens.* **25**: 489-498.
- Aparicio, N., Villegas, D., Araus, J.L., Casadesús, J., Royo, C. 2002.** Relationship between Growth Traits and Spectral Vegetation Indices in Durum Wheat. *Crop Sci.* **42**: 1547-1555.
- Asner, G.P., Martin, R.E. 2008.** Spectral and chemical analysis of tropical forests: Scaling from leaf to canopy levels. *Remote Sens. Environ.* **112**: 3958-3970.
- Atzberger, C. 2004.** Object-based retrieval of biophysical canopy variables using artificial neural nets and radiative transfer models. *Remote Sens. Environ.* **93**: 53-67.
- Atzberger, C., Guérif, M., Baret, F., Werner, W. 2010.** Comparative analysis of three chemometric techniques for the spectroradiometric assessment of canopy chlorophyll content in winter wheat. *Comput. Electron. Agric.* **73**: 165-173.
- Atzberger, C. 2013.** Advances in Remote Sensing of Agriculture: Context Description, Existing Operational Monitoring Systems and Major Information Needs. *Remote Sens.* **5**: 949-981.
- Ayala-Silva, T., Beyl, C.A. 2005.** Changes in spectral reflectance of wheat leaves in response to specific macronutrient deficiency. *Adv. Space Res.* **35**: 305-317.
- Bannari, A., Morin, D., Bonn, F., Huete, A.R. 1995.** A review of vegetation indices. *Remote Sens. Rev.* **13**: 95-120.
- Baret, F., Guyot, G., Major, D.J. 1989.** TSAVI: A Vegetation Index Which Minimizes Soil Brightness Effects On LAI And APAR Estimation. In: IGARSS'89. 12th Canadian Symposium on Remote Sensing. *1989 International Geoscience and Remote Sensing Symposium*. 10-14 July 1989. Vancouver, BC, Canada. vol. 3, pp. 1355-1358.
- Bareth, G. 2009.** GIS- and RS-based spatial decision support: structure of a spatial environmental information system (SEIS). *Int. J. Digit. Earth* **2**: 134-154.
- Barkley, A., Tack, J., Nalley, L.L., Bergtold, J., Bowden, R., Fritz, A. 2014.** Weather, Disease, and Wheat Breeding Effects on Kansas Wheat Varietal Yields, 1985 to 2011. *Agron. J.* **1**: 227-235.
- Barton, C.V.M. 2001.** A theoretical analysis of the influence of heterogeneity in chlorophyll distribution on leaf reflectance. *Tree Physiol.* **21**: 789-795.
- Barton, C.V.M. 2012.** Advances in remote sensing of plant stress. *Plant Soil* **354**: 41-44.
- Beegle, D.B. 2013.** Soil Fertility Management. *Agronomy Guide*. University Park, PA.: The Pennsylvania State University.

* for Chapters 1, 6 and 7

- BGR. 1995.** *Bodenübersichtskarte 1:1000,000 von Deutschland*. Hannover: Bundesanstalt für Geowissenschaften und Rohstoffe (BGR).
- Biskup, B., Scharr, H., Schurr, U., Rascher, U. 2007.** A stereo imaging system for measuring structural parameters of plant canopies. *Plant. Cell Environ.* **30**: 1299-1308.
- Blackburn, G.A. 1998a.** Quantifying chlorophylls and carotenoids at leaf and canopy scales: An evaluation of some hyperspectral approaches. *Remote Sens. Environ.* **66**: 273-285.
- Blackburn, G.A. 1998b.** Spectral indices for estimating photosynthetic pigment concentrations: A test using senescent tree leaves. *Int. J. Remote Sens.* **19**: 657-675.
- Boegh, E., Soegaard, H., Broge, N., Hasager, C.B., Jensen, N.O., Schelde, K., Thomsen, A. 2002.** Airborne multispectral data for quantifying leaf area index, nitrogen concentration, and photosynthetic efficiency in agriculture. *Remote Sens. Environ.* **81**: 179-193.
- Botha, E.J., Leblon, B., Zebarth, B., Watmough, J. 2007.** Non-destructive estimation of potato leaf chlorophyll from canopy hyperspectral reflectance using the inverted PROSAIL model. *Int. J. Appl. Earth Obs. Geoinf.* **9**: 360-374.
- Broge, N.H., Leblanc, E. 2001.** Comparing prediction power and stability of broadband and hyperspectral vegetation indices for estimation of green leaf area index and canopy chlorophyll density. *Remote Sens. Environ.* **76**: 156-172.
- Buschmann, C. 2007.** Variability and application of the chlorophyll fluorescence emission ratio red/far-red of leaves. *Photosynth. Res.* **92**: 261-271.
- Camps-Valls, G., Bruzzone, L., Rojo-Álvarez, J.L., Melgani, F. 2006.** Robust support vector regression for biophysical variable estimation from remotely sensed images. *IEEE Geosci. Remote Sens. Lett.* **3**: 339-343.
- Cao, Q, Cui, Z, Chen, X, Khosla, R, Dao, TH, Miao, Y. 2012.** Quantifying spatial variability of indigenous nitrogen supply for precision nitrogen management in small scale farming. *Precis. Agric.* **13**: 45-61.
- Cao, X., Luo, Y., Zhou, Y., Duan, X., Cheng, D. 2013.** Detection of powdery mildew in two winter wheat cultivars using canopy hyperspectral reflectance. *Crop Prot.* **45**: 124-131.
- Cao, Y, Tang, C, Song, X, Liu, C, Zhang, Y. 2012.** Characteristics of nitrate in major rivers and aquifers of the Sanjiang Plain, China. *J. Environ. Monit.* **14**: 2624-2633.
- Carter, G.A. 1991.** Primary and Secondary Effects of Water Content on the Spectral Reflectance of Leaves. *Am. J. Bot.* **78**: 916-924.
- Casanova, D., Epema, G.F., Goudriaan, J. 1998.** Monitoring rice reflectance at field level for estimating biomass and LAI. *Field Crops Res.* **55**: 83-92.

- Chen, J.M., Cihlar, J. 1996.** Retrieving leaf area index of boreal conifer forests using Landsat TM images. *Remote Sens. Environ.* **55**: 153-162.
- Chen, X., Cui, Z., Vitousek, P.M., Cassman, K.G., Matson, P.A., Bai, J., Meng, Q., Hou, P., Yue, S., Romheld, V., Zhang, F. 2011.** Integrated soil-crop system management for food security. *Proc. Natl Acad. Sci. USA* **108**: 6399-6404.
- Curran, P.J. 1989.** Remote sensing of foliar chemistry. *Remote Sens. Environ.* **30**: 271-278.
- Curran, P.J., Dungan, J.L., Peterson, D.L. 2001.** Estimating the foliar biochemical concentration of leaves with reflectance spectrometry: Testing the Kokaly and Clark methodologies. *Remote Sens. Environ.* **76**: 349-359.
- Darvishzadeh, R., Atzberger, C., Skidmore, A.K., Abkar, A.A. 2009.** Leaf Area Index derivation from hyperspectral vegetation indices and the red edge position. *Int. J. Remote Sens.* **30**: 6199-6218.
- Darvishzadeh, R., Matkan, A.A., Ahangar, A.D. 2012.** Inversion of a Radiative Transfer Model for Estimation of Rice Canopy Chlorophyll Content Using a Lookup-Table Approach. *IEEE J. Sel. Top. Appl. Earth Obs. Remote Sens.* **5**: 1222-1230.
- Daughtry, C.S.T., Walthall, C.L., Kim, M.S., de Colstoun, E.B., McMurtrey III, J.E. 2000.** Estimating corn leaf chlorophyll concentration from leaf and canopy reflectance. *Remote Sens. Environ.* **74**: 229-239.
- Davies, K. 2004.** *Plant Pigments and their Manipulation*. Oxford, UK: Blackwell Publishing.
- Dawson, T.P., Curran, P.J. 1998.** A new technique for interpolating the reflectance red edge position. *Int. J. Remote Sens.* **19**: 2133-2139.
- Dawson, T.P., Curran, P.J., Plummer, S.E. 1998.** LIBERTY—Modeling the Effects of Leaf Biochemical Concentration on Reflectance Spectra. *Remote Sens. Environ.* **65**: 50-60.
- Delalieux, S., van Aardt, J., Keulemans, W., Schrevens, E., Coppin, P. 2007.** Detection of biotic stress (*Venturia inaequalis*) in apple trees using hyperspectral data: Non-parametric statistical approaches and physiological implications. *Eur. J. Agron.* **27**: 130-143.
- Delalieux, S., Auwerkerken, A., Verstraeten, W., Somers, B., Valcke, R., Lhermitte, S., Keulemans, J., Coppin, P. 2009.** Hyperspectral reflectance and fluorescence imaging to detect scab induced stress in apple leaves. *Remote Sens.* **1**: 858-874.
- Dobermann, A., Blackmore, S., Cook, S.E., Adamchuk, V.I. 2004.** Precision farming: challenges and future directions. In: Proceedings of the 4th International Crop Science Congress. 26 September - 1 October 2004. Brisbane, Australia.
- Dorigo, W.A., Zurita-Milla, R., de Wit, A.J.W., Brazile, J., Singh, R., Schaepman, M.E. 2007.** A review on reflective remote sensing and data assimilation techniques for enhanced agroecosystem modeling. *Int. J. Appl. Earth Obs. Geoinf.* **9**: 165-193.

- Eitel, J.U.H., Long, D.S., Gessler, P.E., Hunt, E.R. 2008.** Combined Spectral Index to Improve Ground-Based Estimates of Nitrogen Status in Dryland Wheat. *Agron. J.* **100**: 1694-1702.
- Elachi, C., van Zyl, J. 2006.** *Introduction to the Physics and Techniques of Remote Sensing.* Hoboken, New Jersey: Wiley-Interscience.
- Elowitz, M.R. 2014.** What is Imaging Spectroscopy (Hyperspectral Imaging)? Retrieved 2014-02-08 17:17:00.
- Elvidge, C.D. 1990.** Visible and near infrared reflectance characteristics of dry plant materials. *Int. J. Remote Sens.* **11**: 1775-1795.
- Evans, J.R. 1983.** Nitrogen and Photosynthesis in the Flag Leaf of Wheat (*Triticum aestivum* L.). *Plant Physiol.* **72**: 297-302.
- Fageria, N.K. 2009.** *The use of nutrients in crop plants.* Boca Raton, Florida, USA: CRC Press, Taylor & Francis Group, LLC.
- Féret, J., François, C., Gitelson, A., Asner, G.P., Barry, K.M., Panigada, C., Richardson, A.D., Jacquemoud, S. 2011.** Optimizing spectral indices and chemometric analysis of leaf chemical properties using radiative transfer modeling. *Remote Sens. Environ.* **115**: 2742-2750.
- Filella, I., Serrano, L., Serra, J., Peñuelas, J. 1995.** Evaluating wheat nitrogen status with canopy reflectance indices and discriminant analysis. *Crop Sci.* **35**: 1400-1405.
- Fridgen, J.L., Varco, J.J. 2004.** Dependency of cotton leaf nitrogen, chlorophyll, and reflectance on nitrogen and potassium availability. *Agron. J.* **96**: 63-69.
- Gamon, J.A., Peñuelas, J., Field, C.B. 1992.** A narrow-waveband spectral index that tracks diurnal changes in photosynthetic efficiency. *Remote Sens. Environ.* **41**: 35-44.
- Gao, B. 1996.** NDWI—A normalized difference water index for remote sensing of vegetation liquid water from space. *Remote Sens. Environ.* **58**: 257-266.
- Garbulsky, M.F., Peñuelas, J., Gamon, J., Inoue, Y., Filella, I. 2011.** The photochemical reflectance index (PRI) and the remote sensing of leaf, canopy and ecosystem radiation use efficiencies: A review and meta-analysis. *Remote Sens. Environ.* **115**: 281-297.
- Gastal, F., Lemaire, G. 2002.** N uptake and distribution in crops: an agronomical and ecophysiological perspective. *J. Exp. Bot.* **53**: 789-799.
- Gausman, H.W., Cardenas, R. 1968.** Effect of Soil Salinity on External Morphology of Cotton Leaves. *Agron. J.* **60**: 566-567.
- Gausman, H.W., Allen, W.A., Myers, V.I., Cardenas, R. 1969.** Reflectance and Internal Structure of Cotton Leaves, *Gossypium hirsutum* L. *Agron. J.* **61**: 374-376.

- Gebbers, R., Adamchuk, V.I. 2010.** Precision Agriculture and Food Security. *Science* **327**: 828-831.
- Gianquinto, G., Orsini, F., Fecondini, M., Mezzetti, M., Sambo, P., Bona, S. 2011.** A methodological approach for defining spectral indices for assessing tomato nitrogen status and yield. *Eur. J. Agron.* **35**: 135-143.
- Gitelson, A.A., Merzlyak, M.N., Lichtenthaler, H.K. 1996.** Detection of Red Edge Position and Chlorophyll Content by Reflectance Measurements Near 700 nm. *J. Plant Physiol.* **148**: 501-508.
- Gitelson, A.A., Gritz, Y., Merzlyak, M.N. 2003a.** Relationships between leaf chlorophyll content and spectral reflectance and algorithms for non-destructive chlorophyll assessment in higher plant leaves. *J. Plant Physiol.* **160**: 271-282.
- Gitelson, A.A., Viña, A., Arkebauer, T.J., Rundquist, D.C., Keydan, G., Leavitt, B. 2003b.** Remote estimation of leaf area index and green leaf biomass in maize canopies. *Geophys. Res. Lett.* **30**: 1248.
- Gitelson, A.A., Merzlyak, M.N. 2004.** Non-Destructive Assessment of Chlorophyll, Carotenoid and Anthocyanin Content in Higher Plant Leaves: Principles and Algorithms. In: Remote Sensing for Agriculture and the Environment. 2004. Ella, Greece, pp. 78-94.
- Gnyp, M.L., Miao, Y., Yuan, F., Ustin, S.L., Yu, K., Yao, Y., Huang, S., Bareth, G. 2014a.** Hyperspectral canopy sensing of paddy rice aboveground biomass at different growth stages. *Field Crops Res.* **155**: 42-55.
- Gnyp, M.L., Bareth, G., Li, F., Lenz-Wiedemann, V.I., Koppe, W., Miao, Y., Hennig, S.D., Jia, L., Laudien, R., Chen, X., Zhang, F. 2014b.** Development and Implementation of a Multiscale Biomass Model Using Hyperspectral Vegetation Indices for Winter Wheat in the North China Plain. *Int. J. Appl. Earth Obs. Geoinf.*
- Goel, P.K., Prasher, S.O., Patel, R.M., Landry, J.A., Bonnell, R.B., Viau, A.A. 2003.** Classification of hyperspectral data by decision trees and artificial neural networks to identify weed stress and nitrogen status of corn. *Comput. Electron. Agric.* **39**: 67-93.
- Govindjee, Krogmann, D. 2004.** Discoveries in oxygenic photosynthesis (1727-2003): a perspective. *Photosynth. Res.* **80**: 15-57.
- Gröll, K. 2008.** Use of sensor technologies to estimate and assess the effects of various plant diseases on crop growth and development. Ph.D. thesis, University of Hohenheim.
- Gutiérrez-Rodríguez, M., Reynolds, M.P., Escalante-Estrada, J.A., Rodríguez-González, M.T. 2004.** Association between canopy reflectance indices and yield and physiological traits in bread wheat under drought and well-irrigated conditions. *Aust. J. Agric. Res.* **55**: 1139-1147.

- Guyot, G., Baret, F. 1988.** Utilisation de la haute resolution spectrale pour suivre l'etat des couverts vegetaux. In: *Spectral Signatures of Objects in Remote Sensing*. 18-22 January 1988. Aussois, France.
- Haboudane, D., Miller, J.R., Tremblay, N., Zarco-Tejada, P.J., Dextraze, L. 2002.** Integrated narrow-band vegetation indices for prediction of crop chlorophyll content for application to precision agriculture. *Remote Sens. Environ.* **81**: 416-426.
- Haboudane, D., Miller, J.R., Pattey, E., Zarco-Tejada, P.J., Strachan, I.B. 2004.** Hyperspectral vegetation indices and novel algorithms for predicting green LAI of crop canopies: Modeling and validation in the context of precision agriculture. *Remote Sens. Environ.* **90**: 337-352.
- Haboudane, D., Tremblay, N., Miller, J.R., Vigneault, P. 2008.** Remote estimation of crop chlorophyll content using spectral indices derived from hyperspectral data. *IEEE Trans. Geosci. Remote Sens.* **46**: 423-437.
- Hackl, H., Mistele, B., Hu, Y., Schmidhalter, U. 2013.** Spectral assessments of wheat plants grown in pots and containers under saline conditions. *Funct. Plant Biol.* **40**: 409-424.
- Hansen, P.M., Schjoerring, J.K. 2003.** Reflectance measurement of canopy biomass and nitrogen status in wheat crops using normalized difference vegetation indices and partial least squares regression. *Remote Sens. Environ.* **86**: 542-553.
- Hatfield, J.L., Gitelson, A.A., Schepers, J.S., Walthall, C.L. 2008.** Application of Spectral Remote Sensing for Agronomic Decisions. *Agron. J.* **100**: 117-131.
- Hatfield, J.L., Prueger, J.H. 2010.** Value of Using Different Vegetative Indices to Quantify Agricultural Crop Characteristics at Different Growth Stages under Varying Management Practices. *Remote Sens.* **2**: 562-578.
- Hatfield, P.L., Pinter, P.J. 1993.** Remote sensing for crop protection. *Crop Prot.* **12**: 403-413.
- Heege, H., Reusch, S., Thiessen, E. 2008.** Prospects and results for optical systems for site-specific on-the-go control of nitrogen-top-dressing in Germany. *Precis. Agric.* **9**: 115-131.
- Herrmann, I., Shapira, U., Kinast, S., Karnieli, A., Bonfil, D.J. 2013.** Ground-level hyperspectral imagery for detecting weeds in wheat fields. *Precis. Agric.* **14**: 637-659.
- Huang, W., Lamb, D.W., Niu, Z., Zhang, Y., Liu, L., Wang, J. 2007.** Identification of yellow rust in wheat using in-situ spectral reflectance measurements and airborne hyperspectral imaging. *Precis. Agric.* **8**: 187-197.
- Huang, Z., Turner, B.J., Dury, S.J., Wallis, I.R., Foley, W.J. 2004.** Estimating foliage nitrogen concentration from HYMAP data using continuum removal analysis. *Remote Sens. Environ.* **93**: 18-29.

- Huete, A., Didan, K., Miura, T., Rodriguez, E.P., Gao, X., Ferreira, L.G. 2002.** Overview of the radiometric and biophysical performance of the MODIS vegetation indices. *Remote Sens. Environ.* **83**: 195-213.
- Huete, A.R. 1988.** A soil-adjusted vegetation index (SAVI). *Remote Sens. Environ.* **25**: 295-309.
- Hunt, E.R., Hively, W.D., Fujikawa, S., Linden, D., Daughtry, C.S., McCarty, G. 2010.** Acquisition of NIR-Green-Blue Digital Photographs from Unmanned Aircraft for Crop Monitoring. *Remote Sens.* **2**: 290-305.
- Hunt, E.R., Doraiswamy, P.C., McMurtrey, J.E., Daughtry, C.S.T., Perry, E.M., Akhmedov, B. 2013.** A visible band index for remote sensing leaf chlorophyll content at the canopy scale. *Int. J. Appl. Earth Obs. Geoinf.* **21**: 103-112.
- Inoue, Y., Peñuelas, J. 2006.** Relationship between light use efficiency and photochemical reflectance index in soybean leaves as affected by soil water content. *Int. J. Remote Sens.* **27**: 5109-5114.
- Jacquemoud, S., Baret, F. 1990.** PROSPECT: A model of leaf optical properties spectra. *Remote Sens. Environ.* **34**: 75-91.
- Jacquemoud, S. 1993.** Inversion of the PROSPECT + SAIL canopy reflectance model from AVIRIS equivalent spectra: Theoretical study. *Remote Sens. Environ.* **44**: 281-292.
- Jacquemoud, S., Bacour, C., Poilvé, H., Frangi, J.P. 2000.** Comparison of Four Radiative Transfer Models to Simulate Plant Canopies Reflectance: Direct and Inverse Mode. *Remote Sens. Environ.* **74**: 471-481.
- Jacquemoud, S., Verhoef, W., Baret, F., Zarco-Tejada, P.J., Asner, G.P., Francois, C., Ustin, S.L. 2006.** PROSPECT+SAIL: 15 Years of Use for Land Surface Characterization. In: IGARSS 2006. *2006 IEEE International Conference on Geoscience and Remote Sensing Symposium*. 31 July - 04 August 2006. Denver, Colorado, pp. 1992-1995.
- Jacquemoud, S., Verhoef, W., Baret, F., Bacour, C., Zarco-Tejada, P.J., Asner, G.P., François, C., Ustin, S.L. 2009.** PROSPECT + SAIL models: A review of use for vegetation characterization. *Remote Sens. Environ.* **113**: S56-S66.
- Jégo, G., Pattey, E., Liu, J. 2012.** Using Leaf Area Index, retrieved from optical imagery, in the STICS crop model for predicting yield and biomass of field crops. *Field Crops Res.* **131**: 63-74.
- Justes, E., Mary, B., Meynard, J.M., Machet, J.M., Thelier-Huche, L. 1994.** Determination of a Critical Nitrogen Dilution Curve for Winter Wheat Crops. *Ann. Bot.* **74**: 397-407.
- Kaufman, Y.J., Tanre, D. 1992.** Atmospherically resistant vegetation index (ARVI) for EOS-MODIS. *IEEE Trans. Geosci. Remote Sens.* **30**: 261-270.
- Kim, M.S., Daughtry, C.S.T., Chappelle, E.W., McMurtrey, J.E., Walthall, C.L. 1994.** The use of high spectral resolution bands for estimating absorbed photosynthetically active

- radiation (APAR). In: Proceedings of 6th International Symposium on Physical Measurements and Signatures in Remote Sensing. 17-21 January 1994. Val D'Isere, France: CNES, pp. 299-306.
- Kimura, R., Okada, S., Miura, H., Kamichika, M. 2004.** Relationships among the leaf area index, moisture availability, and spectral reflectance in an upland rice field. *Agric. Water Manage.* **69**: 83-100.
- Knipling, E.B. 1970.** Physical and physiological basis for the reflectance of visible and near-infrared radiation from vegetation. *Remote Sens. Environ.* **1**: 155-159.
- Knyazikhin, Y., Schull, M.A., Stenberg, P., Möttus, M., Rautiainen, M., Yang, Y., Marshak, A., Latorre Carmona, P., Kaufmann, R.K., Lewis, P., Disney, M.I., Vanderbilt, V., Davis, A.B., Baret, F., Jacquemoud, S., Lyapustin, A., Myneni, R.B. 2013.** Hyperspectral remote sensing of foliar nitrogen content. *Proc. Natl Acad. Sci.* **110**: E185-E192.
- Kokaly, R.F., Clark, R.N. 1999.** Spectroscopic Determination of Leaf Biochemistry Using Band-Depth Analysis of Absorption Features and Stepwise Multiple Linear Regression. *Remote Sens. Environ.* **67**: 267-287.
- Koning, R.E. 1994.** Home Page for Ross Koning. Plant Physiology Information Website. Retrieved 2013-12-16 20:46:00.
- Koppe, W., Li, F., Gnyp, M.L., Miao, Y., Jia, L.I.A.N., Chen, X., Zhang, F., Bareth, G. 2010.** Evaluating Multispectral and Hyperspectral Satellite Remote Sensing Data for Estimating Winter Wheat Growth Parameters at Regional Scale in the North China Plain. *Photogramm. Fernerkund. Geoinf.* **2010**: 167-178.
- Kumar, L., Schmidt, K., Dury, S., Skidmore, A. 2001.** Imaging spectrometry and vegetation science. In: **F. D. van der Meer; S. M. de Jong** (Eds.) *Imaging spectrometry*. Dordrecht, the Netherlands: Kluwer Academic Publishers, 111-155.
- Lamb, D.W., Brown, R.B. 2001.** PA—Precision Agriculture: Remote-Sensing and Mapping of Weeds in Crops. *J. Agric. Eng. Res.* **78**: 117-125.
- Lancashire, P.D., Bleiholder, H., Boom, T.V.D., Langelüddeke, P., Stauss, R., Weber, E., Witzemberger, A. 1991.** A uniform decimal code for growth stages of crops and weeds. *Ann. Appl. Biol.* **119**: 561-601.
- Laudien, R., Bareth, G. 2006.** Multitemporal hyperspectral data analysis for regional detection of plant diseases by using a tractor-and an airborne-based spectrometer. *Photogramm. Fernerkund. Geoinf.* **2006**: 217-227.

- le Maire, G., François, C., Dufrêne, E. 2004.** Towards universal broad leaf chlorophyll indices using PROSPECT simulated database and hyperspectral reflectance measurements. *Remote Sens. Environ.* **89**: 1-28.
- Lee, Y., Yang, C., Chang, K., Shen, Y. 2008.** A simple spectral index using reflectance of 735 nm to assess nitrogen status of rice canopy. *Agron. J.* **100**: 205-212.
- Lemaire, G., Jeuffroy, M., Gastal, F. 2008.** Diagnosis tool for plant and crop N status in vegetative stage: Theory and practices for crop N management. *Eur. J. Agron.* **28**: 614-624.
- Li, F., Gnyp, M.L., Jia, L., Miao, Y., Yu, Z., Koppe, W., Bareth, G., Chen, X., Zhang, F. 2008.** Estimating N status of winter wheat using a handheld spectrometer in the North China Plain. *Field Crops Res.* **106**: 77-85.
- Li, F., Miao, Y., Chen, X., Zhang, H., Jia, L., Bareth, G. 2010a.** Estimating winter wheat biomass and nitrogen status using an active crop sensor. *Intel. Autom. Soft Comput.* **16**: 1219-1228.
- Li, F., Miao, Y., Hennig, S., Gnyp, M., Chen, X., Jia, L., Bareth, G. 2010b.** Evaluating hyperspectral vegetation indices for estimating nitrogen concentration of winter wheat at different growth stages. *Precis. Agric.* **11**: 335-357.
- Li, F., Mistele, B., Hu, Y., Chen, X., Schmidhalter, U. 2014.** Reflectance estimation of canopy nitrogen content in winter wheat using optimised hyperspectral spectral indices and partial least squares regression. *Eur. J. Agron.* **52, Part B**: 198-209.
- Li, H., Zhao, C., Huang, W., Yang, G. 2013.** Non-uniform vertical nitrogen distribution within plant canopy and its estimation by remote sensing: A review. *Field Crops Res.* **142**: 75-84.
- Lichtenthaler, H.K. 1987.** Chlorophylls and carotenoids: Pigments of photosynthetic biomembranes. *Methods Enzymol.* **148**: 350-382.
- Martin, M.E., Plourde, L.C., Ollinger, S.V., Smith, M.L., McNeil, B.E. 2008.** A generalizable method for remote sensing of canopy nitrogen across a wide range of forest ecosystems. *Remote Sens. Environ.* **112**: 3511-3519.
- Meroni, M., Rossini, M., Guanter, L., Alonso, L., Rascher, U., Colombo, R., Moreno, J. 2009.** Remote sensing of solar-induced chlorophyll fluorescence: Review of methods and applications. *Remote Sens. Environ.* **113**: 2037-2051.
- Merzlyak, M.N., Gitelson, A.A., Chivkunova, O.B., Rakitin, V.Y. 1999.** Non-destructive optical detection of pigment changes during leaf senescence and fruit ripening. *Physiol. Plantarum* **106**: 135-141.
- Miao, Y., Mulla, D.J., Robert, P.C. 2006.** Identifying important factors influencing corn yield and grain quality variability using artificial neural networks. *Precis. Agric.* **7**: 117-135.

- Miller, J.R., Hare, E.W., Wu, J. 1990.** Quantitative characterization of the vegetation red edge reflectance I. An inverted-Gaussian reflectance model. *Int. J. Remote Sens.* **11**: 1755-1773.
- Mirik, M., Ansley, R.J., Michels, G.J., Elliott, N.C. 2012.** Spectral vegetation indices selected for quantifying Russian wheat aphid (*Diuraphis noxia*) feeding damage in wheat (*Triticum aestivum* L.). *Precis. Agric.* **13**: 501-516.
- Mirik, M., Ansley, R.J., Steddom, K., Jones, D., Rush, C., Michels, G., Elliott, N. 2013.** Remote Distinction of A Noxious Weed (Musk Thistle: *Carduus Nutans*) Using Airborne Hyperspectral Imagery and the Support Vector Machine Classifier. *Remote Sens.* **5**: 612-630.
- Mistele, B., Schmidhalter, U. 2008.** Estimating the nitrogen nutrition index using spectral canopy reflectance measurements. *Eur. J. Agron.* **29**: 184-190.
- Moran, M.S., Inoue, Y., Barnes, E.M. 1997.** Opportunities and limitations for image-based remote sensing in precision crop management. *Remote Sens. Environ.* **61**: 319-346.
- Mulla, D.J. 2013.** Twenty five years of remote sensing in precision agriculture: Key advances and remaining knowledge gaps. *Biosyst. Eng.* **114**: 358-371.
- NASA.** Earth Observatory. Retrieved 2014-02-10 23:45:00.
- Naumann, J., Young, D., Anderson, J. 2009.** Spatial variations in salinity stress across a coastal landscape using vegetation indices derived from hyperspectral imagery. *Plant Ecol.* **202**: 285-297.
- Nguyen, H.T., Lee, B. 2006.** Assessment of rice leaf growth and nitrogen status by hyperspectral canopy reflectance and partial least square regression. *Eur. J. Agron.* **24**: 349-356.
- Oerke, E., Gerhards, R., Menz, G., Sikora, R.A., eds. 2010.** *Precision Crop Protection - the Challenge and Use of Heterogeneity*: Springer Netherlands.
- Ogden, R.T., Miller, C.E., Takezawa, K., Ninomiya, S. 2002.** Functional regression in crop lodging assessment with digital images. *Journal of Agricultural, Biological, and Environmental Statistics* **7**: 389-402.
- Ollinger, S.V., Richardson, A.D., Martin, M.E., Hollinger, D.Y., Frohking, S.E., Reich, P.B., Plourde, L.C., Katul, G.G., Munger, J.W., Oren, R., Smith, M.L., Paw U, K.T., Bolstad, P.V., Cook, B.D., Day, M.C., Martin, T.A., Monson, R.K., Schmid, H.P. 2008.** Canopy nitrogen, carbon assimilation, and albedo in temperate and boreal forests: Functional relations and potential climate feedbacks. *Proc. Natl Acad. Sci.* **105**: 19336-19341.

- Ollinger, S.V., Reich, P.B., Frolking, S., Lepine, L.C., Hollinger, D.Y., Richardson, A.D. 2013.** Nitrogen cycling, forest canopy reflectance, and emergent properties of ecosystems. *Proc. Natl Acad. Sci.* **110**: E2437.
- Oppelt, N. 2002.** *Monitoring of plant chlorophyll and nitrogen status using the airborne imaging spectrometer AVIS.* Ph.D thesis, der Ludwig-Maximilians-Universität München.
- Oppelt, N., Mauser, W. 2004.** Hyperspectral monitoring of physiological parameters of wheat during a vegetation period using AVIS data. *Int. J. Remote Sens.* **25**: 145-159.
- Osborne, S.L., Schepers, J.S., Francis, D.D., Schlemmer, M.R. 2002.** Detection of Phosphorus and Nitrogen Deficiencies in Corn Using Spectral Radiance Measurements. *Agron. J.* **94**: 1215-1221.
- Peng, Y., Gitelson, A.A. 2011.** Application of chlorophyll-related vegetation indices for remote estimation of maize productivity. *Agric. For. Meteorol.* **151**: 1267-1276.
- Peñuelas, J., Gamon, J.A., Fredeen, A.L., Merino, J., Field, C.B. 1994.** Reflectance indices associated with physiological changes in nitrogen- and water-limited sunflower leaves. *Remote Sens. Environ.* **48**: 135-146.
- Peñuelas, J., Baret, F., Filella, I. 1995a.** Semi-empirical indices to assess carotenoids/chlorophyll-a ratio from leaf spectral reflectance. *Photosynthetica* **31**: 221-230.
- Peñuelas, J., Filella, I., Lloret, P., Muñoz, F., Vilajeliu, M. 1995b.** Reflectance assessment of mite effects on apple trees. *Int. J. Remote Sens.* **16**: 2727-2733.
- Peñuelas, J., Pinol, J., Ogaya, R., Filella, I. 1997.** Estimation of plant water concentration by the reflectance Water Index WI (R900/R970). *Int. J. Remote Sens.* **18**: 2869-2875.
- Perry, E.M., Fitzgerald, G.J., Nuttall, J.G., O Leary, G.J., Schulthess, U., Whitlock, A. 2012.** Rapid estimation of canopy nitrogen of cereal crops at paddock scale using a Canopy Chlorophyll Content Index. *Field Crops Res.* **134**: 158-164.
- Pinter, P.J., Hatfield, J.L., Schepers, J.S., Barnes, E.M., Moran, M.S., Daughtry, C.S.T., Upchurch, D.R. 2003.** Remote sensing for crop management. *Photogramm. Eng. Remote Sensing* **69**: 647-664.
- Prabhakar, M., Prasad, Y.G., Vennila, S., Thirupathi, M., Sreedevi, G., Rao, G.R., Venkateswarlu, B. 2013.** Hyperspectral indices for assessing damage by the solenopsis mealybug (Hemiptera: Pseudococcidae) in cotton. *Comput. Electron. Agric.* **97**: 61-70.
- Pu, R., Gong, P., Biging, G.S., Larrieu, M.R. 2003.** Extraction of red edge optical parameters from Hyperion data for estimation of forest leaf area index. *IEEE Trans. Geosci. Remote Sens.* **41**: 916-921.

- Qiao, J., Yang, L., Yan, T., Xue, F., Zhao, D. 2013.** Rice dry matter and nitrogen accumulation, soil mineral N around root and N leaching, with increasing application rates of fertilizer. *Eur. J. Agron.*: 93-103.
- Richter, K., Atzberger, C., Vuolo, F., Weihs, P., D'Urso, G. 2009.** Experimental assessment of the Sentinel-2 band setting for RTM-based LAI retrieval of sugar beet and maize. *Can. J. Remote Sens.* **35**: 230-247.
- Richter, K., Atzberger, C., Vuolo, F., D'Urso, G. 2011.** Evaluation of Sentinel-2 Spectral Sampling for Radiative Transfer Model Based LAI Estimation of Wheat, Sugar Beet, and Maize. *IEEE J. Sel. Top. Appl. Earth Obs. Remote Sens.* **4**: 458-464.
- Rondeaux, G., Steven, M., Baret, F. 1996.** Optimization of soil-adjusted vegetation indices. *Remote Sens. Environ.* **55**: 95-107.
- Salas, E., Henebry, G. 2014.** A New Approach for the Analysis of Hyperspectral Data: Theory and Sensitivity Analysis of the Moment Distance Method. *Remote Sens.* **6**: 20-41.
- Schlemmer, M., Gitelson, A., Schepers, J., Ferguson, R., Peng, Y., Shanahan, J., Rundquist, D. 2013.** Remote estimation of nitrogen and chlorophyll contents in maize at leaf and canopy levels. *Int. J. Appl. Earth Obs. Geoinf.* **25**: 47-54.
- Schlemmer, M.R., Francis, D.D., Shanahan, J.F., Schepers, J.S. 2005.** Remotely measuring chlorophyll content in corn leaves with differing nitrogen levels and relative water content. *Agron. J.* **97**: 106-112.
- Seelan, S.K., Laguetta, S., Casady, G.M., Seielstad, G.A. 2003.** Remote sensing applications for precision agriculture: A learning community approach. *Remote Sens. Environ.* **88**: 157-169.
- Serrano, L., Filella, I., Peñuelas, J. 2000.** Remote Sensing of Biomass and Yield of Winter Wheat under Different Nitrogen Supplies. *Crop Sci.* **40**: 723-731.
- Shou, L., Jia, L., Cui, Z., Chen, X., Zhang, F. 2007.** Using High-Resolution satellite imaging to evaluate nitrogen status of winter wheat. *J. Plant Nutr.* **30**: 1669-1680.
- Sims, D.A., Gamon, J.A. 2002.** Relationships between leaf pigment content and spectral reflectance across a wide range of species, leaf structures and developmental stages. *Remote Sens. Environ.* **81**: 337-354.
- Sims, D.A., Gamon, J.A. 2003.** Estimation of vegetation water content and photosynthetic tissue area from spectral reflectance: a comparison of indices based on liquid water and chlorophyll absorption features. *Remote Sens. Environ.* **84**: 526-537.
- Smith, M., Martin, M.E. 2001.** A plot-based method for rapid estimation of forest canopy chemistry. *Can. J. For. Res.* **31**: 549-555.

- Stafford, J.V. 2000.** Implementing Precision Agriculture in the 21st Century. *J. Agric. Eng. Res.* **76**: 267-275.
- Sun, L., Song, C. 2008.** Evapotranspiration from a freshwater marsh in the Sanjiang Plain, Northeast China. *J. Hydrol.* **352**: 202-210.
- Taub, D.R., Lerdau, M.T. 2000.** Relationship between leaf nitrogen and photosynthetic rate for three NAD-ME and three NADP-ME C4 grasses. *Am. J. Bot.* **87**: 412-417.
- Thenkabail, P.S., Smith, R.B., De Pauw, E. 2000.** Hyperspectral vegetation indices and their relationships with agricultural crop characteristics. *Remote Sens. Environ.* **71**: 158-182.
- Thenkabail, P.S., Smith, R.B., De Pauw, E. 2002.** Evaluation of narrowband and broadband vegetation indices for determining optimal hyperspectral wavebands for agricultural crop characterization. *Photogramm. Eng. Remote Sensing* **68**: 607-621.
- Thenkabail, P.S., Enclona, E.A., Ashton, M.S., Legg, C., De Dieu, M.J. 2004.** Hyperion, IKONOS, ALI, and ETM+ sensors in the study of African rainforests. *Remote Sens. Environ.* **90**: 23-43.
- Thenkabail, P.S., Lyon, J.G., Huete, A. 2012.** *Hyperspectral remote sensing of vegetation*. New York: CRC Press.
- Thenkabail, P.S., Mariotto, I., Gumma, M.K., Middleton, E.M., Landis, D.R., Huemmrich, K.F. 2013.** Selection of Hyperspectral Narrowbands (HNBS) and Composition of Hyperspectral Twoband Vegetation Indices (HVIs) for Biophysical Characterization and Discrimination of Crop Types Using Field Reflectance and Hyperion/EO-1 Data. *IEEE J. Sel. Top. Appl. Earth Obs. Remote Sens.* **6**: 1-13.
- Tilling, A.K., O Leary, G.J., Ferwerda, J.G., Jones, S.D., Fitzgerald, G.J., Rodriguez, D., Belford, R. 2007.** Remote sensing of nitrogen and water stress in wheat. *Field Crops Res.* **104**: 77-85.
- Tilly, N., Hoffmeister, D., Cao, Q., Lenz-Wiedemann, V., Miao, Y., Bareth, G. 2013.** Precise plant height monitoring and biomass estimation with Terrestrial Laser Scanning in paddy rice. *ISPRS Ann. Photogramm. Remote Sens. Spatial Inf. Sci.* **II-5/W2**: 295-300.
- Townsend, P.A., Serbin, S.P., Kruger, E.L., Gamon, J.A. 2013.** Disentangling the contribution of biological and physical properties of leaves and canopies in imaging spectroscopy data. *Proc. Natl Acad. Sci.* **110**: E1074.
- Tucker, C.J. 1979.** Red and photographic infrared linear combinations for monitoring vegetation. *Remote Sens. Environ.* **8**: 127-150.
- Ustin, S.L., Roberts, D.A., Pinzón, J., Jacquemoud, S., Gardner, M., Scheer, G., Castañeda, C.M., Palacios-Orueta, A. 1998.** Estimating Canopy Water Content of Chaparral Shrubs Using Optical Methods. *Remote Sens. Environ.* **65**: 280-291.

- Ustin, S.L., Gamon, J.A. 2010.** Remote sensing of plant functional types. *New Phytol.* **186**: 795-816.
- Ustin, S.L., Riaño, D., Hunt, E.R. 2012.** Estimating canopy water content from spectroscopy. *Israel J. Plant Sci.* **60**: 9-23.
- van der Meer, F.D., de Jong, S.M. 2001.** *Imaging Spectrometry: Basic Principles and Prospective Applications*. Dordrecht: Kluwer Academic Publishers.
- Vargas, L.A., Andersen, M.N., Jensen, C.R., Jørgensen, U. 2002.** Estimation of leaf area index, light interception and biomass accumulation of *Miscanthus sinensis* 'Goliath' from radiation measurements. *Biomass Bioenergy* **22**: 1-14.
- Verhoef, W. 1984.** Light scattering by leaf layers with application to canopy reflectance modeling: The SAIL model. *Remote Sens. Environ.* **16**: 125-141.
- Verrelst, J., Muñoz, J., Alonso, L., Delegido, J., Rivera, J.P., Camps-Valls, G., Moreno, J. 2012.** Machine learning regression algorithms for biophysical parameter retrieval: Opportunities for Sentinel-2 and -3. *Remote Sens. Environ.* **118**: 127-139.
- Viña, A., Gitelson, A.A. 2011.** Sensitivity to Foliar Anthocyanin Content of Vegetation Indices Using Green Reflectance. *IEEE Geosci. Remote Sens. Lett.* **8**: 464-468.
- Wagner, S.C. 2012.** Biological Nitrogen Fixation. *Nature Education Knowledge* **3**: 15.
- Weiss, M., Baret, F., Myneni, R.B., Pragnère, A., Knyazikhin, Y. 2000.** Investigation of a model inversion technique to estimate canopy biophysical variables from spectral and directional reflectance data. *Agronomie* **20**: 3-22.
- Weng, Q. 2011.** *Advances in environmental remote sensing: sensors, algorithms, and applications*: CRC Press LLC.
- Wiegand, C.L., Richardson, A.J. 1990.** Use of Spectral Vegetation Indices to Infer Leaf Area, Evapotranspiration and Yield: I. Rationale. *Agron. J.* **82**: 623-629.
- Xavier, A.C., Vettorazzi, C.A. 2004.** Mapping leaf area index through spectral vegetation indices in a subtropical watershed. *Int. J. Remote Sens.* **25**: 1661-1672.
- Xue, L., Cao, W., Luo, W., Dai, T., Zhu, Y. 2004.** Monitoring leaf nitrogen status in rice with canopy spectral reflectance. *Agron. J.* **96**: 135-142.
- Yao, Y., Miao, Y., Huang, S., Gao, L., Ma, X., Zhao, G., Jiang, R., Chen, X., Zhang, F., Yu, K., Gnyp, M., Bareth, G., Liu, C., Zhao, L., Yang, W., Zhu, H. 2012.** Active canopy sensor-based precision N management strategy for rice. *Agron. Sustain. Dev.* **32**: 925-933.
- Yoder, B.J., Waring, R.H. 1994.** The normalized difference vegetation index of small Douglas-fir canopies with varying chlorophyll concentrations. *Remote Sens. Environ.* **49**: 81-91.

- Yoder, B.J., Pettigrew-Crosby, R.E. 1995.** Predicting nitrogen and chlorophyll content and concentrations from reflectance spectra (400-2500 nm) at leaf and canopy scales. *Remote Sens. Environ.* **53**: 199-211.
- Yu, K., Lenz-Wiedemann, V., Leufen, G., Hunsche, M., Noga, G., Chen, X., Bareth, G. 2012.** Assessing hyperspectral vegetation indices for estimating leaf chlorophyll concentration of summer barley. *ISPRS Ann. Photogramm. Remote Sens. Spatial Inf. Sci.* **1-7**: 89-94.
- Yu, K., Gnyp, M.L., Gao, L., Miao, Y., Chen, X., Bareth, G. 2013a.** Using partial least squares (PLS) to estimate canopy nitrogen and biomass of paddy rice in China's Sanjiang Plain. In: *Workshop on UAV-based Remote Sensing Methods for Monitoring Vegetation*. 9-10 September 2013. Cologne, Germany.
- Yu, K., Li, F., Gnyp, M.L., Miao, Y., Bareth, G., Chen, X. 2013b.** Remotely detecting canopy nitrogen concentration and uptake of paddy rice in the Northeast China Plain. *ISPRS J. Photogramm. Remote Sens.* **78**: 102-115.
- Yu, K., Gnyp, M.L., Gao, L., Miao, Y., Chen, X., Bareth, G. 2014a.** Estimate Leaf Chlorophyll of Rice Using Reflectance Indices and Partial Least Squares. *Photogramm. Fernerkund. Geoinf.* **submitted**.
- Yu, K., Chen, X., Lenz-Wiedemann, V., Bareth, G. 2014b.** Optimizing spectral indices to reduce effects of soil background and canopy structure for the estimation of leaf chlorophyll of barley at different growth stages. *ISPRS J. Photogramm. Remote Sens.* **submitted**.
- Yu, K., Leufen, G., Hunsche, M., Noga, G., Chen, X., Bareth, G. 2014c.** Investigation of Leaf Diseases and Estimation of Chlorophyll Concentration in Seven Barley Varieties Using Fluorescence and Hyperspectral Indices. *Remote Sens.* **6**: 64-86.
- Zarco-Tejada, P.J., Miller, J.R., Noland, T.L., Mohammed, G.H., Sampson, P.H. 2001.** Scaling-up and model inversion methods with narrowband optical indices for chlorophyll content estimation in closed forest canopies with hyperspectral data. *IEEE Trans. Geosci. Remote Sens.* **39**: 1491-1507.
- Zarco-Tejada, P.J., Berjón, A., López-Lozano, R., Miller, J.R., Martín, P., Cachorro, V., González, M.R., de Frutos, A. 2005.** Assessing vineyard condition with hyperspectral indices: Leaf and canopy reflectance simulation in a row-structured discontinuous canopy. *Remote Sens. Environ.* **99**: 271-287.
- Zhang, C., Kovacs, J. 2012.** The application of small unmanned aerial systems for precision agriculture: a review. *Precis. Agric.* **13**: 693-712.

- Zhang, J., Pu, R., Huang, W., Yuan, L., Luo, J., Wang, J. 2012.** Using in-situ hyperspectral data for detecting and discriminating yellow rust disease from nutrient stresses. *Field Crops Res.* **134**: 165-174.
- Zhang, N., Wang, M., Wang, N. 2002.** Precision agriculture—a worldwide overview. *Comput. Electron. Agric.* **36**: 113-132.
- Zhao, D., Reddy, K.R., Kakani, V.G., Reddy, V.R. 2005.** Nitrogen deficiency effects on plant growth, leaf photosynthesis, and hyperspectral reflectance properties of sorghum. *Eur. J. Agron.* **22**: 391-403.
- Zhou, Z., Tong, L. 2005.** The current status, threats and protection way of Sanjiang Plain wetland, Northeast China. *J. Forest. Res.* **16**: 148-152.
- Zinnert, J., Nelson, J., Hoffman, A. 2012.** Effects of salinity on physiological responses and the photochemical reflectance index in two co-occurring coastal shrubs. *Plant Soil* **354**: 45-55.

Eigene Beteiligung an den Veröffentlichungen

An allen vier Artikeln (zwei publizierte Artikel und zwei Manuskripte in Review) habe ich maßgeblich von den Feldmessungen bis hin zur Analyse der Ergebnisse sowie Konzeption und Ausarbeitung der Artikel mitgewirkt, was auch meine Erstautorenschaft in allen vier Artikeln belegt.

Erklärung

Ich versichere, dass ich die von mir vorgelegte Dissertation selbständig angefertigt, die benutzten Quellen und Hilfsmittel vollständig angegeben und die Stellen der Arbeit - einschließlich Tabellen, Karten, und Abbildungen - , die anderen Werken im Wortlaut oder dem Sinn nach entnommen sind, in jedem Einzelfall als Entlehnung kenntlich gemacht habe; dass diese Dissertation noch keiner anderen Fakultät oder Universität zur Prüfung vorgelegt hat; dass sie - abgesehen von unten angegebenen Teilpublikationen - noch nicht veröffentlicht worden ist sowie, dass ich eine solche Veröffentlichung vor Abschluss des Promotionsverfahrens nicht vornehmen werde. Die Bestimmungen der Promotionsordnung sind mir bekannt. Die von mir vorgelegte Dissertation ist von Prof. Dr. Georg Bareth betreut worden.

Köln, den

Folgende Teilpublikationen liegen vor:

Yu, K., Li, F., Gnyp, M.L., Miao, Y., Bareth, G., Chen, X. 2013. Remotely detecting canopy nitrogen concentration and uptake of paddy rice in the Northeast China Plain. *ISPRS J. Photogramm. Remote Sens.* **78**: 102-115.

Yu, K., Leufen, G., Hunsche, M., Noga, G., Chen, X., Bareth, G. 2014. Investigation of leaf diseases and estimation of chlorophyll concentration in seven barley varieties using fluorescence and hyperspectral indices. *Remote Sens.* **6**: 64-86.

Yu, K., Gnyp, M.L., Gao, L., Miao, Y., Chen, X., Bareth, G. 2014. Estimate leaf chlorophyll of rice using reflectance indices and partial least squares. *Photogramm. Fernerkund. Geoinf.* **submitted.**

Yu, K., Chen, X., Lenz-Wiedemann, V., Bareth, G. 2014. Optimizing spectral indices to reduce effects of soil background and canopy structure for the estimation of leaf chlorophyll of barley at different growth stages. *ISPRS J. Photogramm. Remote Sens.* **submitted.**

Curriculum vitae

Kang Yu

Born 1985 in Jiangsu, China

Emails: kyu@uni-koeln.de, yuk@cau.edu.cn

Education

- 1992-1997 Primary school
- 1997-2000 Junior high school
- 2000-2003 Senior high school
- 2003-2007 China Agricultural University, BS in Resources & Environmental Sciences
- 2007-2009 China Agricultural University, MS in Plant Nutrition

Academic career

- 2004-2007 China Agricultural University, Undergraduate Research Program (URP), advisor: Prof. Xinping Chen
- 2007-2009 China Agricultural University, Jiansanjiang project, advisors: Profs. Xinping Chen & Yuxin Miao
- 2009-present University of Cologne, Institute of Geography, PhD student, advisor: Prof. Georg Bareth

List of publications

Peer-reviewed journals:

Yu, K., Li, F., Gnyp, M.L., Miao, Y., Bareth, G., Chen, X. 2013. Remotely detecting canopy nitrogen concentration and uptake of paddy rice in the Northeast China Plain. *ISPRS J. Photogramm. Remote Sens.* **78**: 102-115.

Yu, K., Leufen, G., Hunsche, M., Noga, G., Chen, X., Bareth, G. 2014. Investigation of leaf diseases and estimation of chlorophyll concentration in seven barley varieties using fluorescence and hyperspectral indices. *Remote Sens.* **6**: 64-86.

Yu, K., Gnyp, M.L., Gao, L., Miao, Y., Chen, X., Bareth, G. 2014. Estimate leaf chlorophyll of rice using reflectance indices and partial least squares. *Photogramm. Fernerkund. Geoinf.* **submitted**.

Yu, K., Chen, X., Lenz-Wiedemann, V., Bareth, G. 2014. Optimizing spectral indices to reduce effects of soil background and canopy structure for the estimation of leaf chlorophyll of barley at different growth stages. *ISPRS J. Photogramm. Remote Sens.* **submitted**.

Yao, Y., Miao, Y., Huang, S., Gao, L., Ma, X., Zhao, G., Jiang, R., Chen, X., Zhang, F., Yu, K., Gnyp, M., Bareth, G., Liu, C., Zhao, L., Yang, W., Zhu, H. 2012. Active canopy sensor-based precision N management strategy for rice. *Agron. Sustain. Dev.* **32**: 925-933.

Gnyp, M.L., Yu, K., Aasen, H., Yao, Y., Huang, S., Miao, Y., Bareth, G. 2013. Analysis of crop reflectance for estimating biomass in rice canopies at different phenological stages. *Photogramm. Fernerkund. Geoinf.* **2013**: 351-365.

Gnyp, M.L., Miao, Y., Yuan, F., Ustin, S.L., Yu, K., Yao, Y., Huang, S., Bareth, G. 2014. Hyperspectral canopy sensing of paddy rice aboveground biomass at different growth stages. *Field Crops Res.* **155**: 42-55.

Conference proceedings:

Yu, K., Lenz-Wiedemann, V., Leufen, G., Hunsche, M., Noga, G., Chen, X., Bareth, G. 2012. Assessing hyperspectral vegetation indices for estimating leaf chlorophyll concentration of summer barley. *ISPRS Ann. Photogramm. Remote Sens. Spatial Inf. Sci.* **1-7**: 89-94.

Yu, K., Gnyp, M.L., Gao, L., Miao, Y., Chen, X., Bareth, G. 2013. Using partial least squares (PLS) to estimate canopy nitrogen and biomass of paddy rice in China's Sanjiang Plain. In: *J. Bendig, G. Bareth (Eds.), Proceedings of the UAV-based Remote Sensing Methods for Monitoring Vegetation.* 9-10 September 2013. Cologne, Germany. *Kölner Geographische Arbeiten.*

Gnyp, M.L., Yao, Y., Miao, Y., Yu, K., Huang, S., Dornauf, E., Hütt, C., Lenz-Wiedemann, V.I.S., Laudien, R., Jiang, R., Chen, X., Bareth, G. 2010. Evaluating within-field rice growth variability using Quickbird and Ikonos images in Northeast China. In: *The 3rd ISDE Digital Earth Summit.* 12-14 June, 2010. Nessebar, Bulgaria.

Gnyp, M.L., Yao, Y., Yu, K., Huang, S., Miao, Y., Bareth, G. 2012. Hyperspectral analysis of rice phenological stages in northeast China. *ISPRS Ann. Photogramm. Remote Sens. Spatial Inf. Sci.* **1-7**: 77-82.

Gnyp, M.L., Miao, Y., Yuan, F., Yu, K., Yao, Y., Huang, S. Bareth, G. 2014. Derivative analysis to improve rice biomass estimation at early growth stages. In: *J. Bendig, G. Bareth (Eds.), Proceedings of the Workshop on UAV-based remote sensing methods for monitoring vegetation,* 9-10 September 2013, University of Cologne, Germany. *Kölner Geographische Arbeiten.*